FACULDADE DE ENGENHARIA DA UNIVERSIDADE DO PORTO
Masters in Mechanical Engineering

Master Dissertation

Soil-Structure Interaction modelling for an Offshore Wind Turbine with monopile foundation

Manuel António Rodrigues Franco
up201706755@up.pt

Supervisors
Dr. Pedro Manuel Leal Ribeiro
Mr. Marcos Paulo Halal Lombardi
Dr. Mads Damgaard

August 7, 2022

U. PORTO
FEUP FACULDADE DE ENGENHARIA
UNIVERSIDADE DO PORTO

Abstract

Offshore wind turbines (OWTs) are complex and dynamic sensitive structures. Although very similar to their onshore counterparts, they are usually bigger to resist the hardship of offshore conditions and the environment. These structures can be supported by different sub-structures, where the monopile foundation is the most popular. However, as current OWTs and corresponding foundations increase in size with the desire of having more cost-efficient solutions in the energy industry, there are concerns that current design methods are not applicable. This is corroborated by the increasing number of investigations and studies that present significant differences between the predicted structure behaviour and measured response. It is then important to accurately predict the foundation stiffness, both for future design phases and for the reassessment of existing foundations, by avoiding resonance regions. The amount of uncertainties surrounding the foundation and substructure design is the main difficulty in performing a correct design process that includes all significant factors. These uncertainties make it impossible to have very precise simulation results with simplified models (as even with complex models there is a certain error), as it is unknown which factors have more weight in stabilizing the structure and that may change with time. A rigorous procedure may be employed using a Finite Element Analysis, but it also requires higher computational times and foundation properties from tests that are also expensive. For complex structures, as an OWT, numerical solutions have to be developed. A number of limitations arise from the numerical approach, where experimental modal analysis is able to validate and improve such an approach. Based on these considerations, a simple model is developed using a single Timoshenko p-version finite element. This developed model allowed a study on the stiffness gain through different soil modelling formulation proposals, where an emphasis on natural frequency prediction was performed. The best-presented proposal assured an error inside a 5% bandwidth in relation to the measured fundamental natural frequency on four distinct full-scale testing situations identified through an Operational Modal Analysis process. Nevertheless, to safely design a wind turbine, sufficient damping in the entire structure is important to decrease fatigue damage accumulation during the service life of the wind turbine. Damping source formulations were then considered and its influence on the estimated natural frequency was observed.

Keywords: Offshore Wind Turbine; Soil-Structure Interaction; Modal analysis; Small-strain soil stiffness

Resumo

As turbinas eólicas *offshore* são estruturas complexas e dinamicamente sensíveis. Apesar de serem muito semelhantes às suas contrapartes (*onshore*), são usualmente maiores para resistirem às dificuldades inerentes do ambiente marítimo. Estas estruturas podem ser suportadas por diferentes sub-estruturas, onde a fundação monopilar é a mais popular. Contudo, com o aumento do tamanho das turbinas eólicas e suas fundações à medida que cresce o desejo de soluções mais eficientes em termos de custo na indústria energética, preocupações existem que os métodos de projeto atuais não sejam aplicáveis. Tal é corroborado pelo aumento de investigações e estudos que apresentam diferenças entre os comportamentos previstos e observados destas estruturas. É, então, importante prever de forma precisa a rigidez da fundação, seja para as fases futuras de projeto destas estruturas, seja para a reavaliação das estruturas existentes, evitando regiões de resonância. As incertezas que rodeiam o projeto da fundação e sub-estrutura são a principal dificuldade em realizar um processo correto de projeto que inclua todos os fatores significantes. Estas incertezas impossibilitam a aquisição de resultados muito precisos com modelos simplificados (dado que mesmo com modelos complexos existe um certo erro), dado que não é certo que fatores terão mais peso na estabilização da estrutura e que poderão mudar com o tempo. Um processo rigoroso pode ser elaborado utilizando uma análise de elementos finitos, mas tal requereria elevados tempos computacionais e variadas propriedades sobre a fundação de testes que são também caros. Para estruturas complexas como as turbinas eólicas *offshore*, soluções numéricas são necessárias. A utilização de uma abordagem numérica tem limitações, sendo necessário análises modais experimentais para validar e melhorar estas abordagens. Com base nestas considerações, um modelo simples foi desenvolvido usando um único elemento finito de Timoshenko e de versão p. Este modelo permitiu o estudo de ganho de rigidez com as diferentes propostas de formulação de modelar o solo, onde o foco se centrou na estimação das frequências naturais. A melhor proposta apresentada assegurou um erro dentro de uma banda de 5% de erro em relação à frequência natural fundamental medida em quatro casos distintos de teste em grande escala por via de uma análise modal operacional. Contudo, para projetar de forma segura uma turbina eólica, amortecimento suficiente deverá existir para diminuir a acumulação de danos devido a fadiga durante a vida de serviço da turbina. Consequentemente, foram consideradas formulações para modelar as diferentes fontes de amortecimento, sendo observada a influência que estas têm na frequência natural estimada.

Palavras-Chave: Turbina eólica *offshore*; Interação solo-estrutura; Análise modal; Rigidez do solo em pequenas deformações

Acknowledgments

This thesis would not be possible without the support of many people. To start, I want to thank my parents, Manuel Franco and Cristina Rodrigues, and my cousin Hugo Drumond for their support and presence throughout the thesis timeline.

In terms of academics, I want to take the opportunity to thank my supervisor, professor Pedro Leal Ribeiro, for all the guidance provided. A note also goes to professor Tiago Ferradosa who helped in the start of the thesis with scouring considerations.

I would also like to thank all the personnel in the LaC Department at Vestas for the excellent environment they provided. A special thanks to Marcos Lombardi, my supervisor at Vestas. Words are not enough to describe the immense help that he gave me throughout the thesis, with extreme dedication and availability. Another person that helped a lot with his soil knowledge and making sure that the thesis did not go outside the initial objectives is Mads Damgaard. An acknowledgement is also due to Ana Margarida Antunes who helped with her insight, opinion, and English skills.

A final thank you to all the team in the Formula Student FEUP that allowed me to work in their space, as well as for understanding the situation and supporting me. An appreciation is also noted to Henrique Oliveira for the rides to Vestas.

Table of Contents

List of Figures

List of Tables

List of Abbreviations

API	American Petroleum Institute
BEM	Blade/Beam Element Moment
CPT	Cone Penetration Test
DLC	Design Load Case
DNV	Det Norske Veritas
FEM	Finite Element Method
FLS	Fatigue Limit State
GBS	Gravity-Based Structure
IEC	International Electrotechnical Commission
KC	Keulegan-Carpenter number
LCoE	Levelised Cost of Energy
LM	Lumped Mass
NGI	Norwegian Geotechnical Institute
NREL	National Renewable Energy Laboratory
OCR	Over-Consolidation Ratio
OWT	Offshore Wind Turbine
RNA	Rotor and Nacelle Assembly
SDOF	Single Degree Of Freedom
SLS	Serviceability Limit State
SPT	Standard Penetration Test
SSI	Soil-Structure Interaction
ULS	Ultimate Limit State

List of Symbols

α	Roughness parameter	-
	Wind shear exponent	-
α_0	Steady angle of attack	rad
α_d	Bearing capacity factor	-
β	Dimensionless frequency parameter	-
β_{Stokes}	Stokes number	-
δ	Logarithmic decrement damping	-
ε_c	Reference critical strain	-
η	Loss factor	-
γ'	Effective unit weight of the soil	N/m^3
$\gamma_{0.7}$	Reference strain amplitude	-
γ_c	Cyclic strain amplitude	-
γ_{sat}	Unit weight of the saturated soil	N/m^3
γ_w	Unit weight of water	N/m^3
λ	Shear correction factor	-
λ_w	Wavelength	m
μ_w	Water dynamic viscosity	Pa.s
ν	Poisson ratio of the Structure material	-
ν_s	Soil Poisson ratio	-
ω	Frequency	rad/s
ω_n	Natural frequency	rad/s
ω_w	Wave frequency	rad/s
σ	Mean root of the relative speed between water wave particle and structure	m/s
σ_1	Standard deviation	-
	Principal direction stress	Pa
σ'_h	Horizontal effective stress	Pa
σ_u	Water pore pressure	Pa
σ_v	Total vertical stress	Pa
σ'_v	Vertical effective stress	Pa
ϕ	Modal shape	-
ϕ_0	Steady inflow angle	rad
ϕ_f	Sand friction angle	degree

φ	Angle around the monopile	rad
φ_{att}	Blade angle of attack	rad
ρ	Mass density of the Structure material	kg/m^3
ρ_a	Mass density of air	kg/m^3
ρ_g	Mass density of the marine growth	kg/m^3
ρ_s	Mass density of the soil	kg/m^3
ρ_w	Mass density of water	kg/m^3
ξ	Dimensionless (local) coordinate	-
ζ	Damping ratio	-
ζ_s	Soil damping ratio	-
a_0	Dimensionless frequency	-
A	Beam cross-section area	m^2
	Sand p-y curve parameter	-
A_r	Aerodynamic rotor area	m^2
c	Blade chord length	m
	Damping coefficient	-
c_a	Aerodynamic damping coefficient	N.s/m
c_c	Critical damping coefficient	N.s/m
c_o	Wave phase velocity	m/s
c_s^{hys}	Soil hysteretic damping coefficient	N.s/m^3
c_s^{rad}	Soil radiation damping coefficient	N.s/m^3
c_v	Coefficient of consolidation	m^2/s
c_w^{rad}	Water radiation damping coefficient	N.s/m
c_w^{vis}	Water viscous damping coefficient	N.s/m^3
C_d	Drag coefficient	-
C_d^{blade}	Blade drag coefficient	-
C_{IN}	Soil stiffness influence parameter	-
C_l^{blade}	Blade lift coefficient	-
C_M	Added mass coefficient	-
C_p	Power coefficient	-
C_{PR}	Soil stiffness coefficient	-
d	Structure outside diameter	m
D_r	Relative density of the soil	-
E	Structure material Young's Modulus	Pa
E_D	Energy dissipated in a load cycle by the soil	J
E_s	Young's Modulus of the Soil	Pa
E_S	Energy stored at a maximum strain equal to the cyclic amplitude strain by the soil	J
f	Frequency	Hz
F_D	Drag force	N
F_L	Lift force	N
F_T	Thrust force	N
g	Gravity acceleration	m/s^2
G	Structure material shear modulus	Pa
G_0	Small strain shear modulus	Pa
G_s	Soil shear modulus	Pa

h_w	Wave height	m
$H(x)$	Hankel function	-
I	Moment of area of a beam	m^4
	Turbulence intensity	-
I_l	Soil liquid index	-
I_p	Soil plasticity index	-
I_{ref}	Reference turbulence intensity	-
J	Moment of inertia of a body/beam	$kg.m^2$
J_{clay}	Clay soil strength parameter	-
k	Stiffness	N/m
k'	Stiffness	N/m^2
k_{ini}	Initial stiffness	N/m^3
k_o	Wave number	-
K_o	Lateral earth pressure coefficient	-
k_{PISA}	PISA design model initial stiffness	-
k_s	Soil stiffness	N/m^3
KC	Keulegan–Carpenter number	-
l	Structure/Beam length	m
L	Embedded length of the structure into the soil	m
$L_{embedded}$	Embedded length of the structure into the soil	m
$L_{submerged}$	Submerged length of the structure	m
m	Mass	kg
M_{aero}	Aerodynamic torque	N.m
M_v	Constrained soil modulus	Pa
n	PISA design model curvature parameter	-
N_p	Bearing capacity factor	-
p	Force per unit of length	N/m
P	Power	W
p_u	Soil bearing capacity	N/m
Q	Coefficient	-
R	Radius performed by the blade tip around the rotor centre	m
R_{ext}	External radius of the Structure	m
R_{int}	Internal radius of the Structure	m
S	Scour depth	m
s_u	Soil undrained shear strength	Pa
t	Thickness of the Structure	m
T	Kinetic energy	J
t_g	Marine growth thickness	m
t_p	Drainage time	s
T_{wave}	Wave period	s
U_m	Maximum wave orbital velocity	m/s
v	Speed/Velocity	m/s
V	Speed/Velocity	m/s
V_s	Shear wave velocity of the soil	m/s
V_{wind}	Wind speed	m/s
w	Soil water content	-

y	Lateral displacement (in common literature)	m
y_c	Reference critical lateral displacement	m
z	Depth	m
z_R	Transition depth	m
z_w	Water depth	m

Chapter 1

Introduction

1.1. General introduction

Offshore wind turbines (OWT) have a great prospect of evolution, since offshore sites have an increased proportion of wind energy capacity, as winds are stronger (higher wind speeds) and more stable (lower turbulence) than their onshore counterparts, as well as lower visual pollution. However, the construction and installation of offshore wind turbines are more difficult, from a logistic and engineering point of view, due to its intrinsically demanding characteristics [1–3].

The increased popularity of OWT is leading to further pushes in maximizing energy production and cost reduction. A direct consequence of these objectives is the OWT size increase and consequent advances in aerodynamics and structural integrity of the blades, to achieve an optimal design and operation of the wind turbines, reducing maintenance costs. Other factors such as correct maintenance strategies, increasing reliability, reduction of costs associated with installation, and improving supply chain integration are all steps to further reduce the total levelised cost of energy (LCoE) and improve the overall performance of the OWT. Fig. 1.1 presents the typical costs involved in OWT projects. The reduction in the overall cost of producing a given amount of energy translates to a lower price of the energy provided and an increase in the demand for this type of energy source [3, 4].

The marine environment that surrounds the offshore wind facilities makes them more complex from a design, installation, and operation point of view. An important remark should be made to the fact that optimizing foundation design has a significant potential for even further cost reductions, as, according to Asim et al. [3], the turbine itself costs less than 25% of the overall cost of installation. However, as the OWT is installed further away from shore, reducing the installation costs is a difficult process. It requires a deep analysis of the type of foundation used. The viability of wind farms depends on the development of efficient solutions to a variety of technical and design issues/challenges [5, 6].

A monopile foundation is the predominant technology used in offshore wind farms currently in operation, contemplating more than 70% of the installed support structures, due to its ease of construction in shallow to medium water depths (up to 30 meters). Different geologies/soil layers pierced by the monopile lead to different design considerations and varying length, wall thickness, and diameter. Currently, monopiles are expected to

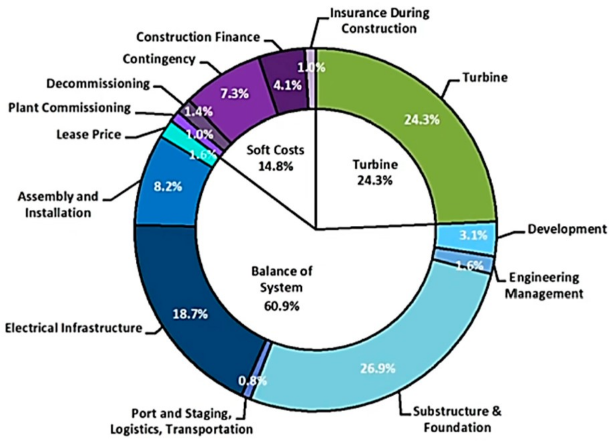

Fig. 1.1. OWT projects typical costs [3].

have outer diameters between four (4) and eight (8) meters, with penetrating lengths up to 40 meters. As such, it's common that the length-diameter ratio of a monopile supporting an OWT is less than six (6). It is important to note that as OWTs increase in size, so will the foundation dimensions. The monopile foundation is usually installed from impact driving, but other installation methods exist [1, 3, 7–10].

The characteristic loads for the design of wind turbines are commonly taken from time-domain aeroelastic response simulations. The design is mainly driven by extreme load cases that have origin from wind and wave loading. As fatigue damage is sensitive to the modal properties of the structure, an increase in the accuracy of the analysis tools used can improve reliability. This increase in reliability leads to a more cost-efficient design, as a less conservative approach can be used [11, 12].

During the OWT service life, besides the wind turbine itself, the foundation is subjected to millions of cycles of loading. As OWT are slender structures, these may operate, due to environmental (wind and wave) and mechanical loads, at frequencies close to their natural frequencies. As such, since these structures are flexible, they are especially dynamically sensitive in terms of their natural frequencies/dynamic loading. The design of offshore wind turbines currently passes through a design of soft-stiff, where there is a tight tolerance for the fundamental natural frequency of the structure when designing the system. A soft-stiff design is a design that tries to situate the fundamental natural frequency of an OWT between the 1P and 2/3P frequencies of a given wind turbine [1, 13].

Since OWT are relatively new structure, very few decent/detailed long-term performance records are available. This means that the design process that is made for 20+ years does not have a real-life comparison/validation. Yet, the accumulated rotation and stiffness change under long-term cyclic loading must be predicted when designing the OWT and its foundation [9, 14].

The monopile foundation is a fixed support structure, which means that the OWT is supported by the seabed. This makes the foundation design and analysis more complex, as it is important to investigate the soil-structure interaction (SSI). Damgaard et al. [15] observed that the consideration of a clamped OWT at a mudline leads to an overestimation of the natural frequencies of the structure while considering the common oil and gas practices regarding the interaction between a pile and the soil would lead to an underestimation. As such, other factors not portrayed in the common practices should be considered to justify this matter, pointing out the importance of the SSI when assessing the modal properties of the structure [13, 16].

Scour is a phenomenon that is linked to the removal of soil around the foundation of a structure, such as monopile foundations for OWTs. The occurrence of scouring leads to a reduction in foundation ultimate capacity and adjacent soil stiffness, altering the OWT dynamic response. Scour can then shift the fundamental frequency of the OWT into a range where resonance may occur. This showcases the importance of predicting not only the foundation behaviour due to a given excitation on the wind turbine but also due to other geological phenomenons that occur and may influence the structure response. If scour is significant, scour protection should be designed to protect the structure's foundation [17–19].

Standards require proper modal properties assessment and estimation but do not present a recommendation in that regard. Effects such as scour, soil permeability, soil non-linear behaviour, cyclic loading, the interaction between two adjacent layers of soil, and marine growth might alter the modal properties of the foundation on a SSI model analysis. Although all these factors might have a relevant influence, the vast majority are associated with a high degree of uncertainty and/or are not well-understood [1, 20–23].

The most common industry approach to SSI analysis comes from the oil and gas standard and it has been shown that this is inaccurate when applying to monopile foundations used in the OWTs. The development of a simple yet accurate approach that replaces this standard is needed for the offshore wind industry, with several modifications being published that try to account for the differences between the piles from these two industries. A more accurate approach will allow further cost reductions [4, 24].

FEM analysis is a possibility to guarantee simulation accuracy if all properties that influence the system's mass, stiffness and damping are known. However, this method is very time-consuming, requiring considerable resources to run. For this reason only, as projects have tight time schedules from a commercial point of view, the method is overlooked when faced with other more simple yet less accurate approaches in regular design routines. The most common model approach consists of a beam on a Winkler foundation. This model is computationally efficient and versatile, allowing non-linear springs to be considered discretely throughout the pile length. Other modelling approaches exist, such as the super-element approach, where the whole foundation is replaced as equivalent matrices of mass, stiffness and damping. Both these methods allow the incorporation of the SSI using a simplified method [24–26].

According to Versteijlen et al. [27], the initial stiffness of the springs that represent the soil reaction for small strain has a big influence on the natural frequencies of an OWT, as it will be the small strain stiffness that defines the modal properties of the support structure. In the majority of the endured vibrations, the OWT is also expected to be in a linear range of the soil response, i.e., the soil response will be linear throughout most of the OWT service life.

The correct estimation of the modal properties of the structure is important, as the natural frequencies allow the designer to understand if resonance occurs and the damping ratio defines the amplitude of vibrations when resonance happens. The fatigue damage is the main design parameter influenced by the modal properties, as even a small change in the considered global stiffness and damping of the system can lead to significant changes in this parameter. Currently, the parameters associated with the foundation coming from SSI models present some degree of uncertainty, while being one of the main influence factors in terms of overall damping and stiffness of the OWT system. A correct estimation of these properties can allow for less conservative designs, reducing the quantity of material needed for a given OWT and thus reducing costs. This is the main drive to develop cost efficient models to predict the structure characteristics and response. [4, 13, 23, 28].

Fig. 1.2 presents the common differences obtained in real-life situations, as reported in the work of Damgaard et al. [15], between the measured and calculated fundamental frequencies of OWTs. The necessity of an improved approach to the SSI to diminish the error seen between measured and predicted natural frequencies of OWTs requires the conception of new formulations regarding soil stiffness. Soil stiffness formulation is the main parameter of uncertainty related to the determination of OWTs natural frequencies. It has been repeatably documented that soil stiffness depends not only on the soil itself but also on the embedded structure properties. Since the common formulations used for slender piles in the oil and gas industry provide significant errors due to not accounting for the embedded structure properties, an effort should be made to include this.

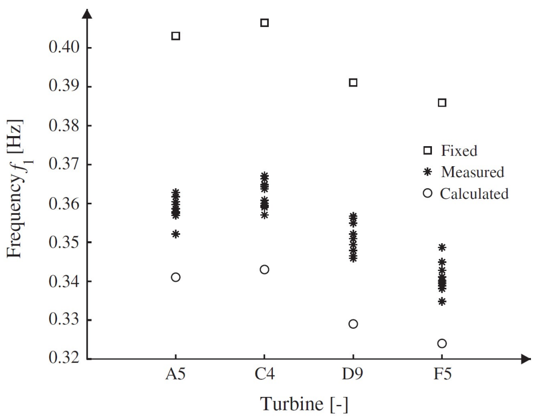

Fig. 1.2. Comparison between measured and calculated undamped fundamental frequencies of different OWTs [15].

1.2. Objectives

The present work intends to formulate a SSI model that can account for different soil influences on the structure and correct current used formulations. As best case scenarios only include a bandwidth error for different soil strata of between 7% and 15% (as seen in different literature), a formulation that can guarantee a smaller bandwidth error is desired.

Since multi-body and modal-based widely used models require considerable computational costs, to facilitate the study and formulation proposals assessment, a simpler model is set to be developed. This simpler model should be considerable faster but without compromising the obtained results by having low accuracy. As such, this developed model should assure that it can provide values within a 2% bandwidth error to controlled and baseline tests when compared with other validated and more complex models.

At the same time, exposure to the different factors that can influence the SSI characteristics, thus influencing the predicted modal properties of the system is desired. The reunion of this information in one place can then help further research and modelling development in this regard. Likewise, an assessment of currently used formulations for damping is attempted, as damping on these kinds of problems is only identified by back-calculating.

1.3. Thesis Layout

This thesis is composed of four main sections: a general introduction to OWTs and their design process (Chapter 2), a literature review on SSI modelling and influences that affect the modal properties of the studied system (Chapter 3), development of a simpler model that allows an easier approach on the study of SSI modelling (Chapter 4), and presentation and comparison of proposed formulations with experimental data from full-scale testing (Chapter 5). The present work focuses on the SSI modelling of an OWT with a monopile foundation, where a modelling approach based on the Winkler method was defined. Due to confidentiality agreements, no explicit results on the full-scale testing will be presented (only errors relative to the experiment's fundamental natural frequency will be presented). Special emphasis on the natural frequencies will be given, as damping influences very little on the natural frequencies obtained and measured.

As a model will be developed, two different models will then be used for results comparison: a newly developed model by the author of the current work and a well-validated model used in Vestas ('benchmark model' from now on). The ground-up developed model aims to be a simple approach to the OWT problem, where one Timoshenko beam element with varying geometry and properties is considered. This simple model will have multi degrees of freedom, defined by the degree of the shape functions used since a p-version finite element will be considered. After the first process of validation with analytical solutions, this model will also be subjected to a calibration process. Generic cases were considered for the analytical validation processes defined. Data regarding a set of different OWTs was consulted and the calibration process was performed comparing with the predicted results from the benchmark model. The well-validated model allows focusing on the influence of the soil, as the rest of the structure is considered to be well validated with full-scale experiments and measurements. However, as it is a computational costly model, it is inefficient to perform different soil stiffness formulations and first-degree optimization on it. Consequently, the simple model developed allows bigger flexibility in this regard. A damping sensitivity study on the developed model is also performed to assess if any damping source has a big impact on the estimated natural frequencies. The development and validation are exposed throughout Chapter 4.

Full-scale testing was performed to identify the natural frequencies of a set of different OWTs embedded in different soil strata. The modal properties identification was performed by an Operational Modal Analysis process. The variety of testing on different soil conditions allows the validation of the assumed soil stiffness formulation, where distinct influencing coefficients and parameters can be modified. Verdicts are then elaborated regarding the formulations considered and what modifications can still be performed. Various influencing factors can be included, but not all will, as there is a lack of correlation that can directly link them to the soil stiffness. This study is performed throughout Chapter 5.

Chapter 2

Offshore Wind Turbines

Horizontal axis wind turbines are vastly preferred and common over vertical axis wind turbines in the offshore wind industry due to higher capabilities of wind harnessing, affordable prices with size escalation, and well-established technology. The main difference between onshore and offshore wind turbines lies in the way the wind turbines are supported. The OWT can be supported as a fixed-bottom or as a floating structure. The fixed-bottom support structure has a foundation fixed to the seabed while floating support structures consist of floating platforms connected to the seabed through mooring cables. Besides the design of the OWT structure (tower with the rotor and nacelle assembly), other elements should be considered and designed in parallel, such as scour protection (depending on the water depth) and foundation (selecting the type most adequate for each case and designing it) [3].

2.1. Structure

An offshore wind turbine (OWT) can be divided into different parts: the Rotor and Nacelle Assembly (RNA) and the support structure (which includes the tower, substructure, and foundation). The foundation will be the part of the support structure that is below the mudline/sea ground level. Fig. 2.1 presents the mentioned division of an OWT system. Another way to see an OWT is to divide it using what it has in common with onshore wind turbines, i.e., wind turbine (RNA and tower) and foundation structure (substructure and foundation) [29].

2.1.1 Wind turbine

A wind turbine is essentially composed of a RNA and a tower. The RNA is mounted on top of the tower and it includes the aerodynamic rotor (rotor and blades), the transmission system, and the generator. The aerodynamic rotor usually has three blades linked to the rotor. The transmission system connects the rotor to the generator allowing a reduction. The transmission system can then be seen as a gearbox. However, although wind turbines regularly contain a gearbox, some do not. Wind turbines that do not have a gearbox are called direct-drive turbines. This depends on the generator installed at the wind turbine. The generator is responsible for the transformation of the mechanical power coming from

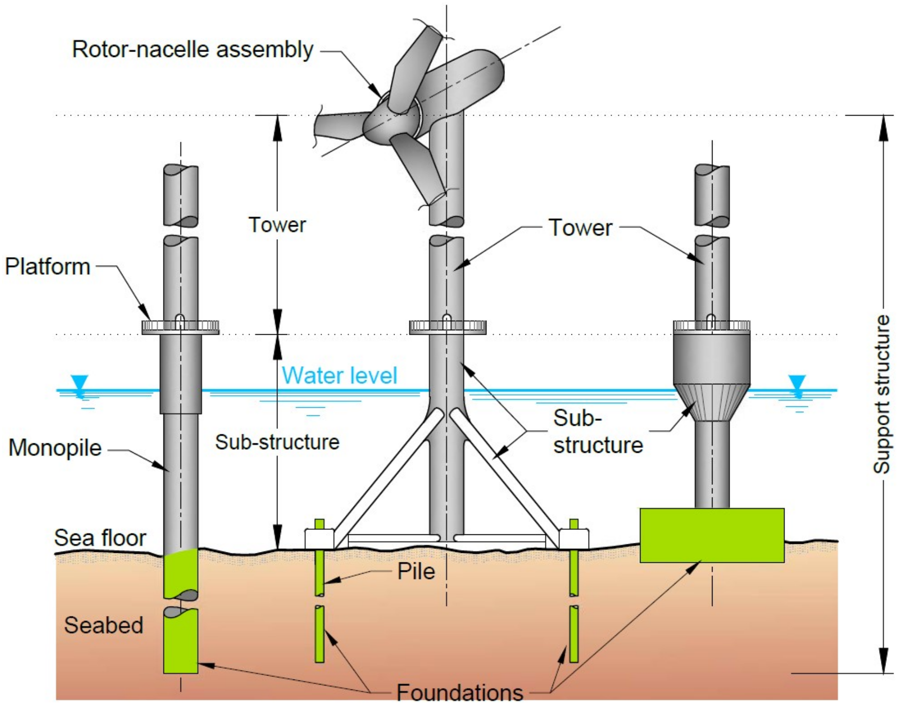

Fig. 2.1. OWT system division [29].

the rotating rotor to electrical power that supplies a power grid. Other components such as control systems and grid connections are also installed at the RNA [1].

It is common practice that the tower diameter and thickness vary with its length. Both of these dimensions decrease in the direction of the tower top, i.e., the outer diameter and thickness at the bottom of the wind turbine will be significantly bigger than at the top of the wind turbine. In a simplified analysis, these variations are regarded as linear. In reality, the tapered section of the tower will have an outer diameter that indeed varies linearly with height but will have sections of constant thickness. These regions of constant thickness come from the manufacturing process of the towers, where a rolling process of a metal sheet can be used [1, 30].

To mitigate vibrations, some towers are installed with damping mechanisms. These devices can take different forms but usually consist of a mass pendulum system. These systems are employed to further decrease dynamic loads applied to the structure, as significant vibrations can exist [31].

2.1.2 Sub-structure and Foundation

Different foundation type sub-structures can be considered. Besides floating sub-structures (that will be briefly introduced), monopod, tripod, jacket, and gravity base foundations should be considered during a design phase of a given OWT. Hybrid solutions can also be contemplated. According to the OWT location (soil and water depth) and environmental characteristics, some solutions can be more advantageous than others. However, currently, as technology developments allow, the monopod sub-structure is the popular choice when designing an OWT. The applicability of these sub-structures with increasing water depth can be seen in Fig. 2.2. This sub-section will give a rough overview of the existing types of sub-structures for OWTs [29, 32].

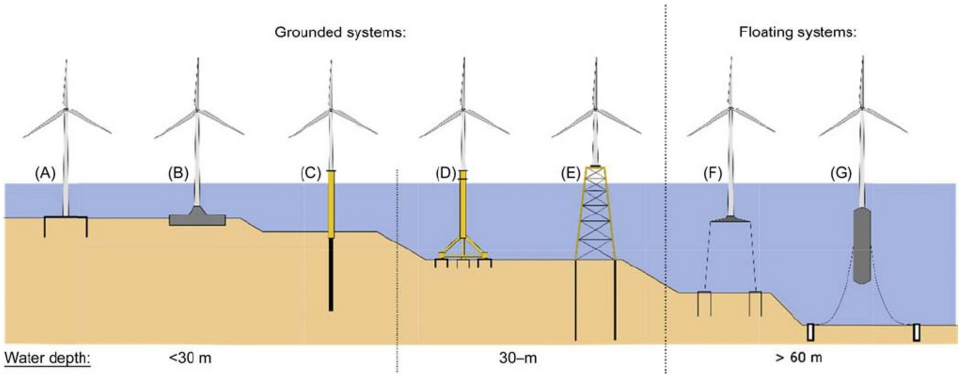

Fig. 2.2. OWT sub-structure types: (A) suction caisson, (B) Gravity base, (C) monopile/monopod, (D) tripod on suction caisson, (E) jacket, (F) tension leg platform, and (G) spar buoy platform [1].

Wave and wind loading generate a significant overturning moment in the foundation. Pile foundations are regularly selected as a foundation for offshore wind turbines since other types of foundations face difficulties to resist this moment. Water depth has a significant weight on the foundation type selection, as different foundations can be more adequate to use or more cost-efficient solutions to employ. Scour is also a phenomenon to take into consideration when selecting the foundation type, as it occurs for shallow water depths, raising the question of if scour protection should be implemented. Note that, as it will be mentioned in future chapters, scour influences significantly the stiffness of the soil and the fundamental natural frequency of the system [32, 33].

The monopile foundation is a fixed-bottom foundation that consists of a large tube-like structure. This support structure is embedded into the seabed through impact driving and/or drilling. These are regularly installed for water depths up to around 30 meters. This is the most common type of foundation used in the offshore wind industry as it is simple to construct and assemble [3, 34].

On monopile foundations, vertical loads are transferred to the surrounding soil through shaft friction and tip resistance. These will generate an axial shear across the length of the monopile. With respect to lateral loads, monopiles transfer them by bending, with the soil reacting to this motion in opposite direction. As it consists of a single structure, a certain degree of flexibility is noted when compared with other types of foundation [2, 26, 34].

A jacket foundation consists of a set of three or four piles embedded into the seabed. This support structure consists of a space frame structure made of welded tubular members. The legs (embedded piles) are usually inclined to increase stability. This foundation can then be considerably stiffer than the monopile foundation, and is more viable, for that reason, for water depths bigger than 30 meters. Nevertheless, vertical piles allow an easier installation. Different installation processes to those used in monopile installation can be used [3, 6, 35].

The suction caisson foundation has a simple installation procedure than the monopile foundation, as this last one requires a considerable amount of equipment. Its installation however may be complicated as some suction caisson have valves to allow the substructure to sink into the soil. This means that these valves need to be operated undersea, requiring robots or divers [6].

Gravity-based structures (GBS) are a type of shallow foundations. This foundation can only be used for shallow water depths, as they are held in place by their weight. Installing this type of foundation for deep water depths is not feasible, as loads will be higher and a heavier, as well as more expensive, structure would be necessary. Concrete is the common selected material for this kind of foundation, as a large volume and high weight are requirements. Nevertheless, steel can also be used for this support structure [36].

A GBS will transfer the loading that it is subjected directly to the soil, in opposition to what is observed for pile-type foundations, where the support structure deflects before transferring the loading to the surrounding soil. As they are shallow installed support structures, a high vulnerability to scour and sinking exists [36].

Fixed-bottom hybrid support structures are also being investigated as a possibility of increasing the foundation stiffness while decreasing costs. Trojnar [37] investigated a hybrid foundation system composed of a footing plate resting on the ground and a vertical monopile embedded in the subsoil. Although small-scale results showed greater lateral stiffness when employing this kind of foundation, there is no knowledge of interest in implementing, for now, this foundation alternative in full-scale. The concept allows a reduction of lateral displacements and a decrease in the bending moment that the monopile is subjected to. The soil reaction is also modified with the application of this hybrid fixed-bottom foundation.

From a given water depth (around 60 meters), fixed-bottom support structures become substantially expensive and commercially not viable solutions. As such, for increased water depths, floating support structures are employed. However, currently, the technology is not fully developed to successfully implement this kind of foundation at a large scale in the offshore wind industry. Different floating structures may be selected, such as tension leg, spar buoy, or semi-submersible support structures [3].

The tension leg support structure consists of three or four mooring cables that connect the floating structure to the seabed. The main difference between this foundation and the rest of the existing floating foundations is the fact that the mooring cables are in tension, providing static support to the OWT. As the substructure increases in this foundation, the tension cables are subjected to larger tensions and thus they are required to get bigger, elevating the costs of installation [3].

The spar buoy support structure consists on a tower-like structure filled with ballast and connected to the seabed through mooring cables. These mooring cables allow the substructure to navigate within a given circle. As such, they are bigger in length than the ones needed for the tension leg type foundation (around 4 times). Their stability under extreme weather conditions is an ongoing research [3].

The semi-submersible support structure consists of attaching buoyant structures to the main substructure. This foundation can have different configurations. Varying the buoyancy of the semi-submersible structures, static stability can be achieved, with the floating substructure being connected to the seabed through mooring cables. Likewise, this foundation has the freedom to navigate within a given circle, as in the case of the spar buoy type foundation [3].

Regarding the freedom to navigate within a given circle, the mooring cables used should be flexible enough to compensate for the movement of the floating platform (bigger cables in length). However, this is an important characteristic of these floating foundations, as it avoids extreme wind loads at the blades of the OWTs, protecting them from potentially structurally damaging loads [3].

2.2. Design Considerations

The design of OWTs has two fronts: the wind turbine design (very similar to onshore and offshore wind turbines) and the foundation design. This is a complex task, as it separates the design of a given structure into multiple joint structures. The main difference between onshore and offshore design is the level of foundation influence on the wind turbine design, as well as the introduction of wave loading on the structure. However, both share the same base principle: the rotor thrust due to a given wind load deflects the tower. This deflection does not occur only in the wind direction application, as vibrations in the fore-aft (rotor alignment direction) and side-to-side (perpendicular direction to the rotor alignment) directions exist. The overall bending moment applied on the tower, related to a variety of loads and dynamic effects (such as the rotation of the blades around the rotor axis), then leads to a complex dynamic response of the tower [3, 23, 28].

The loading acting on OWTs is a combination of different static and dynamic loads. High importance is given to the prediction of the natural frequencies and damping of the general system, as this is what will drive the design to avoid resonance frequency ranges and maximum expected load amplification for different load cases considered in the certification of a given OWT. A set of limit states criteria must be confirmed in the design process to ensure that the OWT will not fail. For example, the wind turbine cannot operate when a permanent rotation of more than 0.5º is in order. Different standards and recommendations rule the OWTs design [14].

Floating OWTs are much more complex structures from a design point of view. Since these OWTs have moving platforms, intense wave loading changes the kinematic conditions of blades. As such, besides the different wave interaction with the structure and different load applications in that regard, also the wind loading will be different, as it is applied on the blades in a different way with a constant variation of kinematic conditions. This design process will not be broached here [3].

The present section will focus on the OWT design considering a monopile as the support structure. The broached topics can, however, generally speaking, be applied to other support structures, as there are several design points in common.

2.2.1 Offshore Wind turbine design

The electrical generation driver in a wind turbine is wind. The wind is the relative movement of air and it can be characterised according to its average wind speed at hub height. Characterisation regarding a 50-year recurrence period of extreme wind conditions can also be performed for a given location. This wind characterisation will then allow the categorisation of a wind turbine into a respective class. This will be the certification class for the wind turbine [1, 38].

Usually, a wind turbine is designed for 20+ years of operation, corresponding to almost 10^8 cycles of loading. The OWT design main drive is a set of extreme/ultimate loads acting on the structure. Fatigue loads are also accounted for during the design. Still, for the correct wind turbine design and certification, a series of design load cases (DLC) have to be run. These load cases include situations of normal operation over short and long periods of time, extreme operating conditions and combined situations to include in fatigue analyses. In a nutshell, the standard IEC 61400-3 (standard that rules the fixed-bottom offshore wind turbine design process) gives a series of DLCs to be computed and analysed in order to simulate all load cases possibilities that a wind turbine will face throughout its lifespan. The OWT should then be able to withstand all inputted conditions [13, 14].

Aeroelastic simulation models are commonly used to account for the complex interactions of the wind turbine's blades with the acting wind aerodynamic loads. Incompressible Navier-Stokes equations are used to run the computational simulations. Blade Element Moment Theory (BEM) is regularly used to study the aeroelastic phenomena in the blades. In this theory, the resultant aerodynamic force applied to the rotor is given as the sum of each blade element's thrust force component. Different resultant forces will exist in the fore-aft and side-side directions [3, 39].

An OWT is subjected to a set of different dynamic loads. These are wind, waves, water currents, and vibrations from rotor and blades induced loads. The main external loads considered have origins in wind and wave loading. The applied loads on a wind turbine (either onshore or offshore) can be divided into more common types [1, 32, 40]:

- Steady loads, associated with a mean wind acting load and inertial/gravity loads;
- Stochastic loads, associated with wind speed variations, i.e., turbulence;
- Resonance-induced loads, mainly associated with matching frequencies between the excitation and the structure, but also due to turbulence;
- Transient loads, associated with loading changes and controller performed alterations, such as gusts and starting/stopping operations;
- Cyclic loads, associated with wind shear, gravity or gyroscopic effects, and yaw motion.

As these loads occur at low frequencies and being wind turbines slender and flexible structures, in this range, wind turbines are dynamically sensitive. The wind turbine performance will then be improved by minimising unwanted loads and maximising the power output [32, 40].

Aasen et al. [4] state that vertical loads are significantly smaller than horizontal loads and bending moments. As such, and as seen in the vast literature, the vertical loads are normally disregarded for simplicity's sake. As such, pitch and surge motions are the ones that influence more the performance of the wind turbine. This is supported by Asim et al. [3] and Achmus et al. [41].

Wave and wind loading are accounted for in simulations as wave and wind probability distributions. The Weibull distribution is widely used as the wind probability distribution. With the design life and wind probability distribution, it is possible to account for the number of hours (time) that a given wind turbine will be subjected to a given wind speed.

A correlation between this time and the respective producing power at the considered wind speed is performed by knowing the power curve of the wind turbine. The lifetime production power of a given wind turbine at a specific location can then be estimated. According to Myers et al. [42], operational conditions are wind-dominated, while extreme conditions are wave-dominated. This difference results in different loading frequency spectra [1, 13].

Wave loading appears as an excitation that introduces relevant oscillation and accelerations to the structure. This type of loading has an excitation frequency close to the fundamental frequency of the wind turbine. This leads to dynamic amplification of loads, which affects the service life of a wind turbine through its fatigue damage [28].

Wind loading drives the rotor of the wind turbine, allowing the generation of electrical power through its rotation. Besides being important to establish reliability for continuous power generation, it is fundamental to understand how the air will behave around the wind turbine, especially the blades. The aerodynamic performance and inherent air interaction with the structure should be studied and understood. For example, vortices may occur at the blade's tip, influencing the aerodynamic forces and moments [3].

As an increasing height is considered, a phenomenon known as wind shear occurs. Wind shear consists of an exponential increase of the wind speed with height. The wind speed at a given height h will be given by Eq. 2.1, where α will be a wind shear exponent. Fig. 2.3 presents the normalised evolution of wind speed with height for wind with an exponent of 0.15. Furthermore, the wind can act on the wind turbine from different angles. There might be up-flow and misalignment angles that lead to different load cases and responses. Fig. 2.4 allows visualization of those angles.

$$V(h) = V_{hub} \cdot \left(\frac{h}{h_{hub}} \right)^{\alpha} \tag{2.1}$$

Wind load cases are then studied usually from extreme load conditions. These are associated with sudden wind gusts. Besides extreme wind load magnitude, extreme direction changes are also studied. An important characteristic of the wind, as a fluid, is the turbulence intensity linked to it. The turbulence intensity can state the wind speed variation within a given time frame. Turbulence is important for relatively short time analyses (up to 10 minutes). As the time frame considered increases (hours and days), other wind factors gain importance. Used for wind modelling, the standard deviation and turbulence intensity can be acquired through Eqs. 2.2 and 2.3, respectively. On Eq. 2.2, the b parameter is usually taken as 5.6 m/s. A general wind field/profile acting on a wind turbine can be visualised in Fig. 2.5 [43].

$$\sigma_1 = I_{ref}\,(0.75 V_{hub} + b) \tag{2.2}$$

$$I = \frac{\sigma_1}{V_{hub}} \tag{2.3}$$

An associated aerodynamic loading consists of the aerodynamic force generated by a blade when passing ahead of the tower. A surging motion can appear and influence wind turbine aerodynamics. With smaller surging amplitudes (and frequencies), a greater stability in power generation and oscillation mitigation is obtained [3].

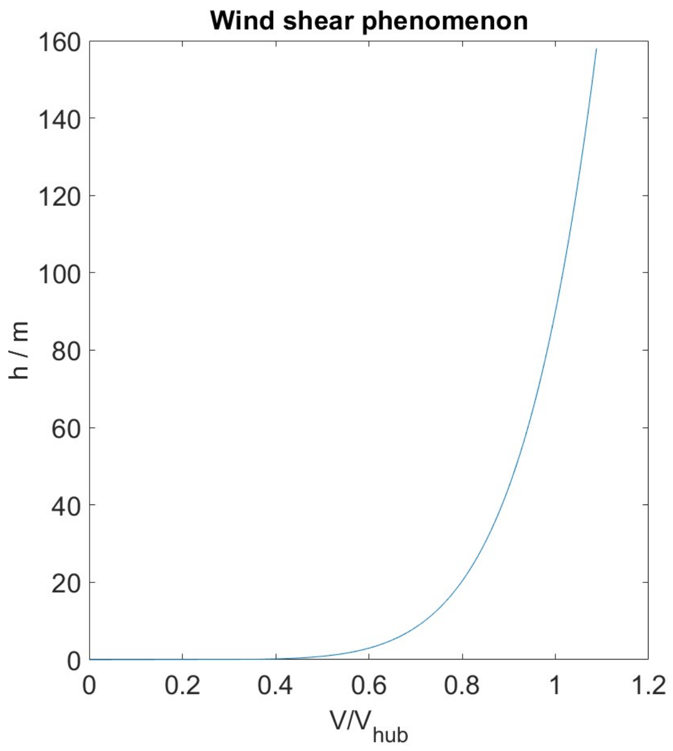

Fig. 2.3. Normalised wind speed evolution with height for the NREL 5-MW Baseline Wind Turbine with $\alpha = 0.15$.

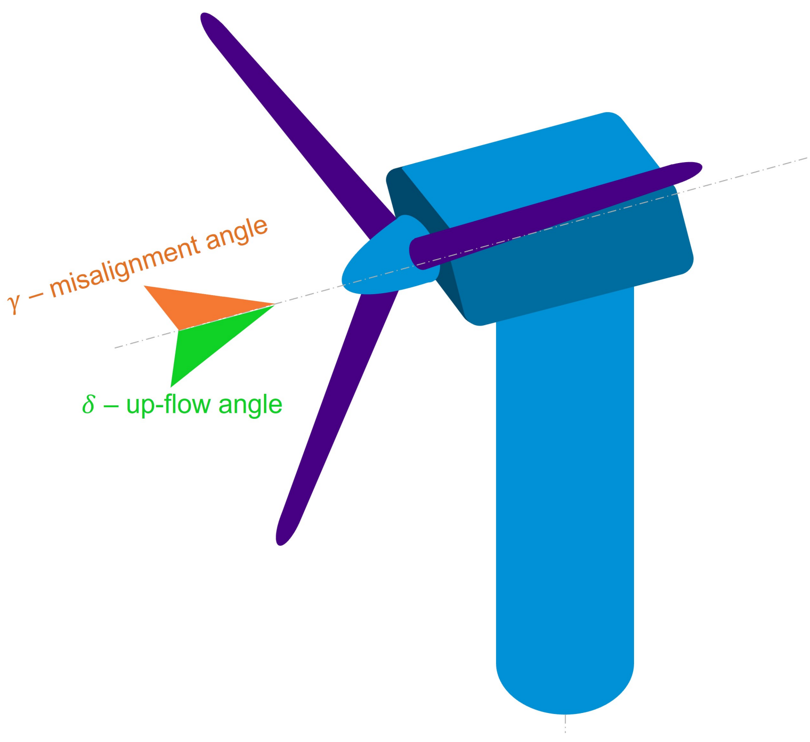

Fig. 2.4. Wind misalignment and up-flow angles in relation to the wind turbine's hub axis.

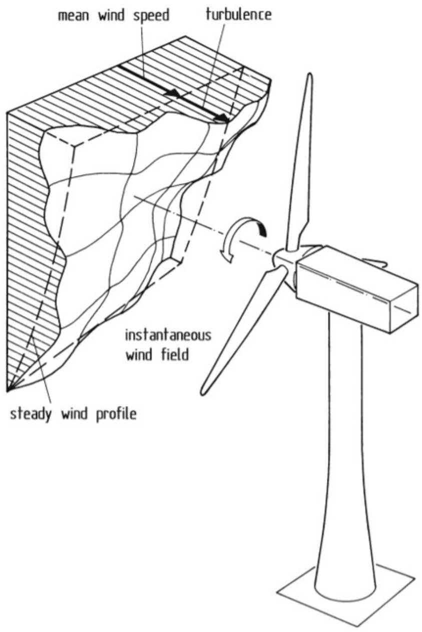

Fig. 2.5. General example of a wind field applied to a wind turbine [44].

To understand the aerodynamic loading, it is necessary to understand how a wind turbine operates. As airflow passes through the wind turbine's blades, an aerodynamic torque is generated and is then transformed into electrical power through a generator. The potential power that lies on the airflow, however, is not fully conversed into electrical power. Putting aside the generator and other components' efficiency, the transformation of the air potential power into aerodynamic power is limited by a theoretical limit known as the Betz limit. This theoretical limit can be achieved by considering the wind turbine rotor as a permeable disc and performing a 1D aerodynamic analysis. As the wind turbine will have more complex phenomena occurring at the blades, the actual power coefficient (that relates the air potential power with the harvested power at the rotor) will always be less than the Betz limit. The Betz limit corresponds to a power coefficient of around 0.59. The power at the rotor due to the generated aerodynamic torque will be given by Eq. 2.4 [1]:

$$P = \frac{1}{2}\rho_a V_{wind}^3 A_r C_p. \tag{2.4}$$

To be able to account for the aerodynamics forces that act on the wind turbine's blades, it is normal to use the Blade Element Momentum (BEM) theory. Its base consists of the general beam element moment approach. BEM then considers a 2D approach to the flow that passes through a wind turbine's blade, where the blade is divided into n annular elements. Fig. 2.6 represents the basic notation used on a blade section. From the represented angles and quantities, special emphasis goes to the steady attack angle α_0 and the steady inflow angle ϕ_0, where θ will be the direction of vibration. Knowing the rotor rotation speed of the blade and the wind speed it is possible to define a tip speed ratio. The tip speed ratio is important to define how much faster the tip of the blade will be rotating than the rotor centre. There will also be a combination of an optimum value of the tip speed ratio in junction with an optimum value of pitch angle that leads to the highest power coefficient [45].

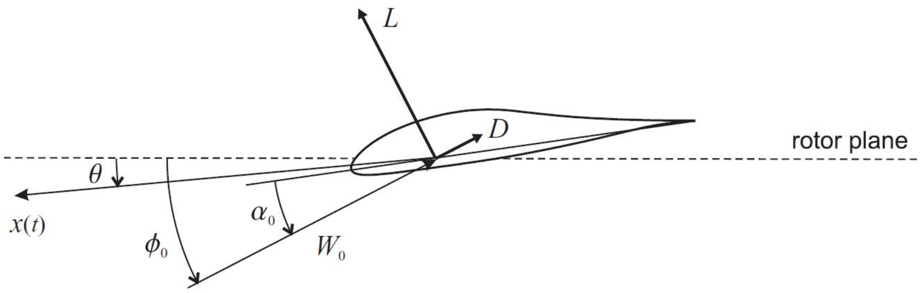

Fig. 2.6. BEM relevant angles [45].

As the airflow passes through a given blade, a high-pressure region is created on the lower part of this component, while a low-pressure region exists on top. These pressure contributions generate a lift force, making the rotor move. At the same time, a drag force will exist. These loads, observable in Fig. 2.6, vary in terms of the wind speed that passes through the blade as well as on its angle of attack. The drag and lift forces are forces that are aligned with the blades' referential. By projecting these forces onto the rotor plane, it is possible to quantify the thrust force and aerodynamic torque applied to the rotor. All the mentioned loads are given by Eqs. 2.5 to 2.8 [44]:

$$F_L = \frac{1}{2} C_l^{blade} \rho_a V_{wind}^2 c; \tag{2.5}$$

$$F_D = \frac{1}{2} C_d^{blade} \rho_a V_{wind}^2 c; \tag{2.6}$$

$$F_T = F_L \cos\phi_0 + F_D \sin\phi_0; \tag{2.7}$$

$$M_{aero} = (F_L \cos\phi_0 - F_D \sin\phi_0) \cdot r. \tag{2.8}$$

Another question regarding wind loading relies on the installation of wind turbines in wind farms. The installation of wind farms can increase wind turbine performance, as downstream turbines can extract energy from vortical flows from upstream turbines. This means that a clear advantage exists in having several wind turbines as opposed to only one. However, if turbines are too close to one another, a turbine will be located within the wake of another one, degrading its performance. A proper analysis is required to avoid this problem. Computational techniques are frequently used to study these effects [3].

Ice accretion and sliding is also a factor that influences the aerodynamic performance of the wind turbine. This phenomenon affects negatively the power generation capacity and increases the loading on the structure. The degradation in power generation is linked to ice accumulation at the edge of a blade. To fully include this effect on aeroelastic simulations, further complex computational models are required. Ice breaking can also induce vibrations with frequencies close to the natural frequencies of the structure. This is an issue only relevant for cold regions, where ice formation can occur [3, 15].

An offshore wind turbine can be designed based on three different configurations, regarding the necessity of avoiding the resonance frequency ranges. Fig. 2.7 presents these three configurations in a frequency domain. These are [1]:

- soft-soft structure
- soft-stiff structure
- stiff-stiff structure

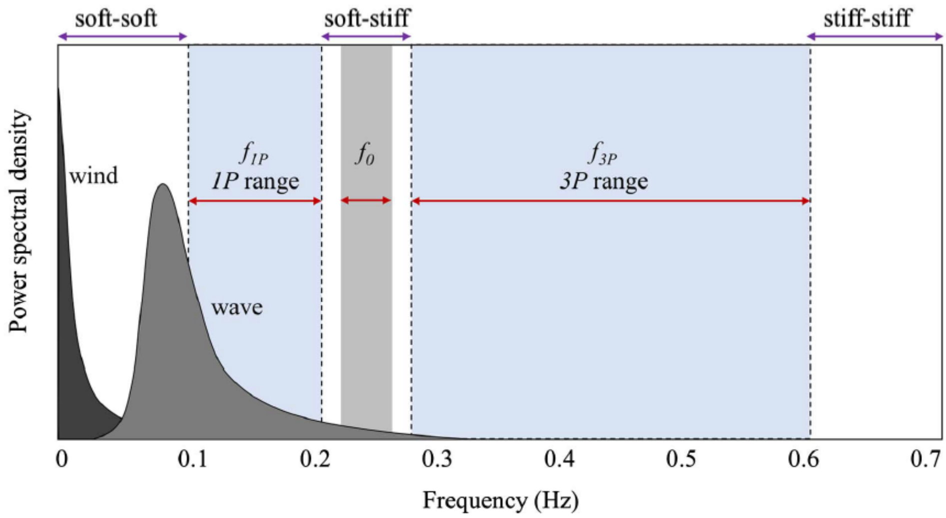

Fig. 2.7. Ranges of excitation, generally speaking, for an OWT in frequency domain [46].

These configurations are defined considering a set of frequency ranges that characterise the wind turbine in terms of rotational frequency. The rotational frequency, commonly known as 1P, defines a lower bound of the operation frequency of the turbine. The blade passing frequency depends on how many blades the wind turbine has. Considering a 3-bladed wind turbine, this frequency is known as 3P and is nothing more than 3 times the 1P frequency. This frequency defines the upper bound of the operation frequency of the turbine. As the wind and wave frequencies, the 1P and 3P frequencies are the main excitation frequencies [30].

The soft-soft structure is a structure that has its fundamental frequency below the 1P frequency range. As the forcing frequencies originated from wind and wave loading are also below this range, this configuration is not used for OWTs.

The soft-stiff structure is a structure that has its fundamental frequency comprehended between the 1P frequency range and the 3P frequency range. This interval is rather small and high precision when designing the structure is required to avoid resonance. In some particular cases, resonance does occur. However, this is the configuration that is regularly employed in the design of wind turbines.

The stiff-stiff structure is a structure that has its fundamental frequency above the 3P frequency range. Although theoretically ideal, it's a difficult configuration to achieve, as both the foundation and the structure itself would have to behave as a stiff body. The amount of material needed to have a stiff structure leads to an exaggerated expensive structure. Besides, as the offshore wind industry tendency is to increase in size, with larger blades and towers, as well as greater masses, the rotation frequency and fundamental frequency of the structure are expected to decrease [15].

The DNV GL-ST-0126 [47] states that, for soft-stiff designs, an absolute relative difference between excitation and natural frequencies above 5% should be verified. Older references stated a relative difference above 10%. These differences are important to avoid the fundamental frequency from entering a resonance frequency range. Controller solutions can be employed to mitigate vibrations if this case cannot be avoided [1, 30, 48].

To correctly design a wind turbine, high accuracy natural frequency predictions are needed. The predicted fundamental natural frequency of the structure leads the design process, influencing the foundation type and overall dimensions selected. However, the natural frequencies do not depend exclusively on the support structure geometry, depending also (and importantly) on the surrounding soil characteristics. The soil-structure interaction drives the obtained foundation stiffness which is important for the determination of the natural frequencies of the wind turbine. More on this subject will be broached in Chapter 3.

2.2.2 Foundation design

As an overall guide, the support structure design goal is to guarantee a stable foundation, where cost minimization is important. This corresponds to mass minimization while assuring that a large number of design constraints are respected, from design criteria to manufacturing and installation. Currently, the design criteria lead to significant conservatism, which means that a given portion of the support structure is not required. It is important to note that this conservatism does not result only from a safety point of view but also from uncertainties in how the soil will behave in long term [42].

It is important to note that offshore foundations must be able to support taller and thus heavier structures, as well as bigger forces and overturning moments than the onshore foundations. This makes the foundation design for OWTs a greater challenge than for their onshore counterparts. A precise prediction of both the bearing capacity of the soil and the foundation stiffness is required for a correct and cost-efficient design, as well as to guarantee that the OWT remains operational and stable during its service life. A relation between the embedded depth of the foundation and its stiffness and bearing capacity exists, as shorter piles will fail earlier than longer piles embedded in the same soil. Monopiles must be designed as to minimise their thickness, but sufficiently large to ensure no yielding takes place [4, 6, 48, 49].

To guarantee that the foundation will support the upper structure and remain stable for the operation of the wind turbine, a set of limit states should be verified. These different limit states verify if the wind turbine will not fail due to soil failure, structure failure, or serviceability failure (conditions that do not allow the wind turbine operation). The geotechnical design comprises three main limit states [24, 40, 46]:

- Ultimate Limit State (ULS) design - it consists of assessing the foundation capacity; typically, extreme load events with preceding cyclic load histories are admitted. This limit state guarantees that the foundation does not collapse due to axial and lateral loads in an extreme case. The ULS can be seen as a lateral displacement at the pile head that corresponds to 10% of the pile diameter.

- Fatigue Limit State (FLS) design - it consists of assessing the foundation stiffness and damping for operational and extreme load events. These modal properties are then used in structural eigenmode analysis.

- Serviceability Limit State (SLS) - it consists of assessing the peak and accumulated deformations and rotations of the OWTs foundation, considering extreme and cyclic loads. This limit state mainly restricts the accumulated permanent rotation, where 0.5º is the maximum allowable head rotation at the seabed under extreme conditions. If 0.25º is assumed as coming from installation tolerances, then the actual and usual allowable limit for head rotation is 0.25º.

Myers et al. [42] in their work stated that by concluding if a given design is strength or stiffness control-oriented, i.e., what is the property that is restricting the design, different considerations can be taken that further help in saving material and mass in the support structure. For example, if stiffness controls the design, the structure is expected to have more reserve capacity than the design imposed capacity, which translates to more material being used than the one needed to satisfy strength design considerations. As such, using the ULS design criterion (strength control design) and the SLS design criterion (stiffness control design) results in different minimum embedment depth of the foundation [50].

Tight tolerances are used in the SLS design criterion. Being the one that usually is more restricting design criterion, it usually governs the design, as it requires a bigger embedment depth. Still, the design should consider all the limit states. Due to its small head rotation, as in some cases, it might be difficult (or actually impossible) to respect it, a relaxed rotation requirement can be considered. However, this relaxation is not always possible due to operation restrictions. It is important to remind that an insufficient design compromises the safety and serviceability of the wind turbine, while a too conservative design leads to higher costs that could be minimised [17, 30, 50].

According to Brinkgreve et al. [50], beyond a given embedded pile length, the rotation becomes independent from this dimension. This is undesirable, as increasing the pile length will not help in reducing the rotation and a portion of the support structure is not being solicited in a relevant way. The authors of that work also explicitly state the importance of the soil stiffness of the upper layers/part of the soil where the pile is embedded. A bigger pile diameter can lead to the necessity of a smaller embedment length. At the same time, a bigger diameter will lead to a stiffer pile that can have more residual stresses, a heavier system, reduced installation drivability and possible worse fatigue conditions.

According to Byrne et al. [6], adding ballast to the foundation after placement increases the foundation performance. While this is interesting, the costs are significant. At the same time, pile bending moments along the pile's length decay more rapidly for flexible piles than for stiff piles [51].

Correct soil characterization is needed to perform a correct foundation design, from strength to deformation and consolidation parameters. The key parameters that are important to consider for the soil will be broached in Chapter 3, where the relative focus will be given to the Soil-Structure Interaction. Different soil modelling approaches will also influence the stiffness and bearing capacity outcome. This subject will also be broached in Chapter 3.

The amount of uncertainties surrounding the foundation and sub-structure design is the main difficulty in performing a correct design process that includes all significant factors. These uncertainties make it impossible to have very precise simulation results with simplified models, as it is unknown which factors have more weight in stabilizing the structure and that may change with time. A rigorous procedure may be employed using FEM analysis, but it also requires higher computational times and foundation properties from tests that are also expensive. Negro et al. [5] stated a series of uncertainties related to foundation design, such as loads combination, scour phenomenon, scour protection, different scale/dimensions, and soil liquefaction. Kementzetzidis et al. [10] presented a series of uncertainties from a geotechnical point of view, where cyclic and dynamic factors were presented. Lateral soil stiffness variation throughout the service life and in storms, as well as dynamic damping from SSI, were presented as the main geotechnical uncertainties.

One major uncertainty in the design of offshore structures, especially wind turbines, is the evolution of the structure throughout its lifespan and how long-term performance will be affected after the foundation is subjected to millions of cycles. As the soil is subjected to cyclic loads from the structure, significant changes in the soil properties can occur. As a result, the foundation stiffness can be altered and, consequently, the natural frequencies can also change. The overall expected evolution of the soil with cyclic loading should be taken into account to design a wind turbine that remains with a fundamental natural frequency outside the excitation frequency ranges. This situation can also be seen as a fatigue problem, where the application of cyclic and dynamic loads leads to smaller bearing capacities and stiffness alterations/degradation. Further attention should also be taken regarding the dynamic amplification of the system response when operating close to the fundamental natural frequency, as higher foundation displacement, and thus higher foundation strain, occur. This can be regarded as a resonance kind of problem [1, 5, 14, 52].

This raises the importance of proper design guidelines regarding the foundation modelling and overall design to ensure a precise and correct simulation of the foundation. Currently, only recommendations on performing a FEM study are in-place on standards [53].

When installing an open-ended pile, a phenomenon known as soil plug can occur. This consists of a portion of soil blocking the end of the pile and not allowing more soil to enter the pile. An incorrect assumption regarding this subject may lead to wrong predictions of pile capacity since the load carrying capacity of plugged and unplugged piles are different. It can also incorrectly misjudge the drivability of the pile, where a plugged pile will require more energy to drive it through the soil, increasing costs and the risk of damaging the pile [54, 55].

This phenomenon is influenced by the permeability and relative density of the soil, as well as by the lateral stress acting on the pile. The vertical stress does not influence directly the soil plugging occurrence. The length of the soil plug depends on the internal skin friction - if the vertical bearing capacity at the pile tip is greater than the internal skin friction, the soil will keep entering the pile. The type of installation of the pile also is preponderant. Note that, according to Fan et al. [22], jacked piles are not used in practice for OWTs installation. As such, the most common practice is impact driving (where soil plugging is of high importance) and drilling (where soil plugging is not relevant for installation) [54, 55].

Any alteration in the fundamental natural frequency, be it an increasing or decreasing frequency, should be taken into account, as these variations lead to the approximation of the fundamental natural frequency to the forcing frequencies range. This approximation is thus associated with resonance problems of the structure. The fatigue damage accumulation is avoided by not coalescing the fundamental frequency of the structure with the operation excitation frequencies. This can be performed by ensuring that the system has sufficient stiffness, mainly soil-related stiffness [14, 15, 56].

Overall, the foundation design should be performed attending to the soil evolution. If due to cyclic loads, the soil gets softer (degrades) with time, then the fundamental frequency of the structure should be closer to the upper bound. However, if the soil hardens with time, then the opposite should be performed. Nevertheless, the soil properties determination inherent uncertainties lead to a foundation design that allows the structure's fundamental frequency to sit, more or less, in the middle of the desired range. This is the most common design practice. Further studies and model developments have to be performed to assure that designing a structure that can have excitation frequencies close to its fundamental frequency is viable since the soil will evolve with time for a more favourable situation. For situations where resonance cannot be avoided, controller solutions have been developed to mitigate its effects [1].

From the necessity of precise natural frequency quantification, an accurate prediction of the foundation stiffness should be performed. This stiffness greatly influences the natural frequencies obtained in the design. The foundation stiffness also plays a big factor in the accumulation of rotation under cyclic loading, affecting the results from the tests regarding the serviceability limit state of permanent rotation [22].

Scour can have a very big negative influence on the structure response. DNV design codes and recommendations [43, 47, 57, 58] present a recommended equilibrium scour depth of 1.3 times the pile diameter to be considered for the ULS and SLS design cases, where the phenomenon is dominated by currents. It is important to acknowledge, however, that in the marine environment, currents, tides and waves, all influence the scour seen. According to Prendergast et al. [17], current-induced scour is when considerable scour depths occur, with wave-induced scour being rather small. Matutano et al. [32] presented a series of different equations for the scour depth prediction, underlining the number of different approaches one can take to broach this subject. Other uncertainties in magnitude and variability of the parameters that govern the scour phenomenon lead to a challenging prediction/estimation of the scour depth that a given foundation will face.

OWTs that are expected to suffer from scour need to be monitored across their service life. The monitoring procedure is based on a long-term plan, where a too conservative approach might lead to unnecessary monitoring activity, which is an additional cost. Even with scour protection, monitoring is important. Scour protection is, however, very costly, which is why not all OWTs that can be subjected to scour have this protection. The deployment of this protection also requires a calm sea state. Overall, the feasibility of a scour protection depends on the site conditions [18, 59]. More on scour will be seen in Chapter 3.

Another factor that should be taken into account, besides the alteration of soil properties, is the interaction of the offshore wind turbine with the water body around it. Apart from the hydrodynamic loading that the structure is subjected to due to waves and currents, the water around the sub-structure will accelerate with the movement of this element. This accelerating body of water can be seen as an added mass. Hydrodynamic damping will also be associated with it. Through the offshore wind turbine lifespan, there is hard marine growth. This marine growth will lead to an increase in the mass of the structure. As a consequence, the overall structure will become softer and with higher damping [2].

Other factors such as noise pollution, disturbance of natural habitats, aquatic animals' migration routes, sensitivity alteration of nearby seismic stations, bird collisions, and damage from impacts are also important when designing an OWT. An effort to minimise the influence of installing a wind turbine in a nature zone should be made, as this will also reduce the problems that the animals that live in/pass through the installation zone of the wind turbines, thus reducing maintenance necessity [3].

2.2.3 Modal properties effects

As in any other dynamic system, operating close to the natural frequencies leads to structural resonance. Resonance conducts the system to large amplitude stresses and high fatigue damage. As such, these regions are avoided in the OWT design [28].

Special attention should be given to forcing frequencies, as the wave loading associated frequencies are variable and can comprehend a wide frequency spectrum. According to Søren [59], the wave frequency of extreme waves is typically between the range of 0.07 and 0.14 Hz, while the wind loading frequency is usually less than 0.1 Hz [17].

First fore-aft and side-side tower modes of wind turbines are the predominant modes of the structure. These, in a soft-stiff design, will be comprehended between 0.1 and 0.5 Hz. These modes will be very close together to each other. The little difference between these two modes results from anisotropy of the moment of inertia of blades and nacelle, as well as significantly different damping characteristics. The fore-aft movement will be highly damped as aerodynamic damping from the rotating blades is significant, while the side-side movement will have negligible aerodynamic damping. As stated before, special attention should be provided to an assessment of foundation stiffness over the typical OWT design life of 20+ years, as in the soft-stiff design, the fundamental frequency (given by the minor frequency of the fore-aft and side-side motions) may vary throughout that timeline [12, 30].

The aeroelastic models regularly used in the wind industry can combine the influencing effect of aerodynamic, elastic, and inertial loads during a load case simulation. With this, they can compute the dynamic aeroelastic response of the structure subjected to a given loading input, as well as its natural modes of vibration. With this, they can compute the dynamic response of the structure subjected to a given loading input and its natural modes of vibration. With these, further calculation of the extreme and fatigue loads can take place, as well as analysis on aeroelastic stability [44].

The wind turbine stability will be assessed through its natural modes. A Cambpell diagram can be drawn to facilitate the visualization of the evolution of the different natural frequency modes with rotor angular speed. It is important to note that each component will have its natural modes and that a structure's natural mode will be composed of a combination of these, i.e., there will not be a pure structural mode of vibration. A given

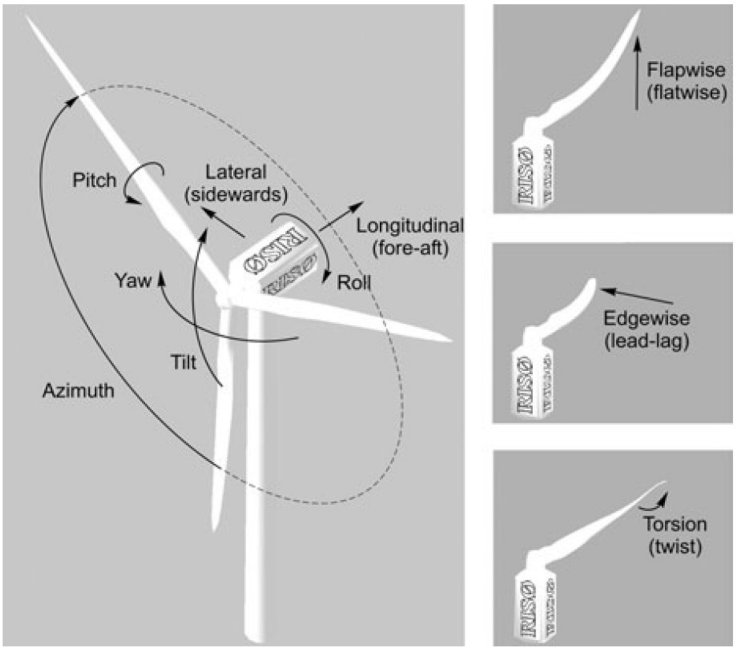

Fig. 2.8. Nomenclature associated to the blade degrees of freedom [45].

mode will have tower and blade natural modes contributions, with the exception of the fixed-free drivetrain torsion. Fig. 2.8 presents the associated nomenclature to the blades' degrees of freedom, while Fig. 2.9 presents the observed blade natural modes and respective Campbell diagram for a 600kW onshore wind turbine. Hansen [45] studied the aeroelastic instabilities that can occur on a wind turbine's blade, where stall and vortex-induced vibrations are the main sources of instability problems.

Being fatigue damage an important design factor for OWTs, both stiffness and damping of the system weigh a lot on the life estimation of a given structure. According to Malekjafarian et al. [23], changes in these properties significantly affect the fatigue damage, with the predicted fatigue life linearly increasing with the damping ratio. The structure will be more sensitive to the damping ratio considered than the resultant moment at mudline from a fatigue damage point of view, as the relationship between stress and fatigue life is non-linear. Shutdowns also have a big effect on the fatigue life, since no significant aerodynamic damping happens to increase the damping ratio of the system. As reported by Aasen et al. [4], for idling periods, the response is dominated by the foundation stiffness and damping, while in operation periods the aerodynamic damping presents itself as the main factor on the damping front.

The damping present in an OWT is composed of a set of different sources of damping. Aerodynamic and soil damping are the main sources of damping, with the first being more significant when the turbine is under operation and the second when the turbine is on idle. The different damping sources will be further presented in Chapter 4.

Aerodynamic damping is very relevant under operating conditions of the wind turbine, as it has a direct impact on the aeroelasticity phenomena that occurs. Considerable damping is achieved when the rotor rotates, modifying the loads applied to the wind turbine. This damping will be proportional to the wind speed that passes through the blades

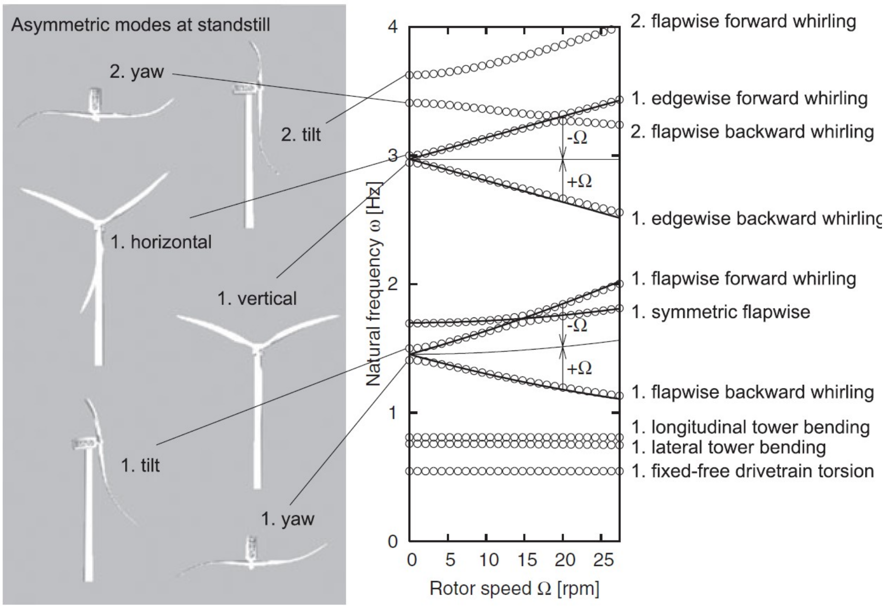

Fig. 2.9. Campbell diagram and respective structure natural modes for a 600 kW onshore wind turbine [45].

[28].

Foundation damping is the most relevant damping source when the OWT is stopped/idle condition, as the aerodynamic damping is very small if not zero. According to Carswell et al. [53], foundation damping incorporation can reduce up to 10% the cyclic loads that the OWT is subjected to. Other damping sources do not have the same weight as foundation damping, although structural damping is still relevant. Some OWTs also have incorporated dampers which greatly contribute to the total damping of the system when on [12, 53].

As documented by Chen et al. [39], the quantification of influence for each individual damping source is very difficult to obtain. As a consequence, the modal damping ratios needed throughout the design phase are difficult to predict, while having a big influence on the dynamic behaviour of the OWT. Dynamic tests after construction may be required to check the validity of assumptions made [60].

Nóren-Cosgriff et al. [12] performed a study regarding the modal properties of an OWT. In their conclusions, they saw that an increased load would result in a small increase in damping, while the fundamental frequency would decrease. Damgaard et al. [31] saw that cross-wind vibration led to increasing fatigue loads, as no significant aerodynamic damping takes place. These authors say that, when the acceleration level increased, the modal damping and natural frequencies decreased. These phenomena were assumed to be related to distinct non-linear soil behaviours.

2.3. Final Remarks

An OWT is composed of the RNA, the tower, the substructure and the respective foundation. The RNA will include an aerodynamic rotor, a transmission system, a generator, and a control system. The monopile foundation is the most common support structure within the offshore wind industry. This foundation type can be seen as the easiest foundation to manufacture and deploy, being possible to install for a considerable water depth range. Its design procedure is also simpler, although it is not the most stable foundation.

A set of several DLCs have to be run in order to certificate a given OWT. However, several uncertainties still exist regarding the soil. These uncertainties are the main reason for investigation and development in this area.

The lateral soil capacity is one of the main limiting factors in the design of OWT monopile foundations, as there is a lack of redundancy in the design due to the nature of loading acting on OWTs. The cyclic loading can cause a failure for smaller amplitudes and before than what was expected when considering monotonic loading.

Minimization of the dynamic amplification is possible by avoiding the areas of resonance (steering clear of coalescence between natural frequencies and forcing frequencies). This avoidance is performed by modifying the stiffness of the structural system (foundation + sub-structure + structure). Besides this step, damping is also required to minimise even further any dynamic amplification. Damping is an important factor to behold, as it is essential for OWTs to avoid excessive fatigue damage accumulation throughout the wind turbine lifespan. If this minimization is not fulfilled, the structure will enter resonance and excessive deformation or even structure collapse can occur. Attention to how the soil stiffness varies with time should also be taken into consideration, as the fundamental frequency will be altered with the stiffness and resonance may occur.

Other phenomena can also alter the stiffness and damping of the structure. Scour was seen as the most common example of these phenomena, where the removal of a portion of the upper soil translates to a stiffness reduction and natural frequency variation. It is important to note that the soil stiffness in the upper part of the soil substantially influences the pile head rotation and the system's fundamental natural frequency obtained.

Overall, further work is necessary to guarantee a safe and viable design process for OWT. Accurate stiffness prediction and damping estimations are needed for proper quantification of the system's modal properties and expected maximum load amplitudes. This is the focus of current investigations regarding not only the design of wind turbine and foundation, but also how the SSI should be modelled (as it will be seen in Chapter 3).

Chapter 3

Soil-Structure Interaction

The vast majority of the predicted natural frequencies of OWT lie below the actual fundamental frequency of the structure. This reported difference that resides inside a 10% bandwidth for the best cases is the result of unconsiderations regarding the influence of different aspects of the soil on the structure. A conservative approach is then used in these cases, leading to a support structure that is unnecessarily large. The incorporation of these interaction effects allows for a more accurate design process, as long as there is a high degree of confidence regarding the influence implementation [7, 46].

The definition of soil parameters is very important for foundation design. As the interaction between the structure and a given soil varies with soil stratum properties, its quantification and estimation affect the modal properties predicted for the structure. Soil parameters that characterise the strength, deformation and consolidation of the soil are necessary to account for the soil's influence on the structure. The evolution of the soil properties with time can also play a vital role in the foundation design for a given structure [52].

The soil-structure interaction (SSI) is important to consider as the relative stiffness between the structure and the foundation may influence the energy and force transferring from one to the other. As the ground can be deformed, a rigid approach, disregarding the flexibility of the foundation, is not a good approach and errors are expected to exist. The structure's response is thus affected when considering this interaction, as the natural frequencies of the structure, the damping ratio, and the soil motion are modified. Consequently, it is relevant to understand that different influences will be seen as different modelling approaches are considered since these can comprise different soil properties and soil-structure relations. Throughout literature and simulation codes, the modelling of the foundation is still processed with poor considerations regarding the SSI [30, 61, 62].

A high degree of uncertainty surrounds the determination of soil properties. Being characterised by a random nature, the calibration of the parameters that define the soil properties is difficult to perform. Yet, a typical underestimation of eigenfrequencies on analyses performed in OWT problems occurs that surpasses the stochastic soil properties, with expected underestimated soil stiffness. As the unconsideration of a SSI leads to higher frequencies than those measured, the introduction of such interaction is necessary. Aspects such as scour, backfilling, and cyclic motion soil modifications can be responsible for a constant alteration on the eigenfrequencies of the structure [15].

The consideration of a soil-structure system conducts to a longer natural period than the one that would be obtained through a completely fixed-base structure. Considering this interaction thus means there will be a softening considered at the structure's foundation. Likewise, an increase in the damping of the foundation-structure system will also occur. As stated by Malekjafarian et al. [23], to obtain a truly optimised design, the SSI should be accurately modelled [7, 61].

Wind turbine models should then consider not only the structure itself but also its substructure and foundation to correctly assess the system response and modal properties. The wind turbine is usually modelled as a lumped mass system, while model variations exist when considering the foundation due to trying to include SSI effects. As Badoni et al. [63] state, the prediction of the response of a structural or mechanical system does not have a unique solution.

Independently from the model used, be it a simplified or a more rigorous model, it is of substantial importance that a precise estimation of the fundamental natural frequency of the structure is performed. Finite element models could be used to approximate in a rigorous way the foundation behaviour as different constitutive soil laws exist that allow a great accuracy on soil response, but the elevated computational cost rules them out of regular use on this subject [30, 53].

According to Sturm et al. [24], further optimization of OWT design would need the implementation of another interface between the structural and the geotechnical designer. However, this new interface would lead to more iterations to be run by both designers, conducting to a longer design period. Reduction of the design period is only possible with a complete understanding of the nature of loads and structural design methodology, where a wide range of loads and/or stiffness quantities are covered.

The stiffness of the system must be well known at small strain to determine the fundamental natural frequency of the structure. Although the loading in offshore wind turbines is of cyclic nature, it is fundamental to first understand the behaviour of the structure due to monotonic loading to expand the knowledge to cyclic loading [64].

Models that consider cyclic loading must include considerations on the hysteresis, and ratcheting behaviour of the soil, as well as the stiffness and possible damping changes that may occur, to correctly obtain the structure's response [64–66].

The main overall concerns when modelling OWT considering the SSI come from inconsistencies between design predictions and measured performances and uncertainties related to soil modelling and soil input parameters/influences. Although the differences seen are not very large, tight operational intervals and dynamic amplification avoidance, as well as an ongoing desire for optimal and cost-efficient methods, promote the investigation of better solutions in this regard [49].

3.1. Soil basics

Soils can be categorised into different types. The most common separation consists on cohesionless and cohesive soils. Sands and gravels are an example of cohesionless soils, while clays are an example of cohesive soils. This division is normally performed through the soil's particle size and shape. As according to Kulhawy [67], clay can be considered soft if it has a maximum undrained shear strength of 50 kPa, while stiff clay will have a minimum undrained shear strength of 100 kPa. However, a proper note should be given to the fact that there is not a consensus on the limits to define a soft or a stiff clay. Meanwhile, sand is characterised by its relative density [33].

The mechanical properties of cohesionless soils are dominated by grain-to-grain contact and friction. As such, the shear strength of sands is derived from the slipping contact friction force at the contact surface between two adjacent particles. Meanwhile, for cohesive soils, chemical and electrical interactions are more important. The shear strength of cohesive soils still plays a major part in the soil resistance, even if a null effective stress is applied [33].

A given soil will be considered saturated when its voids are filled with water. Significant differences can be expected when comparing dry and saturated soil. Although the majority of geotechnical problems have soils partially saturated (voids contain both air and water), it is common to analyse the problem considering one of the extremities: fully dry or fully saturated. Complex constitutive laws and numerical analyses may be needed for the consideration of saturated soils, depending on the problem at hand [33].

The soil can have a drained or undrained nature. This means that different drainage conditions may exist. The drained and undrained conditions are defined from a relation between the consolidation time and the loading time. An undrained condition will be assumed if no significant variation on the soil's water content occurs during loading. The excess water content will, however, be dissipated, as a consolidation process happens. Likewise, an undrained situation can be considered when the consolidation time is significantly larger than the loading time. The soil permeability is interlinked with the soil's drainage capacities. Once again, soil can be partially drained. Nevertheless, for problem considerations, an extremity condition is usually admitted. The drainage condition of the soil is directly linked to its permeability, where a drained condition can be assumed if the soil is very permeable. As according to Jia [33], both undrained or partially drained conditions can be assumed for fine-grained soils beneath offshore shallow foundations. A drainage analysis will be necessary for soils that have high permeability, as a drained condition occurs. Different models, considering either total stress or effective stress, exist to account for the drainage conditions [33].

The effective stress of saturated soils can be determined by performing the difference between the total applied stress on the soil and the water pressure at that same point. Eq. 3.1 presents this relation. The total applied stress can be determined by summing all the applied forces and diving them by the total area of solid and void. It can then be defined as being the total weight per unit of area of the soil and water enclosed in the considered continuum [33]:

$$\sigma_v' = \sigma_v - \sigma_u. \tag{3.1}$$

Likewise, if a soil mass is submerged, or sits below the groundwater table, the water that will reside inside the soil will apply a force on the soil particles around it. This force will be of a buoyant nature, with the water pushing the particles upwards. The magnitude of the force will be equal to the water weight that has been displaced by the particles. Consequently, the net/effective soil weight will be reduced by this buoyant force, as can be seen in Eq. 3.2 [33]:

$$\gamma' = \gamma_{sat} - \gamma_w. \tag{3.2}$$

A mean stress can also be calculated. This will be the sum of the stresses in the main directions, which correspond to the vertical stress ($\sigma_1 = \sigma_v$) and the horizontal stress

($\sigma_2 = \sigma_3 = \sigma_h$), divided by three, as seen in Eq. 3.3 [33, 56, 68]:

$$\sigma_m = \frac{\sigma_1 + \sigma_2 + \sigma_3}{3} = \frac{\sigma_v + 2\sigma_h}{3}. \tag{3.3}$$

The horizontal effective stress can be determined by using the definition of lateral earth pressure coefficient. This coefficient relates the vertical and horizontal effective stresses for a given depth. Specific expressions for this coefficient exist for sands using the knowledge of the internal friction angle. Eq. 3.4 presents this relation in a general way [33, 69]:

$$K_o = \frac{\sigma_h'}{\sigma_v'}. \tag{3.4}$$

Clay is prone to bond with the surrounding water, as it has a net negative charge, while water has a net positive charge. Another property of this soil material is its large specific surface, meaning that clayey soils can absorb a significant amount of water, increasing its volume. The water content on clays will then influence its behaviour by defining four distinct consistency states liquid state, plastic state, semisolid state, and solid state. Clay in its liquid state will not have any strength. In a plastic state, the clay will behave as an elastic material but being easily deformed. A semisolid state will be reached as the clay dries out and cracks start to appear. Crack propagation is a sign that this soil material is losing its plasticity. In solid state, clays exhibit a very brittle behaviour. Fig. 3.1 presents the relation of these states with the Atterberg limits that delimit the clay state, them being the shrinkage limit (SL), the plastic limit (PL), and the liquid limit (LL). These states are quantified by the water content present on the soil, where a plasticity index and a liquid index can be defined as seen in Eqs. 3.5 and 3.6, respectively [33]:

$$I_p = (w_{LL} - w_{PL}) \cdot 100\%; \tag{3.5}$$

$$I_l = \frac{w - w_{PL}}{w_{LL} - w_{PL}} \cdot 100\%. \tag{3.6}$$

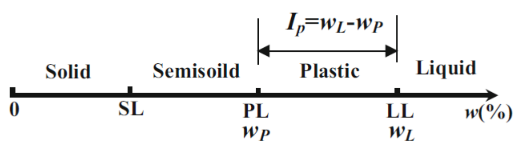

Fig. 3.1. Clay state definition and Atterberg limits with increasing water content [33].

Consolidation consists of a decrease in the volume of voids with an increase in effective stress. Consolidation tends to be more significant for clays than for sands. This phenomenon influences the settlement structure and its influence can be slow-showing. An over-consolidation ratio (OCR) can be defined as the ratio between the maximum value of effective stress in the past and the maximum value in the present. The soil can be considered normally consolidated if the OCR is equal to one. This may mean that the soil has not been subjected to loads greater than the present one. The soil will be called over-consolidated if the OCR is bigger than one. Different geological mechanical factors can be the origin soil over-consolidation. In general, over-consolidation is not relevant for granular soils, like sand. It can, however, highly influence soils as clay. [33].

The principal soil properties are strain-dependent. Inherent properties as the shear modulus and the damping of the soil change with the existing soil strain. Darendeli [70] studied the variation of these two properties with strain, observing that the shear modulus decreased with increasing strain amplitude, while the opposite occur for the soil damping ratio. Consequently, the maximum shear modulus is usually known as the small-strain shear modulus G_0, while the minimum soil damping ratio ζ_{min} occurs for small-strains. Also, the soil properties of existing anisotropy influences the overall strength and stiffness of the soil. This, in turn, alters the soil's natural behaviour when faced with a given excitation. Fig. 3.2 presents an example of the shear modulus degradation with shear strain [7].

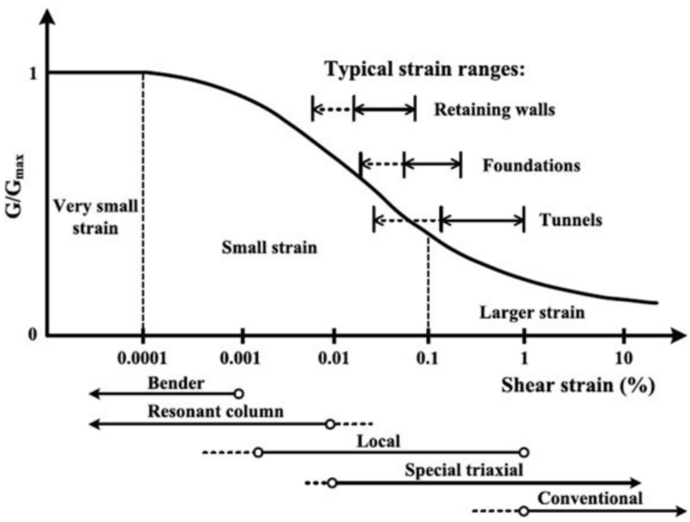

Fig. 3.2. Normalised shear modulus/stiffness degradation with shear strain [71].

The elastic threshold strain γ_{te} is defined as the strain amplitude at which the shear modulus decreases to 98% of its original value (small-strain shear modulus). This threshold defines the point from where the soil behaves elastically but in a non-linear fashion. The cyclic/plastic threshold strain γ_{tc} defines the point from where the deformations become irrecoverable (plastic behaviour) and is determined from the strain amplitude that is associated with a decrease to 80% of the small-strain shear modulus. A reference strain $\gamma_r = \varepsilon_c$ can also be defined by using the strain that corresponds to a shear modulus equal to half of the small-strain shear modulus [70].

The soil Poisson's ratio is a difficult value to obtain and estimate. It depends on the type of the soil, as well as on the soil strain, degree of water saturation and loading frequency. According to Versteijlen et al. [27] common values are 0.3 for sands and 0.45 for cohesive soils. Thota et al. [72] examined different soils in terms of their Poisson's ratio and saw that an increase is expected when the soil is saturated with water.

Besides the lateral strength and stiffness of the soil, the longitudinal/vertical resistance of the soil is also important. This component of soil resistance can be linked to part of the lateral resistance, but more important is what restricts the installation of a given foundation in a certain location. According to Yan et al. [55], the bearing capacity at the tip of a pile will be provided by the soil unit weight, soil cohesion, and soil surcharge. The soil surcharge is induced by the soil that sits above the pile tip and around the pile.

It is important to comprehend that the overall soil stiffness is also highly dependent on the pressure that acts upon it. The soil can behave in a non-linear way during loading, as plastic deformations occur, changing the stiffness of the foundation. Similarly, the damping ratio is affected by the confining pressure, loading frequency and soil plasticity [4, 70, 73, 74].

If the soil is remoulded, a softening process called thixotropy will occur. This phenomenon is then followed by a return to the original state. This return is time-dependent, as the constant water content and porosity affect it. The strength gained after remoulding (due to thixotropy) will be very important for clays [52].

3.2. Soil properties determination

Soil properties estimation is a challenge for geotechnical engineers. Significant differences between field and laboratory measurements occur, as soil condition variability and sample representation are important factors to this. Measurement discrepancies can also be justified by the soil alteration on soil disturbing methods, as removing a sample will hinder the soil's properties. Sampling modifies the existing structure and cementation of the soil, something that occurs throughout millions of years. The associated reliability of the soil properties estimation will be linked to the reliability of the testing performed [69, 70].

The static undrained shear strength, for clays, is an important property that can characterise a given foundation capacity, while the internal friction angle is important to characterise a given sand resistance. For both, knowing the soils Young's modulus can be important. Consequently, certain acquisition reliability is assured. A wide variety of laboratory, field/in-situ test methods exist for the determination of this and other soil properties. Direct shear and triaxial compressional tests are common laboratory test methods, which can be performed on undisturbed or reconstituted soil samples. Vane shear, standard penetration (SPT), and cone penetration (CPT) tests are common field test methods. Seismic wave velocity measurement is an in-situ test method usually performed in tandem with SPT or CPT [52, 63].

The direct shear test is a soil strength test that measures the friction at the interface between two bodies. The shear force is measured using a load cell attached to an actuator that subjects the soil specimen to a lateral load (inducing shear). With the recorded applied load and induced displacement, it is possible to determine a stress-strain curve for different confining pressures [33].

The triaxial shear test is a suitable test for all types of soil, where it is possible to control the drainage condition. This test is very used when a measurement of the water pore pressure is desired. Consequently, it is important to guarantee that the drainage conditions during the test are identical to the ones seen in the field. Three types of triaxial shear tests can be performed, according to the soil consolidation condition in the first stage and the drainage condition in the second stage. These types are the Consolidated-Drained test, Consolidated-Undrained test, and Unconsolidated-Undrained test. Different standards regulate and describe how a triaxial shear test should be performed [33].

Vane shear test is an in-situ test method that correlates a measured torque at failure with the undrained shear strength of the soil. This test method allows a direct and reliable measurement of cohesive soil strength. The shear strength is determined for a given depth of interest [33].

The SPT is a simple and cheap soil property measuring method when compared with other in-situ dynamic soil properties measuring methods. Despite some limitations and a high number of corrections and correlations necessary to reach a soil property estimation, this test method is widely used in geotechnical engineering. This test method consists of driving a thick-walled sample tube using repeated blows from a high-mass hammer. The soil is considered disturbed during the first phase of the penetration. As such, the results are only measured for the remaining penetration. The sum of the number of blows required to drive the sample tube gives the standard penetration resistance and is presented as "N-value" or as "SPT-N value". This resistance, however, does not have a physical meaning. Correlations are then needed to determine a given soil property. Many empirical formulae and correlations exist to relate soil properties with the SPT-N values, but none of them can guarantee a high level of accuracy or quality. The SPT-N values can depend on the equipment used and on the skill of who operates it. These factors should be corrected before entering a design phase that uses the soil properties given by this method. Further corrections for rod length, hole size and use of a liner are needed if alterations to the standard procedures are done. These corrections are especially important for liquefaction evaluation of the soil [33].

The CPT is a similar test method to the SPT, where, instead of a thick-walled sample tube, a steel cone is used. The CPT allows a more accurate estimation of soil properties. This is the reason why this method is vastly used on the offshore industry, even though this is a less used method when compared to the SPT and it cannot be used for very stiff and dense soil conditions. The CPT method, as seen in Fig. 3.3, is the common method applied for the soil properties identification needed for a base soil modelling. The CPT can present a continuous record of its measured properties, although it cannot recover soil samples, as it is possible with the SPT method, and special equipment is necessary. The resolution of CPT method can be related to the size of the cone tip. The cone is connected to a friction sleeve by load cells. These load cells will measure the cone tip resistance and the sleeve resistance during penetration, with the measured data being recorded in increments of depth. Besides the cone tip resistance and sleeve friction, pore pressure and relative density of the pierced soils can also be directly obtained. It is common though to correct the cone resistance for overburden pressure [33].

SPT and CPT measured values can both be linked to other soil properties through a set of correlation expressions. However, by employing these correlations, a tentative of relating a large-strain measurement with a small-strain characteristic needed for a given analysis occurs, resulting in some degree of error. Attention to this should be provided when wanting soil properties estimations through these test methods [27].

Seismic wave velocity measuring uses the concepts of the propagation of seismic waves to determine the soil properties. However, the utilization of only this method through non-destructive tests, such as surface reflection, surface refraction and spectral analysis of surface waves, can have significant drawbacks. This means that a combination of non-destructive and laboratory or destructive field test methods should be performed

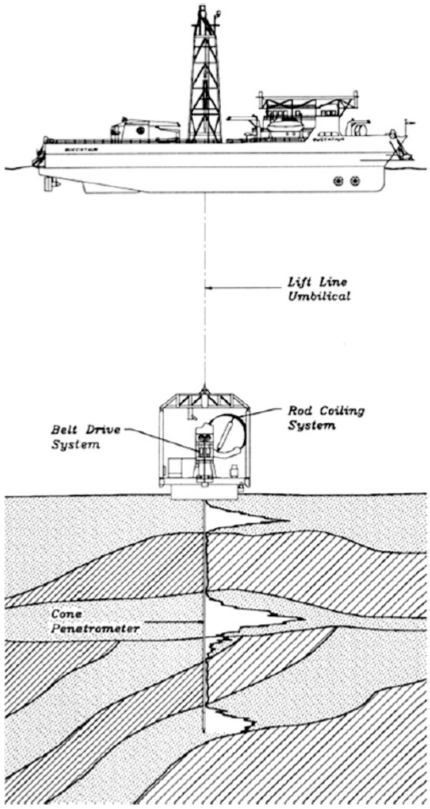

Fig. 3.3. Example of a CPT for offshore applications [33].

to enhance the soil properties estimation. To generate shear waves in the soil, a horizontal impact is necessary. Other types of excitation, such as vertical impacts, a shallow explosion, and operational excitation generate different kinds of seismic waves [33].

Darendeli [70] defends that a small-strain shear modulus in-situ measurement should be performed. For example, by using the shear wave velocity, and knowing the mass density of the soil, it is possible to determine the small-strain shear modulus of the soil, which can be linked to the soil resistance and stiffness. Eq. A.1, in Appendix A, presents this relation. The shear wave velocity can be quantified by in-situ seismic measurements. The shear wave velocity can be assumed constant with depth from depths greater than 80 meters. This situation means that a half-space domain is considered [34, 69, 70].

3.3. Soil influence on OWT performance

The overall stability of any structure is guided by the strength of the local soil. However, especially in offshore structures, more soil properties of the surrounding soil will influence the foundation stiffness and, as a consequence, the structural response of the whole system. The presence of heavy structures can modify the soil properties, influencing the stiffness, damping, and capacity control of the foundation. According to Darendeli [70] a set of factors affect the soil behaviour, namely the strain amplitude, the effective stress, the duration of the confinement state, the number of loading cycles, the strain rate, and the stress history. The considered soil type is also a main factor in the linear and non-linear dynamic soil properties. For example, Abhinav and Saha [26] state that soil stiffness is relatively more important for OWTs found in clayey soils, as underestimations are common [61, 70].

The effects that come from the SSI consideration depend on the foundation typology used. The consideration of SSI effects can also include time-variation of properties, which leads to modal properties variation. Furthermore, these effects should be carefully analysed as their consideration influences the design of the OWT overall structure (mainly the foundation), with resonance avoidance being desired [34].

The soil stratum where a given pile is embedded can be of a complicated nature. Consequently, it can be desired to consider homogeneous soil instead, prioritizing the most common type of soil. However, this can be a highly non-conservative approach. The soil profile with depth influences the degree of the effects of the SSI. Álamo et al. [34] stated that higher variations will occur as the soil becomes softer. Although a higher complexity of the soil characterisation should be noted, according to Gazetas and Dobry [75], the soil reaction at a given depth is essentially independent of what occurs at other depths. This comes from the propagation of waves generated from the soil-structure interface mainly in the horizontal direction, in what can be considered a plane-strain condition.

The usual penetration depth for OWT foundations is less than 50 meters, which means that an assumption of a half-space domain is not correct. In turn, the shear velocity will always vary with depth in these foundations, influencing the actual soil shear modulus, as it is directly linked. This soil property is seen as important to estimate the natural frequencies of the system, as it is normally used for foundation performance evaluation in terms of fatigue and serviceability. The horizontal/lateral response of the structure will then be highly influenced by the non-homogeneity of the soil [51, 52, 62].

According to Darendeli [70], the shear modulus of the soil will increase with the increase of its effective confining pressure, while the soil damping ratio will decrease with the increase of the confining pressure. As a consequence, the shear modulus will be higher for an over-consolidated state, while the soil damping will be lower. This means that the dynamic soil behaviour in terms of small-strains will be less dependent of the vertical effective stress, as a decrease in the void ratio of the soil is responsible for a change in the dynamic response of the soil. When over-consolidation occurs, stiffer soil is then obtained. The effect of confining pressure will be more significant for non-plastic soils, since, for plastic soils (as clays), an increase of soil's plasticity leads to a decrease of the confining pressure influence. Darendeli [70] also saw that over-consolidated soils exhibit some degree of a "memory" regarding their stress history. Meanwhile, Wang et al. [76] observed that, as the sand gets denser, higher strengths and stiffness are achieved. Denser sand will, therefore, have a higher friction angle at one common strain [77].

3.3.1 Soil layers and failure mechanism

The disposition of the soil layers can also affect the overall soil stiffness. Zhang et al. [51] saw that the lateral response of the structure will be highly influenced by the non-homogeneity of the soil and by the pile flexibility. Burd et al. [78] saw that a soft layer in a stiff soil matrix reduces the strength and stiffness of an embedded monopile, with the opposite being true as well. A stiffer layer below the pile tip can also influence the soil resistance acting on the pile. Difficulties in incorporating these influences, especially in simpler models that do not recur to 3D finite elements characterised by constitutive laws, exist. Likewise, according to Álamo [34], the superficial layers of a given soil stratum are the main contributors and influencers of the modal properties found for the structure embedded in such soil stratum. According to Damgaard et al. [13] and to Álamo et al. [34], the Poisson's ratio does not play an important role on soil stiffness determination, as little to no difference was seen for a given soil with distinct ratios.

How the soil fails can be another influencing factor. As different soil failure mechanisms occur, different bearing capacities can be considered. As studied by Zhang and Andersen [7] and by Wang et al. [48], under lateral loading, there is a region where the soil is subjected to a wedge failure and another where a rotational failure mechanism occurs. As can be regarded in Fig. 3.4, the wedge failure mechanism occurs in the upper part of the soil-pile interaction, while the rotational failure occurs around the pile tip. A tension gap can exist due to the pile movement. However, if this gap does not develop, a shallower wedge mechanism depth can occur, as the soil resistance in that region exhibits different behaviour. Wang et al. [48] state that different bearing capacities can be found according to the failure mechanism.

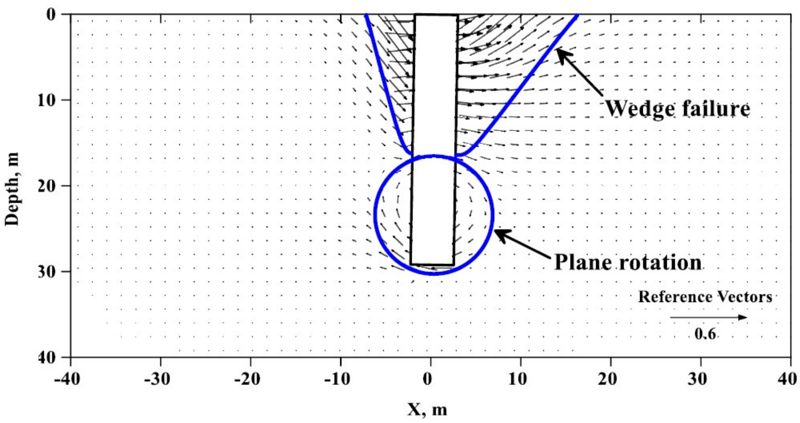

Fig. 3.4. Common soil failure mechanisms around a pile [48].

The division between these two failure mechanisms occurs on the depth where, for rigid piles, a given rotation/pivot point (a point that rotates but does not suffer any lateral displacement in relation to the static situation) exists. The same does not occur for flexible piles, as these essentially do not move near the pile tip and do not have a rotation centre - they can be considered as being clamped at one end. Rigid piles, besides having a pivot point, exhibit significant movement at the pile tip. McAdam et al. [66] saw that the base fixity assumption for a rigid behaving pile (with an aspect ratio of around 5) does not apply [7, 48, 79].

Throughout the literature, relative values of the depth of this rotation centre change. However, a common value lies around a depth that corresponds to 70% of the embedment length. As loading increases, this pivot point lowers into deeper regions, while increasing the eccentricity of the load is reported to move the same point upwards. Sun et al. [80] saw that this depth increased with the pile diameter. Byrne et al. [65] reported an increase in the pivot point for an increase in the lateral pile deflection, which can be seen as a consequence of a given relation between the load applied and the bending moment of the structure. McAdam et al. [66] saw that, although the rotation point moved with changing loads, it tended to a given value. A semi-rigid behaviour can, however, be observed in piles with aspect ratios above five and below ten [7, 48, 65, 66, 76, 80].

As the piles in the offshore wind industry behave in a rigid fashion, a negative deflection at the pile tip will occur. As a consequence, shearing stresses exist around this end, increasing the total lateral resistance. Likewise, as the pile tip also rotates, a moment will also exist due to vertical stresses acting on the pile tip. These effects are not considered in the Standard *p-y* formulation. The PISA design model made an effort to implement these coming from a finite element calibration process [15, 81].

Modifications on the pile diameter/aspect ratio and on the bending stiffness of the structure will change the failure mechanisms. As a consequence, for the same embedment length, a bigger pile diameter will increase the initial stiffness and ultimate bending moment achieved, with the contributions of the base shear and base moment becoming more pronounced. The PISA design model presents a distributed moment to account for a variation around the pile perimeter of vertical shear stresses acting on the pile, as can be seen in Fig. 3.5. As the pile diameter increases, so does this shear resistance increase. Likewise, as the pile engages a larger volume of soil due to a bigger diameter, the stress-strain relationship of the soil in the vicinity of the pile changes [34, 79, 80].

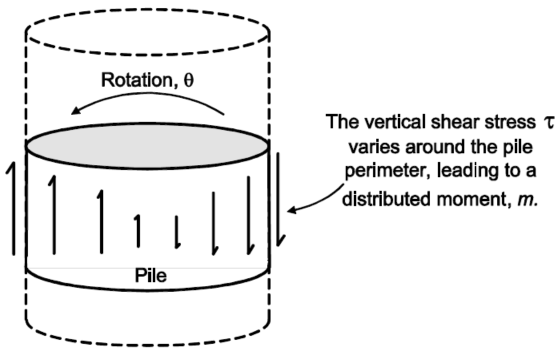

Fig. 3.5. Lateral resistance induced by vertical shear stresses acting on the pile perimeter [82].

Although the corresponding failure mechanisms influence the soil resistance and how it actuates on the structure, Wang et al. [76] admitted that the distribution of the soil pressure can possibly be simplified as a linear distribution by a constant soil resistance coefficient. Those authors saw that, for rigid piles, the pile diameter and aspect ratio did not influence the value of the soil resistance coefficient. Nevertheless, the soil resistance distribution and magnitude along the pile were affected by the soil failure mechanism. The presented approach, however, presents a variety of problems and does not have a direct physical meaning, being an oversimplification of the problem.

In a similar fashion to what was just stated, if a model with high degree of precision is considered, the selection of a complete and accurate soil model is important. As reported by Taborda et al. [83] for a sand model, the movement of the pile leads to an increase of the effective pressure at some regions and a decrease at others. It is then important that the model can capture this occurrence.

3.3.2 Pile installation

An important factor to consider is the soil modification due to the installation of the supporting structure. Different methods exist to install a support structure, where pile driving is the most common installation process for monopile-supported OWTs. After pile installation, the soil surrounding this structure (ultimately the adjacent soil up to 1.5 times the wall thickness of the pile) is expected to be highly remoulded. A partial regain of strength occurs as pore pressure dissipation and thixotropy occurs. The remoulded shear strength can then also be altered as a result of this excess pore pressure dissipation and its distribution. Consequently, the state of the surrounding soil will be highly influenced by the pile installation method selected [7, 9, 52].

It is important to understand that it will be the surrounding soil that has been remoulded that will dictate the interface stiffness on shear, influencing the soil stiffness for lateral solicitations. Likewise, due to pile installation effects, skin friction quantification, a factor that can also help resist an overturning moment applied to the support structure, is subjected to uncertainties. As reported by Fan et al. [9], there is extensive research on the effects of pile installation methods on the axial response of a structure, but no detail was given on the lateral response. Although this influence should be acknowledged, design guidelines do not present a method for its quantification [7, 9].

Fan et al. studied throughout three works (Refs. [9], [22], and [46]) the influence of the pile installation method on numerical simulations (3D finite elements) and small-scale testing on sand, considering three situations: wished-in-place, jacked installation, and pile driving installation. From these, only the last one can be regarded as employable for OWT support structure installation. The wished-in-place situation can be seen as an approximation of the installation by drilling. The impact driving situation, in an overall view, led to the stiffer response, with tests being performed in sand. This installation method allowed densification of the pile surrounding sand, increasing its stiffness. A stiffer axial behaviour for impact driving piles, when compared to jacked piles, had already been seen in the literature. Such is confirmed when assessing that higher vertical stress at the pile tip occurs for impact-driven piles.

Referring to sand, Fan et al. [22] saw that the same void ratio is achieved for pile impact driving, independently of its initial relative density of it. Although given independence from the initial relative density of sand exists in terms of soil properties pile post-installation, a dependence on the ratio between the pile diameter and its thickness can exist, as the soil state is influenced by the effective area ratio of the pile. As stated by Byrne et al. [65] in their work, a possible influence on the soil stiffness regarding the thickness of the pile may exist. The densification that occurs decreases significantly as further away from the pile wall one considers the soil, with densification being more meaningful at shallower depths. When comparing the impact-driven piles with the jacked piles, a noticeable greater area is altered using impact driving, either in the radial or in the vertical directions. The degree of densification that occurs on sands is also bigger for the impact driving case.

If a comparison is performed between the three cases analysed by Fan et al. [46], it is observed that the softest response will be from the wished-in-place situation, while the stiffer response comes from the impact-driven piles. The impact-driven piles, from numerical simulations, exhibit a higher initial stiffness, as well as a bigger soil lateral capacity. It's worth noticing that modelling quantification of the installation process on the soil is a challenging task. As Fan et al. [22] reported, uncertainties still surround this topic. The consideration of a wished-in-place assumption diminishes the computational costs but can lead to an underestimation of the soil's initial stiffness and lateral capacity.

Prendergast and Gavin [17], however, stated that the operational shear modulus of the soil would decrease with pile installation, as large strains are induced on the soil around the pile. At the same time, this effect can be compensated by the increase in confining stress, as over-consolidation develops. Ageing can also increase the initial stiffness of the soil after installation, supporting the data seen by Fan et al. in their work [46].

Consequently, the pile installation method can highly influence the foundation stiffness acquired due to changes in the soil state. Fan et al. [9] state that these changes should be considered in the design phase of the foundation. As reported in their other work, Ref. [46], the response of the structure at low strains will be highly influenced by the effects that result from the installation process. When plastic deformation of the soil occurs, a reduction in the magnitude of influence from the installation process exists. Not considering these effects can then lead to an error when determining the associated modal properties of the system [46].

According to Jia [84], soil plugging can also have an effect on the pile installation resistance and influence on lateral soil resistance. Most open-ended piles, such as common monopiles, are driven into the soil under partially plugged conditions. A partially plugged condition means that, at a given depth, the soil acts as a plug and does not allow more soil to come in. A fully unplugged condition will be a situation where the soil does not restrict the soil from coming inside the pile as it is driven. A fully plugged pile will behave exactly like a closed-ended pile. Even though a partially plugged condition is admitted to be what happens in real life, either fully plugged or fully unplugged conditions are assumed for the design process of a given pile. In the OWT industry, it is common to assume a fully unplugged condition. This can be seen in various literature, but mainly in the work by Fan et al. [46].

3.3.3 Cyclic loading

Cyclic loading is a major aspect of the modal properties variation due to soil characterization alterations. It can be very important to consider cyclic loading for the OWT foundation design, as soil stiffness degradation and permanent deformation take place. Fig. 3.6 presents a perfect example of that. The loads applied to an OWT during a storm are significant, leading to relevant cyclic movement of the structure and, consequently, the soil. Observing Fig. 3.6, the fundamental natural frequency during the storm, due to the extreme movement (even with a stopped turbine) leads to a degradation of the natural frequencies. After the storm, even though there are no more extreme cyclic loads, the effect from before leads to an overall degradation of the natural frequencies. As OWTs operate close to their excitation frequencies, this reduction, over time, can be very harmful to the structure, as resonance can become common [33, 40].

As a consequence, such examples of short-term cyclic loading can induce plastic deformations on the soil that corresponds to a given reduction on the soil shear modulus and overall strength as pore-pressure build-ups. These reductions can lead to failures at

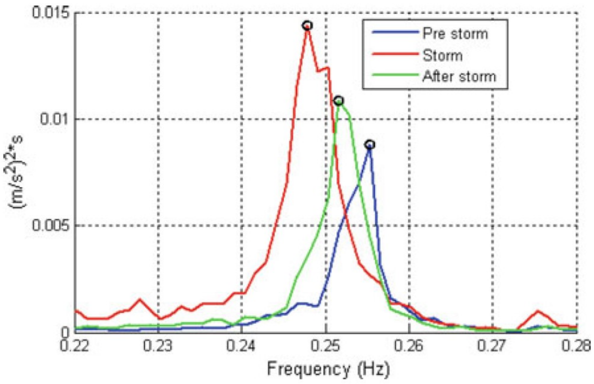

Fig. 3.6. Storm influence on the fundamental natural frequency of an OWT with a GBS foundation [33].

lower load amplitudes than those expected for monotonic loading, impacting the ultimate and serviceability limit states of an OWT. Commonly, natural frequency degradation and accumulated permanent rotation at the mudline level are observed as a result of cyclic loading. It is important to understand that the main reason for failure, as conservative designs are considered, is the serviceability limit state. Usually, 0.5 degrees is assumed as a threshold, where half of it is attributed to construction tolerances. This means that only 0.25 degrees will actually be allowed as a permanent accumulation of rotation. With a varying fundamental natural frequency due to a cyclic loading affecting the soil properties, the structure can get closer to the resonance frequency range, rising load amplitudes and increasing the permanent rotation [85].

There are two types of cyclic loading: short-term (such as storms) and long-term. The short-term cyclic loading, as already broached with the example of a storm occurrence, does not allow the dissipation of pore pressures, decreasing the effective stress and reducing the soil stiffness and strength. Sturm and Andresen [24] also stated this possibility when a storm happens. This is mainly important for clays, as it is more difficult for these to dissipate the water pore pressure. Meanwhile, long-term cyclic loading allows the dissipation of water pore pressure and drained conditions can be assumed. As it will be seen after, in offshore conditions, the soil is usually considered as acting in undrained conditions, but the drainage condition depends on different factors, with significant differences between cohesive and cohesionless soils [15, 74, 85].

According to Carswell et al. [85], soft clays are more susceptible to properties degradation due to cyclic loading, while stiff clays are essentially insensitive. However, according to Gupta and Basu [40], there is not a lot of available information on soil stiffness degradation by long-term cyclic loading in the literature. The existing literature curves in terms of strength and stiffness degradation only relate the expected degradation with shear strain, as was seen in Fig. 3.2. Still, according to Carswell et al. [85], impacts on the soil properties will be more relevant for larger cyclic loads.

As reported in Darendeli's work [70], a relation between the loading stress-strain path of a monotonic loading (backbone curve) and that of cyclic loading can be conceived. Allotey and El Naggar [86] saw that cyclic loading affects soil and pile yielding, gaping, and soil cave-in, where a consequent influence on the soil stiffness and strength occurs.

This, depending on the soil type and depth considered, leads to the formation of hysteresis loops that can take different shapes. Guo et al. [14] stated that the changes in the hysteretic response of the foundation exist with strain amplitude. This can be regarded as the response is of a non-linear nature. Seeing the example of sand on a small-scale model test, Guo et al. [14] observed a consolidation of the soil surrounding the pile, as the sand was cyclically sheared, increasing the stiffness of the soil. It can be said that long-term cyclic loading can increase the soil stiffness for low to medium dense sands, while it can significantly reduce the stiffness when considering clays. The hysteretic response, according to Aasen et al. [4], was confirmed through full-scale measurements of OWTs, where the fundamental frequencies decreased with the increase of loading amplitudes (wind speeds).

For cyclic considerations and overall changing situations through time, like gap formation, a dynamic SSI may be necessary. However, the modelling of such type of SSI requires the specification of interrelated parameters. Difficulties are then encountered to reach the inelastic and non-linear response of the soil with increasing strain. According to Jiang et al. [56], the dynamic SSI can be divided into a kinematic interaction and in an inertial interaction. The kinematic interaction is affected by the soil movement, while the inertial interaction is affected by the mass of the foundation/superstructure [17, 86].

Besides the influence of different cyclic loads in terms of magnitude and phase that leads to different strains, the strain rate will also alter the behaviour of the soil by modifying the soil's properties, mainly its strength and stiffness. This effect depends on the soil type and inherent plasticity. Strain and load rates will also influence the drainage condition of the soil [70, 74, 87].

As seen in the tests carried out for the PISA project and documented in McAdam et al. work [66], the loading rate is more significant in piles with small diameters. The loading rate was seen as an influencing factor of the strength and stiffness of a given soil, with sand presenting a higher capacity of strength for high loading rates. However, clay exhibits a bigger influence dependency on this topic. In those same tests, as well as the ones reported by Byrne et al. [65], a creep-like phenomenon was observed. This can also be an influencing factor on the soil properties modification, as also supported by Zhang et al. [7].

The variation of the structure's fundamental natural frequency with varying loading intensity can indicate the existing non-linear behaviour of the soil. Nóren-Cosgriff and Kaynia [12] saw that a given decrease of the fundamental natural frequency occurred as loading increased. At the same time, damping increased with increasing loading. The then hysteretic nature of the soil is responsible for different stiffness characterisation in accordance with if a loading or unloading process happens [4, 6].

3.3.4 Pore pressure

Soils in offshore sites are expected to be saturated. Consequently, the saturated nature of the soils leads to the development of pore pressure as a result of cyclic strains that occur due to cyclic loading in offshore wind turbines. Pore pressure is defined as the difference between the actual pore pressure and the hydrostatic pressure for still water level. The pore pressure can influence the stiffness of the foundation by changing the effective stress (defined as being the difference between the total stress and the pore pressure) applied to the soil. One should note that pore pressure can also develop in unsaturated soils under cyclic shearing. Pore pressure is regularly associated with soil non-linearities [1, 10, 61, 66].

Pore pressure can have a significant effect on the soil mechanical properties, namely its stiffness and strength. A high-pressure load in offshore structures will be taken by the water pore pressure, reducing the effective stress and the soil's shear resistance and stiffness. The reduction in soil stiffness and strength due to the buildup of soils' water pore pressures should be considered in a nonlinear soil model [88].

According to Damgaard et al. [15], the cyclic motion of the monopile can generate a pore pressure for the saturated soil. The soil stiffness can increase, as the bulk modulus of water is higher than the bulk modulus of the soil matrix material. Damgaard et al. [15] studied the influence of permeability on the soil and saw that an increase of the natural frequencies was possible considering this effect. The increase of permeability promoted a decrease in the natural frequencies. If the structure is loaded slowly, however, no excess pore pressure develops. Especially for the design of OWT foundations in sand, it is important to understand the drainage conditions in existence, as the soil strength and stiffness depend on them [15, 54, 74].

There are significant differences between clays and sands in terms of drainage. While clays typically behave in an undrained manner, sand drainage conditions highly depend on loading rate, drainage length and soil permeability, leading to either drained, partially drained or partially undrained behaviours. It is important to note that sands do not behave in an undrained manner. According to Li et al. [74], a normalised time factor (or, likewise, loading period) can be considered to quantify when a drained or an undrained condition occurs. A factor below 50 means that the pore response is important and an undrained situation can occur. This can be a way to, in a preliminary form, predict the type of drainage condition that the structure will encounter. Eq. 3.7 presents this normalised time factor, where the consolidation factor c_v is defined in Appendix A:

$$T_p = \frac{t_p c_v}{d^2}. \tag{3.7}$$

Due to the distinct drainage conditions expected when considering cohesive versus cohesionless soils, attention should be provided to what kind of model is implemented. While cohesive soils, such as clays, can consider both total and effective stress model considerations due to a common undrained behaviour, cohesionless soils, such as sands, can only be modelled using an effective stress model. This line of thought should continue for layered soils containing both types of soil [81].

As a curiosity, onshore structures embedded in sand are usually considered to be founded on drained soil, as the loading rate is usually slow when compared to the time necessary to drain the excess pore pressure generated from any excitation. It is important to note that soil that behaves in an undrained manner will have a stiffer response, with strain softening at large strains not being considered relevant. This is also true for sand, as dense sands tend to dilate under shear deformation. This dilation enhances the soil properties in an undrained situation since a negative pore pressure is created [74].

Returning to the study performed by Damgaard et al. [15] on the influence of soil permeability, it was observed that for high and low values of permeability, which correlate to fully undrained and drained conditions respectively, the loading rate (frequency) does not alter the soil stiffness. However, for a transient state between these two drainage conditions, the loading rate impacts significantly the soil stiffness obtained. It was found that, in this region, an increase in the loading rate would increase the soil stiffness as well. According to Kementzetzidis et al. [10], the sand permeability will mainly affect the local foundation response, but not in a significant manner the overall dynamics of the OWT structure. At the same time, significant differences can occur in regards to the global damping of the system, primarily under weak vibrations, for partially drained conditions. This corroborates the findings of Damgaard et al. [15], stating that analyses that focus only on the fully drained or undrained conditions can dismiss important factors of the system behaviour.

3.3.5 Liquefaction and scour

As the soils in offshore sites are mainly saturated, liquefaction may occur. Liquefaction consists of the transformation of a substance into a liquid state. This may happen when a given soil is subjected to a fast cyclic loading, being one soil failure important to cover in any structure. An important loss in shear strength occurs in liquefaction, conducting to a global or local failure of the foundation. Liquefaction is a relevant phenomenon for shallow foundations, losing some importance for deep foundations (as pile foundations). This loss in importance comes from the usual penetration of the deep foundations in all soil layers that are susceptible to liquefaction. Liquefaction is only relevant for saturated granular soils (like marine sand) with low compactness level. [87, 88].

Liquefaction is a phenomenon that can be suddenly increased in seismic areas, with a drastic loss of foundation capacity. The initiation of soil liquefaction, according to Jiang and Lin [19], can be determined considering an excess water pore pressure ratio. This ratio relates the excess water pore pressure developed in a free-field soil with the initial soil mean effective stress. According to these, a ratio close to one for the superficial soil layers means that liquefaction is very probable to occur.

Non-linearities can be introduced to the foundation through liquefaction. The changes that come within in terms of soil stiffness, frequency and wavelength of free-field excitation can affect the SSI and, consequently, the overall dynamic response of the structure. As reported by Jiang and Lin [19], this softening effect that comes from an increase in excessive water pore pressure can be incorporated into soil springs.

Scour can also have an effect on the degradation of the foundation stiffness, decreasing the natural frequencies of the whole structure. As this phenomenon alters the modal properties of the OWT, considerable thought should be given to it while designing the foundation of an OWT in a given location. As scour will occur at shallow water depths, inside the usual water depths for fixed-bottom OWTs, the decision on a scour protection to protect the structure from this erosion will also modify the natural frequencies of the system. This phenomenon occurs as sediment transport capacity changes due to currents and waves, as the installation of a structure modifies the water flow of that given region. Significant hole depths surrounding the structure can be found in extensive cases of scouring. Scour is a time-varying phenomenon, where currents and waves influence its development. Either way, a scour depth equilibrium will be reached for a given constant sea condition. The scour depth equilibrium can then be a value that is lower than those used in the design, as foundation design usually considers a maximum scour depth to have a conservative approach to the problem [2, 30, 32, 59, 89, 90].

Scour consists of the removal of soil, be it locally or globally, around a given structure supported by piles or piers. Scour will occur when the near superficial shear stress exceeds the critical shear stress at which sediments are transported. While local scour is the soil removal only on the surrounding area of the embedded structure, global or general scour is related to a general lowering of the ground over a big area. Local scour is mainly due to local water flow changes, with the contraction of flow at the side edges of the pile, formation of a horseshoe vortex at the base in front of the pile, the formation of lee-wake vortices behind the pile, the generation of turbulence, the occurrence of wave breaking, the occurrence of wave reflection, and the occurrence of wave diffraction all being responsible for an increase of the sediment transport capacity and forming scour holes as sediments are removed. This soil removal hinders the ultimate capacity and stiffness of the foundation, which can lead to resonant periods, as the fundamental natural frequency can get closer to the excitation frequencies, as well as compromising the structure's stability. The structure's overall dynamic response will then change due to a gain in flexibility of the structure, as the embedment length gets smaller [30, 56, 59, 66, 89, 90].

The scour status is usually seen by the relation of S/d, where S is the scour depth considering an initial embedment length and d is the pile or pier diameter. To fully characterise a given scour situation, usually, the maximum scour depth and its extension around the structure are quantified. According to Prendergast et al. [89], who saw scour influence on sandy soil, for values up to 0.5 (initial state), no significant influence was regarded. However, for bigger values, as the phenomenon develops, a reduction in the natural frequencies of the system was seen, with the looser sands being more affected than denser ones. The relative density of sands is then important to evaluate the modification of soil properties under scouring conditions. Due to their characteristics, sands are more susceptible to severe scour, while clays do not tend to have significant scour depths developed [69, 90].

According to Briaud et al. [91], the maximum scour depth that can be expected on clayey soils will be very similar to the one verified for sands. However, the scour development for clays is considerable slow when compared with sands. The location of the local scour for these two types of soil will also be different. Scour on clays tends to develop on the sides and behind the pile, while scour on sands develops all around the pile. Yet, these investigators state that the understanding of why the maximum scour depth for these two types of soil is equal is still missing. The influence of scouring on sands and on clays can then be different. Mostafa [90] enumerated a few of these influences for both of these soil types. Scour can:

- For sands...

    1. Reduce the soil ultimate bearing capacity;
    2. Increase the pile head displacement;
    3. Increase the bending moment, with larger piles being necessary to make sure that the pile yield stress is not exceeded.

- For clays...

  1. Lead to a more pronounced effect is observed on stiff clays;
  2. Lead to a more pronounced effect is observed when higher loading amplitudes are applied;
  3. Increase the bending moment.

Scour and liquefaction can occur at the same time. As reported by Jiang and Lin [19], these two phenomena influence the existing SSI. If liquefaction occurs with scouring, the developed scour hole is considered unstable. This transforms local scour into general scour. Likewise, scour is a difficult phenomenon to monitor. Jiang and Lin [19] saw that scour influences more the rotation response of the structure than other dynamic responses. As such, they stated that a good indicator of the scour status can be a correlation with the rotation response of the structure.

As scour varies with time, and since the equilibrium scour depth can change with the alteration of sea conditions (wave and current characteristics change), a time-evolution of scour should be employed for a high accuracy prediction. The common approach to foundation design is to consider the maximum scour depth, which corresponds to a conservative method. Jiang et al. [56] state that the opposite can also be true, i.e., considering an overestimation of the scour depth in the foundation design can lead to a non-conservative design. This statement results from a given underestimation of the maximum lateral acceleration, displacement, and bending moment of the structure. Then, this approach can be considered as incorrect, as equilibrium scour depths do not get close to the maximum scour depth, since backfilling occurs. Backfilling consists of the sediment deposition on the scour holes created. This material tends to have similar properties to the one that has been removed, being possibly consolidated with time due to the compacting effect that waves can have. Scouring and backfilling are two phenomena that occur in parallel. Although some degree of lag between them can exist, with scour developing quicker than backfilling, this is the reason the maximum scour depths predicted are not reached. Consequently, the fundamental natural frequency of an OWT will change throughout the evolution of these processes, until a given equilibrium state is achieved [59, 89].

Simplifying the scour conditions from a local perspective to a general one can lead to the underestimation of the fundamental frequency of the structure. Jiang et al. [56] found that, although a frequency underestimation occurred, an overestimation of the maximum lateral acceleration and bending moment of the structure took place. The same authors found that, when considering local scour dimensions, the main affecting parameter on the natural frequencies was the scour depth, followed by the other characteristic dimensions: scour-hole slope angle and bottom width. Damping considerations, even when considering simplified conditions, are more difficult to analyse [31].

When scour occurs, although some soil is removed as scour holes develop, the adjacent soil is compacted. This was found by Prendergast et al. [89], by Soren and Ibsen [59], by Lin et al. [69], and by Jiang et al. [19, 56]. Consequently, the over-consolidation ratio is expected to vary with depth for a scoured situation, as it is influenced by the severity of the scour. These modifications to the stiffness during scouring are also the result of changes in the relative density and void ratio that come from the consolidation of the adjacent layers subjected to scour. This means that, although a given depth of soil is removed, the superficial layers will now have increased bearing capacities. However, this impact on the adjacent soil layers' properties is limited to a given depth.

The main alteration in the soil properties comes from the increased over-consolidation ratio on adjacent soil layers. This change in the soil properties comes from the unloading process over the remaining soil. The increase in the over-consolidation ratio will then increase the shear modulus and decrease the soil damping. The modification of the over-consolidation ratio means that, besides the modification of the seabed geometry around the structure, also a modification of the soil stress history occurs. As presented by Lin et al. [69], although a significant reduction in the lateral resistance of the structure occurs with scouring, the stress history consideration for the remaining soil leads to an increase in the soil stiffness. This means that certain damping of the negative impact of scour occurs. For the case of sands, the stress history due to scour was found to slightly increase the friction angle, besides increasing the over-consolidation ratio. According to Jiang et al. [56], only the global scour can be seen as affecting the soil properties, with the local scour effects being negligible.

However, if scour protection is added, a stiff superficial layer is added to the foundation soil. This, in turn, raises the fundamental natural frequency of the structure, as the foundation becomes stiffer. Scour protection is used to prevent structural integrity problems due to scour during the lifespan of the OWT. According to Matutatno et al. [32], sizing of the scour protection is a subject that still needs further research, as how scour is predicted influences this protection design [32, 89]. Scour will occur quickly for sands, slowly for clays and will be almost negligible for rocks. Scour protection can be composed of either dumped stone riprap, stone or concrete pitching, soil-cement bagging or grouted fabric mattress, with a horizontal collar/deflector on top. If a scour protection is selected as consisting of rocks and stones, it is important to define the average stone size. This will help characterize the scour protection and define the minimum armour layer thickness. The scour protection has two layers: the armour layer and the filter layer. The armour layer should be at least twice the average stone size. A scour protection consisting of rocks is common. [32, 91, 92].

3.3.6 Gap formation

Besides what was previously presented in terms of cyclic loading, the act of repeatedly moving the structure in different directions can lead to the creation of a gap. These gaps develop mainly on top cohesive soil layers, where a reduction on the properties given the cyclic loading effect makes the gap development easier. Gap formation will also influence the structure's behaviour and overall impedance, as it leads to a lack of contact between the soil and the monopile over a possible significant surface area. As a result, a different response will be obtained, with a reduction in the system's stiffness being expected. This phenomenon then influences the overall dynamics of the structure [25, 65, 66].

Following Pranjoto and Pender work [93], gaping can reduce about half of the lateral stiffness of the pile when compared to no gap development. It has also been reported to be a cause of the degradation of the soil stiffness since as the gap widens, it deepens. This gap will increase further as the magnitude of loading and cycle number increase. A real example of this was observed throughout the tests performed for the PISA project, with both McAdam et al. [66] and Byrne et al. [65] confirming gap formation and consequent influence on the results obtained. According to Carswell et al. [85], gaping occurs as the passive zone behind the pile/structure is loaded beyond the linear range, with the pile being allowed to move freely when reloading occurs until new contact with soil happens. Gap formation can also affect the water pore pressure distribution, as water fills the gap, further affecting the surrounding soil stiffness [94].

Similar to the scour effect, gap formation can have different mechanisms according to the soil type, as different resistances and consolidations exist. Boulanger [95] developed a model where he accounted for gap formation resistance. This resistance took place as a drag and a closure components, where an increased difficulty was introduced to account for the separation between the soil and the structure. This model accounted for the resistance of the soil layers (elastic and plastic components) against the structure movement, the separation between the soil and the structure (gap formation), and the resistance when the structure enters an area where a gap existed (drag component).

The model presented by Boulanger [95] was introduced as being viable for sand and clay. However, gap formation for cohesionless soils (as sands) is difficult to predict, since they are susceptible to cave in and close the gap formed. Still, according to Damgaard et al. [31], some centrifuge tests performed with a pile embedded in sand demonstrate that the soil does not completely cave in. Meanwhile, for clays, an unwanted effect of gap formation is the formation of a permanent residual gap, resulting in an unsupported pile region for small lateral loads. This region can continue to increase as time goes on and the number of cycles increases. However, as a resistance to this separation exists, an additional initial stiffness can be expected. As according to Gupta and Basu [40], gap formation can be disregarded if accurate non-linear elastic soil models are considered, although some differences can be observed. This, however, requires necessarily an elaborate method such as finite elements.

3.3.7 Stiffness and damping overview

Since the soil stiffness is linked to the shear modulus of the soil, as the shear modulus reduces with increasing strain, so will the soil stiffness. Likewise, one can say that the stiffness (or even the soil subgrade reaction modulus) decreases with the pile horizontal displacement. A strain dependence can then be observed. When the Young modulus of the soil reduces, higher damping can be seen. At the same time, a higher fatigue damage equivalent damage occurs, since the fundamental frequency of the structure gets closer to the frequency range that corresponds to wave loading [7, 13, 80, 96].

Prendergast et al. [89] affirm that a direct link between the soil vertical effective stress and the soil strength and stiffness exists. As an excess water pore pressure develops during, e.g., cyclic loading, a reduction in the effective stress occurs. This then means that a reduction in the soil stiffness also happens, dropping the natural frequencies of the structure. Meanwhile, Damgaard et al. [15] demonstrated that a correct consideration of pore pressure generation can improve the predicted natural frequencies of the structure, reducing the error to the measured natural frequencies of OWTs.

Although according to Zdravkovic et al. [73] the soil over-consolidation has no significant impact on the stiffness of the soil, recent research on high over-consolidated aged marine stiff clays concluded that a relevant anisotropy of the soil elastic stiffness exists, with the horizontal Young's moduli exceeding the vertical values that can be measured with any kind of test. Over-consolidation is reported to have a significant effect on the dynamic soil properties when plasticity is involved, as the loading history is accounted through it. Nevertheless, Prendergast et al. [89] saw that stiffness underestimation of heavily over-consolidated soils can occur by using recommended values present in current design codes [70].

In general, a higher soil stiffness can be obtained if less soil plastification occurs. According to Achmus et al. [41], the initial stiffness of a given soil is not affected by its shear strength. Guo et al. [14] reported significant differences in soil stiffness evolution in terms of the soil type. For example, it is common a stiffness degradation to develop as the number of loading cycles increases. However, for sand, it was seen that stiffness increased, instead of decreasing. Reasons for this can rely on a consolidation of the soil, leading to denser sand which, in turn, increases the soil stiffness. The same authors also saw that increasing the loading rate would decrease the stiffness, as strain accumulation of the surrounding soil decreases. Sand stiffness can then be increased with a high strain cyclic loading, contradicting the general idea of stiffness degradation with plasticity.

Soil non-linearities can easily be regarded on the measured natural frequencies, as a variation of the natural frequencies with loading can indicate it. These non-linearities are usually linked to low frequencies, while for high frequencies, non-linearities lose pronouncement and radiation damping increases. A bigger non-linearity will irretrievably be associated with higher dissipated energy, increasing the material damping ratio as the strain amplitude also increases. It is important to note that radiation damping is different from material damping, as will be discussed in Chapter 4. As seen by Allotey and El Naggar [97], the evolution of the hysteretic damping depends on the soil's overall behaviour. A reduction in radiation damping will occur for soil that degrades with time, while an increase will occur for hardening soil. The small-strain material damping will increase with the plasticity index of the soil. The material damping is evaluated using the soil's non-linearity. Its ratio can be calculated by performing the ratio of two areas: the area within a hysteresis loop and an area of maximum potential energy stored in each cycle of motion. In alternative, the Masing behaviour can be considered to evaluate the hysteresis loops that form for a given modulus reduction curve with strain and then obtain the respective material damping [12, 63, 70].

Overall, damping decreases with the increase of the confining stress. In cohesive soils, the obtained damping is associated with existing void ratios. Nevertheless, the contribution of soil damping depends on the relative stiffness found between the structure and the soil, denoting the importance of SSI considerations. Just like for the soil stiffness, the confining pressure affects the soil damping ratio that one encounters at a given foundation. At the same time, a loading increase can increase the overall foundation damping [12, 23, 98, 99].

3.4. Applicable SSI Models

To achieve a high accuracy model, the soil should be modelled by resorting to a soil constitutive law. Nevertheless, to implement this law, a finite element approach is required. A finite element approach consists of a computational costly method, which is highly undesired in the wind industry as design processes are wanted to be performed and validated in a relatively short time (when compared with the overall timeline of the project). This means that a relatively simple approach but sufficiently accurate, such as the Winkler approach, is desired. The cost per accuracy that this method allows together with its simplicity vastly surpasses the costs needed to achieve a very high precision prediction offered by methods such as the finite element approach. Different ways are possible to try and achieve this goal. Jia [96] defends that the action of the lateral soil resistance along the leading face of the pile and the shearing along the toe of the shaft and around the shaft perimeter should be included in order to achieve a correct model.

Two main types of models can be employed to consider the SSI: continuum approaches and subgrade reaction approach. Continuum approaches can be based on FEM analyses, as the soil is treated considering a certain constitutive law. A continuum analysis is then contemplated for the pile embedded in the soil problem. This problem can be solved analytically if the soil is comprehended as a linear material. If not, the solution is only obtained through numerical solving. There are different subgrade reaction approaches, with the main idea being the relation between a local lateral resistance and a local lateral displacement using individual springs to model this relation. Different procedures can then be used to consider this relation [4].

From a computational point of view, as Sturm et al. [24] reports, the design of OWT foundations resorts to simplified and analytical-based methods, instead of FEM-based ones. According to Malekjafarian et al. [23], there are different foundation models that can be employed considering this:

- assuming a rigid foundation (clamped at mudline);
- macro-element/super-element;
- apparent fixity length (equivalent beam and clamped at the bottom);
- pile with discretely distributed springs (Winkler foundation).

Conventional (simplified) design models can, however, be unreliable and non-optimal, leading to substantial errors. In some cases, linear theories are not adequate to predict the displacements in a precise way, with the necessity of introducing non-linearities. As Gazetas [100] states in its work, the computational method selected for obtaining the dynamic behaviour of the structure should reflect the key characteristics of the foundation and surrounding soil [24, 101].

There are different approaches that can be regarded when analysing a Soil-Structure Interaction. The offshore wind turbine problem can be analysed by considering only one plane of action to all three main planes of action. A common approach considers one plane of action, as it is more computationally efficient.

The standard *p-y* method from API and DNV considers only one plane of action. However, this standard was developed for slender piles, with *L/d* ratios relatively high. As such, the application of this standard leads to a considerable error in the calculus of natural frequencies of the structure, as can be seen in the work of Damgaard et al. [15].

As presented by Jia in *Soil Dynamics and Foundation Modelling: Offshore and Earthquake Engineering* [102], different levels of modelling can be admitted. Five distinct levels of modelling can be regarded:

Level 1 The stiffness in each degree of freedom is calculated assuming that the monopile is fixed at a given depth. It can also be performed by applying a small change on the displacement and moment at the pile head, followed by a numerical calculation of the pile stiffness. This approach considers a linear spring stiffness. Consequently, it cannot be applied to situations when the pile is subjected to considerable dynamic forces.

Level 2 A substructure technique is employed. This means that the pile is cut at its top and replaced by a set of non-linear springs and dashpots. Three phases are then needed: *reduction phase*, where pre-calculated load vectors and correspondent stiffness matrix are applied to the pile heads; *solution phase*, where the determination of the response of the pile takes place to then apply on the considered super-structure at the interface between these two elements; *re-tracking phase*, where the forces obtained at the top of the pile should be equal and opposite sign to the ones calculated for the super-structure. The displacement applied from the pile will then allow the re-tracking of the response and loading on the super-structure. This level of modelling combines a (non-)linear analysis of a superstructure with a non-linear analysis of a pile foundation subjected to the calculated forces from the super-structure problem. The substructure approach allows an exact solution for a linear system and can approximate non-linear effects by using an iterative process with equivalent linearization.

Level 3 Each pile is modelled as a beam finite element. The SSI is considered by modelling non-linear springs. This level of modelling can also include the modelling of super-structures. Nevertheless, the most common modelling approach associated with this level is a beam on a non-linear Winkler foundation. A direct approach to the problem can then be assumed. The soil is represented by a set of springs and/or dashpots. The consideration of this soil modelling reduces the computational efforts required for modelling and consequent analysis. This level of modelling also allows the consideration of non-continuous contact, such as slippage and gap formation, between the pile structure and the surrounding soil. Although this is a convenient and versatile approach for pile foundations, the subgrade reaction modulus is usually only governed by the pile displacement at the considered depth, as shear transfer between two adjacent layers is disregarded. Besides the inherent difficulty of determining the soil representing spring stiffness, problems when considering seismic motions also exist.

Level 4 The modelling takes place by considering that the pile is embedded on a homogeneous elastic continuum. Each pile is represented as an infinitely thin linear elastic strip embedded in an elastic medium. The pile-soil interface can be modelled by one of the two methods: considering contact elements, where friction and adhesion parameters are considered, or considering interface elements with normal and tangential stiffness parameters.

Level 5 Similar to the previous level of modelling, a vast complexity is considered in this approach. The modelling consists on a finite element method, which can account for 3D interaction. The soil is considered as finite elements with a complex constitutive law, and the pile is admitted as a beam or solid finite element. Both linear and non-linear, elastic or plastic situations can be considered in this level of modelling. An analysis considering a fully coupled soil-pile-super-structure system is possible without reverting to the independent calculus of soil or super-structure responses.

3.4.1 Rigid foundation approach

The rigid foundation approach does not consider SSI effects. This is the simpler and easier way to represent an OWT problem, as the model will be represented as shown in Fig. 3.7. According to DNV [58], the consideration of the fixed support at the mudline level of the offshore wind turbine can lead to an error up to 20% in natural frequencies obtained. This was also observed in the work of Damgaard et al. [15]. This consideration essentially neglects the SSI phenomena, leading to an overestimation of the fundamental frequency. Still, it is valid as a first estimation, but not valid to use in further modal analyses that may be needed in the design of the OWT. The first estimation can be used at a preliminary stage of the design to decide on wind turbine specifications and foundation type [30, 34].

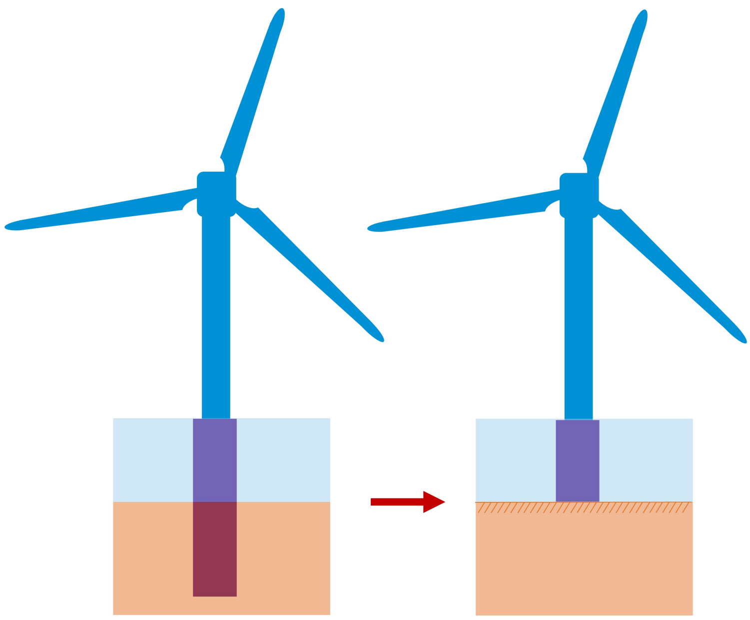

Fig. 3.7. Rigid foundation consideration on OWTs.

By considering the SSI influence, foundation flexibility is introduced, reducing the system's fundamental frequency. This will also change the damping ratio, as soil damping is considered. A flexible foundation allows the existence of tower resonance peaks at lower frequencies than when considering a clamped situation at mudline [11, 34].

3.4.2 Apparent fixity approach

The apparent fixity length model uses the introduction of an equivalent beam to increase the OWT height to the level of clamping. The flexibility introduction due to this beam is correlated with the flexibility gained when considering the foundation. Fig. 3.8 presents this transformation. The beam length and properties depend on the soil properties. The objective is to have a structure that produces the same overall dynamic response as the actual structure. However, according to Koukoura et al. [103], results from this method present large variations for different soil conditions. Therefore, inaccuracies of the natural frequencies increase [11, 16].

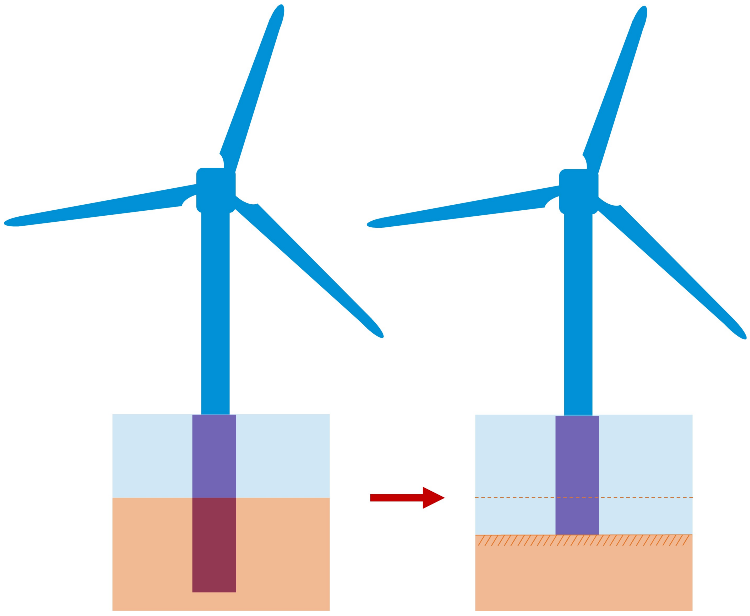

Fig. 3.8. Transformation of the OWT to a SSI-considering model by the apparent fixity approach.

This problem approach is usually linked to simplifications of the structure geometry, which introduces errors even before the method is applied. It is commonly seen in SDOF models this kind of approach to account for the SSI influence on the natural frequencies as it decreases the fundamental frequency with the increase of the system's flexibility. Difficulties regarding the implementation of this method to dynamic problem situations also exist. Consequently, although it can be the simpler method for SSI accountability, the inherent error and existing limitations lead to its relative unpopularity when accuracy is desired.

3.4.3 Super-element approach

Macro or super-elements can represent the soil response in a linear or non-linear fashion. Usually, a linear approach is used. These are often used for shallow foundation representations. This model approach consists of substituting the foundation by a matrix of mass, stiffness and damping that represents the influence of such support at the mudline [62].

These models require a lower computational effort than the most common approach (Winkler foundation), being also easier to calibrate (especially in layered soils) due to their reduced complexity. It is important to understand that, although an easier calibration is possible using this approach if a foundation parameter is changed, a new calibration from scratch has to be performed.

The stiffness and damping of the foundation can be seen as an impedance. The impedance functions that result from here are frequency-dependent and complex-valued, where the real part will represent the stiffness and the imaginary part the damping [34].

If a static problem is considered, the damping component will not appear, with the impedance functions being composed only by the real part. A simple mechanical model of the wind turbine can be considered, as in Fig. 3.9, replacing the whole foundation with a set of 4 springs. These springs restrict the lateral, vertical, and rocking movement of the structure in a simplified one-plane problem. The formulation to reach these spring moduli are obtained from continuum-based numerical analyses or analytical studies and then described by algebraic equations. Ko [30] stated that these can easily be determined through the use of the second Castigliano's theorem [1, 40].

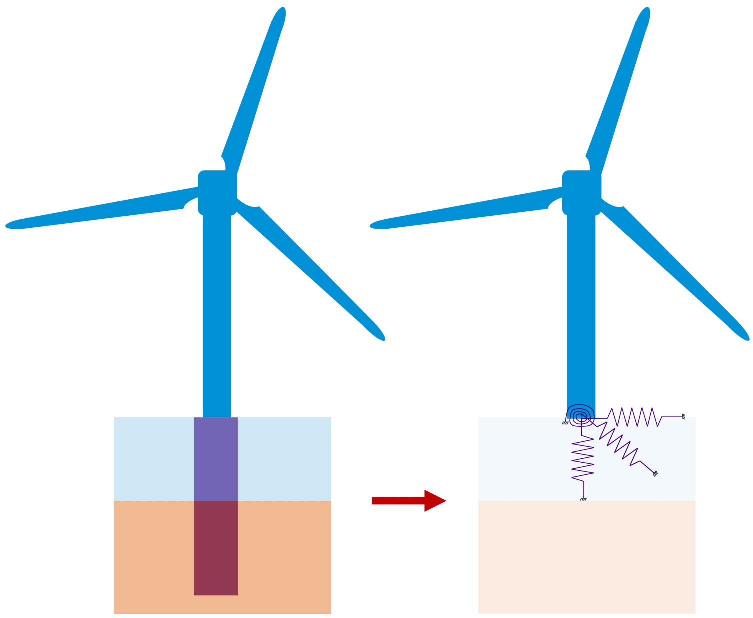

Fig. 3.9. Idealization of offshore wind turbine's foundation through the use of a super-element.

Each represented spring corresponds to a restricted direction. If a dynamic case is studied, these springs, due to the dynamic SSI, depending on the frequency and on the cycles of loading. Different soils have different characteristics and, consequently, different behaviours that should be taken into account by the equivalent springs. According to Ko [30], for eigenfrequency analyses, the vertical stiffness can be disregarded as the lateral response is the predominant response [1, 40].

A proven example of this approach consists of the RedWin project. This project utilises a macro-element at the mudline to simulate the foundation influence. The macro-element considers the soil response as well as the embedded monopile response. Considerations were made in this project to account not only for monotonic loading but also for cyclic loading. For example, the PISA project, a homologous project considering the Winkler foundation, is only valid for monotonic loading, although cyclic considerations are being investigated [24].

3.4.4 Winkler approach

The Winkler foundation consists of the substitution of the surrounding soil by a series of springs across the foundation depth, where a beam supported by a series of uncoupled lateral springs is modelled. Fig. 3.10 presents this approach. This method allows the implementation of non-linear springs, i.e., consideration of the non-linear behaviour of the soil. This foundation representation discretises the foundation, as each node will have a spring associated. Reducing the interval of discretisation will improve the accuracy of the simulation [16, 24, 86, 97].

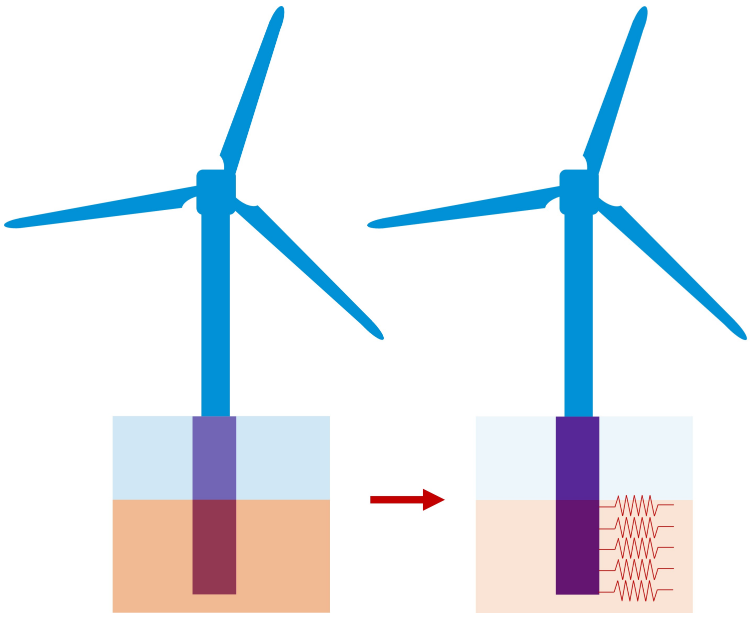

Fig. 3.10. Winkler model approach on the soil resistance applied to an OWT support structure.

Although Wang et al. [16] defend that interaction between springs is accounted for since their stiffness comes from a formulation based on pile experimental tests, as these tests were performed on homogeneous soils, the interaction between springs can only be considered for a given soil type. No interaction with adjacent springs can be considered in this model for a layered type of soil. This can be a drawback, as some degree of coupling is expected to occur in reality due to different properties between different soils as the soil particles will be different and behave in contrasting ways. Byrne et al. [49] state that the Winkler approach, to a given level, can be seen as an oversimplification of the actual response of the soil.

This approach on the foundation issue is an economical way of reaching a satisfactory solution. As it can account for soil non-linearities without significant computational effort and allows a detailed structural modelling, it's a very popular method. The implementation is relatively simple and the consideration of other phenomena, as scour, is easily performed. The Winkler approach can be seen as a good compromise between model accuracy and computational expense [23, 68, 86].

Boulanger et al. [95] proposed a configuration of parallel and series springs to represent the non-linear soil behaviour as well as the gap formation phenomenon that can occur on pile foundations after a given number of cycles. This configuration was used in tandem with a dashpot to include soil damping for a beam on a non-linear Winkler foundation model. At the same time, Gupta and Basu [40] stated that gap formation is not very relevant, as the tight SLS restriction of maximum head rotation of 0.5º does not allow significant gaps to form. As such, in their work, it was concluded that a non-linear elastic analysis is sufficient to obtain a good prediction of the OWT response.

Uncertainties are still inbound regarding the utilization of this approach for dynamic applications. The large deformations from the non-linear and inelastic behaviour of the soil affect the input parameters of this model. The variation of these parameters in these conditions is the main uncertainty [17].

This approach is regularly seen as a versatile and efficient way to consider the interaction between the soil and the structure, as an alternative to FEM approaches. However, the spring stiffness representing this interaction depends only on soil properties and not on the pile properties, which can be seen as questionable according to Damgaard et al. [15]. A bunch of soil influencing factors that might alter soil stiffness are also commonly disregarded when employing this kind of approach, although some correction factors were developed and presented in the literature.

Different soil modelling approaches besides the Winkler model can be used. Dutta and Roy [104] enumerate in their work different soil modelling approaches that can be used for common soil-foundation-structure systems, as well as a critical review of them. These different approaches allow different levels of accuracy from the foundation perspective as they try to surpass the limitations presented by the Winkler formulation. Although the Winkler model is simple for implementation, a given lack of continuity amongst springs exists, as it is based on independent elastic springs. Fig. 3.11 presents all the studied formulations by Dutta and Roy [104]. The quantification of some of the used properties on these models can be, however, difficult. Even for the Winkler model, the determination of springs' stiffness in N/m^3, also known as the coefficient of subgrade reaction, can be complicated as different soil volumes are mobilised according to the foundation area of contact with the soil.

3.4.5 FEM approach

As already stated, the complexity and computational time/cost of finite element models are the main barriers to their regular use, although they allow an increased accuracy by implementing constitutive models. Due to its computational cost, this method cannot be implemented in an efficient way with structural dynamic codes (aeroelastic simulations) that give the structure response [25, 63, 85].

Simplifications on the constitutive models can be performed to try and reduce the computational cost associated. Validity over frequency and load spectra, consistency, the

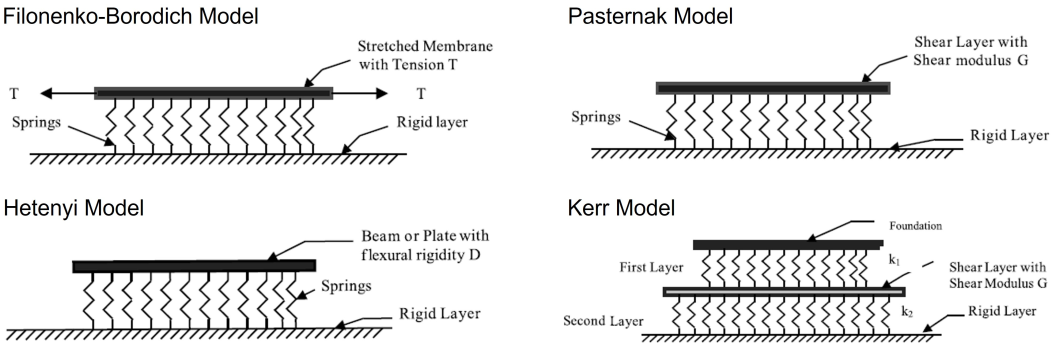

Fig. 3.11. Alternative soil modelling approaches to the Winkler model as according to Dutta and Roy's work [104].

physical meaning of parameters and simplicity are all factors that should influence the selection of the constitutive law for a FEM approach. Still, as full-scale and even small-scale tests can be expensive or incomprehensible complicated to perform, finite element models are more common in investigations. These can capture well the interaction between the soil and the structure, being used as a control reference for a given study. As stated by Versteijlen et al. [27], only by modelling the pile in a 3D continuum can the true interaction mechanisms between the monopile and the surrounding soil be captured [25, 40, 63, 85].

Although, according to Sturm et al. [24], the FEM approach is the only method that provides reasonable results when predicting the load-deformation response of the foundation, the Winkler approach is much more common as it is a versatile, efficient and economical method. However, current projects regarding correct soil modelling for the foundation design of OWTs use both approaches. The PISA and RedWin projects are projects that utilise FEM to calibrate a set of parameters of their model and have a better fitting of the predicted soil reaction. The main advantage is that two approaches are available in these projects, one where FEM is used to calibrate the reaction curves and another where FEM is not necessarily needed [24, 25, 63].

As has been given to understand by Stieng et al. [105], the reduction of computational time is a constant battle in OWT design and analysis in the time domain. The necessity to run a big variety of load cases in order to certificate an OWT makes this a very long and time-consuming process that demands a considerable amount of computational effort. One option to reduce the computational time consists of simulating using the frequency domain instead of the time domain, being considerably faster than time domain solving. However, a lack of precision regarding fatigue estimations is noted, as it does not specifically capture time variations within the system. It is also important to regard that running a dynamic analysis is approximately three times slower than a static analysis, as was verified by Gupta and Basu [40].

3.5. Soil Modelling

For any geotechnical associated problem, a realistic geometry, ground conditions, boundary conditions and material behaviour are required as model inputs to reach an accurate prediction of the analysed system relating to soil interaction. One of the most important soil parameters to define soil stiffness is its shear modulus. Every work on soil stiffness has considerations regarding the shear modulus of the soil analysed.

According to Verrujit [106], to be able to determine the response of a foundation to vibrations, the essential soil parameters are its density, shear modulus, and Poisson's ratio. Gazetas [100] has presented a set of formulae to determine, based on these soil parameters, the equivalent springs (as seen in Fig. 3.9). Although there is literature regarding this type of foundation modelling (super-element approach), this section will only be comprised of foundation modelling concerning the Winkler approach. Still, as offshore in-situ tests are expensive, physical and statistical uncertainties related to soil properties commonly coexist with modelling uncertainties of soil modelling [13, 81].

When considering a monopile foundation, along its length, different soil mechanisms occur. The nature of the response of the monopile influences this behaviour. While flexible piles, as the ones studied for common oil and gas applications, the monopile acts as clamped at its bottom. However, as wider and shorter piles in relative terms (low *L/d* ratio) are used, a more rigid behaviour is observed, with all of the piles rotating in relation to a given point. Multiple studies demonstrate that this pivot point stabilizes between z/L ratios of 0.7 to 0.8 [46, 65, 66, 79, 80].

Zhang et al. [7] studied the application of a *p-y* curve formulation dependent on the soil mechanism that occurred. However, poor physical meaning and definition of the pivot point of the rigid pile are drawbacks of the proposed approach. It is relevant to mention that different soil reactions may exist due to different soil failure mechanisms at different depths. Wang et al. [48] used a similar approach, using different correction parameters for different zones of the pile length, as they verified that the plane rotational failure mechanism affected the soil reaction applied onto the pile.

Throughout the PISA project [6, 49, 50, 64, 81, 82, 107], it was discovered that a set of different soil influences play a vital role in the model approach. The consideration of not only the lateral soil reaction through the modelling of laterally distributed springs but also by modelling a distributed angular spring and local base lateral and angular springs promoted a close representation of the total soil reaction when compared with 3D FEM studies and large-scale tests of monopiles. As monopiles tend to behave in rigid form, significant displacement at the pile end (bottom) can be seen, while flexible piles have essential no displacement at such relative depths. This is an example that strengthens the assumptions performed in this project.

The initial stiffness of the springs that represent the soil reaction force is dependent on the geometry, shape and material properties of both the structure and the soil. Static analysis is sufficient to reach the stiffness values desired. As stated in the previous section, the stiffness can also be represented as a dynamic stiffness (complex number stiffness), that includes the damping as well. This quantity also depends on both the soil and the pile used [27, 40].

The most common way of treating the monopile modelling with consideration of the soil is the Winkler approach. As such, the *p-y* curve theory is regularly implemented by allowing the characterization of the non-linear interaction between the soil and the surrounding soil. Different formulations exist regarding the construction of *p-y* curves since considerable errors have been proven when using oil and gas *p-y* curves for OWT applications. Considerable differences between the piles used in these industries lead to this outcome. Considerable differences were also seen by Zhang et al. [51] between the springs used for horizontal beams on the surface and vertical embedded beams [69, 82].

Soil cyclic effects are often not considered. The RedWin and PISA projects do not include these effects. Soil cyclic effects should, however, be considered for the lifespan performance evaluation of the OWT, as stiffness degradation or consolidation can occur, depending on the soil. Usually, the consideration of these effects is performed by FEMs, where an accurate pore pressure accumulation and cyclic degradation can be modelled. Cyclic effects underline the importance of soil time history [24, 85].

Gap formation is usually not considered for simplicity's sake, as it is complicated to introduce in the model in a proper way since non-linearities are introduced. This can be seen in the work of Boulanger et al. [95]. Besides this Winkler model, only FEM approaches were seen to represent this phenomenon. Damgaard et al. [31] also mention this phenomenon, stating that a shear drag will develop along the side of the pile when the pile returns to the initial position [25, 93].

Different ways exist to model and formulate the soil reaction curves. According to Byrne et al. [81], a simple approach consists in considering the soil as an elastic medium, relating it only to the shear modulus, while more sophisticated approaches consider a non-linear elastic model, including degradation of properties with strain level. Different soil testing can be used to soil properties definition needed in the different formulations.

3.5.1 Shear modulus profile

Prendergast et al. on a series of works (Refs. [17], [68], and [89]) presented different considerations on considering a stiffness profile derived directly from strength variation of the soil with depth. This approach regards the importance given to the stiffness of top layers and does not overestimate at the same level the stiffness of bottom layers as some formulations do. Another advantage of this approach is a degree of independence from the type of soil stratum studied, as no different formulation is needed if a soil stratum is composed of clay and sand or only one of those soil types.

This approach considers the small-strain shear modulus profile with depth and transforms it as subgrade reaction modulus/initial stiffness. The transformation can be performed by resorting to different sets of equations. The most common equations were studied by Prendergast et al. [17] and are presented in Table 3.1. According to the same authors, the representation of the stiffness across the foundation using the shear modulus profile is more realistic of the offshore soil conditions and reflects the importance of soil removal due to scour.

Soil stiffness is a property that is strain-dependent. However, in modal analyses, the small-strain assumption is sufficient, and the small-strain shear modulus provides a good estimation for stiffness calculations. It is important to understand that soil stiffness is expected to depend on soil type, the geometry of the structure and loading type [27, 68].

The small-strain shear modulus depends on the density and stress level of the soil, as well as on ageing and cementation. The number of factors that shear modulus depends on makes it difficult to predict, but geophysical measurement techniques can be used to reach reliable values of the small-strain shear modulus. These measurements are usually not very expensive when comparing them with other soil experiments. Multiple ways exist to estimate the shear modulus through measured values of different soil properties. Soil wave propagation velocity and measured cone tip resistance are the main examples of properties to reach the small-strain shear modulus, as has been broached earlier in this Chapter [68].

Using experimental pile tests, Prendergast et al. [68] performed a comparison between this method and the API Standard regarding scour. They reached the conclusion that using the API approach when scour phenomenon occurs would underestimate the frequency for low scour depth. Meanwhile, their proposed method agreed well with measured frequencies for different scour depths. The resulting soil stiffness profile can be seen in Fig. 3.12, where these two approaches are compared. Special attention should be provided to the fact that how the soil properties, mainly the shear modulus, are obtained influences the estimated stiffness profile.

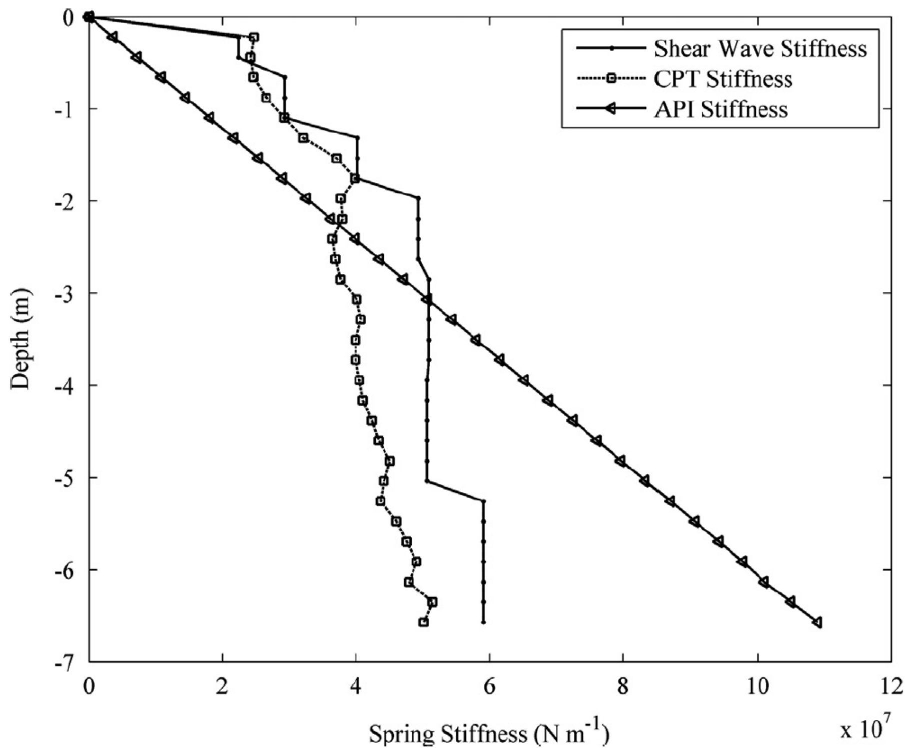

Fig. 3.12. Stiffness derived from the shear modulus profile versus from the API Standard [68].

The different theoretical approaches to considering the soil stiffness from the measured soil moduli are presented in Table 3.1. These were all used by Prendergast and Gavin in their work [17] to study the best formulation. However, all of these are related to slender pile considerations. A slender-like pile (aspect ratio above 10) was studied in this paper. The reader should then acknowledge that the conclusions from this paper cannot be directly extrapolated to the present work.

Table 3.1. Soil stiffness with soil properties as seen in the work of Prendergast and Gavin [17].

Investigator credit	Formula
Biot	$k_s = \frac{0.95E_s}{d\left(1-\nu_s^2\right)}\left[\frac{E_s d^4}{\left(1-\nu_s^2\right)EI}\right]^{0.108}$
Vesic	$k_s = \frac{0.65E_s}{d\left(1-\nu_s^2\right)}\left[\frac{E_s d^4}{EI}\right]^{1/12}$
Meyerhof and Baike	$k_s = \frac{E_s}{d\left(1-\nu_s^2\right)}$
Klopple and Glock	$k_s = \frac{2E_s}{d(1+\nu_s)}$
Selvadurai	$k_s = \frac{0.65E_s}{d\left(1-\nu_s^2\right)}$

3.5.2 API Standard

The API Standard utilises the *p-y* method. It's based on a series of *p-y* curves that were formulated considering long and small diameter piles subjected to a limited number of cycles, i.e, it's based on soil test results and empirical correlations. These piles were tested while embedded in homogeneous soil. Good accuracy regarding the pile head force-deflection response is obtained when employing this approach on piles similar to the ones that gave origin to the *p-y* curves formulation presented in the API Standard. This approach tends to behave in a conservative manner. While undrained conditions were assumed for clays, for sands a drained condition was assumed when developing the *p-y* curves from testing [9, 15, 24, 48, 74].

This method considers a beam on nonlinear Winkler springs, not accounting for the continuous nature of the soil. As stated before, this method applied for OWT has some limitations that lead to an unsatisfactory performance (inaccurate results). It should be noted that the method of installation influences the overall soil reaction and that the *p-y* curves in their normal formulation do not include this effect. According to various literature, horizontal deflections on monopiles with low *L/d* ratios are underestimated and, for small operational loads, underestimations on the foundation stiffness happen. However, these behaviours depend on the type of soil and the extension of displacements. As identified by Wang et al. [79], the API Standard led to an underestimation of the stiffness and lateral ultimate capacity of a low *L/d* ratio pile embedded in soft clay. Meanwhile, as identified by Sun et al. [80], the same standard leads to an overestimation of the initial stiffness for sands [1, 2, 46, 48].

However, independently of the pile diameter and length, the API approach can predict in a satisfactory way the bending moment profile. In some cases, an underestimation can also be remarked for increased depths. Wang et al. [76] stated that this could mean an incorrect model of the *p-y* curves for this depth for large diameter piles. The overestimation of stiffness that also occurs at high depths can be seen as a supporting factor in this matter [48, 76].

Versteijlen et al. [27] stated that different soil reactions could become relevant as the *L/d* ratio decreases. This would explain errors that occur when using this standard oil and gas approach on piles from the offshore wind industry. This is also the base for the PISA design model, as mentioned later in this work. According to Wang et al. [76], although there is now evidence of the relevant contribution of other resistance components, the lateral resistance is still dominated by the laterally distributed reaction.

The effect of pile diameter is not considered in the common *p-y* curves formulation. As this is the main difference between the API approach and the real cases, a variety of modifications have been proposed to include this factor. Damgaard et al. [15] have seen in validated laboratory tests that the initial stiffness of *p-y* curves are highly dependent on pile diameter dimensions. As well, the same set of *p-y* curves are usually used independently of the loading case (either if it is a loading, unloading or reloading case, the same formulation is used). This neglects the effects of permanent deformations and soil damping that may be relevant. As a variable soil stratum is usually the case for embedded piles, different reaction magnitude due to different phenomena (like soil layers interaction) can lead to dissimilarities when comparing with unmodified *p-y* curves [4, 15, 80].

Modifications regarding a better prediction of the ultimate soil resistance, correction parameters, fitting parameters, and others exist to better capture the soil reaction for large diameter piles. Achmus et al. [41] verified that the common API method underestimated significantly the initial stiffness for sands at shallow depths while taking the Thieken and Kallehave modifications provided better predictions. The Kallehave modification accounts for a relation between the strength and the stiffness of the soil. The Thieken modification accounts for small strain soil stiffness, leading to a stiffer response than the Kallehave approach since the latter cannot relate the small strain stiffness with the oedometric stiffness.

Damgaard et al. [31] state that, for modal analysis, a common way to estimate the spring stiffness considered for soil modelling consists of linearising the non-linear *p-y* curves. This linearization can be performed by considering the initial soil stiffness of the non-linear springs or by using the secant or tangent soil stiffness for a given situation. Even when considering cyclic loading (un and reloading paths), a good estimation can be obtained by using the initial stiffness from monotonic loading. Carswell et al. [85] recommend that, for large loads, the fundamental natural frequency determination should be performed by using the secant stiffness of the *p-y* curves.

According to the Standards API [108] and DNV [43, 47], Eqs. 3.8 and 3.9 present the standard force per unit length formulations for sand and clay, respectively, for a static situation. Through these, it is possible to define the initial stiffness of a given soil.

$$p = A \cdot p_u \tanh\left(\frac{k_{ini}z}{A \cdot p_u} y\right) \tag{3.8}$$

$$p = \begin{cases} 0.5 p_u \left(\frac{y}{y_c}\right)^{1/3} & , y \leq 8y_c \\ p_u \, , y > 8y_c \end{cases} \tag{3.9}$$

Different formulations can be encountered for dynamic/cyclic situations. For the case of sands, only the A parameter is modified, with a different definition being employed. However, for clays, a different formulation exists from a given lateral displacement. Eq. 3.10 presents the formulation for a depth where the soil bearing capacity increases with depth, while Eq. 3.11 presents the formulation for a depth where the soil bearing capacity is considered constant. The depth of transition from which the soil bearing capacity can be considered constant is defined as z_R.

$$p = \begin{cases} 0.5p_u\left(\frac{y}{y_c}\right)^{1/3} & , y \leq 3y_c \\ 0.72p_u\left[1-\left(1-\frac{z}{z_R}\right)\frac{y-3y_c}{12y_c}\right] & , 3y_c \leq y \leq 15y_c \\ 0.72p_u\frac{z}{z_R} & , y > 15y_c \end{cases} \tag{3.10}$$

$$p = \begin{cases} 0.5p_u\left(\frac{y}{y_c}\right)^{1/3} & , y \leq 3y_c \\ 0.72p_u & , y > 3y_c \end{cases} \tag{3.11}$$

To reach the initial stiffness of a given soil, as presented in Eq. 3.12, a derivation in order to the lateral displacement of the force per unit length is necessary. After deriving, the lateral displacement is assumed equal to zero. For sand, the formulation is simplified to what is seen in Eq. 3.13, where a linear evolution exists with depth.

$$k' = \left.\frac{\mathrm{d}p}{\mathrm{d}y}\right|_{y=0} \tag{3.12}$$

$$k'_{sand} = k_{ini}z \tag{3.13}$$

Although it is possible to reach an initial stiffness for sand through the formulation presented, for clay this is not possible. If the same process is used, the denominator of the expression will be zero, leading to an undefined case. Consequently, there are common stiffness estimation expressions that allow the quantification of the initial stiffness of this soil type. Eqs. 3.14 and 3.15 present the most common expressions:

$$k'_{clay} = \xi_{emp}\frac{p_u}{d\varepsilon_c^{0.25}}; \tag{3.14}$$

$$k'_{clay} = \frac{0.23p_u}{0.1y_c}. \tag{3.15}$$

If a similar approach is performed without taking the lateral displacement as zero, i.e., just deriving the force per unit length for clay soil, Eq. 3.16 is obtained. It was observed that a good fitting with Eq. 3.15 was achieved when a lateral displacement of 0.001 times the diameter was considered. Consequently, and avoiding the fact that different coefficients are necessary to define an estimation for clay stiffness, the second presented stiffness estimation for clay is more appropriate and easier to use/define.

$$\frac{\mathrm{d}p_{clay}}{\mathrm{d}y} = \frac{p_u}{6y_c}\left(\frac{y_c}{y}\right)^{2/3} \tag{3.16}$$

With the general formulation defined to acquire the initial stiffness of the soil, attention should be provided to the quantification of the different necessary values. These can follow what is present in the Standards or use the modified and proposed expressions from different literature. In a nutshell, Table 3.2 presents all the considered relevant and seen expressions for sands, while Table 3.3 presents all the considered relevant and seen expressions for clays. Further modifications exist on the literature using a set of ratios/dimensionless parameters. Are examples of that the Sørensen [109, 110] and Kallehave [111] approaches on the sand stiffness to account for the rigid behaviour of the structure on the slender-defined API standard curves.

Table 3.2. Sand proposed expressions, as according to Refs. [43], [48], and [76].

Parameter	Formula	Ref.
k_{ini}	$\left(0.008085\phi_f^{2.45} - 26.09\right) 10^6$	[76]
k'_{ini}	$100 K_p \gamma' z$	[48]
K_p	$\tan^2\left(45 + \frac{\phi_f}{2}\right)$	[48]
K_p^{DIN}	$\sqrt{\frac{\left[\left(\frac{1+\sin\phi_f}{1-\sin\phi_f}\right)\left(1+0.53\frac{2\pi}{3\cdot180}\phi_f\right)^{0.26+\frac{5.96\pi}{180}\phi_f}\right]^2}{1+\left(\tan\left(-\frac{2}{3}\phi_f\right)\right)^2}}$	[48]
A	$\begin{cases} 3-0.8\frac{z}{d} \geq 0.9 \text{ , static loading} \\ 0.9 \text{ , cyclic loading} \end{cases}$	[43]
A	$\begin{cases} 2.75 - z\frac{2.75}{0.7L} \text{ , } \frac{z}{L} \leq 0.7 \\ (z-0.7L)\ \frac{2.25}{0.7L} \text{ , } \frac{z}{L} > 0.7 \end{cases}$	[48]
p_u	$\begin{cases} (C_1 z + C_2 d)\,\gamma' z \text{ , } z \leq z_R \\ C_3 d \gamma' z \text{ , } z > z_R \end{cases}$	[43]
p_u	$\frac{11}{16}\gamma' z^{1.5} K_p^{DIN}\left(1+\tan\phi_f\right)\sqrt{d}$	[48]
C_1	$0.115 \cdot 10^{0.0405\phi_f}$	[76]
C_2	$0.571 \cdot 10^{0.022\phi_f}$	[76]
C_3	$0.646 \cdot 10^{0.0555\phi_f}$	[76]

Table 3.3. Clay proposed expressions, as according to Refs. [7], [43], [85], and[112].

Parameter	Formula	Ref.
y_c	$2.5\varepsilon_c d$	[112]
p_u	$\begin{cases} (3s_u + \gamma' z)\,d + J_{clay}\cdot s_u z \text{ , } z \leq z_R \\ 9 s_u d \text{ , } z > z_R \end{cases}$	[43]
p_u	$\left(N_{p0} s_u + \gamma' z\right) d$	[7]
J_{clay}	$\begin{cases} 0.25 \text{ , stiff clays} \\ 0.50 \text{ , soft clays} \end{cases}$	[85]
N_{p0}	$\begin{cases} N_1 - (N_1 - N_2)\left(1 - \frac{z}{\alpha_d d}\right)^{1.35} - (1-\alpha) \text{ , while } N_{p0} \leq N_{pd} \\ N_{pd} = 9.14 + 2.8\alpha \text{ , for remaining cases} \end{cases}$	[7]
N_1	11.94	[7]
N_2	3.22	[7]
α_d	14.5	[7]
α	$\begin{cases} 0 \text{ , smooth interface} \\ 1 \text{ , rough interface} \end{cases}$	[7]

3.5.3 PISA design model

The PISA design model rises from the questionable accuracy provided by only considering a lateral distributed load as common *p-y* curves methods do. The PISA method can be seen as an extension and improvement of the common *p-y* method. This model introduces the inclusion of the resistance from the base shear force, base moment and skin friction, as seen in previous onshore applications. As such, the PISA design model considers four types of springs to simulate the soil reaction [48, 82]:

- Distributed load reaction - in any way similar to what is seen in common *p-y* curves, this component relates the distributed lateral load applied to the foundation and the lateral pile displacement; as such, similar functions to the common *p-y* curves are used.

- Distributed moment reaction - rising from vertical shear stresses developed across the pile length, this component relates a distributed moment applied to the pile with the pile cross-section rotation.

- Base shear reaction - it relates a base shear force with the lateral displacement at the end (bottom) of the foundation.

- Base moment reaction - it relates a base moment with the rotation at the end (bottom) of the foundation.

The distributed angular spring, which is the main innovation in this model, is related to vertical tractions induced on the pile perimeter. These result from existing friction between the soil-pile interface and are expected to be related to the local distributed lateral load, as vertical displacements occur caused by local rotation of the pile's cross-section. Vertical relative movements of active and passive soil wedges can also contribute to these displacements. However, vertical loads resulting from these vertical tractions are disregarded [49, 107].

As literature states that different reactions could exist for low aspect (*L/d*) ratios, the inclusion of these lateral resistance components in the model rises the fundamental frequency of the structure. Then, this approach does indeed close the gap between the predicted and measured responses of piles with lower aspect ratios [78, 82].

A robust model is achieved by using a Timoshenko beam theory, including the influence of shear strains on the overall pile deformation. As soil reaction curves will not be unique, this approach allows appropriate curve definition from dimensionless soil variables, followed by FEM calibration. Throughout the development of the design model, no imposition regarding the parametric curve form was performed, allowing other functions to be implemented. Undrained conditions were considered in this design model. No effect from the installation method was assumed, as a ”wished in place” consideration was performed [49, 78, 107].

The PISA design model neglects the effect of the vertical loads due to the structure weight, as its application does not vary, while representing a small fraction of the vertical capacity of the foundation. The model then assumes that the lateral behaviour is independent from these vertical loads.

Some degree of limitation exists when applying this design model to a layered soil stratum. As a variety of soil is in order, the implementation of the rule-based approach of the method allows for a faster running time of the problem. However, worse results are obtained, as worse fitting is obtained in relation to the real case. Burd et al. [78] studied the application of this design model to non-homogeneous strata. Although a satisfactory estimation was obtained when comparing the results with numerical 3D results, the model performed worse for cases that involved combinations of very soft clays and very dense sands. As a consequence, a possible degradation of the overall soil stiffness should be modelled as strong layers are degraded by softer layers in terms of strength [81].

The tests that were performed for further comparison and calibration of the model developed were conducted by applying an excitation in a single plane. These tests were performed using a monotonic loading. As such, the PISA design model was only developed for this intent, i.e., it is not applicable for cases where load amplitudes exceed the elastic range. Further development is underway to allow the extension of this model for cyclic loading [24, 113].

After calibrating, a 1D finite-element model is achieved, where the OWT is represented as a line mesh of Timoshenko beam finite elements. The soil reaction is introduced by calibrated parametric functions that relate the soil reaction to a given local lateral displacement or rotation. The fidelity of this 1D model is, however, limited: the utilization of a Winkler-like approach does not account for every relevant SSI mechanism; simple functions are used to explain parameters depth variation; imperfect fitting during the calibration [49].

In alternative to the calibration method, a rule-based method was devised to further use the PISA design model in soils where calibration cannot be achieved or a fast estimation is needed. It relies on strength and stiffness parameters, as the soil reaction curves are based on predefined functions that depend on the soil type. Questionable responses can be obtained using this approach, as a poor fitting to the actual soil reaction curves is expected using this approach [82].

Burd et al. [107] verified that for shallow depths/large displacements, a post-peak softening occurred. The authors linked this to a soil dilation phenomenon as represented in their calibration analyses and load numerical data.

According to Wang et al. [76], the PISA design model provides a good estimation of the ultimate bearing capacity and correctly accounts for the diameter and aspect ratio influences on the SSI. At the same time, the same authors state that an overestimation of the structure response can occur. The model leaves open the possibility of different effects integration, such as cyclic loading, multi-directional loading, densification, age hardening and others. Byrne et al. [82] state that cyclic loading consideration is possible by using methods such as the Masing rule or through incorporation in kinematic hardening models. Still, further improvement is needed as stated by Wang et al. [76] and the own design model developers [82].

The rule-based method of the PISA design model imposes the utilization of a set of empirical equations that are based on a specific type of soil. This means that errors are expected to exist when employing them on other soils, even if they are of the same type. The *p*-*y* curve used in this model is comprised of dimensionless parameters to make it a unique formulation for both sand and clay. This formulation can be seen in Eq. 3.17, where the considered parameters are exposed in Table 3.4. Performing the same approach on initial stiffness as seen previously on the API Standard, a common expression can be reached for both sands and clays. This is exposed in Eq. 3.18. Table 3.5 summarizes all the needed quantities to allow the implementation of this design model in a given soil.

$$\bar{p} = \begin{cases} \bar{p_u} \frac{2c}{-b+\sqrt{b^2-4ac}} \ , \bar{y} \leq \bar{y_u} \\ \bar{p_u} \ , \bar{y} > \bar{y_u} \end{cases} \tag{3.17}$$

$$k' = \left.\frac{\mathrm{d}\bar{p}}{\mathrm{d}\bar{y}}\right|_{\bar{y}=0} = \frac{2G_0 k_{PISA}(1-n)}{1-n+|n-1|} \tag{3.18}$$

Table 3.4. PISA design parameters as according to Burd et al. [78].

Parameter	Sand	Clay
Parameter a	$1-2n$	
Parameter b	$2n\frac{\bar{y}}{\bar{y_u}} - (1-n)\left(\frac{\bar{p}}{\bar{p_u}} - \frac{k_{PISA}\bar{y}}{\bar{p_u}}\right)$	
Parameter c	$(1-n)\frac{k_{PISA}\bar{y}}{\bar{p_u}} - n\frac{\bar{y}^2}{\bar{y_u}^2}$	
Normalised distributed load ($\bar{p}$)	$\frac{p}{s_u d}$	$\frac{p}{\sigma_v' d}$
Normalised lateral displacement ($\bar{y}$)	$\frac{G_0 y}{s_u d}$	$\frac{G_0 y}{\sigma_v' d}$

Table 3.5. PISA ruled-base method necessary quantities for sand, soft clay, and stiff clay as according to Burd et al. [78].

Soil type	Parameter	Formula
Sand	n	$0.917+0.06193D_r$
	k_{PISA}	$8.731-0.6982D_r-0.9178\frac{z}{d}$
	p_u	$\sigma_v' d\left[0.3667+25.89D_r+(0.3375-8.9000D_r)\frac{z}{L}\right]$
	$\bar{y_u}$	$146.1-92.11D_r$
Soft clay	n	$0.7204-0.002679\frac{z}{d}$
	k_{PISA}	$12.05-1.547\frac{z}{d}$
	p_u	$s_u d\left[7.743-3.945\exp -0.8456\frac{z}{d}\right]$
	$\bar{y_u}$	173.8
Stiff clay	n	$0.9390-0.03345\frac{z}{d}$
	k_{PISA}	$10.60-1.650\frac{z}{d}$
	p_u	$s_u d\left[10.70-7.101\exp -0.3085\frac{z}{d}\right]$
	$\bar{y_u}$	241.4

3.5.4 Stiffness and damping effects

In order to guarantee that the simulation correctly predicts the structure behaviour, correct model inputs have to be introduced. This has substantial importance when talking about the stiffness assigned to the lateral springs that replace the soil surrounding the OWT monopile. From a modal properties analysis point of view, as performed by various authors, the estimation of a small-strain stiffness (that can also be regarded as initial stiffness), is sufficient to reach the fundamental natural frequency of the structure. The initial stiffness can be defined as a secant stiffness that corresponds to a normalised mudline displacement of 0.001, while a secant stiffness will be the stiffness obtained for a normalised mudline displacement up to 0.04 [19, 40, 46, 68].

The consideration of an initial stiffness is regularly assumed as sufficient since natural frequencies concern vibrations with small amplitude. This comes from the linearity of the eigenproblem and the fundamental natural frequency obtained will not represent the structure modal properties when other conditions, like liquefaction and seismic activity, occur. This is further reinforced by Søren and Larsen [59] on their work. Achmus et al. [41] also stated that due to the low frequencies from wind and wave loading, dynamic effects can be neglected when determining the soil stiffness [19, 40, 68].

According to Achmus et al. [41], the fundamental frequency of an OWT highly depends on the stiffness provided when the system is under unloading and reloading conditions. As the soil stiffness is strain-dependent, these situations lead to differences in the stiffness of the system. Increasing loads, or displacements, leads to an initial stiffness increase. The bounds of the stiffness when considering cyclic loads/displacements also increase with increasing cyclic amplitudes. However, as Achmus et al. [41] found out, relatively decent results are achieved considering the initial stiffness of a monotonic loading condition instead of a un/reloading condition.

The stiffness of the shallow/top layers plays a big part in the system response. Large mudline pile loads can lead the soil surface to enter an inelastic range, increasing soil reaction across the pile length. As such, a higher stiffness at shallower depths will be the main influence factor on the fundamental frequency obtained. Versteijlen et al. [27] reached this conclusion when seeing that the API approach overestimated the stiffness of sand at high depths, but an underestimation of the fundamental natural frequency occurred [27, 85].

Special attention should be given when modelling the scour phenomenon. According to Lin et al. [69], only removing the spring representing the soil layer that has been eroded due to scour is incorrect. This simplification considers the local scour as general scour, which was demonstrated to not incur significant errors, but when scour occurs, a consolidation of adjacent soil layers happens. As such, although a stiffness loss indeed takes place, a stiffness gain is also materialized. Stress history of the soil layers was then seen as important for design aspirations considering scour. Not considering this history leads to an over-conservative design. Also, the utilization of scour protection is expected to increase the foundation stiffness, since a stiffer soil material is used.

A correct estimation of the damping used in the model is important as a higher damping value will lead to lower loads being applied and the necessary material to resist the loading will be less. At the same time, incorrect estimation of high damping values would lead to the design of an OWT that could be susceptible to premature failure. This is an important issue in the wind industry, as guidelines do not include recommended methods of considering damping, resulting in not considering some sources of damping that may be important (over-conservative design) [114].

There are different damping sources, relating to structural, wind, water, and soil interactions. When the OWT is operating, i.e., producing energy, aerodynamic damping is the most relevant damping source. When the OWT is stopped, foundation damping takes place as the most relevant damping source, with structural damping being a relevant source as well. The way these damping sources are modelled is also important, as Rayleigh damping cannot be used for some damping sources [12, 39, 115, 116].

Aerodynamic damping originated from air drag actuating on the rotating blades. The blades oscillate in the airflow due to tower bending vibration. Some air drag is also experienced by the tower itself, but very small values are in order when compared with the ones from the rotating blades. Significant differences from aerodynamic damping in the fore-aft and in the side-side directions are also noted. Aerodynamic damping is influenced by a series of factors, mainly wind speed, blade rotation speed, pitch angle of the blades and yaw angle of the rotor. Underestimations are expected to occur for wind speeds higher than the rated wind speeds [39].

Foundation damping is regarded as damping from the soil. A particularity of this type of damping is that Rayleigh damping cannot be used to correctly represent the foundation damping. although it is regularly used for modelling structural damping (not including damping from tower dampers). Different sources of soil damping according to Malekjafarian et al. [23] are: radiation of elastic waves damping, soil material/hysteretic damping, and pore pressure dissipation (seepage) damping. The bigger influence of soil damping comes from the hysteretic type damping. This source of foundation damping is regarded as the most complex and least understood, as there is no consensus on how to quantify it [4, 23, 53, 116].

The radiation damping is originated from the motion of the monopile as waves from this vibration radiate away from the pile and through the soil. The generated waves carry out some of the transmitted energy of the structure movement, with part of the energy being absorbed. This type of soil damping depends on the excitation frequency, mode of oscillation, the geometry of the system, and overall characteristics of the soil. Usually, for frequencies lower than 1 Hz, this type of damping is disregarded [4, 23, 39, 75].

The hysteretic damping originated from the own soil dissipation of energy due to friction and sliding between soil particles, specially when the soil is cyclically loaded. Strain effects and overall non-linear soil behaviour influence this type of damping. Alterations on the effective stress acting on the soil change the hysteretic damping verified. These alterations can come from water pore pressure changes. This type of damping highly depends on soil strain, being independent of frequency and loading rate [4, 39].

Seepage damping originated from the seepage of pore water between soil particles, equaling the excess pore pressure. This type of damping is of viscous nature and is proportional to the frequency, yet independent of the soil strain level. To understand the degree of influence that this type of damping can introduce, drainage conditions around the monopile should be known. Soils with low permeability (like clays) lead to essentially no seepage damping as the soil behaves in an undrained manner. On medium to high permeability soils (like sands), the seepage damping will depend on loading rate, drainage length and drainage properties of the soil, as drainage occurs. According to Beuckelaers [117], this type of damping only contributes with small damping values on very permeable soils and is thus not usually considered [23].

Damgaard et al. [15] and Kementzetzidis et al. [10] both report the importance of pore-pressure in the global OWT damping. By affecting the effective stresses of the soil and changing permeabilities, different damping values can be obtained.

Structural damping is a structure material associated damping that can have different origins, from material losses to joint friction but relying on the dissipation of energy from the structure when it vibrates. As such, a series of challenges appear to fully model this damping source. Usually, a Rayleigh damping matrix is used. Alternatively, a loss factor associated to the material stiffness is used [23, 39].

Different types of tower dampers exist. The most common OWT structures are the tuned mass dampers. These devices are employed to further reduce loads and vibration amplitudes. When they are active (there is the possibility to turn off these devices), they contribute to a large amount of the damping measured. [23].

Hydrodynamic damping has two sources: wave radiation damping and hydrodynamic drag viscous damping. Wave radiation damping is proportional to wave velocities. Hydrodynamic viscous damping is proportional to the squared wave relative velocities. Hydrodynamic damping is the least important of the different damping sources according to literature. As such, in a variety of studies, it is ignored [39].

Investigations tend to focus on calculating a specific damping source through back-calculation (and assuming linear contributions) or by assuming direct modelling. From experimental tests, usually, only the overall damping is measured, as it is a simpler and straightforward analysis. Different damping ratios are mentioned throughout the literature. If small damping values are expected, the consideration of a loss factor can be used, as the relationship between this parameter and an equivalent damping ratio exists. Introducing plasticity into the model can also avoid some limitations of introducing damping as a viscous source (which is not the case for every damping source). Only considering non-linear (plastic) springs is not correct to include a given damping source [23, 39, 53, 63].

Although there is no consensus on how to model these different damping sources for precise damping estimations, standards recommend the consideration of some of these damping sources. No recommended approach is given in these standards. An estimation is thus performed by using Rayleigh damping, which produces considerable errors. It is also important to have frequency-dependent damping to better represent actual damping phenomena regarding the soil. However, approaches regarding time-independent damping values, such as the one presented by Brinkgreve et al. [116], also exist [23, 53].

3.5.5 Vertical soil modelling

The soil is usually modelled in the vertical direction by considering a series of t-z and Q-z curves. Like the seen *p-y* curves, these curves come from experimental data after piles testing. Likewise, how the soil properties for these are acquired, once again, influences the achieved curves and, thus, the estimated stiffness.

The axial capacity of the soil characterises the vertical bearing capacity of the foundation. It depends on the soil type and on the installation process. Although both tension and compression capacities can be admitted, for monopile foundations, only compression is considered. Proper emphasis is given to the pile installation on the determination of the longitudinal stiffness [29].

Like in lateral soil modelling, different methods exist when modelling. Likewise, different formulations of soil capacities and soil stiffness quantification exist. Soil plugging has a significant effect on the considered modelling of the problem. Consequently, different assessments should be performed to ensure that a correct model is selected for a given case [84]. At the same time, modifications should be performed in order to consider scour effects. ”Liquefiable” curves should be considered in these conditions. According to Jiang et al. [19], these ”liquefiable” curves can be obtained by considering the effective vertical stress into the vertical ultimate soil resistance calculation that is used to define the common t-z and Q-z curves. Pore water pressure is regularly ignored in this formulation.

As little influence has been reported in the literature regarding vertical soil modelling on predominately lateral response problems, this topic will not be further elaborated on. More on this can, although, be regarded in Chapter 17 of *Soil Dynamics and Foundation Modelling: Offshore and Earthquake Engineering* [84] and in the Standard API [108] and/or DNV [43, 47, 58].

3.6. Final Remarks

Geotechnical tests are the most common soil measurement methods employed in the offshore wind industry. Tests such as cone penetration tests (CPT) and laboratory testing of borehole samples are soil disturbing and large-strain measurement methods. These methods raise the question of adequability for the small-strain soil properties assessment. In turn, recorded soil wave data (wave velocities) can allow the determination of more characteristics than what can be achieved with CPT, for example, while being a non-disturbing method. CPT is the regular method used for soil properties identification in offshore conditions. Although more effective parameters can be obtained with this indirect method, a given degree of uncertainty can be associated with it, as outside influence factors can affect the measurement. Backscattering of waves due to contrast between soil layers and lateral soil variability can be a source of uncertainty in this regard. The quality of the estimation can be further impacted by geometric attenuation. Either way, soil wave recording can be seen as an advantageous measuring method over common disturbing methods, as some in-situ characteristics are not lost [27, 70].

The soil stiffness is highly dependent on the interaction between the soil and the structure. This interaction is highly complicated, with many factors being involved. Cyclic loading can lead to a softening or hardening of the soil, changing its stiffness. Other soil properties, such as permeability, shear modulus and ultimate capacity can be linked to soil stiffness. It was also seen that the pile installation method can highly influence the foundation stiffness obtained, as an over-consolidation or densification occurs. Álamo et al. [34] defend that the superficial soil layers are the ones that govern the effects of the SSI on observed modal properties.

As the literature suggests repeatedly, an underestimation of the overall OWT foundation stiffness is performed using common and established procedures in the oil and gas industry. In turn, not considering any kind of SSI, as considering the structure to be clamped, leads to an overestimation of the natural frequencies. However, when considering a SSI, it is easier to find justifications regarding soil stiffness degradation than regarding occurrences of stiffness increases. Consequently, this may suggest that a less correct modelling approach is being employed.

Besides all the limiting factors from the common modelling approach, different soil behaviours might happen in parallel and/or in series with each other. This reinforces that a set of different sources of stiffness increase/decrease might not be considered in the vast majority of the literature. If a high accuracy prediction is wanted, then a dynamic SSI has to be considered. Nevertheless, problems with actually implementing this type of SSI exist, as soil parameters that characterise this interaction are related to each other.

As Malekjafarian et al. [23] resumed in their work and has been exposed here, a lot of challenges still exist in the consideration of SSI. The soil modelling considering the effects that may affect the SSI requires more study, as some of these factors are not even captured using complex constitutive laws. Drainage conditions are not usually considered in the modelling, as proper dynamic SSI is needed. Likewise, seabed changes with time are not usually considered, as an equilibrium or a maximum status are assumed. The loading influence on the modal properties is also disregarded when possible alterations on the modal properties can happen due to it.

In terms of modelling, the Winkler approach is commonly used in the industry, as it is a simple and versatile method. It replaces the soil across the pile embedded length for a series of springs that simulate the soil reaction at different depths. Despite that, it does not account for the interaction between adjacent soil springs, which is a relation that can occur. Common *p-y* curve formulation incurs considerable errors when applied for OWTs foundations, as they were formulated for slender piles than the ones used for OWT applications.

Globally, the approaches to foundation modelling lead to the underestimation of the natural frequencies of the system. This can mean that an underestimation of the soil stiffness is considered, as the rigid foundation approach leads to an overestimation of these same frequencies. Different investigations and tests were and are being performed to reach a simple and versatile approach without the necessity of the computational costly approach of FEMs.

Although a high-precision solution can be obtained, FEM is mainly used in investigation as it is a very time-consuming process. There are projects that only use FEMs to calibrate soil reaction curves present in the model developed. At the same time, solving by resorting to a frequency domain is faster than using a time domain solver. However, it lacks fatigue estimation accuracy. The utilization of a static analysis leads to considerable less computational effort.

The common oil and gas approach presented in API standards (for slender piles) when applied to large diameter and short piles as the ones used in the offshore wind industry results in a significant underestimation of lateral stiffness for clays, while it can overestimate the lateral stiffness for sands, especially at high depths. Similar conclusions are reached for the soil's ultimate capacity. Not considering the base moment and force as well as the skin friction throughout the pile length might be reasons, as presented by the PISA design model. However, the consideration of a more proper lateral distributed resistance through a corrected *p-y* formulation can be sufficient.

A different approach altogether and only dependent on the shear modulus of the soil is also regarded as a promising answer for stiffness estimation throughout the pile length.

This approach departs from experimental testing values of slender piles as it depends more directly on the soil properties, considering the pile-soil interaction as well.

Chapter 4

Model Development

4.1. Vibrations Basics

A dynamic system is usually composed of an elastic element, a mass or inertia, and a damper. These elements allow the system to store and return elastic/potential and kinetic energy, as well as dissipate energy, respectively [118].

A linear elastic element is characterised by a spring with stiffness k. The force that acts on this element will be linearly proportional to the displacement seen in the spring's ends, as presented in Eq. 4.1 and visualised in Fig. 4.1. The units of the spring stiffness will then be N/m. Moreover, a rigid link can be considered by having a spring that has infinite stiffness [30, 118].

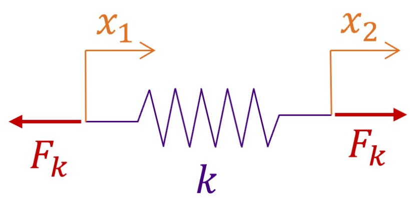

Fig. 4.1. Elastic element representation.

$$F_k = k\left(x_2 - x_1\right) \tag{4.1}$$

If a given system has more than one spring linked to two common ends, an equivalent spring can be devised. The equivalent spring value will depend on the spring combination form. Two parallel springs will lead to a different equivalent stiffness to the one that is obtained by two springs in series. Fig. 4.2 presents these differences and the corresponding formulation as according to what is seen in *Apontamentos de Vibrações de Sistemas Mecânicos* [118]. In short, a parallel configuration will lead to a stiffer system, while a series configuration leads to a softer system.

The dissipative element is characterised by a damper with a damping coefficient c if viscous damping is considered. The force that acts on this element will be linearly proportional to the velocity seen in the damper's ends, as presented in Eq. 4.2 and visualised in Fig. 4.3. The units of the damping coefficient will then be N.s/m [118]:

$$F_c = c\left(\dot{x}_2 - \dot{x}_1\right). \tag{4.2}$$

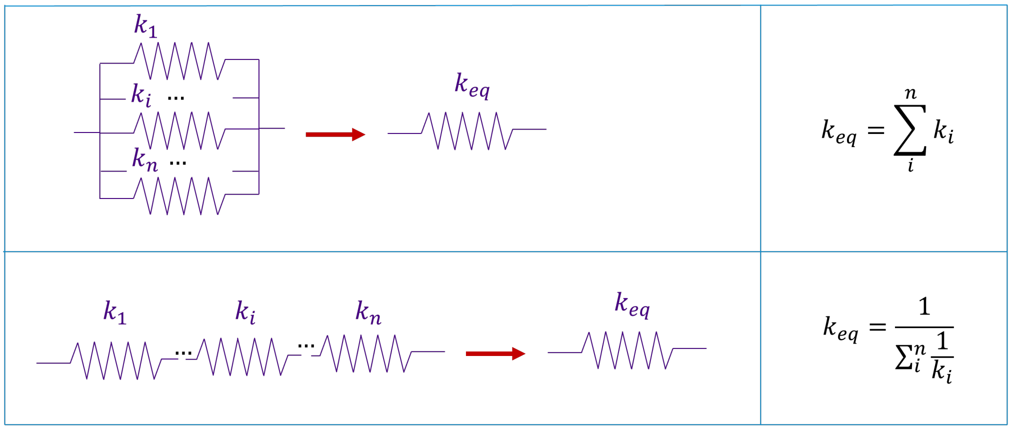

Fig. 4.2. Differences on spring assemblies.

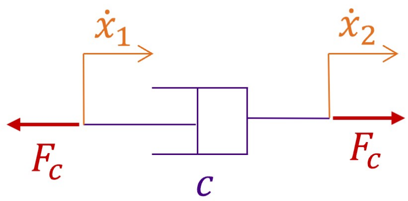

Fig. 4.3. Dissipative element representation.

Other and more complex springs and dampers exist to account for non-linear behaviours. Non-linear springs can be similarly represented as previously seen but the spring stiffness k will now be a function that depends on the spring's displacement. The spring can also, on some occasions, be of a complex nature to account for some dynamic effects. In rigorous form, spring stiffness of complex nature will be called an impedance, where damping is also accounted for. Likewise, different approaches to damping can be regarded, as more sources than viscous-origin damping exist.

The inertial element can be characterised either by a mass m or by an inertia J or even by both. The force that this element is responsible for can be quantified by Newton's second law seen in Eq. 4.3 [118]:

$$F_m = m\ddot{x}. \tag{4.3}$$

Any mechanical system can be transformed into a physical system composed of equivalent dynamic quantities. The dynamic system that is equivalent to the mechanical system will then be fully defined with the quantification of the mass/inertia, damping coefficient, and spring stiffness. The analysis of the vibrations is then performed by writing the mathematical model that defines the system's motion. Through different theorems, such as the d'Alembert principle, or energy methods, such as Hamilton's principle, it is possible to solve the obtained differential equations of motion. Analytical or numerical methods can be used to solve these equations [118].

According to the desired results, a linearization may be required or, at least, recommended. For modal properties analysis, i.e., vibrations analysis, a linearization is required. This may mean, in some cases, that an iterative process will also be required.

Considering one degree of freedom system on a free regime after an impulsive load, different basic quantities can be defined. The undamped natural frequency is an important quantity of a dynamic system. The undamped natural frequency will be given by Eq. 4.4, where the stiffness k and mass m are the equivalent properties of the elastic and inertial elements of the system. In terms of damping, a damping ratio can be defined as seen in Eq. 4.5. The critical damping coefficient c_c, defined in Eq. 4.6, determines the minimum damping at which the system does not oscillate after an impulsive excitation. This means that for damping ratios below the unity, the response to an impulse will be of an oscillatory motion until an equilibrium state is reached; if a damping ratio bigger than one is considered, the response will rapidly tend to the equilibrium state. The damping coefficient c will be the equivalent property of the viscous dissipative element of the system. Then, if damping is considered, a damped natural frequency can be defined as seen in Eq. 4.7 [118].

$$\omega_n = \sqrt{\frac{k}{m}} \tag{4.4}$$

$$\zeta = \frac{c}{c_c} \tag{4.5}$$

$$c_c = 2m\omega_n \tag{4.6}$$

$$\omega_d = \omega_n\sqrt{1-\zeta^2} \tag{4.7}$$

The natural frequency of a structure can then change with modifications to its stiffness and mass. Very small changes can also happen if the structural damping is altered, as what is measured is a damped natural frequency. If an oscillatory response due to an impulsive load is measured, a relation can be reached regarding the oscillatory response period and the natural frequency. This relation is seen in Eq. 4.8. Likewise, a relation regarding the damping can be acquired using the notion of logarithmic decrement. For a single measured period, the relation between the logarithmic decrement and the damping ratio is as seen in Eq. 4.9. For several (N) periods, the formulation in Eq. 4.10 can be used [2, 118].

$$T = \frac{2\pi}{\omega_d} \tag{4.8}$$

$$\begin{gathered} \delta = \ln\left(\frac{x(t_1)}{x(t_2 = t_1 + T)}\right) = \zeta\omega_n T \rightarrow \\ \delta = \frac{2\pi\zeta}{\sqrt{1-\zeta^2}} \rightarrow \zeta = \frac{\delta}{\sqrt{(2\pi)^2+\delta^2}} \end{gathered} \tag{4.9}$$

$$\delta = \frac{1}{N}\ln\left(\frac{x(t_1)}{x(t_N = t_1 + N\cdot T)}\right) \tag{4.10}$$

4.2. Model definition

The dynamic behaviour of a structure can be characterised by its modal parameters, which can be obtained analytically or numerically. For simple structures, such as constant cross-section beams, analytical solutions exist or can be developed. For complex structures, as an OWT, numerical solutions have to be developed, where the division of the structure into a distinct number of elements can be considered. A number of limitations arise from the numerical approach, where experimental modal analysis is able to validate and improve such an approach. Based on these considerations, a simple model is developed [31].

A series of different decisions have to be taken before modelling the structure, from what beam theory should be adopted and general coordinate system possibilities to what solution method should be employed and shape functions utilization. The model developed and presented here is comprised of a simple finite element approach. However, it does not resort to in-depth finite element considerations of body discretisation as common FEM analyses on this subject do. The main goal of this model development is to reach a simplified model that can capture the soil reaction actuating on the structure, giving a representation of the structure with fewer degrees of freedom than what is usual.

Gupta and Basu [40] stated that a complex soil nature should be assumed for a correct foundation representation, as to capture the dynamic behaviour of the structure due to cyclic and dynamic loading. However, as presented in that same work and already mentioned in the present work, running a dynamic analysis is significantly more computationally costly than a static problem. The difference in the results does not tend to be that different for low frequencies. Being the developed model a simplified approach to the OWT problem, static-like springs will be considered with parallel dashpots.

The p-version finite elements are imposed for use in this model development. This finite element version allows the consideration of fewer elements while achieving good displacement compliance. As such, it is the ideal version to obtain a reduction in the degrees of freedom while maintaining the same response accuracy. As every investigation concentrates its efforts using h-version finite elements, this consists of a new approach on OWT simulation.

The h-version finite elements consist of increasing the number of simple elements to increase the model precision. Meanwhile, the p-version finite elements consist of increasing the number of shape functions through the elements.

FEMs can allow high accuracy results to be obtained. Stoykov and Ribeiro [101] stated that sometimes non-linear models have to be developed due to the insufficiency of linear theories to predict the displacements accurately. Consequently, non-linear equations of motion have to be solved by iterative methods, demanding elevated computational effort with h-version finite elements [119].

The p-version finite elements are not prone to locking phenomena (allows the study of thick and thin structures), fewer degrees of freedom can be used without compromising the accuracy of the results, and the mesh is kept constant. The utilization of this version of the finite element also reduces problems due to inter-element discontinuities. Better strain and stress fields can be obtained using p-version finite elements than using h-version finite elements [119, 120].

A common simplification consists of modelling the wind turbine's problems as a Single Degree of Freedom (SDOF), while assuming a concentrated mass at the top of the wind turbine's tower. Calculation errors are, nevertheless, expected, since the majority of simplified approaches do not account for the tapered nature of wind turbines when predicting their natural frequencies. Common errors in SDOF models are the consideration of a higher mass density of the structure to account for different in-tower components and the poor estimation of an equivalent diameter for the tower. A simple calibration procedure could be a possibility to reduce these errors. Further simplifications regarding the foundation flexibility and substructure of OWTs have been performed that increase the error of common SDOF models seen in the literature. Even using linear approximations of the tower's moment of inertia and area leads to considerable errors. These models also do not account for differences in the RNA (inertia moment anisotropy), resulting in only one 1st mode natural frequency instead of two close frequencies (the fundamental natural frequency in the fore-aft and side-side directions). Ko [30] pointed out that attention should be given when applying SDOF models [3, 28, 30].

The model developed will consider a single plane, presenting a slight complexity when compared with SDOF models, but without the difficulties faced by common finite elements and other multi-plane models. However, similar considerations can be taken into consideration as only one element will be considered to represent the whole structure.

Although common underestimation is obtained using the Winkler approach, this approach will be used for the present model development. As common *p-y* curves do not consider the influence of a wide selection of factors that alter the soil stiffness, an attempt to include some of these in a different Winkler approach will take place. A small-strain approach to the soil stiffness was considered, as defended by Burd et al. [107] in their work.

4.2.1 Beam theory

Different beam theories can be considered when modelling. The most common theories are Euler-Bernoulli and Timoshenko. Throughout the literature, in terms of efficiency between accuracy and computational cost, the Euler-Bernoulli is seen as the best choice. Yet, there is no consensus in the beam theory selection, as literature still uses both theories, even when knowing that the Euler-Bernoulli might be a more cost-efficient approach. Gupta et al. [40] studied these beam theories and concluded that the Euler-Bernoulli theory is a beam theory that leads to good natural frequencies accuracy with limited computational cost. [40].

The Timoshenko theory includes the effect of shear deformation and rotatory inertia of the beam cross-section. The shear correction factor can influence the natural frequencies of the beam, as different formulations exist to account for the non-uniform shear stress distribution within the beam cross-section. Burd et al. [107] used the Timoshenko theory to make sure that the PISA design model included the influence of shear strains on the overall pile deformation, maintaining a robust method [40, 120].

The Timoshenko beam theory was considered for the present model development since small differences are noted regarding the computational time between these two beam theories when static loading is considered and to make sure all deformation effects bending related seen in the structure are included. A longitudinal displacement component will also be admitted, as Jia [96] states that axial forces applied on the structure can affect its lateral behaviour.

4.2.2 Coordinates

Using a general element coordinate referential that has its origin in a given point within the element, three coordinates are defined: one in the longitudinal direction (x_1) and two in the transversal direction (x_2 and x_3). Using the common simplification seen in the literature of a single plane approach, as well as considering a Timoshenko beam element, the displacements considering these coordinates will be represented in a different set of variables, seen in Eq. 4.11, that are independent of the x_2 and x_3 coordinates. Fig. 4.4 presents the admitted coordinate referential.

$$\begin{cases} u_1^g(x_1,x_3,t) = u_1(x_1,t) + x_3 \cdot \theta(x_1,t) \\ u_2^g(x_1,x_3,t) = 0 \\ u_3^g(x_1,x_3,t) = u_3(x_1,t) \end{cases} \tag{4.11}$$

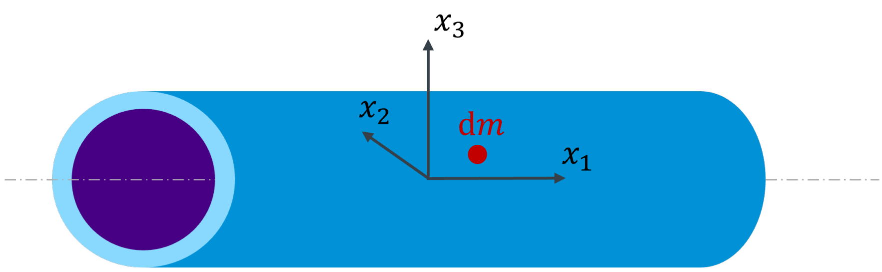

Fig. 4.4. Admitted coordinate referential.

4.2.3 Shape functions

As presented in previous work of Ribeiro (Refs. [119] and [120]), different shape functions are usually employed for different coordinates. However, considering a model with several finite elements, to impose shape function continuity, the same shape functions are proposed for the current problem. The shape function continuity allows displacement and force continuity between different elements. The shape function family f allows this continuity. In alternative, but not allowing the same degree of continuity (continuity only exists displacement-wise), the shape function family g can be used.

Using the representation of **ff** to mean the shape function vector, either considering the shape function family f or g, Eq. 4.12 presents the definition of the local displacements in order to the generalised coordinates. Different vector lengths are possible using this formulation with p-version finite elements, allowing bigger flexibility in the convergence study.

$$\begin{cases} u_1(x_1,t) = \mathbf{ff}_{u_1}^{\mathrm{T}}(x_1) \cdot \mathbf{q}_{u_1}(t) \\ u_3(x_1,t) = \mathbf{ff}_{u_3}^{\mathrm{T}}(x_1) \cdot \mathbf{q}_{u_3}(t) \\ \theta(x_1,t) = \mathbf{ff}_{\theta}^{\mathrm{T}}(x_1) \cdot \mathbf{q}_{\theta}(t) \end{cases} \tag{4.12}$$

It is important to note that the shape functions will be dependent on the longitudinal coordinate x_1, while the generalised coordinate will only be time-dependent. This decomposition of the local coordinates allows algorithm simplification, as time and spatial integration can be separated. The utilization of shape functions also allows an easy transition from individual equations of motion to a representation in matrix form.

4.3. Virtual Work Implementation

The virtual work principle states that the summation of the virtual work performed by all forces applied to a body, including inertia forces, will be zero. The formulation can be seen as the summation between the virtual work provided by inertial, internal and external forces. Eq. 4.13 presents the general equation that represents this principle:

$$\delta W_e + \delta W_i + \delta W_j = 0. \tag{4.13}$$

The several integrals that are presented can be solved using numerical integration methods. As the present work elaborated a Matlab script to implement the developed model, these integrals were performed using Matlab capabilities.

4.3.1 Inertial forces virtual work

The inertial virtual work, represented as δW_j, can be presented as seen in Eq. 4.14. Using previous considerations regarding the Timoshenko beam theory, the Eq. 4.15 can be reached. By applying Eq. 4.12, the structural mass matrix in each displacement component can be obtained. These matrices are presented in Eqs. 4.16 to 4.18, where:

- $\mathbf{M}_{u_1}$ is the structural mass associated with u_1;
- $\mathbf{M}_{u_3}$ is the structural mass associated with u_3;
- $\mathbf{M}_{\theta}$ is the structural mass associated with θ.

$$\delta W_j = -\int_V \rho \left(\delta u_1^g \ddot{u}_1^g + \delta u_2^g \ddot{u}_2^g + \delta u_3^g \ddot{u}_3^g\right) \mathrm{d}V \tag{4.14}$$

$$\delta W_j = -\int_{x_1} \int_S \rho \left(\delta u_1 \ddot{u}_1 + \delta u_3 \ddot{u}_3 + x_3^2 \delta \theta \ddot{\theta}\right) \mathrm{d}S \mathrm{d}x_1 \tag{4.15}$$

$$\delta \mathbf{q}_{u_1} \cdot \left[\int_{x_1} \int_S \rho \cdot \mathbf{ff}_{u_1}(x_1) \cdot \mathbf{ff}_{u_1}^{\mathrm{T}}(x_1) \mathrm{d}S \mathrm{d}x_1\right] \cdot \ddot{\mathbf{q}}_{u_1} = \delta \mathbf{q}_{u_1} \cdot \mathbf{M}_{u_1} \cdot \ddot{\mathbf{q}}_{u_1} \tag{4.16}$$

$$\delta \mathbf{q}_{u_3} \cdot \left[\int_{x_1} \int_S \rho \cdot \mathbf{ff}_{u_3}(x_1) \cdot \mathbf{ff}_{u_3}^{\mathrm{T}}(x_1) \mathrm{d}S \mathrm{d}x_1\right] \cdot \ddot{\mathbf{q}}_{u_3} = \delta \mathbf{q}_{u_3} \cdot \mathbf{M}_{u_3} \cdot \ddot{\mathbf{q}}_{u_3} \tag{4.17}$$

$$\delta \mathbf{q}_{\theta} \cdot \left[\int_{x_1} \int_S \rho \cdot x_3^2 \cdot \mathbf{ff}_{\theta}(x_1) \cdot \mathbf{ff}_{\theta}^{\mathrm{T}}(x_1) \mathrm{d}S \mathrm{d}x_1\right] \cdot \ddot{\mathbf{q}}_{\theta} = \delta \mathbf{q}_{\theta} \cdot \mathbf{M}_{\theta} \cdot \ddot{\mathbf{q}}_{\theta} \tag{4.18}$$

As the surrounding mass around the structure has to be accelerated as well, a similar approach considering an equivalent mass can be employed. This is relevant for the water around the pile, as well as for the water that resides within the pile. Likewise, the added mass due to water can be reached through the virtual work principle, as seen in Eq. 4.19 that sums Eqs. 4.20 and 4.21. However, as water is a fluid, no added mass in the longitudinal and rotational direction is considered. A proper fluid-structure interaction should be conducted for more precise results. Yet, the accuracy gained by considering such interaction does not compensate for the complexity introduced. As such, this equivalent added mass is managed by an empirical parameter, C_M [2].

$$\delta W_j^w = \delta W_j^{w_i} + \delta W_j^{w_e} \tag{4.19}$$

$$\delta W_j^{w_i} = -\int_{x_1}\int_{S_i} \rho_w \left(\delta u_1 \ddot{u}_1 + \delta u_3 \ddot{u}_3 + x_3^2 \delta\theta\ddot{\theta}\right) \mathrm{d}S\mathrm{d}x_1 \tag{4.20}$$

$$\delta W_j^{w_e} = -\int_{x_1}\int_{S_e} \rho_w \left(C_M - 1\right) \left(\delta u_1 \ddot{u}_1 + \delta u_3 \ddot{u}_3 + x_3^2 \delta\theta\ddot{\theta}\right) \mathrm{d}S\mathrm{d}x_1 \tag{4.21}$$

Other influences can be regarded, like marine growth and soil mass acceleration. In these cases, the only difference to the formulation seen for the structural mass resides in the mass density and area considered. Eqs. 4.22 to 4.30 reflect in matrix form all the mass matrices relevant for the main mass matrix of the system, including the added water mass, where:

- $\mathbf{M}_{u_3}^{w_i}$ is the added mass due to water inside the pile on the transversal direction;
- $\mathbf{M}_{u_3}^{w_e}$ is the added mass due to water around the pile on the transversal direction;
- $\mathbf{M}_{u_3}^{s_i}$ is the added mass due to soil inside the pile on the transversal direction;
- $\mathbf{M}_{u_3}^{s_e}$ is the added mass due to soil around the pile on the transversal direction;
- $\mathbf{M}_{\theta}^{s_i}$ is the added inertia due to soil inside the pile;
- $\mathbf{M}_{\theta}^{s_e}$ is the added inertia due to soil around the pile;
- $\mathbf{M}_{u_1}^{g}$ is the added mass due to marine growth on the longitudinal direction;
- $\mathbf{M}_{u_3}^{g}$ is the added mass due to marine growth on the transversal direction;
- $\mathbf{M}_{\theta}^{g}$ is the added inertia due to marine growth.

However, according to Asnaashari et al. [112], marine growth has a negligible effect on the natural frequencies. It was considered as well that the soil added mass can be included in a similar way to the formulation for water added mass.

$$\delta\mathbf{q}_{u_3} \cdot \left[\int_{x_1}\int_{S_i} \rho_w \cdot \mathbf{ff}_{u_3}(x_1) \cdot \mathbf{ff}_{u_3}^{\mathrm{T}}(x_1)\,\mathrm{d}S\mathrm{d}x_1\right] \cdot \ddot{\mathbf{q}}_{u_3} = \delta\mathbf{q}_{u_3} \cdot \mathbf{M}_{u_3}^{w_i} \cdot \ddot{\mathbf{q}}_{u_3} \tag{4.22}$$

$$\delta\mathbf{q}_{u_3} \cdot \left[\int_{x_1}\int_{S_e} \rho_w (C_M - 1)\,\mathbf{ff}_{u_3}(x_1) \cdot \mathbf{ff}_{u_3}^{\mathrm{T}}(x_1)\,\mathrm{d}S\mathrm{d}x_1\right] \cdot \ddot{\mathbf{q}}_{u_3} = \delta\mathbf{q}_{u_3} \cdot \mathbf{M}_{u_3}^{w_e} \cdot \ddot{\mathbf{q}}_{u_3} \tag{4.23}$$

$$\delta\mathbf{q}_{u_3} \cdot \left[\int_{x_1}\int_{S_i} \rho_s \cdot \mathbf{ff}_{u_3}(x_1) \cdot \mathbf{ff}_{u_3}^{\mathrm{T}}(x_1)\,\mathrm{d}S\mathrm{d}x_1\right] \cdot \ddot{\mathbf{q}}_{u_3} = \delta\mathbf{q}_{u_3} \cdot \mathbf{M}_{u_3}^{s_i} \cdot \ddot{\mathbf{q}}_{u_3} \tag{4.24}$$

$$\delta\mathbf{q}_{u_3} \cdot \left[\int_{x_1}\int_{S_e} \rho_s (C_M - 1)\,\mathbf{ff}_{u_3}(x_1) \cdot \mathbf{ff}_{u_3}^{\mathrm{T}}(x_1)\,\mathrm{d}S\mathrm{d}x_1\right] \cdot \ddot{\mathbf{q}}_{u_3} = \delta\mathbf{q}_{u_3} \cdot \mathbf{M}_{u_3}^{s_e} \cdot \ddot{\mathbf{q}}_{u_3} \tag{4.25}$$

$$\delta\mathbf{q}_{\theta} \cdot \left[\int_{x_1}\int_{S_i} \rho_s \cdot x_3^2 \cdot \mathbf{ff}_{\theta}(x_1) \cdot \mathbf{ff}_{\theta}^{\mathrm{T}}(x_1)\,\mathrm{d}S\mathrm{d}x_1\right] \cdot \ddot{\mathbf{q}}_{\theta} = \delta\mathbf{q}_{\theta} \cdot \mathbf{M}_{\theta}^{s_i} \cdot \ddot{\mathbf{q}}_{\theta} \tag{4.26}$$

$$\delta\mathbf{q}_{\theta} \cdot \left[\int_{x_1}\int_{S_e} \rho_s (C_M - 1) \cdot x_3^2 \cdot \mathbf{ff}_{\theta}(x_1) \cdot \mathbf{ff}_{\theta}^{\mathrm{T}}(x_1)\,\mathrm{d}S\mathrm{d}x_1\right] \cdot \ddot{\mathbf{q}}_{\theta} = \delta\mathbf{q}_{\theta} \cdot \mathbf{M}_{\theta}^{s_e} \cdot \ddot{\mathbf{q}}_{\theta} \tag{4.27}$$

$$\delta\mathbf{q}_{u_1} \cdot \left[\int_{x_1}\int_{S_g} \rho_g \cdot \mathbf{ff}_{u_1}(x_1) \cdot \mathbf{ff}_{u_1}^{\mathrm{T}}(x_1)\,\mathrm{d}S\mathrm{d}x_1\right] \cdot \ddot{\mathbf{q}}_{u_1} = \delta\mathbf{q}_{u_1} \cdot \mathbf{M}_{u_1}^{g} \cdot \ddot{\mathbf{q}}_{u_1} \tag{4.28}$$

$$\delta\mathbf{q}_{u_3} \cdot \left[\int_{x_1}\int_{S_g} \rho_g \cdot \mathbf{ff}_{u_3}(x_1) \cdot \mathbf{ff}_{u_3}^{\mathrm{T}}(x_1)\,\mathrm{d}S\mathrm{d}x_1\right] \cdot \ddot{\mathbf{q}}_{u_3} = \delta\mathbf{q}_{u_3} \cdot \mathbf{M}_{u_3}^{g} \cdot \ddot{\mathbf{q}}_{u_3} \tag{4.29}$$

$$\delta\mathbf{q}_{\theta} \cdot \left[\int_{x_1}\int_{S_g} \rho_g \cdot x_3^2 \cdot \mathbf{ff}_{\theta}(x_1) \cdot \mathbf{ff}_{\theta}^{\mathrm{T}}(x_1)\,\mathrm{d}S\mathrm{d}x_1\right] \cdot \ddot{\mathbf{q}}_{\theta} = \delta\mathbf{q}_{\theta} \cdot \mathbf{M}_{\theta}^{g} \cdot \ddot{\mathbf{q}}_{\theta} \tag{4.30}$$

As opposed to water, the soil is a solid comprised of fine particles. As such, it is expected to have some degree of resistance, especially when compressed, in terms of rotation. For this reason, an added mass in θ is also considered. Although the soil will also be accelerated in the longitudinal direction, the inertial effect can be regarded as negligible for a lateral studied problem. Consequently, it is safe to disregard the added soil mass in this direction. As for marine growth, this is a phenomenon that usually occurs linked to the structure, i.e., marine growth is a mass that is physically connected to the structure. Consequently, marine growth can be seen as an added mass in every direction. It does not introduce significant stiffness to the system.

To be possible to introduce these added masses, quantities should be defined in terms of their properties. According to Jia [2], the marine growth mass density is estimated as 1325 kg/m^3, where an average thickness t_g of 45 mm can be used. It is important to note that these quantities may and will vary according to the OWT location and with time. In relation to water mass density, according to the report of the International Towing Tank Conference [121], a value around 1027 kg/m^3 can be used. Resorting again to Jia's *Soil Dynamics and Foundation Modeling Offshore and Earthquake Engineering* [2], the added mass coefficient can be considered equal to two (2), if the KC number remains below five (5) and the Stokes number has a very high value, as it is expected for calm sea states.

Besides these distributed masses, localised/lumped masses can be considered too in this model. Eq. 4.31 presents the virtual work from a rigid body type of inclusion to the beam model. Components, such as the RNA, will be introduced to the model using this kind of approach. Eqs. 4.32 to 4.34 present the corresponding matrices, where:

- $\mathbf{M}_{u_1}^{LM}$ is the added lumped mass on the longitudinal direction;
- $\mathbf{M}_{u_3}^{LM}$ is the added lumped mass on the transversal direction;
- $\mathbf{M}_{\theta}^{LM}$ is the added lumped inertia.

$$\delta W_j^{LM} = -\int_{x_1} \delta\left(x_1 - x_1^i\right)\left\{m_i \cdot \left[\delta u_1 \ddot{u}_1 + \delta u_3 \ddot{u}_3\right] + J_i \cdot \delta\theta\ddot{\theta}\right\} \mathrm{d}x_1 \tag{4.31}$$

$$\mathbf{M}_{u_1}^{LM} = m_i \cdot \mathbf{ff}_{u_1}\left(x_1^i\right) \cdot \mathbf{ff}_{u_1}^T\left(x_1^i\right) \tag{4.32}$$

$$\mathbf{M}_{u_3}^{LM} = m_i \cdot \mathbf{ff}_{u_3}\left(x_1^i\right) \cdot \mathbf{ff}_{u_3}^T\left(x_1^i\right) \tag{4.33}$$

$$\mathbf{M}_{\theta}^{LM} = J_i \cdot \mathbf{ff}_{\theta}\left(x_1^i\right) \cdot \mathbf{ff}_{\theta}^T\left(x_1^i\right) \tag{4.34}$$

In some occurrences, a correction to the mass and inertia properties may be needed as the components are not located at a point within the analysed structure/beam, i.e., might have a given offset. For these, Steiner's theorem can be used. However, as points with absolute velocity will more certainly be considered, a small error will be carried out when only using Eq. 4.35, as given by the specified theorem (where x_i is the centre of mass of the contemplated rigid body). In other words, the direct application of this theorem in these applications is not entirely correct. Another term is introduced due to the relative movement of the structure and points considered, as can be regarded in a simple example using the energy approach presented below.

$$J_{x_{i+1}} = J_{x_i} + m_{x_i} \cdot \left(x_{i+1} - x_i\right)^2 \tag{4.35}$$

Assume that a clamped beam has a rigid body of mass m_G and inertia J_G at its free extremity, as seen in Fig. 4.5. With G being the centre of gravity of the rigid body and O the top of the beam, where $\bar{OG} = e$, the kinetic energy can be calculated by Eq. 4.36. Assuming that the rotation of the beam is given by θ and that it remains equal throughout the considered points, an estimation for the linear velocity of G can be reached (Eq. 4.37), leading to the kinetic energy seen in Eq. 4.38.

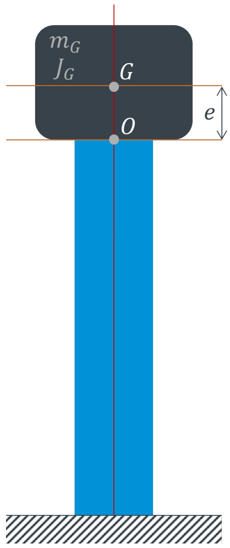

Fig. 4.5. Example of a clamped beam with a rigid body on its extremity.

$$T = \frac{1}{2} m_G \cdot v_G^2 + \frac{1}{2} J_G \cdot \dot{\theta}^2 \tag{4.36}$$

$$v_G \approx v_O + e \cdot \dot{\theta} \tag{4.37}$$

$$T = \frac{1}{2} m_G \cdot v_O^2 + m_G \cdot e \cdot v_O \cdot \dot{\theta} + \frac{1}{2} \left(J_G + m_G \cdot e^2 \right) \cdot \dot{\theta}^2 \tag{4.38}$$

An extra component ($m_G \cdot e \cdot v_O \cdot \dot{\theta}$) is then seen in the kinetic energy for the point O, which proves that another term is introduced if the point considered on the beam does not have null velocity. However, as the linear and angular velocities of the structure are not expected to be high, for simplicity's sake, this term is assumed to not play a significant part in this translation of rigid body properties. Although it is incorrect to apply Steiner's theorem directly, it is not expected to influence significantly the results obtained. Consequently, for the model developed, only Steiner's theorem is considered when acquiring the equivalent mass and inertia on the top of the wind turbine tower.

4.3.2 Internal forces virtual work

The internal virtual work, usually represented as δW_i, can be presented as seen in Eq. 4.39. Since the internal forces come from achieved deformations and consequent stresses, further considerations are needed. Eqs. 4.40 and 4.41 present the relations necessary to solve this issue and translate the Eq. 4.39 into the previous unknown variables (without defining new unknown variables).

$$\delta W_i = -\int_V (\delta\varepsilon_{x_1x_1} \cdot \sigma_{x_1x_1} + \delta\gamma_{x_1x_3} \cdot \tau_{x_1x_3})\,\mathrm{d}V \tag{4.39}$$

$$\begin{cases} \sigma_{x_1x_1} = E \cdot \varepsilon_{x_1x_1} \\ \tau_{x_1x_3} = \lambda \cdot G \cdot \gamma_{x_1x_3} \end{cases} \tag{4.40}$$

$$\begin{cases} \varepsilon_{x_1x_1} = \frac{\partial u_1}{\partial x_1} + x_3 \frac{\partial \theta}{\partial x_1} \\ \gamma_{x_1x_3} = \frac{\partial u_3}{\partial x_1} + \theta \end{cases} \tag{4.41}$$

After substituting the unknown quantities for their correspondent relation, it is possible to reach the structural stiffness. Special attention should be given to the λ parameter, known as the shear correction factor. Within the literature, different formulations exist to quantify this factor. According to Kaneko [122], the best shear correction factor for beams with a circular section is given by the formulation expressed in Eq. 4.42.

$$\lambda = \frac{6 + 12 \cdot \nu + 6 \cdot \nu^2}{7 + 12 \cdot \nu + 4 \cdot \nu^2} \tag{4.42}$$

The resulting stiffness matrices that come from the formulation of Eq. 4.39 are presented in Eqs. 4.43 to 4.48. These are denoted as:

- $\mathbf{K}_{u_1}^{E}$ is the structural stiffness due to the Young's modulus of the structure's material associated with u_1;
- $\mathbf{K}_{\theta}^{E}$ is the structural stiffness due to the Young's modulus of the structure's material associated with θ;
- $\mathbf{K}_{u_3}^{G}$ is the structural stiffness due to the shear modulus of the structure's material associated with u_3;
- $\mathbf{K}_{u_3\theta}^{G}$ is the structural stiffness due to the shear modulus of the structure's material associated with u_3 and θ;
- $\mathbf{K}_{\theta u_3}^{G}$ is the structural stiffness due to the shear modulus of the structure's material associated with θ and u_3;
- $\mathbf{K}_{\theta}^{G}$ is the structural stiffness due to the shear modulus of the structure's material associated with θ.

$$\delta\mathbf{q}_{u_1} \cdot \left[\int_{x_1}\int_S E \cdot \frac{\partial \mathbf{ff}_{u_1}(x_1)}{\partial x_1} \cdot \frac{\partial \mathbf{ff}_{u_1}^{\mathrm{T}}(x_1)}{\partial x_1} \mathrm{d}S\mathrm{d}x_1\right] \cdot \mathbf{q}_{u_1} = \delta\mathbf{q}_{u_1} \cdot \mathbf{K}_{u_1}^{E} \cdot \mathbf{q}_{u_1} \tag{4.43}$$

$$\delta\mathbf{q}_{\theta} \cdot \left[\int_{x_1}\int_S E \cdot x_3^2 \cdot \frac{\partial \mathbf{ff}_{\theta}(x_1)}{\partial x_1} \cdot \frac{\partial \mathbf{ff}_{\theta}^{\mathrm{T}}(x_1)}{\partial x_1} \mathrm{d}S\mathrm{d}x_1\right] \cdot \mathbf{q}_{\theta} = \delta\mathbf{q}_{\theta} \cdot \mathbf{K}_{\theta}^{E} \cdot \mathbf{q}_{\theta} \tag{4.44}$$

$$\delta\mathbf{q}_{u_3} \cdot \left[\int_{x_1}\int_S \lambda G \cdot \frac{\partial \mathbf{ff}_{u_3}(x_1)}{\partial x_1} \cdot \frac{\partial \mathbf{ff}_{u_3}^{\mathrm{T}}(x_1)}{\partial x_1} \mathrm{d}S\mathrm{d}x_1\right] \cdot \mathbf{q}_{u_3} = \delta\mathbf{q}_{u_3} \cdot \mathbf{K}_{u_3}^{G} \cdot \mathbf{q}_{u_3} \tag{4.45}$$

$$\delta \mathbf{q}_{u_3} \cdot \left[\int_{x_1} \int_S \lambda G \cdot \frac{\partial \mathbf{ff}_{u_3}(x_1)}{\partial x_1} \cdot \mathbf{ff}_\theta^{\mathrm{T}}(x_1)\, \mathrm{d}S \mathrm{d}x_1 \right] \cdot \mathbf{q}_\theta = \delta \mathbf{q}_{u_3} \cdot \mathbf{K}^G_{u_3\theta} \cdot \mathbf{q}_\theta \tag{4.46}$$

$$\delta \mathbf{q}_\theta \cdot \left[\int_{x_1} \int_S \lambda G \cdot \mathbf{ff}_\theta(x_1) \cdot \frac{\partial \mathbf{ff}^{\mathrm{T}}_{u_3}(x_1)}{\partial x_1} \mathrm{d}S \mathrm{d}x_1 \right] \cdot \mathbf{q}_{u_3} = \delta \mathbf{q}_\theta \cdot \mathbf{K}^G_{\theta u_3} \cdot \mathbf{q}_{u_3} \tag{4.47}$$

$$\delta \mathbf{q}_\theta \cdot \left[\int_{x_1} \int_S \lambda G \cdot \mathbf{ff}_\theta(x_1) \cdot \mathbf{ff}_\theta^{\mathrm{T}}(x_1)\, \mathrm{d}S \mathrm{d}x_1 \right] \cdot \mathbf{q}_\theta = \delta \mathbf{q}_\theta \cdot \mathbf{K}^G_\theta \cdot \mathbf{q}_\theta \tag{4.48}$$

Relevant to note that coupling will occur as seen in Eqs. 4.46 and 4.47.[1] The nature of this coupling is related to the bending phenomenon of the structure, relating the displacement u_3 with θ.

4.3.3 External forces virtual work

There are several external forces that can be regarded as acting on the structure. Main external forces come from soil reactions and forces that are interlinked with damping effects. As such, the virtual work can be separated in soil reaction forces and dissipative forces. It was considered that no significant sea current loads are present and that the hydrostatic water pressure is applied around all the perimeter of the monopile, producing a zero-net force.

Soil reaction forces

If a section of the foundation/monopile is considered at a given depth, the generalised position of the spring that replaces the surrounding soil can be defined as presented in Fig. 4.6. The Figure considers a displacement u_3 in the x_3 direction, while φ is assumed as starting from the x_2 axis.

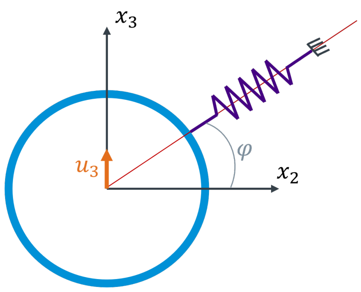

Fig. 4.6. Cross-section consideration of soil reaction.

If a force in the x_3 direction is applied, it is expected that only a portion of the surrounding soil will act to oppose the acting force. As such, only half of the pile (equivalent to say $0 \leq \varphi \leq \pi$) will actively oppose this loading in a simplified approach. Assuming that the soil will react in the normal direction of the monopile, the continuum spring load for a given cross-section of the monopile will be given by Eq. 4.49. The virtual work provided by this external force is given by Eq. 4.50.

$$\mathrm{d}F_k = -k_s \cdot u_3 \sin \varphi \tag{4.49}$$

[1]It's pertinent to note that one matrix will be the transpose of the other.

$$\delta W_e = -\int_0^{\pi} \int_{x_1} \delta u_3 \cdot k_s \cdot u_3 \sin^2(\varphi) \cdot R_{ext} \mathrm{d}x_1 \mathrm{d}\varphi \tag{4.50}$$

The spring stiffness, known as k_s, is defined as a force per volume (N/m^3) and it represents an equivalent stiffness. This equivalent stiffness means that different representations and considerations can be regarded in the stiffness formulation. It was also assumed that the modelled springs will deform a quantity Δl equal to $u_3 \cdot \sin\varphi$. As such, the soil resistance as an added stiffness in matrix form, $\mathbf{K}_s$, can be observed in Eq. 4.51.

$$\delta \mathbf{q}_{u_3} \cdot \left[\int_0^{\pi} \int_{x_1} k_s \cdot \sin^2(\varphi) \cdot R_{ext} \cdot \mathbf{ff}_{u_3}(x_1) \cdot \mathbf{ff}_{u_3}^{\mathrm{T}}(x_1) \, \mathrm{d}x_1 \mathrm{d}\varphi \right] \cdot \mathbf{q}_{u_3} = \delta \mathbf{q}_{u_3} \cdot \mathbf{K}_s \cdot \mathbf{q}_{u_3} \tag{4.51}$$

As Versteijlen et al. [27] state in their work, it is incorrect to consider an initial stiffness of soil representing springs without taking into account the geometry of the pile. As the springs represent the interaction between the soil and the structure, modelling the soil springs as independent from the pile geometry will lead to non-real results. The same author stresses out the importance of the stiffness from the shallow layers. According to Jiang and Lin [19], the maximum depth to which one can consider a given layer as shallow is 2.5 times the pile diameter. It is expected, as it was presented in Chapter 3, that their stiffness will greatly influence the natural frequencies of the structure. The formulated proposals for soil modelling will be presented in Chapter 5.

Although other soil reaction components take important roles on the global soil reaction acting on the pile, as documented in the PISA project, only a lateral reaction was considered in the present work due to available data and simplification. If more information can be gathered and validated in this regard, these soil reaction components should be considered and modelled.

Dissipative forces

Structural damping

Structural damping can be defined by a loss factor, η. Some literature mentions common values for structural material loss factors. Eq. 4.52 presents the relation found in *Introduction to Finite Element Vibration Analysis* [123], where a division by the frequency is necessary to allow a constant damping matrix. The variables associated are denoted as:

- $\mathbf{C}_{u_1}$ is the structural damping associated with u_1;
- $\mathbf{C}_{u_3}$ is the structural damping associated with u_3;
- $\mathbf{C}_{u_3\theta}$ is the structural damping associated with u_3 and θ;
- $\mathbf{C}_{\theta u_3}$ is the structural damping associated with θ and u_3;
- $\mathbf{C}_{\theta}$ is the structural damping associated with θ.

$$\mathbf{C}_{struc} = \begin{bmatrix} \mathbf{C}_{u_1} & \mathbf{0} & \mathbf{0} \\ \mathbf{0} & \mathbf{C}_{u_3} & \mathbf{C}_{u_3\theta} \\ \mathbf{0} & \mathbf{C}_{\theta u_3} & \mathbf{C}_{\theta} \end{bmatrix} = \frac{\eta}{\omega} \begin{bmatrix} \mathbf{K}_{u_1}^E & \mathbf{0} & \mathbf{0} \\ \mathbf{0} & \mathbf{K}_{u_3}^G & \mathbf{K}_{u_3\theta}^G \\ \mathbf{0} & \mathbf{K}_{\theta u_3}^G & \mathbf{K}_{\theta}^E + \mathbf{K}_{\theta}^G \end{bmatrix} \tag{4.52}$$

Cook [124] used a loss factor (η) of 0.0047 for steel structures, while Damgaard et al. [13] mentioned a value of 0.01 for steel monopiles. These values are within or very close to the limits mentioned for steel structures in *Structural Vibration: Analysis and Damping* [125]. As the damping matrix will depend on the frequency, a given frequency should be defined to quantify the structural damping matrix. As the first natural frequencies are the main concern, the damping matrix will be constructed to consider an early estimation of the first natural frequency.

According to Damgaard et al. [31], a change in temperature can alter the natural frequencies of the system. As temperature changes, a change on the mechanical properties of the structure also occurs. A change in 5% was stated to happen in very extreme conditions (variation of more than 150 ºC), leading to a variation of 0.5% in the fundamental frequency of the structure. The influence in damping was even smaller and depicted as insignificant. Thus, this influence factor will not be considered further.

If a tuner mass damper exists in the tower, further considerations should be devised. However, usually, in full-scale tests, these devices are turned off. If this is not the case, further considerations comprising a dynamic system with an additional degree of freedom should be considered to include the damping of this device.

Soil radiation damping

In a similar fashion to what was seen with the soil stiffness considerations, only half of the monopile is assumed to be subjected to the soil damping phenomena. Likewise, the damping force will act in a normal direction to the pile's surface, leading to the formulation seen in Eq. 4.53. Eqs. 4.54 and 4.55 present the external virtual work produced by this force and its representation in matrix form, $\mathbf{C}_s^{rad}$.

$$\mathrm{d}F_c^{rad} = -c_s^{rad} \cdot \dot{u}_3 \sin\varphi \tag{4.53}$$

$$\delta W_e = -\int_0^{\pi} \int_{x_1} \delta u_3 \cdot c_s^{rad} \cdot \dot{u}_3 \sin^2\varphi \cdot R_{ext} \mathrm{d}x_1 \mathrm{d}\varphi \tag{4.54}$$

$$\boldsymbol{\delta}\mathbf{q}_{u_3} \cdot \left[\int_0^{\pi} \int_{x_1} c_s^{rad} \cdot \sin^2\varphi \cdot R_{ext} \cdot \mathbf{ff}_{u_3}(x_1) \cdot \mathbf{ff}_{u_3}^{\mathrm{T}}(x_1) \, \mathrm{d}x_1 \mathrm{d}\varphi \right] \cdot \dot{\mathbf{q}}_{u_3} = \boldsymbol{\delta}\mathbf{q}_{u_3} \cdot \mathbf{C}_s^{rad} \cdot \dot{\mathbf{q}}_{u_3} \tag{4.55}$$

According to Badoni and Makris [63], the soil radiation damping coefficient, c_s^{rad} can be given through the shear wave velocity influencing parameters. For the interest of the current work, the damping coefficient should be a quantity per unit of area [N.s/m^3]. As such, the expression from Ref. [63] was divided by the total embedded length of the pile and the pile half diameter, as seen in Eq. 4.56. The coefficient Q, dimensionless frequency a_0, and shear wave velocity of the soil can all be obtained by using the expressions present in Appendix A. The damping coefficient expression is similar to the one analytically developed by Gazetas and Dobry [126] for flexible piles embedded in layered soils.

$$c_s^{rad} = Q \cdot a_0 \cdot \rho_s V_s \frac{2d}{L_{embedded}\pi d} \tag{4.56}$$

According to Shirzadeh et al. [28] and Damgaard et al. in Refs. [31] and [13], there are several studies on the fact that no significant influence comes from radiation damping for frequencies below 1 Hz. Still, a damping ratio value of 0.12% is regularly presented as a reference for a pile diameter of 4.7 meters, water depth of 20 meters and a fundamental frequency of 0.3 Hz.

Soil hysteretic damping

The same assumption as before maintains for the current case. Eq. 4.57 presents the force considered. Eqs. 4.58 and 4.59 present the external virtual work produced by this force and its representation in matrix form, $\mathbf{C}_s^{hys}$.

$$\mathrm{d}F_c^{hys} = -c_s^{hys} \cdot \dot{u}_3 \sin\varphi \tag{4.57}$$

$$\delta W_e = -\int_0^{\pi} \int_{x_1} \delta u_3 \cdot c_s^{hys} \cdot \dot{u}_3 \sin^2\varphi \cdot R_{ext} \mathrm{d}x_1 \mathrm{d}\varphi \tag{4.58}$$

$$\delta \mathbf{q}_{u_3} \cdot \left[\int_0^{\pi} \int_{x_1} c_s^{hys} \cdot \sin^2\varphi \cdot R_{ext} \cdot \mathbf{ff}_{u_3}(x_1) \cdot \mathbf{ff}_{u_3}^{\mathrm{T}}(x_1) \, \mathrm{d}x_1 \mathrm{d}\varphi \right] \cdot \dot{\mathbf{q}}_{u_3} = \delta \mathbf{q}_{u_3} \cdot \mathbf{C}_s^{hys} \cdot \dot{\mathbf{q}}_{u_3} \tag{4.59}$$

The soil hysteretic damping can be defined by using the definition of the loss factor, η_s, in a similar way to what was seen previously. According to Malekjafarian et al. [23], the loss factor can be related to a damping coefficient, c_s^{hys}, through Eq. 4.60. For the interest of the current work, the damping coefficient c_s^{hys} should be a quantity per unit of area [N.s/m^3]. As such, the expression from Ref. [23] was divided by the total embedded length of the pile.

$$c_s^{hys} = 2 \cdot \zeta_s \frac{G_s}{\omega \cdot L_{embedded}} \tag{4.60}$$

The soil damping ratio ζ_s can be obtained through empirical values in a work performed by Darendeli [70] on that matter. That author studied a variable amount of different soils, from sand to clay, and formulated a damping variation with strain. It is recommended to use the minimum value of those presented in that work, considering an effective vertical pressure of 1 atmosphere. As such, a minimum soil damping ratio of 0.8% is set. This recommendation is provided to avoid an overestimation of the soil damping.

Alternatively, the HSsmall model presents a definition of soil hysteretic damping for small-strain. This definition directly gives the soil damping ratio and is given as the ratio between the energy dissipated in a load cycle (E_D) by the energy stored at a maximum strain equal to the cyclic amplitude strain (E_s), as possible to observe in Eq. 4.61 [116].

$$\zeta_s = \frac{E_D}{4\pi E_S} \tag{4.61}$$

$$E_D = \frac{4G_0\gamma_{0.7}}{0.385} \left[2\gamma_c - \frac{\gamma_c}{1 + \frac{\gamma_{0.7}}{0.385\gamma_c}]} - \frac{2\gamma_{0.7}}{0.385} \ln\left(1 + \frac{0.385\gamma_c}{\gamma_{0.7}}\right) \right] \tag{4.62}$$

$$E_S = \frac{G_0\gamma_c^2}{2 + \frac{2 \cdot 0.385\gamma_c}{\gamma_{0.7}}} \tag{4.63}$$

Difficulties in quantifying the strain that one could encounter in the model exist. Gazetas and Dobry [126] proposed a strain-displacement relation on their work that helps overcome these difficulties. This relation makes it possible to write the cyclic strain γ_c

in function of the lateral displacement u_3, as seen in Eq. 4.64. However, the utilization of such a relation would lead to an iterative algorithm, demanding further computational cost. For this reason, this approach is not recommended for a simple model application.

$$\gamma_c(x_1) = \frac{1+\nu_s}{2.5d} u_3(x_1) \tag{4.64}$$

According to Damgaard et al. [31], as this source of damping results from the dissipation of energy by slippage of grains, this phenomenon is frequency independent. Consequently, for a given deformation (soil strain), this damping source can be approximated to an equivalent material viscosity. This represents another approach on this subject.

Soil seepage damping

Soil seepage damping is a form of damping that will not be considered in this work. As little information regarding it was found and as small-strain will be considered in the formulation of the analysed problem, this type of damping will be disregarded.

Water radiation damping

Johanning [127] presented a set of equations to define the hydrodynamic damping of a large-scale surface piercing circular cylinder. Taking these equations into account for the current work, Eq. 4.65 can be considered as an estimation for the damping coefficient due to wave radiation, c_w^{rad}. As a consequence, a concentrated instead of a distributed damping force should be admitted. This implies the utilization of a Dirac function that will be one when $x_1 = x_1^p$. Eq. 4.66 represents the damping matrix $\mathbf{C}_w^{rad}$ expected. The presented expression results from equalling the dissipated energy with the energy over a cycle if the structure oscillation is harmonic. This approach is similar to what was seen in Eq. 4.61.

$$c_w^{rad} = \frac{8\omega_n \rho_w R_{ext}^3 \sinh\left(k_o L_{submerged}\right)}{\sinh\left(2k_o L_{submerged}\right) + 2k_o L_{submerged}} \frac{\left(e^{-i\nu} \cdot \mathrm{H}(k_o R_{ext})\right)^2}{k_o R_{ext}} \tag{4.65}$$

$$\mathbf{C}_w^{rad} = c_w^{rad} \left[\int_{x_1} \delta\left(x_1 - x_1^p\right) \mathbf{ff}_{u_3}(x_1) \cdot \mathbf{ff}_{u_3}^{\mathrm{T}}(x_1)\, \mathrm{d}x_1\right] \tag{4.66}$$

Using this approach by Johanning [127], besides using a Hankel function (which uses Bessel functions for its definition), introduces the utilization of a number named as wave number k_o. This wave number can be estimated. Appendix B presents the approach used to obtain the wave number, admitting that the wave period is between 6 and 10 seconds [2], and a water depth between 20 and 30 meters.

According to Haslum [128], hydrodynamic radiation for a calm sea state (long wave periods) can be safely disregarded. Even for short wave periods, the radiation component of the hydrodynamic damping is not of much importance. According to Kementzetzidis et al. [10], wave radiation can be disregarded for frequencies lower than 1 Hz (similar to what was presented for soil radiation damping). A damping ratio, however, can be taken into account. According to References [28], [31], and [39], the wave radiation damping

[2]These values were seen as calm sea state wave periods, as consulted from WindFinder on the final days of June 2022.

ratio is expected to fall between 0.11% and 0.24%. One should notice that the uncertainty around these values is considerable. A damping ratio of 0.12% can be taken for the rest of the present analysis.

Water viscous damping

The same assumption as the one performed for the soil is done here. Considering that the damping force will act in a normal direction to the pile's surface, a similar virtual work equation can be reached. Eq. 4.67 shows the matrix form regarding the water viscous damping, $\mathbf{C}_w^{vis}$.

$$\delta\mathbf{q}_{u_3}\cdot\left[\int_0^{\pi}\int_{x_1} c_w^{vis}\cdot\sin^2\varphi\cdot R_{ext}\cdot\mathbf{ff}_{u_3}(x_1)\cdot\mathbf{ff}_{u_3}^T(x_1)\mathrm{d}x_1\mathrm{d}\varphi\right]\cdot\dot{\mathbf{q}}_{u_3}=\delta\mathbf{q}_{u_3}\cdot\mathbf{C}_w^{vis}\cdot\dot{\mathbf{q}}_{u_3} \tag{4.67}$$

The usual expression in literature for the water viscous damping coefficient c_w^{vis} is given by Eq. 4.68, as seen in the work of Chen and Duffour [39]. Attention should be given to the fact that the resulting damping coefficient is N.s/m. However, difficulties in defining the root mean of the relative speed between the water wave-particle and the pile (σ_r) and the modal shape (φ) in advance. Consequently, an alternative expression is suggested. The Eq. 4.69 is based on the proposed equation by Tao and Cai [129], where their equation was divided by the total submerged length of the pile and the pile half perimeter to reach a damping coefficient that consists of a quantity per unit of area [N.s/m^3]. The assumed expression results from an equivalence between Morison's equation and an alternative expression that relates the drag force by using an equivalent linear damping coefficient c_w^{vis}, where a pile-like structure (spar with heave plate) is considered.

$$c_w^{vis}=\int_{x_1}\frac{1}{2}\rho_w\cdot\frac{d}{L_{submerged}}\cdot C_d\sqrt{\frac{8}{\pi}}\sigma_r(x_1)\cdot\phi^2(x_1)\mathrm{d}x_1 \tag{4.68}$$

$$c_w^{vis}=\frac{1}{3}\cdot\mu_w\cdot\beta_{Stokes}\cdot\frac{2d}{L_{submerged}\pi d}\cdot KC\cdot C_d \tag{4.69}$$

Chen and Duffour [39] observed that no significant influence came from the varying drag coefficient C_d. As such, in order to simplify the problem, and remove a nonlinear dependence from the damping, a fixed value for the drag coefficient of 0.74 is considered (according to the drag coefficient for a cylindrical rod perpendicular to the flow with an aspect ratio *L/d* of 5, present in *Applied Fluid Dynamics Handbook* [130]).

As the Keulegan-Carpenter number (*KC*) depends on the relative speed between the water wave-particle and the structure, a fixed KC value is suggested for simplification. According to Chen and Duffour [39], for large diameter monopiles submerged in water, the KC number expected will be low (around 10^-2), while the Stokes parameter will be large. A value less than five (5) is imposed. It is important to state that a low KC is associated with inertia-dominated forces, while high KC values are associated with notable drag-related forces. In Appendix B, it can be seen a formulation to define this dimensionless number. In the same Appendix, a formulation for the Stokes number can also be found. Using the same wave characteristics stated before for the water radiation damping and assuming a maximum wave height of 2.1 meters [3], a value near $2\cdot10^{-2}$ for

[3]Value equivalent to 50% more than seen in very calm days, as consulted from WindFinder on the final days of June 2022.

KC is obtained.

According to Chen and Duffour [39], the overall water/hydrodynamic damping can be disregarded. As OWTs' size increases, the damping ratio associated to this damping source decreases significantly. According to Shirzadeh et al. [28], the water viscous-origin damping will have less influence than the water radiation damping. As the radiation damping generally tends to be ignored for low frequencies, following this line of thought, so should the water viscous damping.

Aerodynamic damping

Aerodynamic damping is a damping source that is dependent on the wind speed that passes through the wind turbine. A higher wind speed will generate a higher damping force. However, the aerodynamic damping depends on the motion direction, i.e., a fore-aft movement will be highly damped, while a side-side movement will not. The fore-aft movement is comprehended to be aligned (or very close) with the wind loading direction, which means that the wind will attenuate the wind turbine movement on that direction. In the side-side direction, however, little to no resistance from the wind will exist, as it consists of a perpendicular direction to the fore-aft direction. The aerodynamic damping in the side-side direction can then be safely disregarded.

If it is considered that the OWT will be stopped, no significant aerodynamic damping will be present. Chen and Duffour [39] mentioned that, for a parked turbine, damping ratios between 0.08% and 0.24% can be seen. In a similar approach to what was stated for the wave radiation damping, a damping ratio can be considered as an estimation of the low damping expected from this source instead of just neglecting its existence.

Considering an equivalent (concentrated at one point) damping at the tower top, $\mathbf{C}_a$, leads to the formulation seen in Eq. 4.71. It imposes the utilization of the Dirac function, where the function will be one when $x_1 = x_1^t$. The quantification of the damping coefficient consists of a complex task. Chen and Duffour [39] presented a method for its determination. Due to the intrinsic complexity of such an approach and attending to the specific characteristics of the analysed OWT experimental testing conditions, Eq. 4.70 is a proposed simplification for the present case of a 3-blade wind turbine for the aerodynamic damping coefficient c_a. The complete expression can be consulted in the Chen and Duffour [39], as they present all the deductions behind it.

$$c_a = 3\rho_a \frac{V_{wind}}{\sin^2(\alpha_0)} c \left(C_d^{blade} \sin(\alpha_0) + C_l^{blade} \cos(\alpha_0) \right) R \tag{4.70}$$

$$\mathbf{C}_a = c_a \cdot \left[\int_{x_1} \delta\left(x_1 - x_1^t\right) \mathbf{ff}_{u_3}(x_1) \cdot \mathbf{ff}_{u_3}^{\mathrm{T}}(x_1)\,\mathrm{d}x_1 \right] \tag{4.71}$$

According to EngineersEdge.com [131], the air density for an ambient temperature of 10 ºC is 1.246 kg/m^3, with a dynamic viscosity of 1.778×10^{-5}. It is worth mentioning that for a shutdown test, the blades are pitch in such a way that α_0 is equal to 90º. For the blade drag coefficient, following common values in literature and easily found in Electrical Academia website [132], a value of 0.04 is adopted.

4.3.4 Equations of motion

The equations of motion can be obtained by adding the contribution of each type of virtual work together. By the virtual work principle, the summation of all virtual works will be equal to zero as shown in Eq. 4.13. The construction of matrices allows the presentation of the equations of motion in a more compact and friendly exposition, where the unknowns will be the generalised coordinates. This representation for the case of a free vibration (no loading) is seen in Eq. 4.72, as it comes from Eq. 4.13.

$$\begin{aligned}
&\begin{bmatrix} \mathbf{M}_{u_1}+\mathbf{M}^g_{u_1} & \mathbf{0} & \mathbf{0} \\ \mathbf{0} & \mathbf{M}_{u_3}+\mathbf{M}^w_{u_3}+\mathbf{M}^g_{u_3}+\mathbf{M}^s_{u_3} & \mathbf{0} \\ \mathbf{0} & \mathbf{0} & \mathbf{M}_\theta+\mathbf{M}^g_\theta+\mathbf{M}^s_\theta \end{bmatrix} \cdot \begin{Bmatrix} \ddot{\mathbf{q}}_{u_1} \\ \ddot{\mathbf{q}}_{u_3} \\ \ddot{\mathbf{q}}_\theta \end{Bmatrix} \\
&+ \begin{bmatrix} \mathbf{C}_{u_1} & \mathbf{0} & \mathbf{0} \\ \mathbf{0} & \mathbf{C}_{u_3}+\mathbf{C}^{rad}_s+\mathbf{C}^{hys}_s+\mathbf{C}^{vis}_w+\mathbf{C}^{rad}_w+\mathbf{C}_a & \mathbf{C}_{u_3\theta} \\ \mathbf{0} & \mathbf{C}_{\theta u_3} & \mathbf{C}_\theta \end{bmatrix} \cdot \begin{Bmatrix} \dot{\mathbf{q}}_{u_1} \\ \dot{\mathbf{q}}_{u_3} \\ \dot{\mathbf{q}}_\theta \end{Bmatrix} \\
&+ \begin{bmatrix} \mathbf{K}^E_{u_1} & \mathbf{0} & \mathbf{0} \\ \mathbf{0} & \mathbf{K}^G_{u_3}+\mathbf{K}_s & \mathbf{K}^G_{u_3\theta} \\ \mathbf{0} & \mathbf{K}^G_{\theta u_3} & \mathbf{K}^E_\theta+\mathbf{K}^G_\theta \end{bmatrix} \cdot \begin{Bmatrix} \mathbf{q}_{u_1} \\ \mathbf{q}_{u_3} \\ \mathbf{q}_\theta \end{Bmatrix} = \begin{Bmatrix} \mathbf{0} \\ \mathbf{0} \\ \mathbf{0} \end{Bmatrix}
\end{aligned} \tag{4.72}$$

It should be noted that the solution of the integrals as presented in previous subsections is computationally costly. As such, a variable change to reach each individual sub-matrix presented in Eq. 4.72 is suggested. By changing the general coordinate x_1 to a dimensionless local coordinate ξ that has a value between -1 and $+1$, a simplification either in shape functions and in integral elaboration is achieved. A Jacobian determinant is then needed to perform these changes, as demonstrated in Eq. 4.73. The derivative chain rule can be applied to reach the derivative of the shape functions to x_1 from shape functions defined on the coordinate ξ, as shown in Eq. 4.74.

$$x_1 = \frac{l}{2}\xi \rightarrow \xi = \frac{2}{l}x_1 \rightarrow \mathrm{d}x_1 = \frac{l}{2}\mathrm{d}\xi \rightarrow \frac{\mathrm{d}\xi}{\mathrm{d}x_1} = \frac{2}{l} \tag{4.73}$$

$$\frac{\mathrm{d}\mathbf{ff}_i(x_1)}{\mathrm{d}x_1} = \frac{\mathrm{d}\mathbf{ff}_i(\xi)}{\mathrm{d}\xi}\frac{\mathrm{d}\xi}{\mathrm{d}x_1} \tag{4.74}$$

After the matrices are computed, an eigenproblem solution can be devised. Following a similar approach as to the one presented by Meirovitch [133], it is possible to solve the equations of motion, if desired. Eqs. 4.75 and 4.76 present the initial steps for this, where the introduction of a second variable is necessary to reduce the degree of derivation associated to the problem. The modal properties can be retrieved as presented in another of Meirovitch work [134]. These are presented in Eqs. 4.78 and 4.79.

$$\begin{aligned}
&\begin{cases} [\mathbf{M}]\cdot\{\ddot{\mathbf{q}}\}+[\mathbf{C}]\cdot\{\dot{\mathbf{q}}\}+[\mathbf{K}]\cdot\{\mathbf{q}\}=\{\mathbf{0}\} \\ [\mathbf{I}]\cdot\{\mathbf{y}\}-[\mathbf{I}]\cdot\{\dot{\mathbf{q}}\}=\{\mathbf{0}\} \end{cases} \rightarrow \\
&\rightarrow \begin{bmatrix} [\mathbf{M}] & [\mathbf{C}] \\ [\mathbf{0}] & -[\mathbf{I}] \end{bmatrix} \cdot \begin{Bmatrix} \{\dot{\mathbf{y}}\} \\ \{\dot{\mathbf{q}}\} \end{Bmatrix} + \begin{bmatrix} [\mathbf{0}] & [\mathbf{K}] \\ [\mathbf{I}] & [\mathbf{0}] \end{bmatrix} \cdot \begin{Bmatrix} \{\mathbf{y}\} \\ \{\mathbf{q}\} \end{Bmatrix} = \begin{Bmatrix} \{\mathbf{0}\} \\ \{\mathbf{0}\} \end{Bmatrix}
\end{aligned} \tag{4.75}$$

$$\begin{Bmatrix} \{\mathbf{y}\} \\ \{\mathbf{q}\} \end{Bmatrix} = \mathrm{e}^{\lambda t}\cdot \begin{Bmatrix} \{\mathbf{y}_0\} \\ \{\mathbf{q}_0\} \end{Bmatrix} \tag{4.76}$$

$$\lambda \begin{bmatrix} [\mathbf{M}] & [\mathbf{C}] \\ [\mathbf{0}] & -[\mathbf{I}] \end{bmatrix} \cdot \begin{Bmatrix} \{\mathbf{y}_0\} \\ \{\mathbf{q}_0\} \end{Bmatrix} = - \begin{bmatrix} [\mathbf{0}] & [\mathbf{K}] \\ [\mathbf{I}] & [\mathbf{0}] \end{bmatrix} \cdot \begin{Bmatrix} \{\mathbf{y}_0\} \\ \{\mathbf{q}_0\} \end{Bmatrix} \tag{4.77}$$

$$\lambda_r = -\sigma_r + i\omega_r \tag{4.78}$$

$$\zeta_r = \frac{\sigma_r}{|\lambda_r|} \tag{4.79}$$

Reminding that this is the approach taken in the Matlab script developed, Matlab incorporated capacities allow the solution of the eigenproblem seen in Eq. 4.77. The solution will take the form of Eq. 4.78. The natural frequency will be the imaginary part of the solution, while the damping ratio will be given by the real part and after performing the operation seen in Eq. 4.79. As numerical solutions are obtained from Matlab, solutions that consider a null eigenfrequency represent a highly damped solution and should not be considered. It is important to note that the analysed problem does not have a natural mode with a frequency equal to zero.

4.4. Model Validation

4.4.1 Tower validation with analytical transversal vibrating beam solutions

Resorting to *Apontamentos de Vibrações de Sistemas Mecânicos* [118], it is possible to retrieve the analytical solutions for a constant circular cross-section beam. These can then be compared with the solutions obtained through the simplified developed model using a single element as the beam. Table 4.1 presents the analytical roots of the transversal vibrating beam problem for different boundary conditions. Eq. 4.80 allows the transformation of these roots to natural frequencies.

Table 4.1. First significant natural frequencies for beams [118].

Boundary condition	Root ($\beta_i l$)
free-free	4.7300
clamped-clamped	4.7300
hinge-hinge	π
clamped-free	1.8751

$$f_i = \frac{(\beta_i l)^2}{2\pi} \sqrt{\frac{EI}{\rho A l^4}} \tag{4.80}$$

Tables 4.3 and 4.4 present a summary of the convergence and validation studies performed. The values presented in Table 4.1, besides considering a constant cross-section beam, are based on the Bernoulli-Euler beam theory. As such, in order to validate the model developed, the natural frequencies should be lower than the ones obtained through the analytical method, but of the same order as them. This is due to the consideration of the rotational inertia and shear deformation in the Timoshenko beam theory.

For the validation study, a constant cross-section beam was considered to directly compare the results to the analytical ones. Meanwhile, for the convergence study, a linear variation of thickness and external radius of the cylinder beam was considered. For both studies, no damping was considered and no lumped mass or other influence was added. Table 4.2 presents the dimensions and properties of the considered circular beam used in these tests to represent a very simplified version of a random OWT tower.

Table 4.2. Validation beam properties and dimensions.

Property	Value	[Unit]
E	210	GPa
ρ	7800	kg/m^3
ν	0.3	
R_{ext}	2.75	m
t	0.05	m
l	80	m

The case of clamped-free was taken as a case to conclude the number of shape functions that are needed to have a solution convergence. This is presented in Table 4.3. The longitudinal displacement is not relevant in a bending problem. Consequently, the number of shape functions for the longitudinal component was not increased in the convergence study. Using this simple beam, convergence regarding the third decimal house is achieved with the minimal number of shape functions (6), while convergence for the fourth decimal house is achieved from 10 shape functions, as observed in Table 4.3. As in reality there is no need for more precision in natural frequency determination, and the variability of the fifth and remaining decimals is not seen as important. This leads to the conclusion that a minimal of 12 shape functions should be used to have coherent results, recommending that 15 shape functions should be used for a good result acquisition, and at least 20 shape functions for a high degree of accuracy. It is important to note once again that this convergence study relies in a constant cross-section beam, which is far simpler case than the real geometry of OWTs.

Table 4.3. Convergence study performed considering a constant cross-section, non-damped structure and a clamped-free boundary condition.

No. Shape Functions	Undamped natural frequency [Hz]
$p_{u_1} = p_{u_3} = p_{tt} = 6$	0.86997
$p_{u_1} = 6; p_{u_3} = p_{tt} = 8$	0.86987
$p_{u_1} = 6; p_{u_3} = p_{tt} = 10$	0.86984
$p_{u_1} = 6; p_{u_3} = p_{tt} = 12$	0.86982
$p_{u_1} = 6; p_{u_3} = p_{tt} = 15$	0.86980
$p_{u_1} = 6; p_{u_3} = p_{tt} = 17$	0.86980
$p_{u_1} = 6; p_{u_3} = p_{tt} = 19$	0.86979
$p_{u_1} = 6; p_{u_3} = p_{tt} = 21$	0.86979
$p_{u_1} = 6; p_{u_3} = p_{tt} = 23$	0.86979
$p_{u_1} = 6; p_{u_3} = p_{tt} = 25$	0.86978

The values presented in Table 4.4 for the model natural frequencies were obtained using 20 shape functions for each coordinate, as it is the shape function number that corresponds to convergence. However, as it is possible to observe in Table 4.3, 15 shape functions is an acceptable number of shape functions in terms of balance between computational cost and solution precision. Throughout the performed studies, it was seen that using 20 or more shape functions with a single element can lead to numerical issues in terms of solving the presented integrals. Consequently, it is advised to use a maximum of 18 shape functions. These numerical issues mean that more elements should be used. Still, for simplicity's sake and seeing that a given convergence is obtained by using more than 15 shape functions, the division of the structure into more elements can be disregarded.

Table 4.4. Model validation frequencies (Hz), after convergence study, with the beam analytical natural frequencies (Hz).

Condition	free-free	clamped-clamped	hinged-hinged	clamped-free
Analytical f	5.563	5.563	2.454	0.874
Model f	5.433	5.336	2.428	0.870

Throughout every analysed case of analytical validation, the model developed presented a smaller fundamental natural frequency than the analytical obtained one. Once more, the introduction of the rotational influence by using Timoshenko beam elements instead of the Euler-Bernoulli beam elements as the ones from the analytical solution led to this situation. For that reason, the model is then considered validated for the analytical shown cases, i.e., from a simple beam point of view.

4.4.2 Tower validation with developed analytical transversal vibrating beam solutions, considering a rigid body

Considering a beam clamped on one side and free on the other side with a rigid body (concentrated mass and inertia), an analytical solution was developed to further validate the model approach. This solution assumes a homogeneous and isotropic beam and assumes that the mass centre of the rigid body coincides with the top point of the beam. Simplifying further the problem of what can be considered a very simple approach to a wind turbine problem, it is imposed that the mass centre of the rigid body coincides with the free-end of the beam. Fig. 4.7 presents this simple system.

Attending to the boundary conditions, shown in Eq. 4.81, a general solution in space $V(x)$ can be deployed as presented in Eq. 4.82. The solution regarding time is not important for the purpose of the current exposition and will be disregarded from here on in. Note that the β parameter is related to ω through Eq. 4.80.

$$\begin{cases} x=0: \begin{cases} v(0,t)=0 \\ \frac{\partial v(0,t)}{\partial x}=0 \end{cases} \\ x=l: \begin{cases} -EI\frac{\partial^2 v(l,t)}{\partial x^2} = J_{RNA}\frac{\partial^3 v(l,t)}{\partial x \partial t^2} \\ EI\frac{\partial^3 v(l,t)}{\partial x^3} = m_{RNA}\frac{\partial^2 v(l,t)}{\partial t^2} \end{cases} \end{cases} \tag{4.81}$$

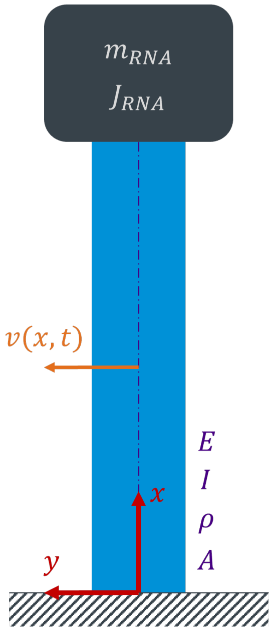

Fig. 4.7. Beam clamped at one end and connected to a rigid body at the other end.

$$V(x) = A_1 \cosh(\beta x) + A_2 \sinh(\beta x) + A_3 \cos(\beta x) + A_4 \sin(\beta x) \tag{4.82}$$

Applying the boundary conditions, the general solution can be simplified and an overall problem equation reached. Eq. 4.83 shows the developed general problem equation in an equivalent matrix representation. The problem is further solved by equaling the determinant of the matrix of the equation system to zero to obtain non-trivial solutions.

$$\begin{bmatrix} D_{11} & D_{12} \\ D_{21} & D_{22} \end{bmatrix} \cdot \begin{Bmatrix} A_1 \\ A_2 \end{Bmatrix} = \begin{Bmatrix} 0 \\ 0 \end{Bmatrix}$$
$$\begin{cases} D_{11} = (\cosh(\beta l) + \cos(\beta l)) - \frac{J}{\rho A}\beta^3(\sinh(\beta l) + \sin(\beta l)) \\ D_{12} = (\sinh(\beta l) + \sin(\beta l)) - \frac{J}{\rho A}\beta^3(\cosh(\beta l) - \cos(\beta l)) \\ D_{21} = (\sinh(\beta l) - \sin(\beta l)) - \frac{M}{\rho A}\beta(\cosh(\beta l) - \cos(\beta l)) \\ D_{22} = (\cosh(\beta l) + \cos(\beta l)) - \frac{M}{\rho A}\beta(\sinh(\beta l) - \sin(\beta l)) \end{cases} \tag{4.83}$$

After determining the natural frequencies by solving the previously stated system in order to βl and using the relation seen in Eq. 4.80, the mode shapes can also be found. Using a given relation between A_2 and A_1 of the existing ones from Eq. 4.83, where a value is assumed for one of the constants, it is possible to plot a given mode shape of the studied structure.

Table 4.5 presents the values obtained to validate the developed model in this matter. The study considered a constant section beam, with the dimensions and properties seen in Table 4.2 plus a rigid body with a concentrated mass of 400 tonnes and an inertia of 60×10^6 kg.m^2 on the free extremity of the beam. A set of different shape function numbers was studied to confirm convergence. Similar conclusions to the ones presented in the previous sub-section were reached, with 20 shape functions being used to validate the model.

Table 4.5. Model validation frequency regarding a constant section beam that is clamped at one end and has a rigid body at the other end.

Analytical f	Model f
0.426 Hz	0.424 Hz

This validation case is very similar to an analytical case of a clamped onshore wind turbine. A validation considering a more close representation of an offshore wind turbine and validation of soil and water interferences on the structure was searched, but insufficient data led to the impossibility of implementing such validation process.

4.5. Model calibration

As some simplifying considerations are applied to make an easier modelling approach, a model calibration should be performed to ensure that the results obtained do not derive from the model itself, but from the inputted properties and OWT characteristics. As such, this sub-section presents the steps necessary to carry out a correct model calibration.

Model calibration can be based on another model if this model is well validated with experimental data. From this starting point, first, the tower of the wind turbine is calibrated using HAWC2-like software with well-validated simulation.

Before starting the model calibration itself, the differences in modelling led to differences in the overall mass of the structure. By dividing the actual mass of the structure by the calculated mass of the simulated structure, a mass correction factor can be obtained. This mass correction is then employed to the mass density of the structure material to ensure that the same structural mass is reached. Regarding stiffness, a direct correction factor does not exist. As a consequence, having the natural frequencies from a well-validated situation, an iterative process has to be carried out to reach the stiffness correction factor that accounts for the minimal error considering both the fore-aft and side-side fundamental frequencies. Special attention is provided to the fundamental frequencies as these were found to be the main influence factor on the deformed shape of the structure.

An initial step was performed to correct the mass of the structure, as it is possible that the model used to represent the OWT is not entirely identical to the OWT itself. A possible cause are simplifications of linear variations for a given section of the structure. Consequently, the actual mass of the structure should be inputted. A mass correction factor is then given by Eq. 4.84:

$$M_{corr} = \frac{m_{real}}{m_{calc}} = \frac{m_{real}}{\rho \pi \int_0^l \left(R_{ext}^2(x) - R_{int}^2(x)\right) \mathrm{d}x}. \tag{4.84}$$

As significant differences can occur regarding the total mass of the structure, then significant differences, with more weight on the results obtained, can occur regarding the overall system stiffness. Appendix C shows the analytical approach given on the subject, where a general stiffness correction factor equal to the cubic of the mass correction factor was achieved. This assumption was validated recurring to natural frequencies comparison with the benchmark model. Relative errors for problems considering only the tower with top mass and no foundation (the tower is considered clamped at its bottom and free at the top) below 1% were registered.

Throughout this study of correction factors, it was seen that the main stiffness influencer regarding first mode bending is the component $\mathbf{K}_{\theta}^{E}$. This can also be explicated by analysing the equations in Appendix C. Summarizing, the fact that this stiffness component is defined by the difference between the fourth power outer radius and the fourth power inner radius compensates for the variation seen by the difference of the squared outer radius and the squared inner radius. The following and more correct approach is then to correct not the overall stiffness matrix with a single correction factor, but to use different correction factors, depending on the formulation difference. As only this component, $\mathbf{K}_{\theta}^{E}$, has a different formulation, being defined by the difference of 4th power elements, while the rest of the stiffness components all are defined by the difference of squared elements, The stiffness correction factor stated before should then be applied to this component, and a stiffness correction factor equal to the mass correction factor should be applied for all remaining components. Eq. 4.85 then states the stiffness correction factor that was used to correct the structural stiffness of the modelled OWT:

$$\begin{cases} K_{corr} = {M_{corr}}^{3}, \text{ applied to } \mathbf{K}_{\theta}^{E} \\ K_{corr} = M_{corr}, \text{ applied to the rest} \end{cases} . \tag{4.85}$$

Given the simplifications performed, only the tower was calibrated. The whole structure, accounting for the monopile and transition piece was not considered, as their connection consists of a grouted mass. This grouted mass introduces extra stiffness and mass to the structure. This quantification, however, is not known and the literature does not present a realistic approach to this matter. As such, during the modelling of the structure, this connection was seen as being a variation of a section and an equivalent section was assumed to reach the stiffness and mass values of this connection. However, if the grouted mass is known, a mass correction can take place for all the structures, but difficulties with stiffness quantification of the connection can still exist.

This calibration process then allows the generalization of the developed model for different cases without the necessity of a calibration study beforehand. Thus, by knowing the real mass of the tower, both the mass and stiffness correction factors can be computed and the model calibrated as such. It is important to note that this process is only valid if a linear approximation is considered for the variation of the outer diameter and thickness of the tower.

4.6. Damping sources sensitivity

The previously presented damping formulations consist of literature recommendations and simplifications. As a consequence, they may be wrong about the desired conditions of implementation. This sub-section pretends to show, in a simplified manner, the degree of influence that the proposed formulation for different damping sources has on the fundamental frequency of the OWT. If a given damping source has an influence lower than 0.1%, then it is safe to disregard the formulation of that damping source entirely from the model. Attention should be provided to the fact that this does not necessarily mean that the damping source does not exist or significantly influence the fundamental natural frequency of those conditions, it means that the proposed formulation does not create a significant influence to be considered in the model.

The structural damping is considered the base damping source, being the reference for all remaining damping analyses. The introduced damping effect from a given damping source will be compared to the influence that structural damping has when compared to an undamped situation. A hypothetical OWT was then considered to perform this analysis. The tower of this hypothetical OWT is given by the characterisation seen in Table 4.2, while the support structure is characterised by what is seen in Table 4.6. For simplification, the transition piece that usually exists will not be included in this defined generic OWT structure. A rigid body to simulate the RNA was considered. Its properties are as defined previously in the sub-section referring to the validation of the model with a rigid body. A supposed blade length (described circumference radius) of 60 meters was admitted. The air was assumed to be subjected to 10 ºC and a wind speed of 8 m/s. A generic soil will also be used for this investigation. The soil stratum considered is represented in Fig. 4.8.

Table 4.6. Generic support structure properties and dimensions.

Property	Value	[Unit]
E	210	GPa
ρ	7800	kg/m^3
ν	0.3	
R_{ext}	3.25	m
t	0.07	m
$L_{embedded}$	24	m
$L_{submerged}$	20	m

The presented generic soil properties were based on different literature that studied OWT responses considering SSI effects. For the clay layer, Refs. [39] and [53] were consulted. For the sand layers, Refs. [11], [16], and [39] were consulted. For the assumption of the Poisson's ratio, Refs. [59] and [72] were consulted. Once again, this soil stratum is a generic assumption and does not represent any specific location. The sand-clay-sand disposition consists of a commonly seen stratum in literature and allows the implementation of the damping sources on different soil types.

Table 4.7 presents all the damping influence results on the undamped fundamental frequency of a generic hypothetical OWT. The consideration of damping, even when admitting all damping sources, lead to a relative difference on the fundamental natural frequency of 0.04%. This means that even tho a combined damping ratio of around 2% was observed, decreasing the undamped fundamental natural frequency from 0.2539 Hz to 0.2538 Hz, the impact on the fundamental frequency of the system is negligible. Consequently, it is safe to disregard damping altogether and perform the analyses from an undamped point-of-view.

As only the stationary condition was studied, the present study also supports the statements of Nóren-Cosgriff and Kaynia [12]. They said that, for a stationary wind turbine, the OWT damped response would be dominated by the soil damping, Meanwhile, for an

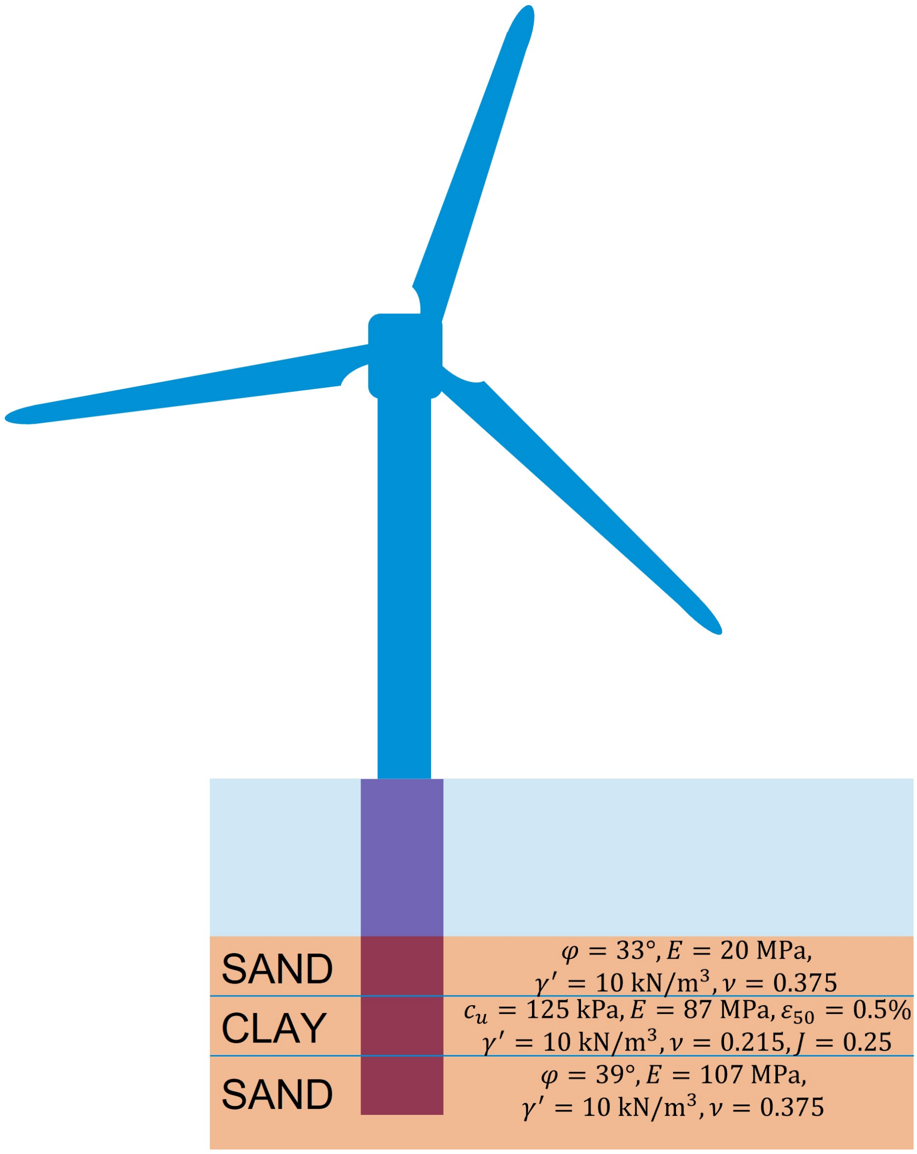

Fig. 4.8. Generic soil stratum considered for the investigation of the influence of damping source formulations on the fundamental frequency.

Table 4.7. Influencing quantification of different damping sources on the undamped fundamental frequency of a generic OWT.

Damping source	Influence
Structural	0.01%
Aerodynamic	0.00%
Soil radiation	0.02%
Soil hysteresis	0.02%
Water radiation	0.00%
Water viscous	0.00%
All sources	0.04%

operating OWT, aerodynamic damping is expected to be dominating damping source, as reported by various literature.

Shirzadeh et al. [28] state that the principal hydrodynamic damping is due to the water radiation, as structure deflections and relative velocities are small and lead to smaller values of water viscous damping. In this study, they provided similar degrees of impact on the fundamental natural frequency. Either way, the impact seen was negligible for both hydrodynamic sources and conclusions cannot be drawn on this topic.

4.7. Model Limitations

The developed model can be seen as a very simplified approach when compared with the real system. The model considers that a linear variation of the outer diameter and thickness occurs in the tapered sections of the OWT structure. Although a calibration process is performed, this process still has some degree of error associated to it, besides only considering the tower of the wind turbine. This is important, as the grout part that connects the monopile to the transition piece is considered through an equivalent outer diameter and thickness, i.e., in this connection region, it is considered that the transition piece and the monopile are one single (together) piece.

Limitations then exist that will be responsible for the error that may be found when using the formulated model. As the soil stiffness formulation will be developed considering the results from the developed model, employing that formulation in a well-validated model can also result in discrepancies.

Starting with the simpler one-element model, the system can substitute the whole foundation through a rigid connection (clamped boundary condition), as well as replace the RNA with a concentrated mass plus inertia. These are very simple and common simplifications performed throughout the literature. However, these simplifications do not capture the contribution of different vibration modes from different structural components besides the tower, as well as considering an overly stiff foundation.

As reported by Damgaard et al. [15], the fixed wind turbine has higher natural frequencies than the ones measured. This is a consequence of having an overly stiff foundation than in reality. As such, a simplified one-element model is usually upgraded to a multi-element model where soil interaction is considered. Damgaard et al. [15] also reported that considering common *p-y* curves to account for the soil reaction on the pile that composes the OWT foundation leads to a softer foundation than in reality. The reasons why that happens have been exposed elsewhere in this work.

The consideration of only considering cylinder beam elements leads to the utilization of lumped mass and inertia to substitute other elements that are not included in that definition, such as the RNA. A note should be performed as to say that the RNA will have different inertia if a different direction is considered. This is due to the eccentricity created by the blades and rotor.

On the simpler one-element model, the only damping considered was the structural damping. If the results would be compared with the real-life wind turbine damping, increased damping would be noted, as other sources of damping would be present. Since the one element model is used to validate the structural properties and characteristics of the model, with the results being compared to the results from the model used at Vestas, these are not limitations. However, when considering the multi-element model and a more complex one-element model, besides the structural damping, other sources of damping have to be considered. As such, some sources of damping that are commonly disregarded in the literature have been considered/formulated. This consideration might be non-conservative, as the different damping sources quantification have different origins and were retrieved from various literature reviews, some of which did not specifically broach the monopile OWT. Besides that, some damping coefficients are not constant and are frequency-dependent. In order to simplify, the coefficients were calculated using a linear fundamental natural frequency. Some errors may come from this simplification.

Considering all these points, it's possible to consider the position of the developed model. Being the developed model a single element p-version model where the soil interaction is also accounted for, the limitation of the clamped situation does not apply. However, numerical resolution can be a problem when using high degrees shape functions, especially for large structures with high geometric variability (due to soil properties or geometry) throughout their length. These limitations can lead to a poor resolution of the obtained result, as convergence is only possible for the first decimal numbers. As the natural frequencies are commonly reported up to four decimal numbers for high precision, if this is guaranteed, this limitation can be disregarded. Still, some errors can occur from this source.

Another limitation comes from the SSI consideration. Different approaches are reported in the literature, from considering a linear behaviour to a complex constitutive law for the soil, with hardening or softening. As to simplify the problem at hand, a small strain situation was considered for the soil behaviour. This consideration is acceptable in modal properties analysis, as small displacements are usually considered. However, the cyclic and overall dynamic behaviour of the soil will have an important influence on the general properties of the soil with time. This means that considering a small strain situation might be a good approximation to linearise the soil reaction, but might not include the soil changes that happen in long term. This might be the most important limitation of the model. A set of parallel and/or series springs, where each spring represents a given influence factor on the soil stiffness, can be considered to try and account for different aspects and non-linearities of the soil.

As different effects on the SSI take place in terms of the existing lateral resistance, the developed model and overall approach to the problem considered only the direct lateral resistance of the soil. No base shear or moment was considered. Likewise, no distributed influence of the shear stress across the pile length was considered. The consideration of these contributions can help increase the overall soil stiffness, as literature states that they are important for rigid-like-behaving piles.

4.8. Final remarks

A simple model was developed using a single Timoshenko p-version finite element to represent the OWT. A convergence study was performed to determine the minimum degree of the shape functions that guarantees a convergence result to the fourth decimal number. Numerical issues can occur for very large structures when using a very high degree for the shape functions. Although this problem can occur, for the case studied a shape function number can be used that assures convergence for the decimal number intended. For the developed model, 15 shape functions were seen as an acceptable minimum number of shape functions, 18 shape functions were defined as the number of shape functions that avoid numerical issues, and 20 shape functions are the minimum number assumed to obtain a very high degree of precision on the result acquired.

It was observed throughout the developed model and follow-up studies that the shape functions in the u_1 direction have no direct effect on the lateral behaviour of the structure. This happens as there is no coupling between the effects on this direction with the ones that are linked with lateral deflection (bending) - u_3 and θ. To further reduce computational costs, the shape functions number in this direction can be reduced to a low value (as, for example, six) or be scrapped altogether. This is also admitted in several works, although often not explicitly said. For this reason, no soil stiffness was modelled in this direction.

Two analytical validations were performed, one considering a constant section beam with different boundary conditions and another considering a constant section beam clamped at one end and with a rigid body attached at the other end. As the analytical result is obtained using the Euler-Bernoulli theory, the model should produce lower natural frequencies, as the rotation of the section is considered. This was confirmed in every analytical situation considered.

To further validate the model, as simplifications regarding the linear variation of the tapered areas of the tower were assumed, a calibration was performed by comparing the values obtained from the developed model with the values obtained from a benchmark model. Correcting first the mass of the structure and relating it with the stiffness correction expected, a good fit with an error of less than 2% for the side-side and fore-aft natural frequencies was obtained. These errors were deemed acceptable as the benchmark model consists of a modal approach model and the developed model consists of a single element model with concentrated masses to represent other components.

Due to the nature of the model itself, several limitations exist. Considering the overall simplicity of the model, a given error is expected to occur. The correction performed to calibrate the model is not perfect and the number of shape functions and overall numerical integration performed to reach the final values can introduce errors. The consideration of other components as point masses instead of a connected body also does not allow for the full influence on the natural mode of the structure.

The SSI is another source of limitation. The simple consideration and how it was considered throughout the model development, the introduction of more complex ways of modelling the soil are not viable. The introduction of non-linear behaviours, as well as hardening/softening coming from cyclic and stress history of the soil, need an iterative process that was not considered in the model formulation. The developed model only considers a small-strain (initial) stiffness of the soil, as it assumes that the lateral displacements are very low and no significant strain is developed on the soil. A set of influence factors/coefficients were considered to try and introduce these influences in a very simple and uncomplicated way.

Difficulties were faced when modelling each damping source, as no direct and general formulation is widely proposed, and neither there is a verified way to identify the contribution of each damping source. As such, a suitability test had to be performed. As stated in different literature, the non-existence of proper damping formulation for each damping source might lead to errors as a damping source that can be important is disregarded.

The overall take on damping regarding the present work was to dismiss any damping source and work with the undamped frequencies of the system. This decision resulted from a study regarding the influence on the natural frequencies from the different damping sources. Nevertheless, the main body of the developed code model, present in Appendix D, contains the different damping sources formulation. The damping disregard was performed through an input file.

Chapter 5

Experimental versus modelling results

The studied OWTs are located at the Norther Offshore Wind farm. Fig. 5.1 presents the overview map of all the OWTs there installed. The studied OWTs are the WTG07, WTG22, WTG33, and WTG37. The soils where their monopiles are embedded consists on a combination of sand and clay layers, where the soils are predominately composed by clay with the exception of the case of the WTG07. Fig. 5.2 presents an OWT structure example from *Assessment of the dynamic behaviour of saturated soil subjected to cyclic loading from offshore monopile wind turbine foundations* [15] that is very similar to the ones studied here. It is important to remind that the developed model considers a linear variation of the outer diameter and thickness on all tapered sections present in the considered structure.

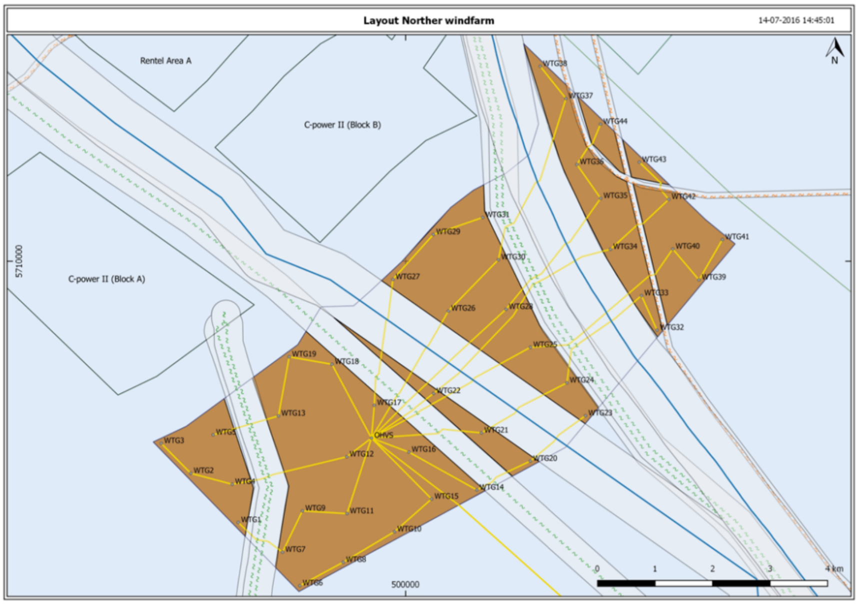

Fig. 5.1. Overview map of the Norther Offshore Wind farm [135].

The tests performed on the mentioned OWTs are not standstill turbine tests, they are a form of decay tests and other low wind operational data tests. Consequently, different factors that are difficult to account for exist. The formulated damping estimations pre-

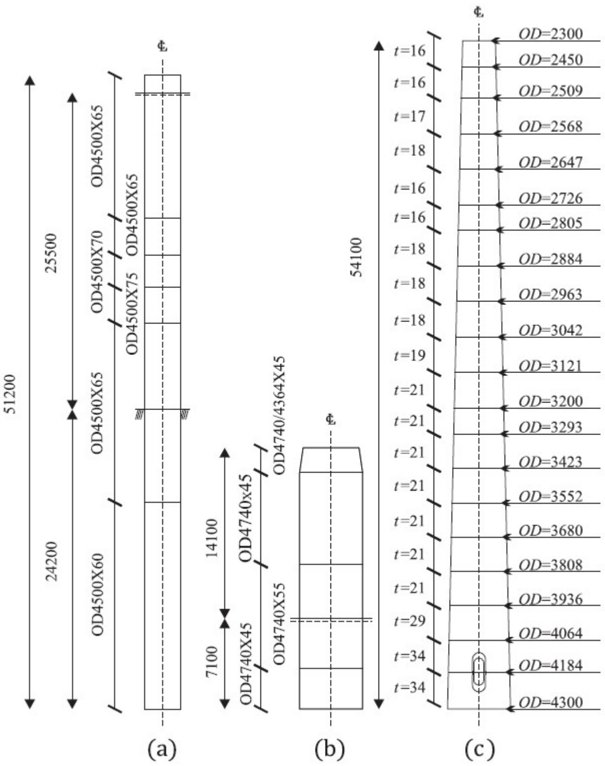

Fig. 5.2. Geometry of an offshore wind turbine structure: (a) monopile foundation, (b) transition piece, and (c) tower [15].

sented in Chapter 4 considered a standstill situation. This means that a slight error can exist when considering a damped situation.

As the first frequencies of the fore-aft and side-side modes are very close together, some degree of coupling is expected between these. The dynamic energy will be transferred from the highest damped mode to the lowest, leading to an impossible acquisition of pure modes. Inaccurate estimations of the modal damping might be obtained due to this occurrence. However, in ”rotor-stop”/shutdown (decay) tests a very small influence of external forces exist, leading to a close pure mode vibration/excitation [31].

According to Nóren-Cosgriff and Kaynia [12], usually there isn’t a preferred direction for the wind and waves to act on the wind turbine. This means that there isn’t a clear dominant direction of loading application. As loading varies from location to location, available data can contradict this. For the present case, this data is not available. It was assumed that all relevant loads are applied on a same plane of action.

Due to a Non-Disclosure Agreement, the results from the experimental tests, as well as the simulated values using a validated model of the tested OWTs cannot be shown. Consequently, all data from here on out will be normalised. The normalization will be based on different quantities, attending to the property analysed. A priority to present errors and relative increase/decrease will then be performed.

5.1. Soil modelling proposals

As the objective of the present work is to introduce different and new ways of representing the Soil-Structure Interaction associated to OWTs, a set of different formulations were developed. A small-strain stiffness (initial stiffness) was considered throughout the several proposals presented and analysed. Wanting to consider in an explicit way the connection between soil and structure properties, at the start the soil shear modulus formulation was used as a base. Table 5.1 presents a summary of every soil modelling proposal elaborated. These proposals are then explained, one by one on the remaining of this section.

Table 5.1. Soil modelling proposals summary.

Proposal	Formulation
Proposal 1	$k_s = \frac{E_s}{2R_{ext}(1-\nu_s^2)} \left[\frac{E_s(2\pi R_{ext})^4}{EI}\right]^{1/12} \frac{p_u}{\pi R_{ext}\sigma_v' OCR} \left(\frac{L}{2R_{ext}}\right)^{\frac{2R_{ext}}{L}}$
Proposal 2	$k_s = \frac{E_s OCR^{0.25}}{2R_{ext}(1-\nu_s^2)} \left[\frac{E_s OCR^{0.25}(2\pi R_{ext})^4}{EI}\right]^{1/12} \frac{p_u}{\pi R_{ext}\sigma_v' OCR} \left(\frac{L}{2R_{ext}}\right)^{\frac{2R_{ext}}{L}}$
Proposal 3	$k_s = \frac{2}{\pi R_{ext}} \left[\frac{E_s OCR^{0.25}(2\pi R_{ext})^4}{EI}\right]^{1/12} \frac{p_u}{\pi R_{ext}\sigma_v' OCR} \left(\frac{L}{2R_{ext}}\right)^{\frac{2R_{ext}}{L}} \begin{cases} k_{ini}\cdot z, \text{ for sand} \\ \frac{0.23p_u}{0.1y_c}, \text{ for clay} \end{cases}$
Proposal 4	$k_s = \frac{4G_s OCR^{0.25}}{2R_{ext}} \left[\frac{E_s OCR^{0.25}(2\pi R_{ext})^4}{EI}\right]^{1/12} \frac{p_u}{\pi R_{ext}\sigma_v' OCR} \left(\frac{L}{2R_{ext}}\right)^{\frac{2R_{ext}}{L}}$
Proposal 5	$k_s = k_s^{base/prop.X} + \frac{2}{\pi R_{ext}} \frac{p_u}{y_c}(2C_d + 80)$

Considering the work done by Prendergast and Gavin [17] and using the Vesic expression presented in that work as a formulation base (see Eq. 5.1), a general formulation can be derived. This general formulation is presented in Eq. 5.2, where two main influence inputs can be regarded: C_{PR}, which is a coefficient that accounts for the presence of soil around the pile (its minimum value should be 0.65, as given by Vesic expression, and a maximum value of double the minimum value), and C_{IN}, which is a coefficient that allows further correction of the soil stiffness attending to different influences.

$$k_s = \frac{0.65E_s}{2R_{ext}(1-\nu_s^2)} \left[\frac{E_s\,(2R_{ext})^4}{EI}\right]^{1/12} \tag{5.1}$$

$$k_s = \frac{C_{PR}E_s}{2R_{ext}(1-\nu_s^2)} \left[\frac{E_s\,(2R_{ext})^4}{EI}\right]^{1/12} C_{IN} \tag{5.2}$$

The necessity of implementing correction factors arises from the fact that the Vesic formulation comes from a slender approach on the subject. Consequently, Eq. 5.1 is used for situations where an infinite flexible beam can be considered, with the soil being an elastic-isotropic and homogeneous medium. This is disclosed on his work [136], as well as on the first solution formulation performed by Biot [137]. Likewise, the API Standard also presents a formulation that consists on a slender approach.

The C_{PR} coefficient should be 0.65 if soil is considered to exist only at one side, or 1.3 if soil is considered to be fully in contact on both sides. Studies performed by Ashford and

Juirnarongrit stated in Prendergast and Gavin work [17] have shown that a value of 1.0 provides close agreement between the upper and lower bound of estimations and accounts for the possibility of gap formation. This parameter can then empirically be changed to better suit a given soil condition, although no guideline is provided.

The C_{IN} intends to include all possible non-stated influence into the stiffness calculation. Examples of these influences are the over-consolidation ratio of the soil, vertical/horizontal soil stress at a given depth, soil bearing capacity, etc. A special attention should be given to ensure that this coefficient remains dimensionless, as the stiffness considered should be a quantity of N/m^3. The most important influences on the SSI problem in hand have been broached in Chapter 3.

The first proposal, seen in Eq. 5.3, utilizes the same coefficient as the modified Vesic expression ($C_{PR} = 1.0$) and tries to account for the pressure variation with depth, using a dimensionless relation based on the one used in the PISA design model for dimensionless pressure, as well as considering an influence of the aspect ratio of the pile. Different steps were taken to reach this final proposal, with different dimensionless pressure factors studied. Meanwhile, the aspect ratio factor is an expression that will only be valid for aspect ratios bigger than 3. As the studied structures have aspect ratios between 3 and 5, this is not a problem.

$$k_s = \frac{E_s}{2R_{ext}(1-\nu_s^2)} \left[\frac{E_s\,(2\pi R_{ext})^4}{EI}\right]^{1/12} \frac{p_u}{\pi R_{ext}\sigma_v' OCR} \left(\frac{L}{2R_{ext}}\right)^{\frac{2R_{ext}}{L}} \tag{5.3}$$

Regarding in more detail the steps taken to reach the first proposal, a differentiation between sand and clay soils was first performed for the dimensionless pressure factor, but low correction for clay was deemed insufficient. Also the connection between two soil properties doesn't present the relation of the capacity of the soil and the acting force/-pressure acting on it. Consequently, a general approach was used considering the bearing capacity of the soil and the effective vertical stress.

As stress history is important in the soil properties evolution throughout time, the over-consolidation ratio was considered. Although, according to Zdravkovic et al. [73], this factor doesn't influence the stiffness in a significant way, it was deemed essential the incorporation of a stress history influence. Furthermore, there isn't consensus on if and how the over-consolidation influences the soil stiffness due to its anisotropic nature. The multiplication of this ratio with the effective vertical stress leads to the pre-consolidation effective stress, which correlates with the stress history of the soil.

$$C_{p_u} = \begin{cases} \frac{p_u}{\pi R_{ext}\sigma_v'} \text{, sand} \\ \frac{p_u}{\pi R_{ext}s_u} \text{, clay} \end{cases} \rightarrow C_{p_u} = \frac{p_u}{\pi R_{ext}\sigma_v'} \rightarrow C_{p_u} = \frac{p_u}{\pi R_{ext}\sigma_v' OCR} \tag{5.4}$$

As the necessary data to correctly quantify the over-consolidation ratio was not available, it was estimated for clays by using the expression present in Appendix A, Eq. A.4, while for sands a certain percentage of the limit OCR was assumed. The limit OCR expression is presented in the same Appendix mentioned. The percentage considered is presented in Eq. A.5 of that same Appendix.

However, a note should be given to the uncertainty of this expression as it sits. It's the author opinion that a different influence factor should be considered to account for the stress history, since stress history can increase or decrease the stiffness of the soil. An example of a situation that could lead to different results is scour. As scour occurs, part of the soil is removed, while the adjacent soil layers increase in their over-consolidation, altering all the soil properties of the adjacent layers in the process. A more detailed study with this factor in different conditions should then be performed to validate the utilization of this factor.

Likewise, after performing a series of tests, it was observed that this influence factor as it is formulated will tend to infinite when the denominator tends to zero. Consequently, it was set that this influence factor is only viable for depths bigger than 1 meter. This reference depth was regularly seen as the point where a stiffness increase, specially on superficial clay layers, occurred. Attention to this should then be provided. For the superficial layers, half of this influence factor at the 1 meter depth mark as considered, admitting that this factor would decrease in direction to the mudline level.

The dimensionless influence parameter ($C_{IN} = C_{p_u}$), seen in Eq. 5.4, also considered the half of the outer perimeter of the structure and not only the diameter, as the outer perimeter is expected to better represent the line of influence. Using the same line of thought, a π was introduced inside the bending relation between the soil reaction and the structure bending moment, as a more direct meaning can be achieved, since the soil modulus doesn't act on a diameter, it would act on a perimeter or area. For this reason, as the the structure is comprised of a circular beam, a π would appear in the formulation.

Using as inspiration the expression that relates two adjacent layers in a soil stratum composed by two soil layers present in Jia's *Soil Dynamics and Foundation Modeling Offshore and Earthquake Engineering* [2], a proposal for the aspect ratio factor was elaborated. Before reaching the seen expression in Eq. 5.3, a relation similar to the one seen in the previously mentioned book equation was formulated, where an effort was done to have a parameter close to the unity for high aspect ratios (common of oil and gas piles). However, the first formulated expression was elaborated and had two degrees of freedom in terms of adjusting the factor. Consequently, a simpler expression was assumed, accounting for an increase in stiffness for rigid piles in agreement with what was seen in literature. This influence parameter is represented in Eq. 5.5 with its evolution, and a plot can be regarded in Fig. 5.3. Through this plot it is evidently observed that a significant effect (increase of up to 40%) only exists for aspect ratios below 10, which are the common ratios seen in the wind industry when employing monopiles. The final proposed equation for the aspect ratio influence factor is only valid for aspect ratios larger than 3.

$$C_{Ld} = \frac{3}{2}\left(\frac{L}{2R_{ext}}\right)^{-1.18} + 1 \rightarrow C_{Ld} = \left(\frac{L}{2R_{ext}}\right)^{\frac{2R_{ext}}{L}} \tag{5.5}$$

This, once again, raises the importance of further validation considering simpler situations that can be tested, as the ones performed by Prendergast et al. while investigating the scour effect (Refs. [68] and [89]). Besides the validation of these individual influence factors, its combined influence should also be seen. Missing available information didn't allow for any validation on this regard.

Following the results seen in Darendeli's work [70], where an increase of the soil shear modulus occurs as a bigger over-consolidation ratio is considered, it was considered that all soil moduli should be multiplied by the over-consolidation ratio. This is the base for

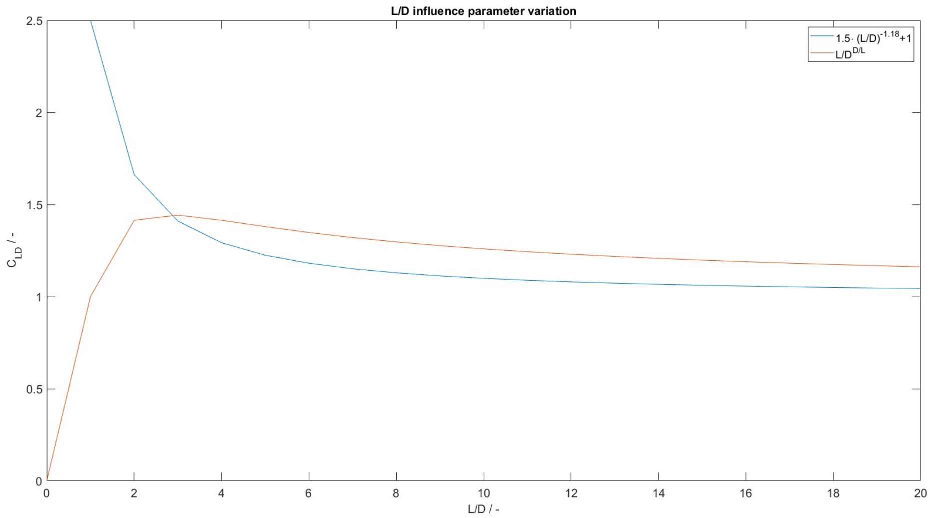

Fig. 5.3. *L/d* influence parameter variation with different aspect ratios.

the second proposal, and it consists on a direct modification of the first proposal. However, the increase of the soil moduli is not linear. After analysing the data made available by Darendei [70], a shear stress increase close to $OCR^{0.25}$ was observed. Eq. 5.6 presents the proposed stiffness formulation accounting for a direct influence on the soil moduli:

$$k_s = \frac{E_s OCR^{0.25}}{2R_{ext}(1-\nu_s^2)} \left[\frac{E_s OCR^{0.25} \left(2\pi R_{ext}\right)^4}{EI} \right]^{1/12} \frac{p_u}{\pi R_{ext} \sigma_v' OCR} \left(\frac{L}{2R_{ext}} \right)^{\frac{2R_{ext}}{L}} . \tag{5.6}$$

After extensively analysing the previous proposals, a third proposal was derived considering the API/DNV Standard approach/stiffness and correcting it with the same influence factors as the ones present in the first proposal. Additionally, the bending influence factor as seen in the Vesic formulation was introduced to account for the SSI. The same exponent was considered for the sake of simplicity. An important note should be remarked as the initial stiffness obtained from the Standards come from deriving the *p*-*y* curves expressions. This leads to a stiffness of $\mathrm{N/m^2}$, so a further correction should be implemented if a subgrade modulus reaction (stiffness in $\mathrm{N/m^3}$) is desired. As a consequence, while using the same base expression, instead of using a continuous method by integrating, as used in the developed model, it is necessary to discretise the stiffness. For such, to reach an equivalent spring force, the spring stiffness per unit length is multiplied by the spacing between successive springs and by the lateral displacement. Although the direct application of the previous expressions could be made, since it was considered that those expressions are applied to the normal of the pile and then integrated around it, for the discrete approach, a pre-multiplication by $\pi/2$ if it is considered than only half of the pile circumference will be subjected to soil resistance or by π if all of the pile circumference is assumed to be subjected to a soil reaction. Eq. 5.7 presents the corrected soil stiffness for a discrete approach:

$$k_s' = \int_0^{\pi} k_s \sin^2(\varphi) R_{ext} \mathrm{d}\varphi = k_s \frac{\pi}{2} R_{ext} . \tag{5.7}$$

With this in mind, the third proposal ended up as seen in Eq. 5.8. Again, the same considerations were taken into account as the ones for the second proposal, since this is an evolution that takes into account more of the soil characteristics than the first proposal.

$$k_s = \frac{2}{\pi R_{ext}} \left[\frac{E_s OCR^{0.25} \left(2\pi R_{ext}\right)^4}{EI} \right]^{1/12} \frac{p_u}{\pi R_{ext} \sigma'_v OCR} \left(\frac{L}{2R_{ext}} \right)^{\frac{2R_{ext}}{L}} \begin{cases} k_{ini} \cdot z, \text{ for sand} \\ \frac{0.23 p_u}{0.1 y_c}, \text{ for clay} \end{cases} \tag{5.8}$$

All the considerations applied on the Vesic formulation were admitted to be applied on the API Standard since it's also based on a slender/flexible structure and the analysed structure is consisted of a rigid-like structure. An added factor that is common to the previous proposal is also admitted to link the soil reaction with the bending of the structure (through its bending moment). This is supported by the fact that, for rigid-like behaved piles, as according to Zhang et al. [51], the soil stiffness will be dependent on the soil elastic parameters and overall dimensions of the pile.

According to Zhang and Andersen [7], when considering a fully rough and bonding interface between the soil and the structure, a soil stiffness around 4 times the soil shear modulus is obtained. As such, the fourth proposal will regard this as the starting point, i.e., the starting point is what can be regarded in Eq. 5.9. As to account the SSI, a correction factor based on the Vesic formulation was added. Introducing all remaining and already presented factors, the final expression for the fourth proposal is given by Eq. 5.10.

$$k_s = \frac{4G_s}{2R_{ext}} \tag{5.9}$$

$$k_s = \frac{4G_s OCR^{0.25}}{2R_{ext}} \left[\frac{E_s OCR^{0.25} \left(2\pi R_{ext}\right)^4}{EI} \right]^{1/12} \frac{p_u}{\pi R_{ext} \sigma'_v OCR} \left(\frac{L}{2R_{ext}} \right)^{\frac{2R_{ext}}{L}} \tag{5.10}$$

This proposal is expect to present similar values to the ones presented by the second proposal. Since both approaches consider the soil moduli, the stiffness profile evolution with depth will have the same relative shape. Consequently, only a multiplying factor will differ from these two proposals.

It is then important to note that the different formulations can be open to alterations in terms of coefficients. The exponent seen in the general formulation, Eq. 5.2, can also be altered to a value up to 0.108, as seen in the formulation presented by Biot in Prendergast and Gavin's work [17]. The way that the dimensionless coefficient takes place on Eqs. 5.4 and 5.5 can also be altered. In the case of Eq. 5.4, the bearing capacity can be divided by either the full or the half pile perimeter. In the case of Eq. 5.5, the value that multiplies the aspect ratio can also be altered. These alterations weren't explored at its full potential, i.e., no optimization study regarding these coefficients was performed.

Different formulations can quantify the soil bearing capacity as presented in several literature. Although the bearing capacities given by the standards are used by default, the choice of this formulation should rely on what is expected to best represent the soil. A study was performed with formulations from Refs. [7], [48], [85], [93], and [112]. As from the standard sand is usually overestimated in terms of stiffness, the bearing capacity used throughout the different proposals was the one defined by the Standard, since alternatives gave a higher sand bearing capacity, increasing further its stiffness. By the contrary, clays are usually underestimated in terms of stiffness. As such, a different formulation from the standard was considered. This formulation, as proposed by Yu and presented in Zhang and Andersen's work [7], is presented in Table 3.3.

Besides altering the soil stiffness formulation, different effects can also be added. This can be seen as the case relating the gap formation related stiffness. A certain stiffness is related to this phenomenon, since a resistance has to be overcome in order for separation between soil and pile to occur. This contribution can then be added to the already calculated soil stiffness. Boulanger [95] developed a non-linear model to represent this phenomenon in sand and clay with a common set of parameters. Fig. 5.4 presents the suggested model by Boulanger [95], where the gap formation component (parallel springs of closure and drag phenomena) is in series with the elastic and plastic components. However, it is expected that the gap develops on one side of the pile, while the other is compressed, which means that one side is connected to the gap formation component, while the other is connected to the elastic-plastic component. Consequently, on the current work, it's the author's opinion that these springs should not be in series but in parallel with the elastic-plastic springs. As no plasticity is considered in the present work, a simple summation of stiffness results on the expected equivalent soil stiffness [25, 95, 138].

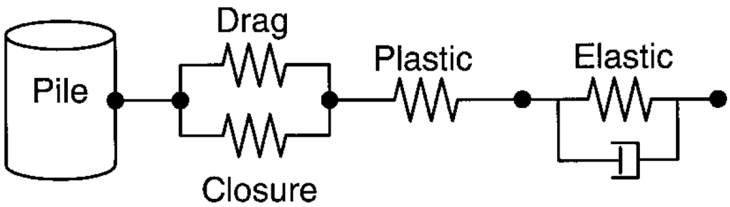

Fig. 5.4. Boulanger's proposed soil model [95].

Eqs. 5.11 to 5.14 present the relevant initial stiffness desired for use in the final proposal. Eqs. 5.11 and 5.13 present the *p*-*y* curve formulated by Boulanger [95] for the drag and closure components of the gap formation, respectively. By considering that $y_0^g = p_0^d = 0$ and $y_0^+ = -y_0^- = \frac{y_c}{100}$, and using the estimation by Wilson in the work of Boulanger [95] of $C_d \approx 0.3$, it's possible to use the following derived equations presented in Eqs. 5.12 and 5.14.

$$p^d = C_d p_u - \left(C_d p_u - p_0^d\right) \frac{y_c}{y_c + 2|y^g - y_0^g|} \tag{5.11}$$

$$k'_{drag} = \left.\frac{\mathrm{d}p^d}{\mathrm{d}y^g}\right|_{y^g=0} = \frac{2C_d p_u}{y_c} \tag{5.12}$$

$$p^c = 1.8p_u \left[\frac{y_c}{y_c + 50\left(y_0^+ - y^g\right)} - \frac{y_c}{y_c - 50\left(y_0^+ - y^g\right)}\right] \tag{5.13}$$

$$k'_{closure} = \left.\frac{\mathrm{d}p^c}{\mathrm{d}y^g}\right|_{y^g=0} = \frac{80p_u}{y_c} \tag{5.14}$$

However, using the standard derived formulation, an overestimation is expected to occur in sands, so the adding of this effect would only worsen this fact. At the same time, clay is expected to be underestimated. Observing the *p*-*y* curves from the Boulanger model as it was, little to no influence was seen in sands, but some differences were already observed in clays. Fig. 5.5 presents the reported differences. Since missing information exists regarding the critical displacement y_c for sands and using the little apparent influence on them of gap formation, the proposed added stiffness is only applied to clay soil layers. The fact that sand is a cohesionless soil also supports this assumption, as this soil more easily fills the void when a gap formation occurs. The added stiffness is then given by Eq. 5.15, with the final proposal being given by Eq. 5.16, where any stiffness proposal seen before can be considered.

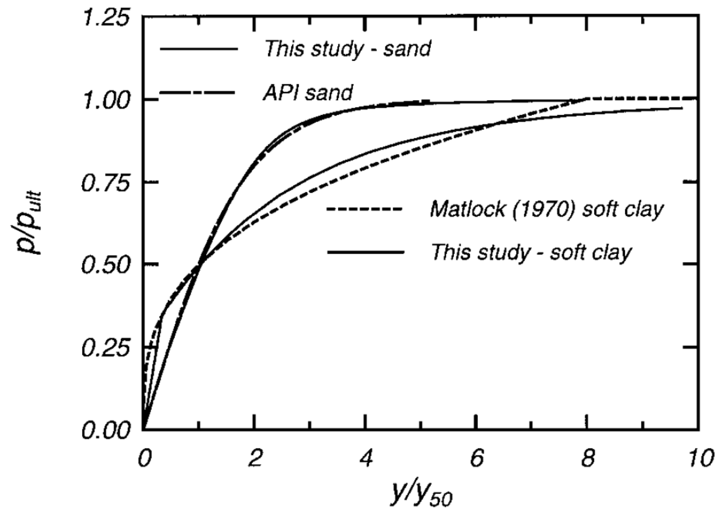

Fig. 5.5. Boulanger model influence on soil reaction curves [95].

$$k_{gap} = \frac{2}{\pi R_{ext}} \left(k'_{closure} + k'_{drag} \right) \tag{5.15}$$

$$k_s = k_s^{proposal} + k_{gap} \tag{5.16}$$

The Standard API *p*-*y* curves will be used for reference. Although it is a method that has been proved to develop some error when applied to OWTs cases, it still is the common formulation used when recurring to natural frequencies estimation and pile response in this industry. Following what was already presented in Chapter 3, the relevant stiffness can be defined as seen in Eq. 3.12. However, different approaches can be taken when defining the necessary parameters for the standard *p*-*y* curves by applying literature suggested expressions. Still, the majority of the majority of quantities will be defined by resorting to the common applied in the Standard. Refs. [48], [76], [85], and [112] were consulted for this matter. The PISA design model was not considered, as the estimation for the relative density seen in Eq. A.7 on Appendix A leads to values outside the scope of applicability of the presented expressions in Chapter 3.

Another reference that will be considered throughout testing will be the modified Vesic expression. This expression consists on the Vesic expression seen in Eq. 5.1, but with a coefficient equal to 1.0, instead of 0.65. A note should be performed that some differences are expected to occur, as the inputted data comes from a table with soil layer properties and not a continuous data acquisition of properties as seen in the various works of Prendergast et al. (Refs. [17], [68], and [89]). This can introduce relevant differences on the natural frequencies acquired.

5.1.1 Proposals discussion

As different factors were considered, a proper discussion on representativity should be performed. The representativity can be analysed through the soil stiffness evolution and what is commonly seen in literature. Attention should although be provided to the fact that there isn't a guide on how the soil stiffness profile should evolve with depth.

Proposals 1, 2, and 4 all have the same evolution shape. For sands a continuous increase with depth exists, while for clays a decrease can occur for a given layer due to the opposite evolution of the over-consolidation ratio with depth. This difference on soil type is the result of a different degree of evolution between the bearing capacity and the over-consolidation ratio. A constant amplification of the stiffness occurs from Proposal 1 to Proposal 2 and, finally, to Proposal 4. A steeper decrease with depth due to the over-consolidation ratio can be seen in Proposal 4.

Nevertheless, if Proposal 5 is considered with the Proposal 4 stiffness, then these effects are reverted, i.e., on clay layers, an increase of stiffness occurs with depth, like on sand layers. Still, a considerable step can exist in terms of stiffness level as different soil type layers are considered. This results from the unconsideration of the gap formation resistance on sand layers.

Regarding Proposal 3, a clear stiffness increase occurs with depth throughout the different layers. The consideration of the over-consolidation correction can lead to a slightly decreasing, almost constant, stiffness on clay layers. This means that the logic defying problem of an decreasing stiffness with depth doesn't exist here. The consideration of this proposal with Proposal 5 leads, again, to an increasing stiffness with depth through all the soil layers. Once more, considerable steps can be observed when changing between different soil type layers.

It is important to note that the available data can also influence how the stiffness profile is shaped. On the present work, constant properties were made available for each soil layer. In reality, these properties will vary with depth, even in the same soil layer. This means that different soil measuring/testing methods can lead to the acquisition of different data with different levels of accuracy, which, in turn, influence the stiffness profile with depth.

Comparing all proposals, except the last one (as it increases the clay layer stiffness only), for clays, similar stiffness are obtained. Meanwhile, for sands, a considerable higher stiffness is obtained for Proposal 3 compared with the rest, specially for high depths. This will be related to what was seen previously on Chapter 3, where an overestimation of the sand initial stiffness tends to occur for the calculated sand initial stiffness from the API/DNV Standard. One should also take into account that the API/DNV Standard base proposal (Proposal 3) will estimate a higher stiffness for sand layers even though significant discrepancies exist in terms of the Young's modulus. If indeed the soil shear modulus plays a vital role on the soil stiffness, the base formulation for soil stiffness calculation shouldn't provide a higher stiffness to a soil layer that has a smaller modulus that adjacent soil layers. This, however, occurs with Proposal 3, while Proposals 1, 2, and 4 already account explicitly for this moduli difference.

Nevertheless, according to Wang et al. [48], the initial stiffness of sand will be influenced by its angle of internal friction and/or by its relative density. Although the soil shear and Young moduli can be linked to these properties, a more correct approach for sands should be the direct interpolation of its stiffness using the angle of internal friction. For this reason, Proposal 3 can be more accurate on this soil type stiffness estimation. If this is indeed the case, then a significant different approach on clay stiffness estimation should be provided, as the correctly used estimation will vastly underestimate clay layers stiffness.

An existing incongruence that can be seen in the influencing factors resides on the bearing capacity factor. As pore pressure increases, the vertical effective stress decreases. This is reported to decrease the stiffness, but, as the factor as formulated, an increase will be seen. Nevertheless, it is expected that the bearing capacity of the soil to also decrease with the increase of pore pressure, which can compensate the decrease in the vertical effective shear stress. The magnitude of the relative influence between these two values with the pore pressure and liquefaction of the soil is unknown, but it was admitted that no increase in stiffness would occur with these phenomena. This can also mean that a factor relating the liquefaction of the soil may be missing to fully define the soil bearing capacity influence factor. Overall, more thought and validation should be given to the pressure influence on soil stiffness with depth.

5.1.2 Out of scope influences

A lot of relevant factors were not included in the models developed and used due to their complicated origins and formulations or undefined formulation. An example of a complicated influence formulation relies in the cyclic loading impact on the soil behaviour, as, depending on the soil, degradation or further consolidation can occur (although degradation is a more common and conservative approach on the matter). An example of undefined formulation is the effect of installation.

Cyclic loading can either increase or decrease the natural frequencies of the structure. The type of occurrence regarding this type of soil fatigue origin, is usually linked to a degradation of soil, with gap formation and loss in soil strength reducing the natural frequencies. However, for some types of soil, consolidation can occur as a consequence of cyclic excitations. This consolidation will then increase the soil stiffness and strength, rising the structure natural frequencies. Further understanding of these phenomena and correct prediction of what type of situation will occur are fundamental to model this influence source.

The time varying behaviour of the soil results from its all-time changing properties. Cyclic loading, as already stated, can harden or soften the soil. A more complex soil modelling approach should then be considered when admitting cyclic loads. An excellent example is modelling ratcheting effects as seen in various works. The adoption of a kinematic hardening soil model was not adopted in the present work, but, with the introduction of time-dependent loads and varying soil properties, such a model should be employed, as stated by Malekjafarian et al. [23].

Fan et al. in their work (Refs. [9], [22], and [46]) found that impact driving, the most common installation method of monopiles in the offshore wind industry, does significantly influence the initial stiffness of the soil. Although a predicted gain in soil stiffness between 40 % and 55 % is expected when considering sands, no formulation was developed and all the studies used experimental or numerical analyses (from elaborated FEM) data. This means that no application can be derived for the current study regarding this effect. The consideration of this influence is expected to rise the natural frequencies of the OWT.

An important influence on the natural frequencies is the scour phenomenon. However, this phenomenon was not considered in developed model or soil stiffness influence, as no information regarding scour was made available. Consequently, assuming values would lead to an extensive study on how scour changes the natural frequencies, as the more correct approach would be to estimate using the service life time up to the moment of analyse, which may need information that is not available. As stated in Chapter 3, scour will not only change the overall embedded length of the pile, but will also change the properties of the upper soil layers. This quantification is also difficult to perform without pre-scour data and after-scour data.

The soil anisotropy is another factor that is hard to account for. A given test to measure the soil properties can provide the stiffness and strength of the soil in one direction, but when the structure excites the soil in a different direction, distinct resistance can be found. This phenomenon is hard to properly quantify, as the soil can significantly vary from location to location and different factors are responsible for the anisotropic behaviour of the soil. The simplification of soil layers as horizontal can also be an influencing factor on the soil resistance and stiffness.

5.2. Full-scale testing

The experimental testing was conducted in four OWTs (WTG07, WTG22, WTG33, and WTG37) at Norther wind farm, Belgium (see Fig. 5.1), and included the measurement of the following signals (with acquisition frequency of at least 10 Hz):

- Tower top accelerations, for both fore-aft and side-side directions [m/s^2];
- Wind speed [m/s];
- Relative wind direction [deg];
- Generator and rotor speeds [rpm];
- Grid power output [kW].

The aforementioned sensors are by default embedded in each wind turbine generator unit during its manufacturing process. To estimate the frequency of the tower's first fore-aft mode, the turbines were tested according to the following two operational approaches:

1. **Shutdown / short pause in production**: a pause in energy production was carried out by rapidly increasing the blades' pitch angles up to about 90 degrees (close to feathered position) and, due to the consequent fast decrease in the aerodynamic loads (loss in torque and thrust), stopping the rotor from spinning and, thus, the power generation. This sudden modification in the aerodynamic thrust level serves as a means for exciting the tower fore-aft vibration modes (aligned with the upwind direction). A qualitative illustration of this procedure is depicted in Figs. 5.6 and 5.7;

2. **Normal production**: under stabilized wind conditions (low standard deviation in speed and relative direction of the wind) the signal-to-noise ratio can be greatly increased, allowing acquisition of data in terms of tower acceleration, which is desirable for the estimation of modes frequency.

Although the first of the listed procedures consists of producing a dynamic response typical of a decay test (thus allowing for the identification of both frequency and damping), the meteorological conditions in which the tests were performed (low wind speeds) were not the ideal for obtaining a signal-to-noise ratio high enough for accurate damping estimation. Nevertheless, for frequency estimation purposes it is enough to select signal windows with relatively stable generator rotation speed and pitch angles of the blades (see averages and standard deviations for the signals in Figs. 5.7a and 5.7b), since both experimentally and numerically calculated damping levels are very low. Moreover, the shutdown / short pause procedure is also valuable for differentiating the fore-aft from the frequencies of the side-side modes (since the vibration amplitudes of the former are usually more than twice as high as those from the latter).

The second procedure consisted of the data acquisition from the turbines in normal operation (power production). For that purpose, a Fast Fourier Transform was performed in the signals acquired in stabilized wind conditions and the obtained tower fore-aft frequencies were averaged. For all tested turbines, the resulting frequencies were almost a perfect match with the ones obtained from the first procedure [139].

5.3. Results

This section intends to present the results regarding the three previous main proposals and the added influence of gap formation in clays. These results will be compared with experimental natural frequencies. The reference fundamental natural frequency using the simple API Standard, without any correction factor will also be considered. Due to confidentiality, all presented results will be represented by relative errors concerning the measured fundamental natural frequency.

A benchmark model from Vestas was also used to have a reference point for the obtained results through the developed model. This benchmark model consists of an aeroelastic model based on the FLEX5 code. A modal-based approach is then used, i.e., the wind turbine modal shapes are obtained from the individual mode shapes of each component. Aerodynamics and aeroelastic codes are used for the determination of the wind turbine's response in the time domain or even in the frequency domain. These can also

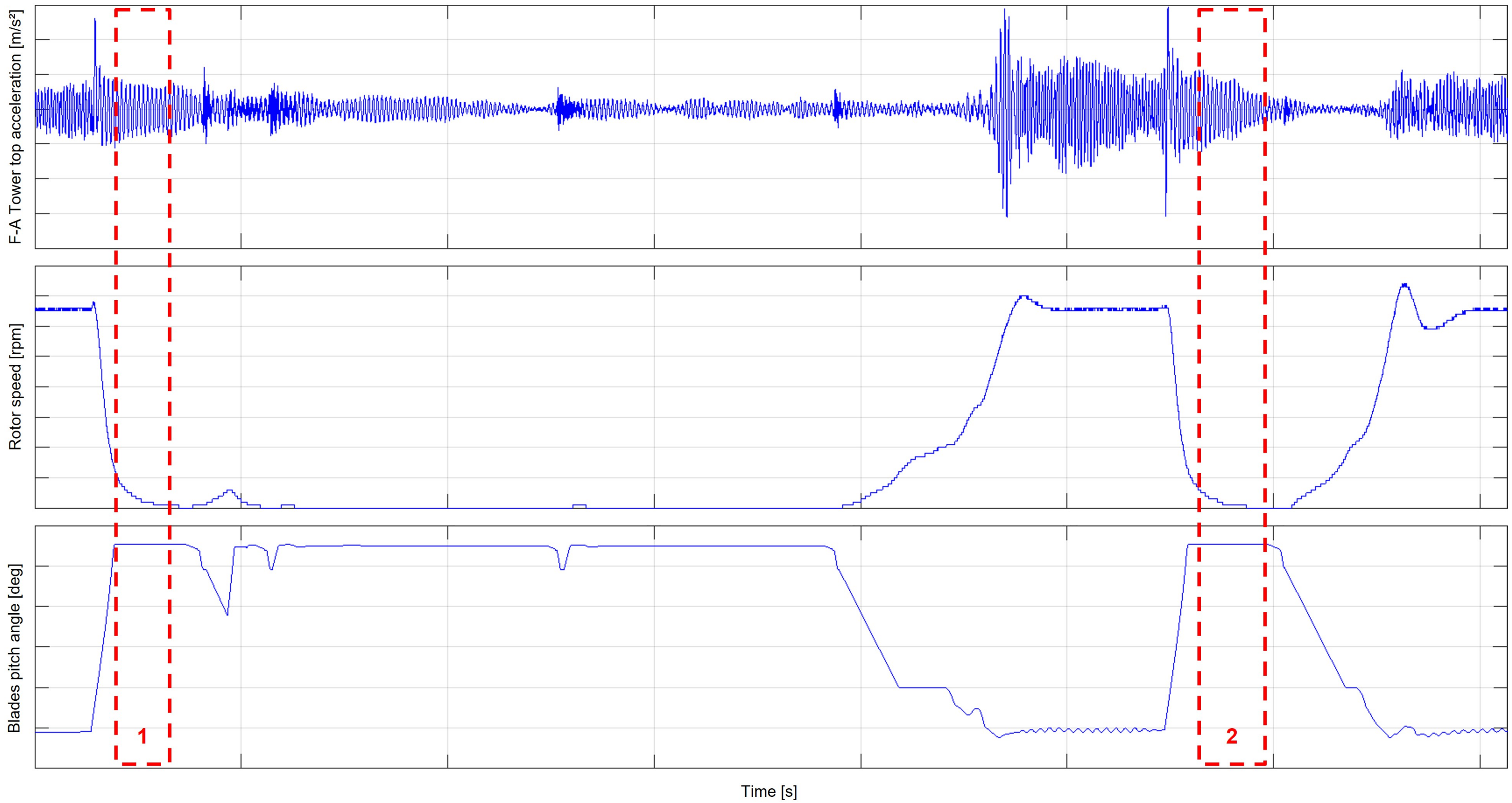

Fig. 5.6. Qualitative illustration of the main signals utilized in the modal characterization of the tested wind turbines. The response windows corresponding to the two shutdown procedures are enclosed by red rectangles 1 and 2 (dashed lines); details are shown in Figs. 5.7a and 5.7b, respectively.

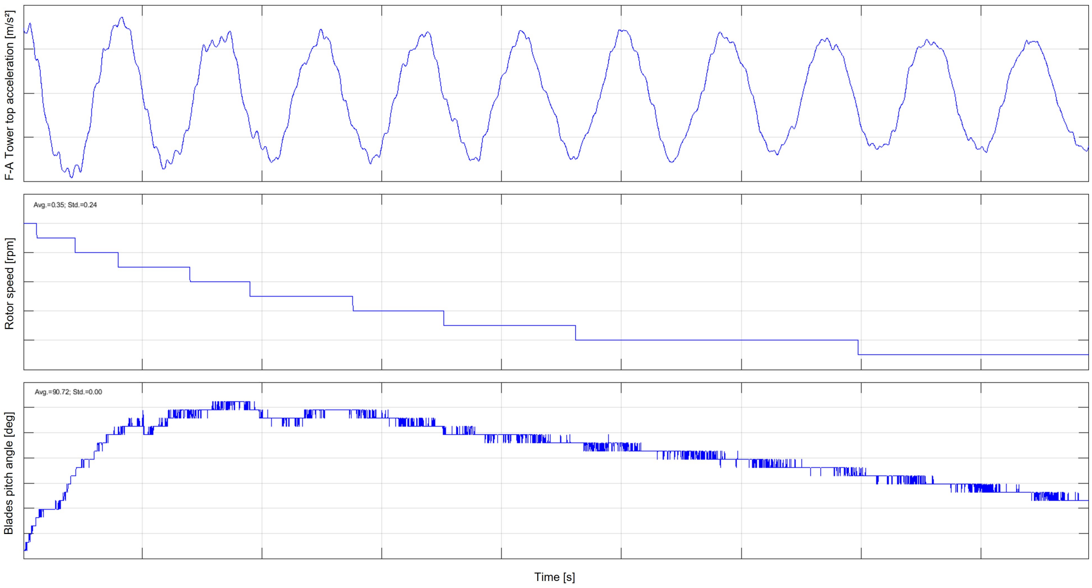

(a) Detail from the first shutdown window depicted in the signal from Fig. 5.6. It is worth mentioning the averages in rotor speed (lowest possible) and pitch angle (90 deg), as well as the associated low standard deviations for both variables.

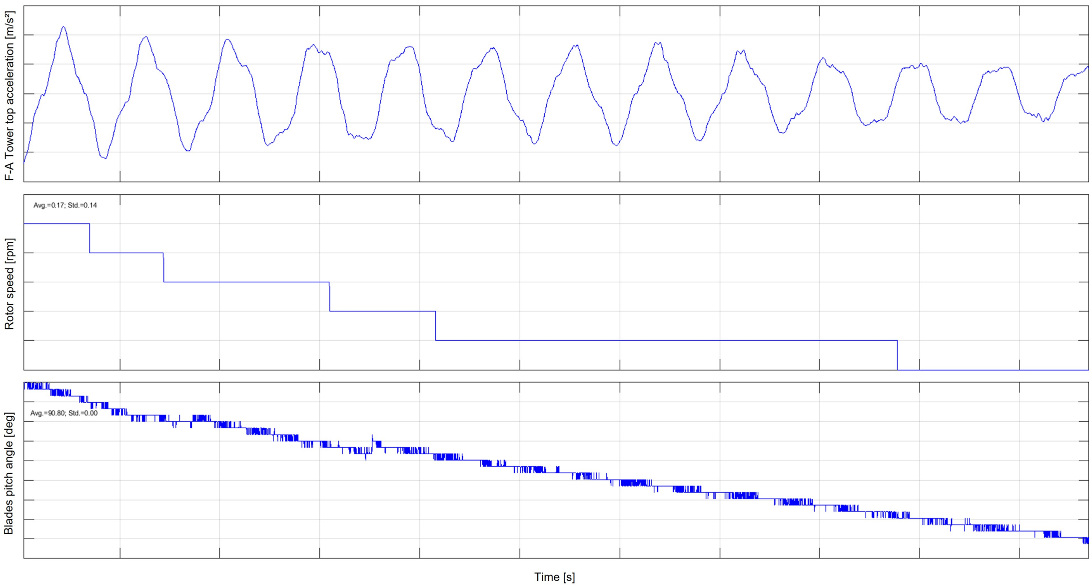

(b) Detail from the second shutdown window depicted in the signal from Fig. 5.6. It is worth mentioning the averages in rotor speed (lowest possible) and pitch angle (90 deg), as well as the associated low standard deviations for both variables.

Fig. 5.7. Response windows corresponding to the two shutdown procedures.

then model the physics around the interaction of the wind turbine with the surrounding turbulent wind field [140].

From here on in, data related to the Fore-Aft movement of the OWT will be presented. As a first point of reference, the natural frequencies from benchmark model and the developed model using the Standard approach were calculated. These results in relation to the measured first mode natural frequency of the OWT are presented in Table 5.2.

Table 5.2. Errors to the measured Fore-Aft frequency of each OWT.

Source	WTG07	WTG22	WTG33	WTG37
Benchmark model	-12.41%	-11.12%	-4.76%	-7.26%
Modified Vesic	-29.98%	-16.51%	-14.96%	-18.43%
API Standard	-12.16%	-7.40%	-2.32%	-9.17%
Proposal 1	-12.24%	-3.34%	-7.17%	-6.23%
Proposal 2	-10.77%	-3.09%	-5.48%	-5.08%
Proposal 3	-7.45%	-0.84%	-0.71%	-3.43%
Proposal 4	-9.58%	-2.13%	-4.23%	-3.78%
Proposal 5 $\left(k_s^{prop.3}\right)$	-4.83%	2.09%	0.27%	-0.22%
Proposal 5 $\left(k_s^{prop.4}\right)$	-5.36%	1.96%	-0.85%	-0.27%

Three references are then denoted: the frequency from a benchmark model at Vestas without accounting for rotor motion, the calculated frequencies using the API Standard and the modified Vesic stiffness approach through the developed model. The benchmark model frequency represents the status-quo of the currently used approach on the SSI considerations of the OWT design process. The developed model calculated frequency using the small-strain stiffness of API Standard *p-y* curves allows a direct comparison with the status-quo of the current design estimation for the natural frequencies. It also allows to draw some conclusions regarding the developed model's applicability. As it can be seen in Table 5.2, a close correspondence between the benchmark model and the developed model considering the API Standard exists. Differences that may exist are both due to the considered clay stiffness estimation and the overall approach to the soil model. Finally, the developed model calculated frequency considering the Modified Vesic proposition of soil stiffness permits a direct comparison with a slender and infinite beam approach on what is considered a rigid beam behaviour case.

Consulting Table 5.2, it is clear that the modified Vesic approach to the problem leads to a vast underestimation of the natural frequencies of the OWT. This is due to, as it was previously stated, the nature of the formulation considering the slender behaviour of the embedded structure. Consequently, the modified Vesic formulation leads to an overall smaller soil stiffness magnitude. This formulation led always to the smaller calculated/predicted natural frequencies. It can then be considered as a lower bound for the natural frequencies estimation, while the clamped tower consideration can be seen as an upper bound.

Studying all the proposals through Table 5.2, Proposal 5 is deemed as the best proposal. Proposals 1 and 2 presented similar results to the API Standard in some situations. This means that the implementation of these proposals wouldn't lead to any relevant advantage that the already well-studied Standard curves. However, Proposal 4, which has a similar approach to these proposals, presented better results, although significant errors could still be seen for the soil without clay governing properties. Proposal 3 presented very good results for cases WTG22 and WTG33. These predominately clayey locations also presented a distinct separation between sand and clay layers. For the cases where this distinct separation did not occur, an error has built up, with an important emphasis on the non-predominately clayey soil (WTG07). By assuming the added resistance due to gap formation, Proposal 5, natural frequency estimations within a $\pm 5\%$ bandwidth error were obtained for all the OWT locations. The consideration of this gap formation added resistance led to better results in all locations, except for the WTG22 case, where a slight overestimation when compared to Proposal 3, occurred.

Fig. 5.8 presents the results as errors concerning the measured first mode Fore-Aft natural frequency of each OWT. A grey bandwidth is also represented in the graph to denote a $\pm 5\%$ error bandwidth. In this figure, the best proposal from those previously mentioned is represented. Two alternatives to this proposal are considered, one using Proposal 3 and another using Proposal 4 as the base formulation for it.

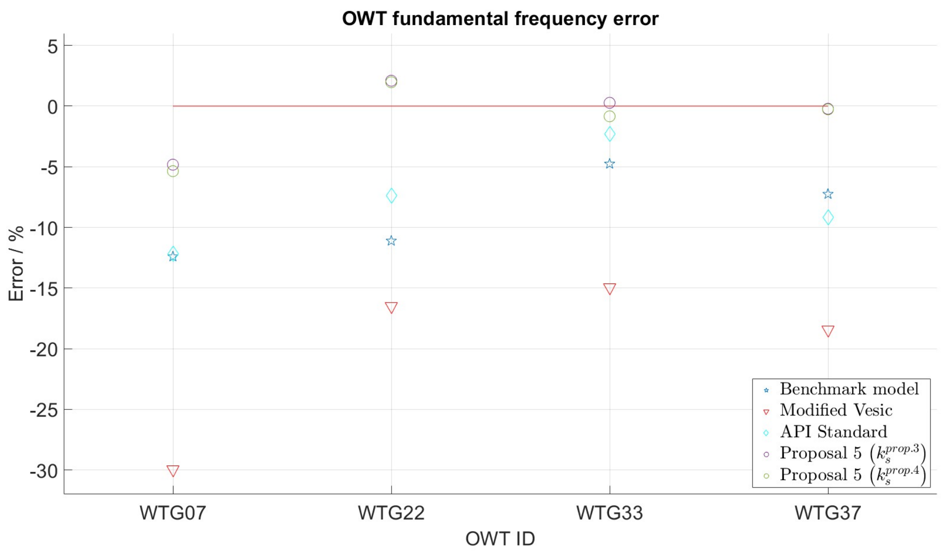

Fig. 5.8. Errors to the measured Fore-Aft frequency of each OWT.

From what can be seen, only Proposal 5 with Proposal 3 as a base is within the 5% bandwidth for all OWT locations admitted. The highest error was observed for the WTG07 OWT, where mixed soil was present, i.e., no soil type is predominate in that location. The remaining cases are locations predominately governed by clayey soils, where the best proposal, independently of its base, managed to be within a 2% bandwidth. A result from the developed model inside this bandwidth can then be corrected through the use of a more accurate model that accounts for different element dynamics, as the developed model can have numerical-related errors.

Fig. 5.9 presents the general tendency followed by the calculated fundamental natural frequency versus the experimental frequencies. The displayed frequencies are normalised by using the average of the experimental natural frequencies of all tested OWTs. As it can be observed, the model is capable to follow the same tendency registered from the full-scale testing, with the exception of the WTG07 OWT. Once again, it is important to remember that this is the OWT that is not embedded on a predominately clayey soil.

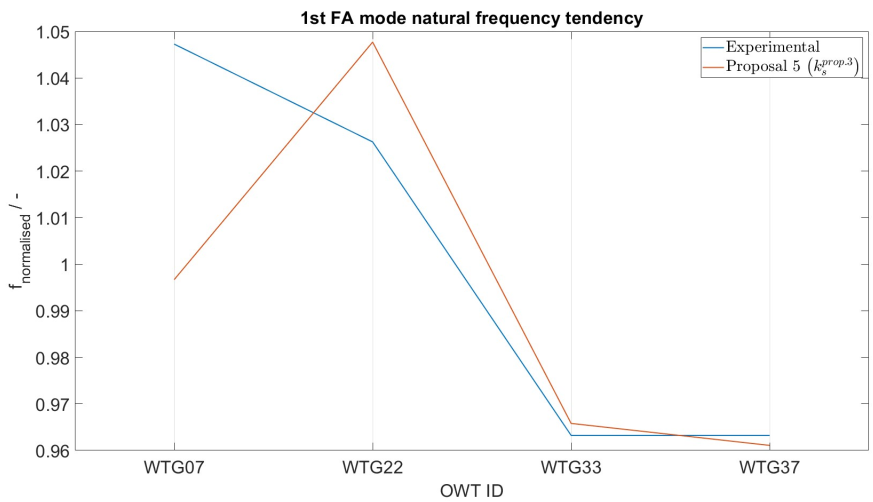

Fig. 5.9. Estimated fundamental frequency tendency versus the experimental fundamental frequency tendency.

Considering Proposal 5, different natural frequency error changes were seen from the base formulation assumed (Proposals 3 and 4). As Proposal 5 only augments the clay stiffness estimation when compared with Proposal 3, relevant differences were observed for the cases where clay was present predominately present in surface layers. For cases where clay was situated in deeper regions, the changes were not so abrupt. This comes then to confirm that the shallower soil layers contribute more to the estimated natural frequencies of the structure than those in deeper regions.

It should be noted that pile installation, an effect that wasn't considered in the present soil modelling, has, more or less, the same influence on sands that the proposed aspect ratio influence factor. Table 5.3 presents the errors to the measured natural frequencies, if a 40% increase in sand stiffness is considered (as it is the minimum increase presented in the work of Fan et al. [46]) while using Proposal 5. It can be seen that the influence is not that significant in terms of natural frequencies increase. However, pile installation can also increase other soil properties, increasing its effective influence on the natural frequencies and stiffness estimation.

Source	WTG07	WTG22	WTG33	WTG37
Proposal 5 $\left(k_s^{prop.3}\right)$	-4.83%	2.09%	0.27%	-0.22%
Proposal 5 $\left(k_s^{prop.3}\right)$ and P.I. effects	-4.79%	2.09%	0.71%	-0.22%

Table 5.3. Comparison between considering a 40% increase in sand stiffness due to Pile Installation (P.I.) and not considering.

5.4. Final Remarks

Different proposals for the soil stiffness consideration were presented. The consideration of different base formulations as well as different influence factors was discussed. A tentative to introduce a direct relation between the bending of the monopile and the reaction of the soil was also performed. This tentative is important as the SSI should be accounted for in the soil stiffness calculation. Only the deemed best and fully developed proposals were presented and used for results comparison.

Throughout the formulation studies, it was noted that the main influence on fundamental natural frequency came from the top soil layers. As different stiffness profiles were obtained, significant differences were observed to occur with ease at the deep soil layers, but that itself did not increase in a relevant way the natural frequencies. It was when the shallower soil layers changed in stiffness that the more noted alterations in the natural frequencies happened.

Although a set of factors were included to account for important factors that change the soil stiffness profile, different influences regarding the soil were not considered in the modelling of the presented problem. Reasons such as complicated origins and unknown formulations led to this decision. Some limitations on the data available had also some weight on the decision. Uncertainties would be introduced if considerations were made regarding these topics, as well as considering specific situations that would only be viable for the studied cases. The disregarded factors could increase or decrease the natural frequencies acquired.

It can then be said that the best-proposed formulation is viable to use in predominately clayey soils, where, in these conditions, an error of around 2% is expected. For soils that have considerable soil type variations, a slightly bigger error can be expected. This may be related to the effects of adjacent soil layer interactions. The model wasn't tested for conditions where predominately sandy soil existed. However, by using the API Standard as the base of the best-formulated proposal, a decent estimation is expected in those conditions. Nonetheless, further work should be performed to validate and correct the proposed formulation.

Chapter 6

Conclusion

6.1. Conclusions

Offshore wind turbines are complex structures. Although similar to their counterpart onshore wind turbines, the introduction of a bigger and complex sub-structure, as well as being installed in an offshore environment, leads to further considerations on the soil behaviour. The overall SSI of the system plays a bigger role in the modal properties on OWT, where a monopile foundation is usually selected. The demand for more energy leads to the necessity of installing bigger wind turbines, which, consequently, need bigger foundations, increasing the area of interaction between the soil and the structure.

An increase in OWT foundation can lead to a more rigid behaviour of the structure. With current Standards being formulated for slender foundations coming from the oil and gas industry, a significant error is seen in terms of modal properties, mainly in the fundamental natural frequency of the OWT. As there is a dependency of the soil stiffness with strain and variation of soil properties with soil-related phenomena, such as scour and other environmental occurrences, the quantification of the soil stiffness throughout time will change. This is significantly important for short piles that behave rigidly. The soil stiffness calculation should, then, focus on these points to ensure that the modal properties of the system are correctly predicted.

As common soil stiffness formulations fail to account for this variety of phenomena, several investigators have broached the topic to find correction factors and different formulations to get closure to the actual stiffness of a given soil stratum. However, there is not a lot of consensus on the literature or proper exposition of conclusions. Instead of an exhausting study on soil stiffness formulation, the utilization of finite elements for the prediction of the structure response is getting more common, as complex constitutive soil laws can be employed. Yet, finite element analyses are very computational expensive procedures. For this reason, a simple approach as the one based on the Winkler approach (beam on a Winkler spring foundation) is commonly used and is the support for the API and DNV Standards. Different approaches to soil foundation can though be considered.

The current work presented a set of simple formulations to correct the common expressions used based on the Winkler approach. The Winkler approach was selected as the most common approach on the subject. A simple model of one element composed of a p-version finite Timoshenko element was developed to easily conclude the soil stiffness formulations. The formulations were developed considering a small-strain condition. The utilization of a simple model allowed a fast and computationally efficient process to conclude on the assumptions performed. A validation process followed by a correction/calibration procedure was elaborated considering analytical solutions from the Euler-Bernoulli theory and a well-validated benchmark model.

The developed model presented a convergence to the fourth decimal number with a shape function degree of 12. However, as the convergence study was performed on a constant section beam, a slighter slower convergence is expected. Consequently, a degree of 20 for the shape functions would guarantee the desired convergence for a more complex structure. Due to the utilization of a single element, numerical issues may appear due to a high shape function degree, which led to the decision to maximise the shape function degree to 18, which is a good balance between result accuracy and numerical issues minimisation.

Regarding the modal properties study, an emphasis was performed on the first mode natural frequencies. As the first natural modes are the ones responsible for the majority of soil reaction, i.e., the first natural modes dominate the structure's response, they tend to be the main focus during modal properties analyses. After performing a sensitivity study on the influence of the different damping sources on the natural frequencies and observing a meaningless influence, the comparison between the estimated natural frequencies from the benchmark and developed models and the experimental natural frequencies was performed considering an undamped situation. Five main proposals were presented. From these, two proposals, Proposals 3 and 5 allowed always a smaller error than what was acquired using the benchmark model and the API Standard on the developed model. Proposal 5 allowed a constant error smaller than 5% for all the studied cases, meeting the initial work goals. Significant differences were then verified using the proposed formulations, as the benchmark model and the API Standard in the developed model both had errors on a 12.5% bandwidth. It was also observed the non-applicability of direct slender approaches, such as the Modified Vesic formulation, on rigid-like behaved piles.

6.2. Future works

The present work considers a Winkler approach, as it is widely used in the industry and throughout literature studies. Besides the pros and cons that it has when compared to other approaches (like the super-element approach), other methods exist for foundation modelling. Models such as the Pasternak model and the Hetenyi model are possibilities to model a given soil that has not been investigated for this application. The consideration of a different and more complete foundation model considering the soil as a spring foundation and the explicit inclusion of the structure properties on that model may beneficially influence the SSI modelling.

Similarly, a more complex and accurate model can be developed. Using p-version shell finite elements for the structure modelling can increase the accuracy of the estimated results, without the cost of the h-version FEM approach. The utilization of shell elements is more than compatible with this type of problem.

It has to be noted that a good evaluation of the soil properties at a given instant in time, as well as before and after installation of a wind turbine are necessary to have a good guide on what properties have changed and quantify the degree of influence of different aspects that are assumed to alter the modal properties of an OWT. Without proper and very detailed properties of the soil, analyses regarding the SSI effects are not possible. Likewise, performing a given analysis with estimations of parameters leads to a high degree of uncertainty, as well as the possibility of incurring significant errors from the real situation.

The consideration of a time-independent SSI is sufficient for a first indication of the fundamental natural frequency interval at a given moment after the OWT installation. However, as time progresses, storms (cyclic high loads), cyclic movements, degradation natured phenomena (scour), and other occurrences affect the modal properties found in this same OWT. Consequently, a time-varying analysis should be performed to account for all these effects, since they vary with time.

Likewise, the inherent non-linear behaviour of the soil modifies the expected soil stiffness with increasing strain. This means that different mechanisms will be in place for considerable movements of the structure. The present work only considered a situation of small strain, where these mechanisms do not influence. Although small-strain situations are common, as storms and similar extreme loads occur, it is expected that the non-linear and plastic behaviours of the soil to be very significant.

Nonetheless, other SSI influences that were not modelled can play an important part in the structure's modal properties. As so, besides trying to validate the proposed influencing factors, a further study on how these different influences can be included in the model should exist.

Due to the inherent developed model simplicity, a one-dimensional/plane case was considered. The introduction of a second plane (and eventually torsion) allows the introduction of existing misalignment concerning wind and wave loading, as well as the yaw misalignment, and wind direction changes. These can also have an impact on the estimated structure response.

As it is difficult to achieve a very precise prediction of the structure's response even with complex models, a statistical approach should be considered. In order to better comprehend and predict the overall response of the structure, statistical notions can be introduced for the analysis of this kind of problem.

References

[1] T. Letcher. *Wind Energy Engineering: A Handbook for Onshore and Offshore Wind Turbines*. Elsevier Science, 2017. ISBN: 9780128094297. URL: https://books.google.pt/books?id=hRZ2DQAAQBAJ.

[2] Junbo Jia. "Offshore Structures and Hydrodynamic Modeling". In: *Soil Dynamics and Foundation Modeling: Offshore and Earthquake Engineering*. Cham: Springer International Publishing, 2018, pp. 269–313. ISBN: 978-3-319-40358-8. DOI: 10.1007/978-3-319-40358-8_9. URL: https://doi.org/10.1007/978-3-319-40358-8_9.

[3] Taimoor Asim et al. "A Review of Recent Advancements in Offshore Wind Turbine Technology". In: *Energies* 15.2 (2022). ISSN: 1996-1073. DOI: 10.3390/en15020579. URL: https://www.mdpi.com/1996-1073/15/2/579.

[4] S. Aasen et al. "Effect of foundation modelling on the fatigue lifetime of a monopile-based offshore wind turbine". In: *Wind Energy Science* 2.2 (2017), pp. 361–376. DOI: 10.5194/wes-2-361-2017. URL: https://wes.copernicus.org/articles/2/361/2017/.

[5] Vicente Negro et al. "Monopiles in offshore wind: Preliminary estimate of main dimensions". In: *Ocean Engineering* 133 (2017), pp. 253–261. ISSN: 0029-8018. DOI: https://doi.org/10.1016/j.oceaneng.2017.02.011. URL: https://www.sciencedirect.com/science/article/pii/S0029801817300690.

[6] Byron W. Byrne and Guy T. Houlsby. "Assessing Novel Foundation Options for Offshore Wind Turbines". In: (2005). URL: https://www.researchgate.net/profile/Byron-Byrne/publication/265874157_Assessing_Novel_Foundation_Options_for_Offshore_Wind_Turbines/links/552d717c0cf21acb092175c2/Assessing-Novel-Foundation-Options-for-Offshore-Wind-Turbines.pdf.

[7] Youhu Zhang and Knut H. Andersen. "Soil reaction curves for monopiles in clay". In: *Marine Structures* 65 (2019), pp. 94–113. ISSN: 0951-8339. DOI: https://doi.org/10.1016/j.marstruc.2018.12.009. URL: https://www.sciencedirect.com/science/article/pii/S0951833918300698.

[8] B. Yeter, Y. Garbatov, and C. Guedes Soares. "Numerical and experimental study of the ultimate strength of a monopile structure". In: *Engineering Structures* 194 (2019), pp. 290–299. ISSN: 0141-0296. DOI: https://doi.org/10.1016/j.engstruct.2019.05.074. URL: https://www.sciencedirect.com/science/article/pii/S0141029618328189.

[9] Shengsheng Fan, Britta Bienen, and Mark F. Randolph. “Centrifuge study on effect of installation method on lateral response of monopiles in sand”. In: *International Journal of Physical Modelling in Geotechnics* 21.1 (2021), pp. 40–52. DOI: 10.1680/jphmg.19.00013. eprint: https://doi.org/10.1680/jphmg.19.00013. URL: https://doi.org/10.1680/jphmg.19.00013.

[10] Evangelos Kementzetzidis et al. “Geotechnical aspects of offshore wind turbine dynamics from 3D non-linear soil-structure simulations”. In: *Soil Dynamics and Earthquake Engineering* 120 (2019), pp. 181–199. ISSN: 0267-7261. DOI: https://doi.org/10.1016/j.soildyn.2019.01.037. URL: https://www.sciencedirect.com/science/article/pii/S026772611731182X.

[11] Erica Bush and Lance Manuel. “Foundation models for offshore wind turbines”. In: *47th AIAA Aerospace Sciences Meeting including The New Horizons Forum and Aerospace Exposition*. DOI: 10.2514/6.2009-1037. eprint: https://arc.aiaa.org/doi/pdf/10.2514/6.2009-1037. URL: https://arc.aiaa.org/doi/abs/10.2514/6.2009-1037.

[12] Karin Norén-Cosgriff and Amir M. Kaynia. “Estimation of natural frequencies and damping using dynamic field data from an offshore wind turbine”. In: *Marine Structures* 76 (2021), p. 102915. ISSN: 0951-8339. DOI: https://doi.org/10.1016/j.marstruc.2020.102915. URL: https://www.sciencedirect.com/science/article/pii/S0951833920302070.

[13] M. Damgaard, L.V. Andersen, and L.B. Ibsen. “Dynamic response sensitivity of an offshore wind turbine for varying subsoil conditions”. In: *Ocean Engineering* 101 (2015), pp. 227–234. ISSN: 0029-8018. DOI: https://doi.org/10.1016/j.oceaneng.2015.04.039. URL: https://www.sciencedirect.com/science/article/pii/S0029801815001201.

[14] Zhen Guo et al. “Model Tests on the Long-Term Dynamic Performance of Offshore Wind Turbines Founded on Monopiles in Sand”. In: *Journal of Offshore Mechanics and Arctic Engineering* 137.4 (Aug. 2015). 041902. ISSN: 0892-7219. DOI: 10.1115/1.4030682. eprint: https://asmedigitalcollection.asme.org/offshoremechanics/article-pdf/137/4/041902/6245078/omae_137_04_041902.pdf. URL: https://doi.org/10.1115/1.4030682.

[15] M. Damgaard et al. “Assessment of the dynamic behaviour of saturated soil subjected to cyclic loading from offshore monopile wind turbine foundations”. In: *Computers and Geotechnics* 61 (2014), pp. 116–126. ISSN: 0266-352X. DOI: https://doi.org/10.1016/j.compgeo.2014.05.008. URL: https://www.sciencedirect.com/science/article/pii/S0266352X14000974.

[16] M. Wang et al. “Derivation and validation of soil-pile-interaction models for offshore wind turbines”. In: July 2013, pp. 181–188.

[17] L.J. Prendergast and K. Gavin. “A comparison of initial stiffness formulations for small-strain soil–pile dynamic Winkler modelling”. In: *Soil Dynamics and Earthquake Engineering* 81 (2016), pp. 27–41. ISSN: 0267-7261. DOI: https://doi.org/10.1016/j.soildyn.2015.11.006. URL: https://www.sciencedirect.com/science/article/pii/S0267726115002869.

[18] A. Schendel et al. "Processes and evolution of scour around a monopile induced by tidal currents". In: *Coastal Engineering* 139 (2018), pp. 65–84. ISSN: 0378-3839. DOI: https://doi.org/10.1016/j.coastaleng.2018.05.004. URL: https://www.sciencedirect.com/science/article/pii/S0378383917306038.

[19] Wenyu Jiang and Cheng Lin. "Lateral responses of monopile-supported offshore wind turbines in sands under combined effects of scour and earthquakes". In: *Soil Dynamics and Earthquake Engineering* 155 (2022), p. 107193. ISSN: 0267-7261. DOI: https://doi.org/10.1016/j.soildyn.2022.107193. URL: https://www.sciencedirect.com/science/article/pii/S0267726122000422.

[20] *Dynamic Mudline Damping for Offshore Wind Turbine Monopiles*. Vol. Volume 9A: Ocean Renewable Energy. International Conference on Offshore Mechanics and Arctic Engineering. V09AT09A025. June 2014. DOI: 10.1115/OMAE2014-23406. eprint: https://asmedigitalcollection.asme.org/OMAE/proceedings-pdf/OMAE2014/45530/V09AT09A025/4432361/v09at09a025-omae2014-23406.pdf. URL: https://doi.org/10.1115/OMAE2014-23406.

[21] R. A. Oriani. "Hydrogen Embrittlement of Steels". In: *Annual Review of Materials Science* 8.1 (1978), pp. 327–357. DOI: 10.1146/annurev.ms.08.080178.001551. eprint: https://doi.org/10.1146/annurev.ms.08.080178.001551. URL: https://doi.org/10.1146/annurev.ms.08.080178.001551.

[22] Shengsheng Fan, Britta Bienen, and Mark F. Randolph. "Effects of Monopile Installation on Subsequent Lateral Response in Sand, Part I: Pile Installation". In: *Journal of Geotechnical and Geoenvironmental Engineering* 147.5 (2021), p. 04021021. DOI: 10.1061/(ASCE)GT.1943-5606.0002467. eprint: https://ascelibrary.org/doi/pdf/10.1061/\%28ASCE\%29GT.1943-5606.0002467. URL: https://ascelibrary.org/doi/abs/10.1061/%5C%28ASCE%5C%29GT.1943-5606.0002467.

[23] Abdollah Malekjafarian et al. "Foundation damping for monopile supported offshore wind turbines: A review". In: *Marine Structures* 77 (2021), p. 102937. ISSN: 0951-8339. DOI: https://doi.org/10.1016/j.marstruc.2021.102937. URL: https://www.sciencedirect.com/science/article/pii/S0951833921000058.

[24] Hendrik Sturm and Lars Andresen. "On the Use of the Finite Element Method for the Design of Offshore Wind Turbine Foundations". In: *Desiderata Geotechnica*. Ed. by Wei Wu. Cham: Springer International Publishing, 2019, pp. 193–204. ISBN: 978-3-030-14987-1.

[25] Mohammad Mahdi Memarpour et al. "Cyclic lateral response of pile foundations in offshore platforms". In: *Computers and Geotechnics* 42 (2012), pp. 180–192. ISSN: 0266-352X. DOI: https://doi.org/10.1016/j.compgeo.2011.12.007. URL: https://www.sciencedirect.com/science/article/pii/S0266352X11002011.

[26] K.A. Abhinav and Nilanjan Saha. "Dynamic Analysis of an Offshore Wind Turbine Including Soil Effects". In: *Procedia Engineering* 116 (2015). 8th International Conference on Asian and Pacific Coasts (APAC 2015), pp. 32–39. ISSN: 1877-7058. DOI: https://doi.org/10.1016/j.proeng.2015.08.261. URL: https://www.sciencedirect.com/science/article/pii/S1877705815019165.

[27] W.G. Versteijlen, A.V. Metrikine, and K.N. van Dalen. “A method for identification of an effective Winkler foundation for large-diameter offshore wind turbine support structures based on in-situ measured small-strain soil response and 3D modelling”. In: *Engineering Structures* 124 (2016), pp. 221–236. ISSN: 0141-0296. DOI: https://doi.org/10.1016/j.engstruct.2016.06.007. URL: https://www.sciencedirect.com/science/article/pii/S0141029616302723.

[28] R. Shirzadeh et al. “Experimental and computational damping estimation of an offshore wind turbine on a monopile foundation”. In: *Journal of Wind Engineering and Industrial Aerodynamics* 120 (2013), pp. 96–106. ISSN: 0167-6105. DOI: https://doi.org/10.1016/j.jweia.2013.07.004. URL: https://www.sciencedirect.com/science/article/pii/S0167610513001359.

[29] Patrick Berthelot et al. *Recommendations for planning and designing foundations of offshore wind turbines*. Version 2.1. Comité Français de Mécanique des Sols et de Géotechnique, Oct. 2020. URL: https://www.cfms-sols.org/sites/default/files/rapport_final_eoliennes_offshore_angl_2020-10-30_version_web_-_archive.pdf.

[30] Yung-Yen Ko. “A simplified structural model for monopile-supported offshore wind turbines with tapered towers”. In: *Renewable Energy* 156 (2020), pp. 777–790. ISSN: 0960-1481. DOI: https://doi.org/10.1016/j.renene.2020.03.149. URL: https://www.sciencedirect.com/science/article/pii/S0960148120304821.

[31] M. Damgaard et al. “Cross-wind modal properties of offshore wind turbines identified by full scale testing”. In: *Journal of Wind Engineering and Industrial Aerodynamics* 116 (2013), pp. 94–108. ISSN: 0167-6105. DOI: https://doi.org/10.1016/j.jweia.2013.03.003. URL: https://www.sciencedirect.com/science/article/pii/S0167610513000603.

[32] Clara Matutano et al. “Scour prediction and scour protections in offshore wind farms”. In: *Renewable Energy* 57 (2013), pp. 358–365. ISSN: 0960-1481. DOI: https://doi.org/10.1016/j.renene.2013.01.048. URL: https://www.sciencedirect.com/science/article/pii/S0960148113000864.

[33] Junbo Jia. “Soil Behavior”. In: *Soil Dynamics and Foundation Modeling: Offshore and Earthquake Engineering*. Cham: Springer International Publishing, 2018, pp. 3–74. ISBN: 978-3-319-40358-8. DOI: 10.1007/978-3-319-40358-8_1. URL: https://doi.org/10.1007/978-3-319-40358-8_1.

[34] Guillermo M. Álamo et al. “Dynamic soil-structure interaction in offshore wind turbines on monopiles in layered seabed based on real data”. In: *Ocean Engineering* 156 (2018), pp. 14–24. ISSN: 0029-8018. DOI: https://doi.org/10.1016/j.oceaneng.2018.02.059. URL: https://www.sciencedirect.com/science/article/pii/S0029801818302087.

[35] Madjid Karimirad. *Offshore mechanics: Structural and Fluid Dynamics for Recent Applications*. eng. First edition. Hoboken NJ, USA: John Wiley and Sons Ltd, 2018. ISBN: 9781119216636.

[36] Srinivasan Chandrasekaran. “Introduction to Offshore Platforms”. In: *Dynamic Analysis and Design of Offshore Structures*. New Delhi: Springer India, 2015, pp. 1–24. ISBN: 978-81-322-2277-4. DOI: 10.1007/978-81-322-2277-4_1. URL: https://doi.org/10.1007/978-81-322-2277-4_1.

[37] Krzysztof Trojnar. “Multi scale studies of the new hybrid foundations for offshore wind turbines”. In: *Ocean Engineering* 192 (2019), p. 106506. ISSN: 0029-8018. DOI: https://doi.org/10.1016/j.oceaneng.2019.106506. URL: https://www.sciencedirect.com/science/article/pii/S002980181930647X.

[38] International Electrotechnical Commission, ed. *IEC 61400-1: Wind turbines - Part 1: Design requirements*. Geneva, Switzerland, 2005.

[39] Chao Chen and Philippe Duffour. “Modelling damping sources in monopile supported offshore wind turbines”. In: *Wind Energy* 21.11 (2018), pp. 1121–1140. DOI: https://doi.org/10.1002/we.2218. eprint: https://onlinelibrary.wiley.com/doi/pdf/10.1002/we.2218. URL: https://onlinelibrary.wiley.com/doi/abs/10.1002/we.2218.

[40] Bipin K. Gupta and Dipanjan Basu. “Offshore wind turbine monopile foundations: Design perspectives”. In: *Ocean Engineering* 213 (2020), p. 107514. ISSN: 0029-8018. DOI: https://doi.org/10.1016/j.oceaneng.2020.107514. URL: https://www.sciencedirect.com/science/article/pii/S0029801820305278.

[41] Martin Achmus et al. “Un- and reloading stiffness of monopile foundations in sand”. In: *Applied Ocean Research* 84 (2019), pp. 62–73. ISSN: 0141-1187. DOI: https://doi.org/10.1016/j.apor.2019.01.001. URL: https://www.sciencedirect.com/science/article/pii/S014111871830573X.

[42] A.T. Myers et al. “Strength, stiffness, resonance and the design of offshore wind turbine monopiles”. In: *Engineering Structures* 100 (2015), pp. 332–341. ISSN: 0141-0296. DOI: https://doi.org/10.1016/j.engstruct.2015.06.021. URL: https://www.sciencedirect.com/science/article/pii/S0141029615003971.

[43] Det Norske Veritas, ed. *DNV-OS-J101 - Design of Offshore Wind Turbine Structures*. May 2014.

[44] E. Hau and H. Renouard. *Wind Turbines: Fundamentals, Technologies, Application, Economics*. SpringerLink: Bücher. Springer Berlin Heidelberg, 2013. ISBN: 9783642271519. URL: https://books.google.dk/books?id=KeNEAAAAQBAJ.

[45] M. H. Hansen. “Aeroelastic instability problems for wind turbines”. In: *Wind Energy* 10.6 (2007), pp. 551–577. DOI: https://doi.org/10.1002/we.242. eprint: https://onlinelibrary.wiley.com/doi/pdf/10.1002/we.242. URL: https://onlinelibrary.wiley.com/doi/abs/10.1002/we.242.

[46] Shengsheng Fan, Britta Bienen, and Mark F. Randolph. “Effects of Monopile Installation on Subsequent Lateral Response in Sand, Part II: Lateral Loading”. In: *Journal of Geotechnical and Geoenvironmental Engineering* 147.5 (2021), p. 04021022. DOI: 10.1061/(ASCE)GT.1943-5606.0002504. eprint: https://ascelibrary.org/doi/pdf/10.1061/\%28ASCE\%29GT.1943-5606.0002504. URL: https://ascelibrary.org/doi/abs/10.1061/%5C%28ASCE%5C%29GT.1943-5606.0002504.

[47] Det Norske Veritas, ed. *DNVGL-ST-0126 - Support structures for wind turbines*. 2016.

[48] H. Wang et al. “Quantifying the influence of pile diameter on the load transfer curves of laterally loaded monopile in sand”. In: *Applied Ocean Research* 101 (2020), p. 102196. ISSN: 0141-1187. DOI: https://doi.org/10.1016/j.apor.2020.102196. URL: www.sciencedirect.com/science/article/pii/S0141118719302433.

[49] Byron W. Byrne et al. “PISA design model for monopiles for offshore wind turbines: application to a stiff glacial clay till”. In: *Géotechnique* 70.11 (2020), pp. 1030–1047. DOI: 10.1680/jgeot.18.P.255. eprint: https://doi.org/10.1680/jgeot.18.P.255. URL: https://doi.org/10.1680/jgeot.18.P.255.

[50] Ronald Brinkgreve et al. “Validation and Application of a New Software Tool Implementing the PISA Design Methodology”. In: *Journal of Marine Science and Engineering* 8.6 (2020). ISSN: 2077-1312. DOI: 10.3390/jmse8060457. URL: https://www.mdpi.com/2077-1312/8/6/457.

[51] Chenrong Zhang, Jian Yu, and Maosong Huang. “Winkler load-transfer analysis for laterally loaded piles”. In: *Canadian Geotechnical Journal* 53.7 (2016), pp. 1110–1124. DOI: 10.1139/cgj-2015-0394. eprint: https://doi.org/10.1139/cgj-2015-0394. URL: https://doi.org/10.1139/cgj-2015-0394.

[52] Ben He, Shaoli Yang, and Knut H. Andersen. “Soil parameters for offshore wind farm foundation design: A case study of Zhuanghe wind farm”. In: *Engineering Geology* 285 (2021), p. 106055. ISSN: 0013-7952. DOI: https://doi.org/10.1016/j.enggeo.2021.106055. URL: https://www.sciencedirect.com/science/article/pii/S0013795221000661.

[53] Wystan Carswell et al. “Influence of foundation damping on offshore wind turbine monopile design loads”. In: *Marine Structures* 83 (2022), p. 103154. ISSN: 0951-8339. DOI: https://doi.org/10.1016/j.marstruc.2021.103154. URL: https://www.sciencedirect.com/science/article/pii/S0951833921002045.

[54] Aparna Verma and S. M. Ali Jawaid. “Development of Soil Plug in Pipe Pile: A Review”. In: *International Journal of Applied Engineering Research* 13.11 (2018), pp. 8929–8935. ISSN: 0973-4562.

[55] Shu-wang Yan et al. “Pit bearing capacity effect on status of soil plug during pile driving in ocean engineering”. In: *China Ocean Engineering* 25.2 (June 2011), pp. 295–304. ISSN: 0890-5487. DOI: 10.1007/s13344-011-0024-7. URL: https://doi.org/10.1007/s13344-011-0024-7.

[56] Wenyu Jiang, Cheng Lin, and Min Sun. “Seismic responses of monopile-supported offshore wind turbines in soft clays under scoured conditions”. In: *Soil Dynamics and Earthquake Engineering* 142 (2021). ISSN: 0267-7261. DOI: https://doi.org/10.1016/j.soildyn.2020.106549. URL: https://www.sciencedirect.com/science/article/pii/S0267726120311751.

[57] Det Norske Veritas, ed. *DNV-RP-C205 - Environmental Conditions and Environmental Loads*. Apr. 2014.

[58] Det Norske Veritas and Riso National Laboratory, eds. *Guidelines for Design of Wind Turbines*. Denmark, 2002.

[59] Søren Peder Hyldal Sørensen and Lars Bo Ibsen. "Assessment of foundation design for offshore monopiles unprotected against scour". In: *Ocean Engineering* 63 (2013), pp. 17–25. ISSN: 0029-8018. DOI: https://doi.org/10.1016/j.oceaneng.2013.01.016. URL: https://www.sciencedirect.com/science/article/pii/S0029801813000383.

[60] Filipe Magalhães et al. "Damping estimation using free decays and ambient vibration tests". In: *Mechanical Systems and Signal Processing* 24.5 (2010). Special Issue: Operational Modal Analysis, pp. 1274–1290. ISSN: 0888-3270. DOI: https://doi.org/10.1016/j.ymssp.2009.02.011. URL: https://www.sciencedirect.com/science/article/pii/S0888327009000727.

[61] Junbo Jia. "Soil–Structure Interaction". In: *Soil Dynamics and Foundation Modeling: Offshore and Earthquake Engineering*. Cham: Springer International Publishing, 2018, pp. 177–190. ISBN: 978-3-319-40358-8. DOI: 10.1007/978-3-319-40358-8_5. URL: https://doi.org/10.1007/978-3-319-40358-8_5.

[62] Ingrid B. Løken and Amir M. Kaynia. "Effect of foundation type and modelling on dynamic response and fatigue of offshore wind turbines". In: *Wind Energy* 22.12 (2019), pp. 1667–1683. DOI: https://doi.org/10.1002/we.2394. eprint: https://onlinelibrary.wiley.com/doi/pdf/10.1002/we.2394. URL: https://onlinelibrary.wiley.com/doi/abs/10.1002/we.2394.

[63] Deepak Badoni and Nicos Makris. "Nonlinear response of single piles under lateral inertial and seismic loads". In: *Soil Dynamics and Earthquake Engineering* 15.1 (1996), pp. 29–43. ISSN: 0267-7261. DOI: https://doi.org/10.1016/0267-7261(95)00027-5. URL: www.sciencedirect.com/science/article/pii/0267726195000275.

[64] Byrne, Byron W. et al. "PISA: new design methods for offshore wind turbine monopiles". In: *Rev. Fr. Geotech.* 158 (2019), p. 3. DOI: 10.1051/geotech/2019009. URL: https://doi.org/10.1051/geotech/2019009.

[65] Byron W. Byrne et al. "Monotonic laterally loaded pile testing in a stiff glacial clay till at Cowden". In: *Géotechnique* 70.11 (2020), pp. 970–985. DOI: 10.1680/jgeot.18.PISA.003. eprint: https://doi.org/10.1680/jgeot.18.PISA.003. URL: https://doi.org/10.1680/jgeot.18.PISA.003.

[66] Ross A. McAdam et al. "Monotonic laterally loaded pile testing in a dense marine sand at Dunkirk". In: *Géotechnique* 70.11 (2020), pp. 986–998. DOI: 10.1680/jgeot.18.PISA.004. eprint: https://doi.org/10.1680/jgeot.18.PISA.004. URL: https://doi.org/10.1680/jgeot.18.PISA.004.

[67] F H Kulhawy and P W Mayne. *Manual on estimating soil properties for foundation design*. Aug. 1990. URL: https://www.osti.gov/biblio/6653074.

[68] L.J. Prendergast et al. "An investigation of the changes in the natural frequency of a pile affected by scour". In: *Journal of Sound and Vibration* 332.25 (2013), pp. 6685–6702. ISSN: 0022-460X. DOI: https://doi.org/10.1016/j.jsv.2013.08.020. URL: https://www.sciencedirect.com/science/article/pii/S0022460X13006858.

[69] Cheng Lin et al. "Scour effects on the response of laterally loaded piles considering stress history of sand". In: *Computers and Geotechnics* 37.7 (2010), pp. 1008–1014. ISSN: 0266-352X. DOI: https://doi.org/10.1016/j.compgeo.2010.08.009. URL: https://www.sciencedirect.com/science/article/pii/S0266352X10001138.

[70] Mehmet Baris Darendeli. "Development of a new family of normalized modulus reduction and material damping curves". PhD thesis. 2001. URL: http://hdl.handle.net/2152/10396.

[71] Junbo Jia. "Dynamic and Cyclic Properties of Soils". In: *Soil Dynamics and Foundation Modeling: Offshore and Earthquake Engineering*. Cham: Springer International Publishing, 2018, pp. 75–108. ISBN: 978-3-319-40358-8. DOI: 10.1007/978-3-319-40358-8_2. URL: https://doi.org/10.1007/978-3-319-40358-8_2.

[72] Sannith Kumar Thota, Toan Duc Cao, and Farshid Vahedifard. "Poisson's Ratio Characteristic Curve of Unsaturated Soils". In: *Journal of Geotechnical and Geoenvironmental Engineering* 147.1 (2021), p. 04020149. DOI: 10.1061/(ASCE)GT.1943-5606.0002424. eprint: https://ascelibrary.org/doi/pdf/10.1061/\%28ASCE\%29GT.1943-5606.0002424. URL: https://ascelibrary.org/doi/abs/10.1061/%5C%28ASCE%5C%29GT.1943-5606.0002424.

[73] Lidija Zdravkovic et al. "Ground characterisation for PISA pile testing and analysis". In: *Géotechnique* 70.11 (2020), pp. 945–960. DOI: 10.1680/jgeot.18.PISA.001. eprint: https://doi.org/10.1680/jgeot.18.PISA.001. URL: https://doi.org/10.1680/jgeot.18.PISA.001.

[74] Shuzhao Li, Youhu Zhang, and Hans Petter Jostad. "Drainage conditions around monopiles in sand". In: *Applied Ocean Research* 86 (2019), pp. 111–116. ISSN: 0141-1187. DOI: https://doi.org/10.1016/j.apor.2019.01.024. URL: https://www.sciencedirect.com/science/article/pii/S0141118718306217.

[75] George Gazetas and Ricardo Dobry. "Simple Radiation Damping Model for Piles and Footings". In: *Journal of Engineering Mechanics* 110.6 (1984), pp. 937–956. DOI: 10.1061/(ASCE)0733-9399(1984)110:6(937). eprint: https://ascelibrary.org/doi/pdf/10.1061/\%28ASCE\%290733-9399\%281984\%29110\%3A6\%28937\%29. URL: https://ascelibrary.org/doi/abs/10.1061/%5C%28ASCE%5C%290733-9399%5C%281984%5C%29110%5C%3A6%5C%28937%5C%29.

[76] Huan Wang et al. "Influence of Pile Diameter and Aspect Ratio on the Lateral Response of Monopiles in Sand with Different Relative Densities". In: *Journal of Marine Science and Engineering* 9.6 (2021). ISSN: 2077-1312. DOI: 10.3390/jmse9060618. URL: https://www.mdpi.com/2077-1312/9/6/618.

[77] Lidija Zdravkovic et al. "Numerical modelling of large diameter piles under lateral loading for offshore wind applications". In: June 2015. ISBN: 978-1-138-02848-7. DOI: 10.1201/b18442-105.

[78] Harvey J. Burd et al. "Application of the PISA design model to monopiles embedded in layered soils". In: *Géotechnique* 70.11 (2020), pp. 1067–1082. DOI: 10.1680/jgeot.20.PISA.009. eprint: https://doi.org/10.1680/jgeot.20.PISA.009. URL: https://doi.org/10.1680/jgeot.20.PISA.009.

[79] Lizhong Wang et al. "A unified lateral soil reaction model for monopiles in soft clay considering various length-to-diameter (L/D) ratios". In: *Ocean Engineering* 212 (2020), p. 107492. ISSN: 0029-8018. DOI: https://doi.org/10.1016/j.oceaneng.2020.107492. URL: https://www.sciencedirect.com/science/article/pii/S0029801820305060.

[80] Yilong Sun et al. "Nonlinear lateral response of offshore large-diameter monopile in sand". In: *Ocean Engineering* 216 (2020), p. 108013. ISSN: 0029-8018. DOI: https://doi.org/10.1016/j.oceaneng.2020.108013. URL: https://www.sciencedirect.com/science/article/pii/S0029801820309586.

[81] Byron Byrne et al. "PISA: New Design Methods for Offshore Wind Turbine Monopiles". In: Offshore Site Investigation And Geotechnics: Smarter Solutions For Future Offshore Developments. Offshore Site Investigation and Geotechnics Committee ofthe Society for Underwater Technology. London, UK: Society for Underwater Technology, Sept. 2017, pp. 142–161. URL: https://www.researchgate.net/publication/320863997_PISA_New_Design_Methods_for_Offshore_Wind_Turbine_Monopiles.

[82] B. W. Byrne et al. "New design methods for large diameter piles under lateral loading for offshore wind applications". English. In: *Frontiers in Offshore Geotechnics III - Proceedings of the 3rd International Symposium on Frontiers in Offshore Geotechnics, ISFOG 2015*. 3rd International Symposium on Frontiers in Offshore Geotechnics, ISFOG 2015 ; Conference date: 10-06-2015 Through 12-06-2015. CRC Press / Balkema - Taylor & Francis Group, 2015, pp. 705–710. ISBN: 9781138028500.

[83] David M. G. Taborda et al. "Finite-element modelling of laterally loaded piles in a dense marine sand at Dunkirk". In: *Géotechnique* 70.11 (2020), pp. 1014–1029. DOI: 10.1680/jgeot.18.PISA.006. eprint: https://doi.org/10.1680/jgeot.18.PISA.006. URL: https://doi.org/10.1680/jgeot.18.PISA.006.

[84] Junbo Jia. "Axial Force–Displacement of Piles: t-z and Q-z Curve". In: *Soil Dynamics and Foundation Modeling: Offshore and Earthquake Engineering*. Cham: Springer International Publishing, 2018, pp. 521–557. ISBN: 978-3-319-40358-8. DOI: 10.1007/978-3-319-40358-8_17. URL: https://doi.org/10.1007/978-3-319-40358-8_17.

[85] W. Carswell et al. “Natural frequency degradation and permanent accumulated rotation for offshore wind turbine monopiles in clay”. In: *Renewable Energy* 97 (2016), pp. 319–330. ISSN: 0960-1481. DOI: https://doi.org/10.1016/j.renene.2016.05.080. URL: https://www.sciencedirect.com/science/article/pii/S0960148116304906.

[86] Nii Allotey and M. Hesham El Naggar. “A numerical study into lateral cyclic nonlinear soil–pile response”. In: *Canadian Geotechnical Journal* 45.9 (2008), pp. 1268–1281. DOI: 10.1139/T08-050. eprint: https://doi.org/10.1139/T08-050. URL: https://doi.org/10.1139/T08-050.

[87] Junbo Jia. “Bearing Capacity of Shallow Foundations”. In: *Soil Dynamics and Foundation Modeling: Offshore and Earthquake Engineering*. Cham: Springer International Publishing, 2018, pp. 413–433. ISBN: 978-3-319-40358-8. DOI: 10.1007/978-3-319-40358-8_12. URL: https://doi.org/10.1007/978-3-319-40358-8_12.

[88] Junbo Jia. “Liquefaction”. In: *Soil Dynamics and Foundation Modeling: Offshore and Earthquake Engineering*. Cham: Springer International Publishing, 2018, pp. 227–250. ISBN: 978-3-319-40358-8. DOI: 10.1007/978-3-319-40358-8_7. URL: https://doi.org/10.1007/978-3-319-40358-8_7.

[89] L.J. Prendergast, K. Gavin, and P. Doherty. “An investigation into the effect of scour on the natural frequency of an offshore wind turbine”. In: *Ocean Engineering* 101 (2015), pp. 1–11. ISSN: 0029-8018. DOI: https://doi.org/10.1016/j.oceaneng.2015.04.017. URL: https://www.sciencedirect.com/science/article/pii/S002980181500092X.

[90] Yasser E. Mostafa. “Effect of Local and Global Scour on Lateral Response of Single Piles in Different Soil Conditions”. In: *Engineering* 4.6 (2012), pp. 297–306. DOI: 10.4236/eng.2012.46039. URL: http://dx.doi.org/10.4236/eng.2012.46039.

[91] Jean-Louis Briaud et al. “SRICOS: Prediction of Scour Rate in Cohesive Soils at Bridge Piers”. In: *Journal of Geotechnical and Geoenvironmental Engineering* 125.4 (1999), pp. 237–246. DOI: 10.1061/(ASCE)1090-0241(1999)125:4(237). eprint: https://ascelibrary.org/doi/pdf/10.1061/\%28ASCE\%291090-0241\%281999\%29125\%3A4\%28237\%29. URL: https://ascelibrary.org/doi/abs/10.1061/%5C%28ASCE%5C%291090-0241%5C%281999%5C%29125%5C%3A4%5C%28237%5C%29.

[92] Junbo Jia. “Scour for Pile Foundations”. In: *Soil Dynamics and Foundation Modeling: Offshore and Earthquake Engineering*. Cham: Springer International Publishing, 2018, pp. 589–600. ISBN: 978-3-319-40358-8. DOI: 10.1007/978-3-319-40358-8_20. URL: https://doi.org/10.1007/978-3-319-40358-8_20.

[93] *Gapping effects on the lateral stiffness of piles in cohesive soil*. Pacific Conference on Earthquake Engineering. 2003. eprint: http://db.nzsee.org.nz/2003/View/Paper096s.pdf.

[94] Lidija Zdravkovic et al. “Finite-element modelling of laterally loaded piles in a stiff glacial clay till at Cowden”. In: *Géotechnique* 70.11 (2020), pp. 999–1013. DOI: 10.1680/jgeot.18.PISA.005. eprint: https://doi.org/10.1680/jgeot.18.PISA.005. URL: https://doi.org/10.1680/jgeot.18.PISA.005.

[95] Ross W. Boulanger et al. “Seismic Soil-Pile-Structure Interaction Experiments and Analyses”. In: *Journal of Geotechnical and Geoenvironmental Engineering* 125.9 (1999), pp. 750–759. DOI: 10.1061/(ASCE)1090-0241(1999)125:9(750). eprint: https://ascelibrary.org/doi/pdf/10.1061/\%28ASCE\%291090-0241\%281999\%29125\%3A9\%28750\%29. URL: https://ascelibrary.org/doi/abs/10.1061/%5C%28ASCE%5C%291090-0241%5C%281999%5C%29125%5C%3A9%5C%28750%5C%29.

[96] Junbo Jia. “Lateral Force-Displacement of Piles - p-y Curve”. In: *Soil Dynamics and Foundation Modeling: Offshore and Earthquake Engineering*. Cham: Springer International Publishing, 2018, pp. 481–519. ISBN: 978-3-319-40358-8. DOI: 10.1007/978-3-319-40358-8_16. URL: https://doi.org/10.1007/978-3-319-40358-8_16.

[97] Nii Allotey and M. Hesham El Naggar. “Generalized dynamic Winkler model for nonlinear soil–structure interaction analysis”. In: *Canadian Geotechnical Journal* 45.4 (2008), pp. 560–573. DOI: 10.1139/T07-106. eprint: https://doi.org/10.1139/T07-106. URL: https://doi.org/10.1139/T07-106.

[98] Thomas Benz. “Small-Strain Stiffness of Soils and its Numerical Consequences”. PhD thesis. Stuttgart, Germany: Institut für Geotechnik Universität Stuttgart, 2007. ISBN: 978-3-921837-55-9.

[99] H. Bolton Seed and I. M. Idriss. *Soil Moduli and Damping Factors for Dynamic Response Analyses*. Dec. 1970.

[100] George Gazetas. “Foundation Vibrations”. In: *Foundation Engineering Handbook*. Ed. by Hsai-Yang Fang. Boston, MA: Springer US, 1991, pp. 553–593. ISBN: 978-1-4615-3928-5. DOI: 10.1007/978-1-4615-3928-5_15. URL: https://doi.org/10.1007/978-1-4615-3928-5_15.

[101] S. Stoykov and P. Ribeiro. “Nonlinear forced vibrations and static deformations of 3D beams with rectangular cross section: The influence of warping, shear deformation and longitudinal displacements”. In: *International Journal of Mechanical Sciences* 52.11 (2010). Special Issue on Non-linear Oscillations, pp. 1505–1521. ISSN: 0020-7403. DOI: https://doi.org/10.1016/j.ijmecsci.2010.06.011. URL: https://www.sciencedirect.com/science/article/pii/S0020740310001591.

[102] Junbo Jia. “Capacity Control, Modeling of Pile Head Stiffness, and Mitigation Measures to Increase Pile Capacity”. In: *Soil Dynamics and Foundation Modeling: Offshore and Earthquake Engineering*. Cham: Springer International Publishing, 2018, pp. 465–480. ISBN: 978-3-319-40358-8. DOI: 10.1007/978-3-319-40358-8_15. URL: https://doi.org/10.1007/978-3-319-40358-8_15.

[103] Christina Koukoura, Anand Natarajan, and Allan Vesth. “Identification of support structure damping of a full scale offshore wind turbine in normal operation”. In: *Renewable Energy* 81 (2015), pp. 882–895. ISSN: 0960-1481. DOI: https://doi.org/10.1016/j.renene.2015.03.079. URL: https://www.sciencedirect.com/science/article/pii/S0960148115002700.

[104] Sekhar Chandra Dutta and Rana Roy. “A critical review on idealization and modeling for interaction among soil–foundation–structure system”. In: *Computers & Structures* 80.20 (2002), pp. 1579–1594. ISSN: 0045-7949. DOI: https://doi.org/10.1016/S0045-7949(02)00115-3. URL: https://www.sciencedirect.com/science/article/pii/S0045794902001153.

[105] Lars Einar S. Stieng et al. “Relative Assessment of Fatigue Loads for Offshore Wind Turbine Support Structures”. In: *Energy Procedia* 80 (2015). 12th Deep Sea Offshore Wind R&D Conference, EERA DeepWind’2015, pp. 229–236. ISSN: 1876-6102. DOI: https://doi.org/10.1016/j.egypro.2015.11.426. URL: https://www.sciencedirect.com/science/article/pii/S187661021502158X.

[106] Arnold Verruijt. “Foundation Vibrations”. In: *An Introduction to Soil Dynamics*. Dordrecht: Springer Netherlands, 2010, pp. 385–394. ISBN: 978-90-481-3441-0. DOI: 10.1007/978-90-481-3441-0_15. URL: https://doi.org/10.1007/978-90-481-3441-0_15.

[107] Harvey J. Burd et al. “PISA design model for monopiles for offshore wind turbines: application to a marine sand”. In: *Géotechnique* 70.11 (2020), pp. 1048–1066. DOI: 10.1680/jgeot.18.P.277. eprint: https://doi.org/10.1680/jgeot.18.P.277. URL: https://doi.org/10.1680/jgeot.18.P.277.

[108] American Petroleum Institute, ed. *Recommended practice for planning, designing and constructing fixed offshore platforms – working stress design*. Apr. 2008.

[109] Søren Peder Hyldal Sørensen. “Soil-Structure Interaction For Nonslender, Large-Diameter Offshore Monopiles”. English. Vol 1: number of pages 31 pp, PDF for print. 202 pp. Include the articles: Review of Laterally Loaded Monopiles Employed as the Foundation for Offshore Wind Turbines - 48 pp. Testing of Laterally Loaded Rigid Piles with Applied Overburden Pressure - 7 pp. Revised Expression for the Static Initial Part of P-Y Curves for Piles in Sand - 40 pp. Assessment of Scour Design for Offshore Monopiles Unprotected Against Scour - 42 pp. PhD thesis. 2012.

[110] Søren Peder Hyldal Sørensen. “Soil-Structure Interaction For Nonslender, Large-Diameter Offshore Monopiles”. English. Vol 2: number of pages: 241 pp., PDF for print. 327 pp. Inkludrerer artiklerne: Small-scale quasi-static tests on non-slender piles situated in sand - Test results. - 241pp. Small-scale cyclic tests on non-slender piles situated in sand - Test results. 75 pp. PhD thesis. 2012.

[111] *Modification of the API P-y Formulation of Initial Stiffness of Sand*. Vol. All Days. SUT Offshore Site Investigation and Geotechnics. SUT-OSIG-12-50. Sept. 2012. eprint: https://onepetro.org/SUTOSIG/proceedings-pdf/OSIG12/All-OSIG12/SUT-OSIG-12-50/1642410/sut-osig-12-50.pdf.

[112] Erfan Asnaashari et al. "Finite Element Modelling and In Situ Modal Testing of an Offshore Wind Turbine". In: *Journal of Vibration Engineering & Technologies* 6 (Aug. 2018). DOI: 10.1007/s42417-018-0018-3.

[113] Harvey J. Burd et al. "New data analysis methods for instrumented medium-scale monopile field tests". In: *Géotechnique* 70.11 (2020), pp. 961–969. DOI: 10.1680/jgeot.18.PISA.002. eprint: https://doi.org/10.1680/jgeot.18.PISA.002. URL: https://doi.org/10.1680/jgeot.18.PISA.002.

[114] W. Carswell et al. "Foundation damping and the dynamics of offshore wind turbine monopiles". In: *Renewable Energy* 80 (2015), pp. 724–736. ISSN: 0960-1481. DOI: https://doi.org/10.1016/j.renene.2015.02.058. URL: https://www.sciencedirect.com/science/article/pii/S0960148115001743.

[115] Christof Devriendt et al. "Damping estimation of an offshore wind turbine on a monopile foundation". In: *IET Renewable Power Generation* 7.4 (2013), pp. 401–412. DOI: https://doi.org/10.1049/iet-rpg.2012.0276. eprint: https://ietresearch.onlinelibrary.wiley.com/doi/pdf/10.1049/iet-rpg.2012.0276. URL: https://ietresearch.onlinelibrary.wiley.com/doi/abs/10.1049/iet-rpg.2012.0276.

[116] R. B. J. Brinkgreve, M. H. Kappert, and P. G. Bonnier. "Hysteretic damping in a small-strain stiffness model". In: *Numerical Models in Geomechanics* (2007). Ed. by Pande and Pietruszczak, pp. 737–742. URL: https://communities.bentley.com/products/geotech-analysis/w/plaxis-soilvision-wiki/46056/hysteretic-damping-in-a-small-strain-stiffness-model.

[117] William Beuckelaers. "Numerical Modelling of Laterally Loaded Piles for Offshore Wind Turbines". PhD thesis. Jan. 2017.

[118] José Dias Rodrigues. *Apontamentos de Vibrações de Sistemas Mecânicos*. Porto, Portugal: Departamento de Engenharia Mecânica da Faculdade de Engenharia da Univerisdade do Porto, Jan. 2020.

[119] P. Ribeiro and G.H.M. van der Heijden. "Elasto-plastic and geometrically nonlinear vibrations of beams by the p-version finite element method". In: *Journal of Sound and Vibration* 325.1 (2009), pp. 321–337. ISSN: 0022-460X. DOI: https://doi.org/10.1016/j.jsv.2009.03.009. URL: https://www.sciencedirect.com/science/article/pii/S0022460X09002272.

[120] Pedro Ribeiro. "A p-version, first order shear deformation, finite element for geometrically non-linear vibration of curved beams". In: *International Journal for Numerical Methods in Engineering* 61.15 (2004), pp. 2696–2715. DOI: https://doi.org/10.1002/nme.1180. eprint: https://onlinelibrary.wiley.com/doi/pdf/10.1002/nme.1180. URL: https://onlinelibrary.wiley.com/doi/abs/10.1002/nme.1180.

[121] *Fresh Water and Seawater Properties*. Apr. 2011. URL: https://ittc.info/media/4048/75-02-01-03.pdf.

[122] T. Kaneko. "On Timoshenko's correction for shear in vibrating beams". In: *Journal of Physics D: Applied Physics* 8.16 (Nov. 1975), pp. 1927–1936. DOI: 10.1088/0022-3727/8/16/003. URL: https://doi.org/10.1088/0022-3727/8/16/003.

[123] Maurice Petyt. *Introduction to Finite Element Vibration Analysis*. 2nd ed. Cambridge University Press, 2010. DOI: 10.1017/CBO9780511761195.

[124] Michael Ferris Cook. "Damping Estimation, Response Prediction and Fatigue Calculation of an Operational Single Pile Platform". USA: Massachusetts Institute of Technology, Jan. 1982.

[125] C.F. Beards. "2 - The vibration of structures with one degree of freedom". In: *Structural Vibration: Analysis and Damping*. Ed. by C.F. Beards. Oxford: Butterworth-Heinemann, 1996, pp. 10–82. ISBN: 978-0-340-64580-2. DOI: https://doi.org/10.1016/B978-034064580-2/50004-1. URL: https://www.sciencedirect.com/science/article/pii/B9780340645802500041.

[126] George Gazetas and Ricardo Dobry. "Horizontal Response of Piles in Layered Soils". In: *Journal of Geotechnical Engineering* 110.1 (1984), pp. 20–40. DOI: 10.1061/(ASCE)0733-9410(1984)110:1(20). eprint: https://ascelibrary.org/doi/pdf/10.1061/\%28ASCE\%290733-9410\%281984\%29110\%3A1\%2820\%29. URL: https://ascelibrary.org/doi/abs/10.1061/%5C%28ASCE%5C%290733-9410%5C%281984%5C%29110%5C%3A1%5C%2820%5C%29.

[127] L. Johanning, P.W. Bearman, and J.M.R. Graham. "Hydrodynamic Damping of a Large Scale Surface Piercing Circular Cylinder in Planar Oscillatory Motion". In: *Journal of Fluids and Structures* 15.7 (2001), pp. 891–908. ISSN: 0889-9746. DOI: https://doi.org/10.1006/jfls.2001.0388. URL: https://www.sciencedirect.com/science/article/pii/S0889974601903883.

[128] Herbjoern Alf Haslum. "Simplified Methods Applied to Nonlinear Motion of Spar Platforms". PhD thesis. Trondheim, Norway: Norges teknisk-naturvitenskapelige universitet, July 2000.

[129] Longbin Tao and Shunqing Cai. "Heave motion suppression of a Spar with a heave plate". In: *Ocean Engineering* 31.5 (2004), pp. 669–692. ISSN: 0029-8018. DOI: https://doi.org/10.1016/j.oceaneng.2003.05.005. URL: https://www.sciencedirect.com/science/article/pii/S0029801803001732.

[130] R. D. Blevins. *Applied Fluid Dynamics Handbook*. New York, USA, 1984. URL: https://ui.adsabs.harvard.edu/abs/1984vnr..book.....B.

[131] *Viscosity of Air, Dynamic and Kinematic*. Accessed on 2022-07-04. Engineers Edge. URL: https://www.engineersedge.com/physics/viscosity_of_air_dynamic_and_kinematic_14483.htm.

[132] *Wind Turbine Blade Aerodynamics*. Accessed on 2022-07-05. Electrical Academia. URL: https://electricalacademia.com/renewable-energy/wind-turbine-blade-aerodynamics/.

[133] Leonard Meirovitch. *Computational methods in structural dynamics*. Rockville, Maryland, USA: Sijthoff & Noordhoff International Publishers, 1980. ISBN: 90 286 0580 0.

[134] Leonard Meirovitch. *Analytical Methods in Vibrations*. USA: The MacMillan Company, 1967.

[135] *Norther Offshore Wind Farm*. Accessed on 2022-07-05. Norther. URL: https://www.norther.be/.

[136] Aleksandar B. Vesic. "Beams on Elastic Subgrade and the Winkler's Hypothesis". In: (1971), pp. 845–850.

[137] M. A. Biot. "Bending of an Infinite Beam on an Elastic Foundation". In: *Journal of Applied Mechanics* (203 Mar. 1937).

[138] Ross W. Boulanger et al. *Pile Foundations in Liquefied and Laterally Spreading Ground During Earthquakes: Centrifuge Experiments & Analyses*. California, USA, Sept. 2003. URL: https://faculty.engineering.ucdavis.edu/boulanger/wp-content/uploads/sites/71/2014/09/Boulanger_et_al_CGM03_01.pdf.

[139] D. J. Ewins. *Modal Testing: Theory, Practice and Application*. 2nd ed. July 2009. ISBN: 978-0-863-80218-8.

[140] Martin Felix Jørgensen. "Aerodynamic and Mechanical System Modelling". English. PhD thesis. 2013. ISBN: 978-87-7475-370-4.

[141] Timur. *The waves and the wind. Calculation of wave characteristics*. 2021. URL: https://planetcalc.com/4406/.

[142] Paul Webb. "Chapter 10: Waves". In: *Introduction to Oceanography*. Pressbooks, Aug. 2021. URL: https://rwu.pressbooks.pub/webboceanography/.

[143] Rick Salmon. *Introduction to Ocean Waves*. San Diego, USA. eprint: http://www-pord.ucsd.edu/rsalmon/111.textbook.pdf.

[144] R.L. Soulsby and J. V. Smallman. Oxfordshire, USA: Hydraulics Research Wallingford, Feb. 1986. eprint: https://eprints.hrwallingford.com/112/1/SR76-method-calculating-orbital-velocity-waves.pdf.

[145] Majid Bhinder and Jimmy Murphy. "Evaluation of the Viscous Drag for a Domed Cylindrical Moored Wave Energy Converter". In: *Journal of Marine Science and Engineering* 7 (Apr. 2019), p. 120. DOI: 10.3390/jmse7040120.

Appendixes

Appendix A

Relevant to the quantification of the soil radiation damping, the shear wave velocity of the soil can be defined as seen in Eq. A.1 and presented by Gupta and Basu [40]. This quantity can also be seen as very important to define the shear modulus profile of the soil, as different soil analysis methods exist to measure the shear wave velocity of the soil with depth. The presented relation then allows for the quantification of the shear modulus, which is linked to the soil stiffness.

$$V_s = \sqrt{\frac{G_s}{\rho_s}} \tag{A.1}$$

The dimensionless frequency as presented in Eq. A.2 from Gupta and Basu work [40], allows the calculation of the soil radiation damping. This quantity represents the excitation frequency on a pile like structure embedded into the soil in a dimensionless form.

$$a_0 = \frac{\omega \cdot R_{ext}}{V_s} \tag{A.2}$$

The soil radiation damping can vary with depth, as there will be a difference between shallower and deeper layers. According to Jiang and Lin [19], a shallower depth will be limited to a depth equal to 2.5 times the respective pile diameter. Considering this, the Q coefficient that governs the soil radiation damping coefficient can be given by Eq. A.3 as according to Gazetas and Dobry [126] and to Badoni and Makris [63].

$$Q = \begin{cases} 2\left(1+\frac{3.4}{\pi(1-\nu_s^2)}\right)^{1.25}\left(\frac{\pi}{4}\right)^{0.75} & , z \leq 2.5d \\ 4\left(\frac{\pi}{4}\right)^{0.75} & , z > 2.5d \end{cases} \tag{A.3}$$

According to Jia [33], the over-consolidation ratio for clays can be estimated as seen in Eq. A.4. Other expressions exist throughout the literature, but the majority come from experimental data or pressure relations regarding stress history. This expression was used as values obtained using it cross-checked some of the consulted literature. For the sand, a difference in the limit over-consolidation ratio was assumed. This relation is shown in Eq. A.5. The value was arbitrary but selected considering that more than a third of the limit value would occur. The overall meaning of the over-consolidation ratio is the ratio between the pre-consolidation effective stress and the vertical effective stress, as seen in Eq. A.6.

$$OCR_{clay} \approx \left(\frac{4s_u}{\sigma_v'}\right)^{1.25} \tag{A.4}$$

$$OCR_{sand} = \frac{2}{3} OCR_{limit} \tag{A.5}$$

$$OCR = \frac{\sigma_p'}{\sigma_v'} \tag{A.6}$$

For some soil modelling approaches, other properties besides the ones made available by Vestas are necessary. An example of that is the relative density of sand layers. Resorting to the expression presented by Prendergast et al. [89], it is possible to relate it to known quantities, as seen in Eq. A.7.

$$D_r = \frac{1}{2.91} \ln\left(\frac{q_c}{60 \cdot (\sigma_v')^{0.7}}\right) \tag{A.7}$$

As the drainage condition influences the stiffness encountered in the soil, it can be important to predict it. As such, to reach a value of the drainage normalised time factor seen in Eq. 3.7, it is necessary to quantify the coefficient of consolidation c_v. This is giving in Eq. A.8. The constrained modulus M_v necessary for the determination of this coefficient is presented in Eq. A.9 [74].

$$c_v = \frac{M_v k_p}{\gamma_w} \tag{A.8}$$

$$M_v = \frac{(1-\nu_s)\,E_s}{(1+\nu_s)\,(1-2\nu_s)} \tag{A.9}$$

A Dirac function is widely utilised in mathematics. It represents the situation of a step, where it is zero until a given value and, from that point on, it will be unitary. Eq. A.10 represents this common function:

$$\delta(x-x_p) = \begin{cases} 0\ ,\ x \leq x_p \\ 1\ ,\ x > x_p \end{cases} \quad . \tag{A.10}$$

Appendix B

This Appendix intends to present the selected approach regarding wave shape characterisation, important for the definition of the water viscous damping. For the following characterisation three sources were consulted: *The waves and the wind. Calculation of wave characteristics* [141], *Introduction to Oceanography* [142], and *Introduction to Ocean Waves* [143].

Waves propagate in a sine-like style. However, they cannot be described as this function. For this reason different wave related quantities are defined to best capture the wave propagation shape, such as wave number, wave length, phase velocity and wave period. These quantities can be defined as shown in Eqs. B.1 to B.3:

$$\lambda_w = \frac{2\pi}{k_o}; \tag{B.1}$$

$$c_o = \frac{\omega_w}{k_o}; \tag{B.2}$$

$$T_{wave} = \frac{2\pi}{\omega_w}. \tag{B.3}$$

Using the dispersion law, it is possible to use a relationship between the frequency of the waves ω_w and the wave number. By employing the linear wave theory for a free surface, Eq. B.4 can be written. Depending on the relation of the water depth with the wavelength, a possible simplification can be performed.

$$\omega_w^2 = g \cdot k_o \tanh\left(k_o z_w\right) \tag{B.4}$$

Waves can be considered to happen in deep water when the depth is more than half of the wavelength. This means the relation and simplification seen in Eq. B.5. As such, the wave frequency can be obtained according to Eq. B.6.

$$z_w \geq \frac{\lambda_w}{2} \rightarrow \tanh\left(k_o z_w\right) \approx 1 \tag{B.5}$$

$$\omega_w^2 = g \cdot k_o \tag{B.6}$$

Waves can be assumed to occur in shallow waters if the depth is less than one-twentieth of the wavelength. The corresponding relation and simplification can be seen in Eq. B.7. The consequent wave frequency can be obtained by using Eq. B.8.

$$z_w \leq \frac{\lambda_w}{20} \tag{B.7}$$

$$\omega_w^2 = g \cdot z_w \cdot k_o^2 \tag{B.8}$$

For the cases in between, the so-called transitional depths, there is no viable simplification. Consequently, a numerical approach should be performed to obtain the wave frequency by using Eq. B.4. Different numerical/iteration methods exist to reach this solution, from a simple fixed point iteration method to the Newton-Raphson method. The bisection method was used in the present work.

After defining the overall shape of the waves, it is possible to define the maximum orbital velocity of the waves. This can be determined by using Eq. B.9, as presented in *A direct method of calculating bottom orbital velocity under waves* [144]. The determination of this quantity can then be used for an estimation of the Keulegan-Carpenter number, as defined by Eq. B.10, seen in the work of Bhinder and Murphy [145].

$$U_m = \frac{\omega_w h_w}{2 \sinh\left(k_o z_w\right)} \tag{B.9}$$

$$KC = \frac{U_m T_{wave}}{\lambda_w} \tag{B.10}$$

Also important to the characterization of a fluid flow is the Stokes number. This number defines a ratio between the response time of a particle and a characteristic time scale of the fluid considered. The Stokes number can be defined by Eq. B.11, as retrieved from Tao and Cai's work [129]:

$$\beta_{Stokes} = \frac{\left(2R_{ext}\right)^2 \cdot \rho_w \omega_w}{2\pi\mu_w}. \tag{B.11}$$

Appendix C

As non-perfect and simple approaches are considered in the model developed, correction factors are necessary to guarantee that the model will correctly predict the structure's response. Structural mass and stiffness matrices are then affected by these approaches. A correction factor that conducts to little or no error concerning the real-life observed response is desired. Different steps have to be performed to reach the desired error minimization.

Depending on the overall structure modelling used, the system may require stiffness and mass gain or stiffness and mass loss. It is recommended that only one dimension of the structure varies differently from the real variation. For the studied problem, this dimension was the thickness, where a linear variation was considered, leading to a heavier and stiffer structure than in reality.

Before entering the stiffness correction, a mass correction should be performed to ensure that the modelled structure has the same mass as the real structure. Eqs. C.1 to C.4 show the process to define the mass correction factor, where m_c is the calculated mass and m_r is the real mass. Eq. C.3 states that calculating the mass with exact dimensions would lead to the real mass. The mass correction factor can then be defined by Eq. C.4.

$$m = \rho V = \rho\pi \int_0^l \left(R_{ext}^2(x) - R_{int}^2(x)\right) \mathrm{d}x \tag{C.1}$$

$$\begin{aligned} m_c = \tfrac{\pi l \rho}{2} &\int_{-1}^{+1} \left[R_{ext}^2(\xi) - \left(R_{ext}(\xi) - t(\xi)\right)^2\right] \mathrm{d}\xi \\ = \tfrac{\pi l \rho}{2} &\int_{-1}^{+1} [2R_{ext}t - t^2]\, \mathrm{d}\xi \end{aligned} \tag{C.2}$$

$$\begin{cases} m_r = \frac{\rho\pi l}{2} M_{corr} \int_{-1}^{+1} \left[2R_{ext}t - t^2\right] \mathrm{d}\xi \\ m_r = \frac{\rho\pi l}{2} \int_{-1}^{+1} \left[2R_{ext_t}t_t - t_t^2\right] \mathrm{d}\xi \end{cases} \tag{C.3}$$

$$M_{corr} = \int_{-1}^{+1} \frac{2R_{ext_t}t_t - t_t^2}{2R_{ext}t - t^2} \mathrm{d}\xi \tag{C.4}$$

An analytical approach to the stiffness correction factor presents itself as a challenge. Contrary to the mass, there is no unique expression that quantifies the stiffness of a structure as a scalar quantity. Instead, stiffness is characterised by a set of stiffness matrices. Still, Eqs. C.5 to C.8 present an initial approach to the quantification of a stiffness correction factor in a similar way to what was seen for the mass. By ignoring the shape functions product (the reason why a matrix is then built), it is seen in Eq. C.5 that the stiffness will be defined with an integral that is identical to the one in Eq. C.2. As such, for this stiffness case, the stiffness correction factor should be equal to the mass correction factor, as both are subjected to the same error. Looking through the structural stiffness equations present in Chapter 4, only one stiffness matrix is defined by using a different integral. This stiffness component is presented (without its shape functions) in Eq. C.6. This will be the term subjected to a bigger error, as it has elements powered to four. Consequently, the stiffness correction factor for this component will be different from the rest.

$$\begin{aligned} K_{u_3} &= \tfrac{2\pi\lambda G}{l}\int_{-1}^{+1}\left[2R_{ext}t - t^2\right]\mathrm{d}\xi \\ &= \tfrac{2\pi\lambda G}{l}M_{corr}\int_{-1}^{+1}\left[2R_{ext_t}t_t - t_t^2\right]\mathrm{d}\xi \end{aligned} \tag{C.5}$$

$$K_\theta^E = \int_{-1}^{+1}\left(\frac{E\pi}{2l}\left[R_{ext}^4 - R_{int}^4\right] + \frac{\pi l\lambda G}{2}\left[R_{ext}^4 - R_{int}^4\right]\right)\mathrm{d}\xi \tag{C.6}$$

$$\begin{aligned} R_{ext}^4 - R_{int}^4 &= \left(R_{ext}^2 - R_{int}^2\right)\left(R_{ext}^2 + R_{int}^2\right) \\ &= 4R_{ext}^3 t - 6R_{ext}^2 t^2 + 4R_{ext}t^3 - t^4 = 2R_{ext}^2\left(2R_{ext}t - t^2\right) - \left(2R_{ext}t - t^2\right)^2 \end{aligned} \tag{C.7}$$

$$K_\theta^E = \frac{E\pi}{2l}\int_{-1}^{+1}\left[2R_{ext}^2\left(2R_{ext}t - t^2\right) - \left(2R_{ext}t - t^2\right)^2\right]\mathrm{d}\xi \tag{C.8}$$

As can be observed in Eq. C.8, although the expression seen in the integral of Eq. C.4 that defines the mass correction factor, it's multiplied or by itself or by a quantity that depends on the coordinate. Focusing on the portion that has the bigger power concerning the expression that is linked to the mass correction factor (which will be the squared one), an approach can be made. This approach considers that the equivalent correction factor will be linked to the highest power associated with the mass correction factor, independently of the corresponding sign. As known, squaring the integral and squaring the content of the integral and then performing the integral leads to different results. If the expression, however, is substituted inside the integral, the mass correction factor will also be squared. Only considering this would lead to some considerable error, as other factors are presented to influence this stiffness. However, by admitting that the equivalent integral will lead to, approximately a value of the cube of the previously highlighted expression, then it can be reached that the stiffness correction factor would be equal to the cube of the mass correction factor. This line of thought can be seen in Eqs. C.9 to C.11.

$$u = 2R_{ext}t - t^2 \rightarrow 2R_{ext}^2 u - u^2 \tag{C.9}$$

$$\int u^2 du = u^3 \rightarrow \left(2R_{ext}t - t^2\right)^3 = M_{corr}^3\left(2R_{ext_t}t_t - t_t^2\right)^3 \tag{C.10}$$

$$K_{corr} \approx M_{corr}^3 \tag{C.11}$$

After this assumption, using a benchmark model, testing was performed to conclude the relative error acquired. Through these series of tests, a good correlation between natural frequencies from the developed model and the well-validated model was observed. Errors below 1% were registered, with a maximum error of 2% noted. As such, this assumption is valid, although its demonstration can raise doubts.

Appendix D

```
close all
format long

%Inputs
inputquest=questdlg('Select one of the inputs available.','Structure Input','Input Tower Only', 'Input Whole Structure', 'Input Test Beam', 'Input Whole Structure');
switch inputquest
    case 'Input Tower Only'
        InputSDOFTower
    case 'Input Whole Structure'
        InputSDOFOWT
    case 'Input Test Beam'
        InputAnTest
end
load shapefunctionsff.mat
omega=omega_exp;

%% Shape functions
opts.Interpreter='tex';
p=inputdlg({'Number of shape functions for the u_1 displacement:','Number of shape functions for the u_3 displacement:','Number of shape functions for the \theta rotation:'},'Number of shape functions (for a free-free element)',[1 80],{'6','18','18'},opts);
p_u1=str2double(p{1});
p_u3=str2double(p{2});
p_tt=str2double(p{3});
if p_u1+p_u3+p_tt <=15 && bcb+bct>=1
    p_u1=8;
    p_u3=8;
    p_tt=8;
    msgbox('The number of shape functions were changed to 8 to ensure that the problem is solved.','Warning')
end
    FF_u1=FF;
    FF_u3=FF;
    FF_tt=FF;
    dFF_u1=dFF;
    dFF_u3=dFF;
    dFF_tt=dFF;
    FdF_u3tt=FdF;
    FF_u1(p_u1(1,1)-1:length(f)-2,:)=[];
    FF_u1(:,p_u1(1,1)-1:length(f)-2)=[];
    dFF_u1(p_u1(1,1)-1:length(df)-2,:)=[];
    dFF_u1(:,p_u1(1,1)-1:length(df)-2)=[];
```

```
        FF_u3(p_u3(1,1)-1:length(f)-2,:)=[];
        FF_u3(:,p_u3(1,1)-1:length(f)-2)=[];
        dFF_u3(p_u3(1,1)-1:length(df)-2,:)=[];
        dFF_u3(:,p_u3(1,1)-1:length(df)-2)=[];
        FF_tt(p_tt(1,1)-1:length(f)-2,:)=[];
        FF_tt(:,p_tt(1,1)-1:length(f)-2)=[];
        dFF_tt(p_tt(1,1)-1:length(df)-2,:)=[];
        dFF_tt(:,p_tt(1,1)-1:length(df)-2)=[];
        FdF_u3tt(p_u3(1,1)-1:length(df)-2,:)=[];
        FdF_u3tt(:,p_tt(1,1)-1:length(f)-2)=[];

%% Matrix assembly
dimMKC=p_u1+p_u3+p_tt;
G=@(xi) E(xi)./(2.*(1+nu(xi))); %Pa - material shear modulus
lambda=@(xi) (6+12.*nu(xi)+6*nu(xi).^2)./(7+12.*nu(xi)+4.*nu(xi).^2); % - shear correction factor

%function handles
M_u1=zeros(p_u1,p_u1);                                        % Structural mass u1 direction
Mlm_u1=zeros(p_u1,p_u1);                                      % Lumped mass (RNA) u1 direction
Mg_u1=zeros(p_u1,p_u1);                                       % Marine growth mass u1 direction
K_u1=zeros(p_u1,p_u1);                                        % Structural stiffness u1 direction
for i=1:p_u1
    for j=1:p_u1
        %Mass matrices
        fM_u1=@(xi) rho.*(Rext(xi).^2-Rint(xi).^2).*FF_u1{i,j}(xi);
        M_u1(i,j)=0.5.*pi.*l.*integral(fM_u1,-1,1);
            Mlm_u1(i,j)=m_RNA.*FF_u1{i,j}(1);
            for m_addi=1:length(m_Tadd)
                Mlm_u1(i,j)=Mlm_u1(i,j)+m_Tadd(m_addi).*FF_u1{i,j}(xi_Tadd(m_addi));
            end
                fMg_u1=@(xi) zmg(xi).*rho_g.*((Rext(xi)+t_g).^2-Rext(xi).^2).*FF_u1{i,j}(xi);
                Mg_u1(i,j)=0.5*pi*l*integral(fMg_u1,-1,1);
        %Stiffness matrices
        fK_u1=@(xi) E(xi).*(Rext(xi).^2-Rint(xi).^2).*dFF_u1{i,j}(xi);
        K_u1(i,j)=2.*pi.*integral(fK_u1,-1,1)./l;
    end
end
M_u3=zeros(p_u3,p_u3); %Structural mass u3 direction
Mlm_u3=zeros(p_u3,p_u3); %Lumped mass (RNA) u3 direction
```

```
Mwi_u3=zeros(p_u3,p_u3); %Inner water added mass u3 direction
Mwe_u3=zeros(p_u3,p_u3); %Outer water added mass u3 direction
Mg_u3=zeros(p_u3,p_u3); %Marine growth mass u3 direction
Msi_u3=zeros(p_u3,p_u3); %Inner soil added mass u3 direction
Mse_u3=zeros(p_u3,p_u3); %Outer soil added mass u3 direction
K_u3=zeros(p_u3,p_u3); %Structural stiffness u3 direction
K_s=zeros(p_u3,p_u3); %Soil stiffness u3 direction
Cw_vis=zeros(p_u3,p_u3); %Water viscous damping u3 direction
Cw_rad=zeros(p_u3,p_u3); %Water radiation damping u3 direction
Cs_rad=zeros(p_u3,p_u3); %Soil radiation damping u3 direction
Cs_hys=zeros(p_u3,p_u3); %Soil hysteresis damping u3 direction
Ca=zeros(p_u3,p_u3); %Aerodynamic damping u3 direction
for i=1:p_u3
    for j=1:p_u3
        %Mass matrices
        fM_u3=@(xi) rho.*(Rext(xi).^2-Rint(xi).^2).*FF_u3{i,j}(xi);
        M_u3(i,j)=0.5.*pi.*1.*integral(fM_u3,-1,1);
            Mlm_u3(i,j)=m_RNA.*FF_u3{i,j}(1);
            for m_addi=1:length(m_Tadd)
                Mlm_u3(i,j)=Mlm_u3(i,j)+m_Tadd(m_addi).*FF_u3{i,j}(xi_Tadd(m_addi));
            end
                fMwi_u3=@(xi) zmw(xi).*rho_w.*(Rint(xi).^2).*FF_u3{i,j}(xi);
                Mwi_u3(i,j)=0.5.*pi.*1.*integral(fMwi_u3,-1,1);
                fMwe_u3=@(xi) zmw(xi).*rho_w.*((C_M-1).*((Rext(xi)+t_g).^2)).*FF_u3{i,j}(xi);
                Mwe_u3(i,j)=0.5.*pi.*1.*integral(fMwe_u3,-1,1);
                fMg_u3=@(xi) zmg(xi).*rho_g.*((Rext(xi)+t_g).^2-Rext(xi).^2).*FF_u3{i,j}(xi);
                Mg_u3(i,j)=0.5*pi*1*integral(fMg_u3,-1,1);
                fMsi_u3=@(xi) zcs(xi).*frho_s(xi).*(Rint(xi).^2).*FF_u3{i,j}(xi);
                Msi_u3(i,j)=0.5.*pi.*1.*integral(fMsi_u3,-1,1);
                fMse_u3=@(xi) zcs(xi).*frho_s(xi).*(C_M-1).*(Rext(xi).^2).*FF_u3{i,j}(xi);
                Mse_u3(i,j)=0.5.*pi.*1.*integral(fMse_u3,-1,1);
        %Stiffness matrices
        fK_u3=@(xi) lambda(xi).*G(xi).*(Rext(xi).^2-Rint(xi).^2).*dFF_u3{i,j}(xi);
        K_u3(i,j)=2.*pi.*integral(fK_u3,-1,1)./1;
            fKs=@(xi) k_s(xi).*FF_u3{i,j}(xi).*Rext(xi);
            K_s(i,j)=0.25.*pi.*1.*integral(fKs,-1,1);
        %Damping matrices
                beta=@(xi) (zmg(xi).*(4.*(Rext(xi)+t_g).^2.*rho_w.*omegawave)./(2.*pi.*mu_w))+((1-zmg(xi)).*(4.*Rext(xi).^2.*rho_w.*omegawave)./(2.*pi
```

```
.*mu_w));
                wka=wk.*d_m1/2;
                fCw_vis=@(xi) zcw(xi).*(1/3).*mu_w.*beta(xi).*KC.*2.*Rext(xi).*C_d.*FF_u3{i,j}(xi).*Rext(xi);
            Cw_vis(i,j)=0.25.*pi.*1.*integral(fCw_vis,-1,1).*2./((l_TP1-l_M1).*pi.*d_m1);
            dY1=0.5.*(bessely(0,wka)-bessely(2,wka));
            dJ1=0.5.*(besselj(0,wka)-besselj(2,wka));
            helpfunccwrad=real((exp(-sqrt(-1).*atan(dY1/dJ1))).^2.*((wka.*besselh(1,wka)).^(-1)).^2);
            cw_rad=@(xi) 8.*rho_w.*(Rext(xi)).^3.*(sinh(wk.*(l_TP1-l_M1))).^2.*helpfunccwrad.*omega_exp./(wka.*(sinh(2.*wk.*(l_TP1-l_M1))+2.*wk.*(l_TP1-l_M1)));
            fCw_rad=@(xi) zcw(xi).*cw_rad(xi).*FF_u3{i,j}(xi);
            xi_cwrad=2.*(l_M1+(l_TP1-l_M1)/2)./l-1;
            Cw_rad(i,j)=fCw_rad(xi_cwrad);
            a0=@(xi) (omega.*Rext(xi))./(fV_s(xi));
            fCs_rad=@(xi) zcs(xi).*Q(xi).*a0(xi).*(fgamma_s(xi)./9.81).*fV_s(xi).*2.*Rext(xi).*FF_u3{i,j}(xi).*Rext(xi);
            Cs_rad(i,j)=0.25.*pi.*1.*integral(fCs_rad,-1,1).*2./(l_M1.*pi.*d_m1);
            fCs_hys=@(xi) zcs(xi).*(2.*zeta_s.*fG_s(xi))./(omega.*l_M1).*FF_u3{i,j}(xi).*Rext(xi);
            Cs_hys(i,j)=0.25.*pi.*1.*integral(fCs_hys,-1,1);
            Re_ca=Vx*cb*rho_a/(mu_a);
            if Re_ca<10^4
                msgbox('The Reynolds number for a blade is situated below the considered estimation for the blade drag coefficient.','Warning')
            end
            if strcmp(favsss,'Fore-Aft')==1
                ca=(rho_a.*3.*Vx.*cb.*C_dblade.*R)*(1-InpTWpar);
            elseif strcmp(favsss,'Side-Side')==1
                ca=0;
            end
            Ca(i,j)=ca.*FF_u3{i,j}(1);
    end
end
M_tt=zeros(p_tt,p_tt);  %Structural inertia theta direction
Mlm_tt=zeros(p_tt,p_tt); %Lumped inertia theta direction
Mg_tt=zeros(p_tt,p_tt); %Marine growth mass theta direction
Msi_tt=zeros(p_u3,p_u3); %Inner soil added mass theta direction
Mse_tt=zeros(p_u3,p_u3); %Outer soil added mass theta direction
K_ttG=zeros(p_tt,p_tt); %Structural stiffness (G) theta direction
K_ttE=zeros(p_tt,p_tt); %Structural stiffness (E) theta
```

```
        direction
for i=1:p_tt
    for j=1:p_tt
        %Mass matrices
        fM_tt=@(xi) rho.*(Rext(xi).^4-Rint(xi).^4).*FF_tt{i,j}(xi);
        M_tt(i,j)=0.125.*pi.*l.*integral(fM_tt,-1,1);
        Mlm_tt(i,j)=J_RNA.*FF_tt{i,j}(1);
            fMg_tt=@(xi) zmg(xi).*rho_g.*((Rext(xi)+t_g).^4-Rext(xi).^4).*FF_tt{i,j}(xi);
            Mg_tt(i,j)=0.125*pi*l*integral(fMg_tt,-1,1);
            fMsi_tt=@(xi) zcs(xi).*frho_s(xi).*(Rint(xi).^4).*FF_tt{i,j}(xi);
            Msi_tt(i,j)=0.125.*pi.*l.*integral(fMsi_tt,-1,1);
            fMse_tt=@(xi) zcs(xi).*frho_s(xi).*(C_M-1).*(Rext(xi).^4).*FF_tt{i,j}(xi);
            Mse_tt(i,j)=0.125.*pi.*l.*integral(fMse_tt,-1,1);
        %Stiffness matrices
        fK_ttG=@(xi) lambda(xi).*G(xi).*(Rext(xi).^2-Rint(xi).^2).*FF_tt{i,j}(xi);
        K_ttG(i,j)=0.5.*pi.*l.*integral(fK_ttG,-1,1);
        fK_ttE=@(xi) E(xi).*(Rext(xi).^4-Rint(xi).^4).*dFF_tt{i,j}(xi);
            K_ttE(i,j)=0.5.*pi.*integral(fK_ttE,-1,1)./l;
    end
end
K_u3tt=zeros(p_u3, p_tt);
for i=1:p_u3
    for j=1:p_tt
        fK_u3tt=@(xi) lambda(xi).*G(xi).*(Rext(xi).^2-Rint(xi).^2).*FdF_u3tt{i,j}(xi);
        K_u3tt(i,j)=pi.*integral(fK_u3tt,-1,1);
    end
end
        K_ttu3=transpose(K_u3tt);

        M=zeros(dimMKC);
        M(1:p_u1,1:p_u1)=Mcorr.*M_u1+Mg_u1+Mlm_u1;
        M(p_u1+1:p_u1+p_u3,p_u1+1:p_u1+p_u3)=Mcorr.*M_u3+Mwi_u3+Mwe_u3+Mg_u3+Mlm_u3+Msi_u3+Mse_u3;
        M(p_u1+p_u3+1:p_u1+p_u3+p_tt,p_u1+p_u3+1:p_u1+p_u3+p_tt)=Mcorr.*M_tt+Mg_tt+Mlm_tt+Mse_tt+Msi_tt;
        K=zeros(dimMKC);
        K(1:p_u1,1:p_u1)=Mcorr.*K_u1;
        K(p_u1+1:p_u1+p_u3,p_u1+1:p_u1+p_u3)=Mcorr.*K_u3+K_s;
        K(p_u1+p_u3+1:p_u1+p_u3+p_tt,p_u1+p_u3+1:p_u1+p_u3+p_tt)=Mcorr^3.*K_ttE+Mcorr.*K_ttG;
        K(p_u1+1:p_u1+p_u3,p_u1+p_u3+1:p_u1+p_u3+p_tt)=Mcorr.*
```

```
        K_u3tt;
        K(p_u1+p_u3+1:p_u1+p_u3+p_tt,p_u1+1:p_u1+p_u3)=Mcorr.*K_ttu3;
        C=zeros(dimMKC);
        C(1:p_u1,1:p_u1)=(eta./omega).*Mcorr.*K_u1;
        C(p_u1+1:p_u1+p_u3,p_u1+1:p_u1+p_u3)=(eta./omega).*Mcorr.*K_u3+Cw_vis+Cw_rad+Cs_rad+Cs_hys+Ca;
        C(p_u1+p_u3+1:p_u1+p_u3+p_tt,p_u1+p_u3+1:p_u1+p_u3+p_tt)=(eta./omega).*(Mcorr^3.*K_ttE+Mcorr.*K_ttG);
        C(p_u1+1:p_u1+p_u3,p_u1+p_u3+1:p_u1+p_u3+p_tt)=(eta./omega).*Mcorr.*K_u3tt;
        C(p_u1+p_u3+1:p_u1+p_u3+p_tt,p_u1+1:p_u1+p_u3)=(eta./omega).*Mcorr.*K_ttu3;

%% Boundary conditions
% Boundary condition on the left of the element
ru1l=0;
ru1r=0;
ru3l=0;
ru3r=0;
rttl=0;
rttr=0;
if bc(1,1)==1 %clamped condition
    ru1l=1;
    ru3l=2;
    rttl=1;
    M(1,:)=[];
    M(:,1)=[];
    K(1,:)=[];
    K(:,1)=[];
    C(1,:)=[];
    C(:,1)=[];
    M((p_u1+1)-ru1l:(p_u1+2)-ru1l,:)=[];
    M(:,(p_u1+1)-ru1l:(p_u1+2)-ru1l)=[];
    K((p_u1+1)-ru1l:(p_u1+2)-ru1l,:)=[];
    K(:,(p_u1+1)-ru1l:(p_u1+2)-ru1l)=[];
    C((p_u1+1)-ru1l:(p_u1+2)-ru1l,:)=[];
    C(:,(p_u1+1)-ru1l:(p_u1+2)-ru1l)=[];
    M((p_u1+p_u3+1)-ru1l-ru3l,:)=[];
    M(:,(p_u1+p_u3+1)-ru1l-ru3l)=[];
    K((p_u1+p_u3+1)-ru1l-ru3l,:)=[];
    K(:,(p_u1+p_u3+1)-ru1l-ru3l)=[];
    C((p_u1+p_u3+1)-ru1l-ru3l,:)=[];
    C(:,(p_u1+p_u3+1)-ru1l-ru3l)=[];
elseif bc(1,1)==2 %hinge condition
    ru1l=1;
    ru3l=1;
    rttl=0;
```

```
        M(1,:)=[];
        M(:,1)=[];
        K(1,:)=[];
        K(:,1)=[];
        C(1,:)=[];
        C(:,1)=[];
        M((p_u1+1)-ru1l,:)=[];
        M(:,(p_u1+1)-ru1l)=[];
        K((p_u1+1)-ru1l,:)=[];
        K(:,(p_u1+1)-ru1l)=[];
        C((p_u1+1)-ru1l,:)=[];
        C(:,(p_u1+1)-ru1l)=[];
elseif bc(1,1)==3 %u1 roller condition
        ru1l=0;
        ru3l=1;
        rttl=0;
        M(p_u1+1,:)=[];
        M(:,p_u1+1)=[];
        K(p_u1+1,:)=[];
        K(:,p_u1+1)=[];
        C(p_u1+1,:)=[];
        C(:,p_u1+1)=[];
elseif bc(1,1)==4 %u3 roller condition
        ru1l=1;
        ru3l=0;
        rttl=0;
        M(1,:)=[];
        M(:,1)=[];
        K(1,:)=[];
        K(:,1)=[];
        C(1,:)=[];
        C(:,1)=[];
end
% Boundary condition on the right of the element
if bc(end,2)==1 %clamped condition
        ru1r=1;
        ru3r=2;
        rttr=1;
        M(p_u1-1-(ru1l+ru3l+rttl),:)=[];
        M(:,p_u1-1-(ru1l+ru3l+rttl))=[];
        K(p_u1-1-(ru1l+ru3l+rttl),:)=[];
        K(:,p_u1-1-(ru1l+ru3l+rttl))=[];
        C(p_u1-1-(ru1l+ru3l+rttl),:)=[];
        C(:,p_u1-1-(ru1l+ru3l+rttl))=[];
        M((p_u1+p_u3-1)-ru1r-(ru1l+ru3l+rttl):(p_u1+p_u3)-ru1r-(ru1l
            +ru3l+rttl),:)=[];
        M(:,(p_u1+p_u3-1)-ru1r-(ru1l+ru3l+rttl):(p_u1+p_u3)-ru1r-(
            ru1l+ru3l+rttl))=[];
```

```
        K((p_u1+p_u3-1)-ru1r-(ru1l+ru3l+rttl):(p_u1+p_u3)-ru1r-(ru1l+ru3l+rttl),:)=[];
        K(:,(p_u1+p_u3-1)-ru1r-(ru1l+ru3l+rttl):(p_u1+p_u3)-ru1r-(ru1l+ru3l+rttl))=[];
        C((p_u1+p_u3-1)-ru1r-(ru1l+ru3l+rttl):(p_u1+p_u3)-ru1r-(ru1l+ru3l+rttl),:)=[];
        C(:,(p_u1+p_u3-1)-ru1r-(ru1l+ru3l+rttl):(p_u1+p_u3)-ru1r-(ru1l+ru3l+rttl))=[];
            M(end-1,:)=[];
            M(:,end-1)=[];
            K(end-1,:)=[];
            K(:,end-1)=[];
            C(end-1,:)=[];
            C(:,end-1)=[];
    elseif bc(end,2)==2 %hinge condition
        ru1r=1;
        ru3r=1;
        rttr=0;
        M(p_u1-1-(ru1l+ru3l+rttl),:)=[];
        M(:,p_u1-1-(ru1l+ru3l+rttl))=[];
        K(p_u1-1-(ru1l+ru3l+rttl),:)=[];
        K(:,p_u1-1-(ru1l+ru3l+rttl))=[];
        C(p_u1-1-(ru1l+ru3l+rttl),:)=[];
        C(:,p_u1-1-(ru1l+ru3l+rttl))=[];
        M((p_u1+p_u3-1)-ru1r-(ru1l+ru3l+rttl),:)=[];
        M(:,(p_u1+p_u3-1)-ru1r-(ru1l+ru3l+rttl))=[];
        K((p_u1+p_u3-1)-ru1r-(ru1l+ru3l+rttl),:)=[];
        K(:,(p_u1+p_u3-1)-ru1r-(ru1l+ru3l+rttl))=[];
        C((p_u1+p_u3-1)-ru1r-(ru1l+ru3l+rttl),:)=[];
        C(:,(p_u1+p_u3-1)-ru1r-(ru1l+ru3l+rttl))=[];
    elseif bc(end,2)==3 %u1 roller condition
        ru1r=0;
        ru3r=1;
        rttr=0;
        M(p_u1+p_u3-1-(ru1l+ru3l+rttl),:)=[];
        M(:,p_u1+p_u3-1-(ru1l+ru3l+rttl))=[];
        K(p_u1+p_u3-1-(ru1l+ru3l+rttl),:)=[];
        K(:,p_u1+p_u3-1-(ru1l+ru3l+rttl))=[];
        C(p_u1+p_u3-1-(ru1l+ru3l+rttl),:)=[];
        C(:,p_u1+p_u3-1-(ru1l+ru3l+rttl))=[];
    elseif bc(end,2)==4 %u3 roller condition
        ru1r=1;
        ru3r=0;
        rttr=0;
        M(p_u1-1-(ru1l+ru3l+rttl),:)=[];
        M(:,p_u1-1-(ru1l+ru3l+rttl))=[];
        K(p_u1-1-(ru1l+ru3l+rttl),:)=[];
        K(:,p_u1-1-(ru1l+ru3l+rttl))=[];
```

```
        C(p_u1-1-(ru1l+ru3l+rttl),:)=[];
        C(:,p_u1-1-(ru1l+ru3l+rttl))=[];
end
ru1=ru1r+ru1l;
ru3=ru3r+ru3l;
rtt=rttr+rttl;

%% Eigen problem
A=[-inv(M)*C,-inv(M)*K;eye(size(M,1),size(C,2)), zeros(size(M,1)
    ,size(K,2))];
% [eigV,eigMv]=eigs(A,12,'smallestabs');
[eigV,eigMv]=eig(A);
dMv=diag(eigMv);
trucnat=find(abs(real(dMv)./abs(dMv))<=.99 & imag(dMv)>eps);
[natfreq,indeig]=sortrows([(imag(dMv(trucnat)))./(2.*pi),-real(
    dMv(trucnat))./(abs(dMv(trucnat)))]);
disp(natfreq(1:6,:))

%% Decay test
TESTde=questdlg('Do you want to perform a decay test?','Decay
    test','Yes','No','No');
switch TESTde
    case 'Yes'
        TESTdetype=questdlg('Do you want a step or impulse
            excitation?','Type of decay test','Step','Impulse','
            Impulse');
        switch TESTdetype
            case 'Step'
                TESTdetype=1;
            case 'Impulse'
                TESTdetype=2;
        end
        opts.Interpreter='tex';
        ns=inputdlg({'Newmark parameter \delta:','Newmark
            parameter \alpha','Newmark time step (\delta t) [s]:'
            ,'Maximum simulation time [s]:'},'Newmark solution'
            ,[1 50],{'0.5','0.25','0.01','600'},opts);
        Npdelta=str2double(ns{1});
        Npalpha=str2double(ns{2});
        deltat=str2double(ns{3});
        timemax=str2double(ns{4});
        if TESTdetype==1
            Nmtitle='Newmark method response to a step like
                excitation';
        else
            Nmtitle='Newmark method response to an impulse like
                excitation';
        end
```

```
if bct>0
    bc(2,end)=0;
    msgbox('The defined top boundary condition was not "free". This was changed.','Warning')
end
Nsize=timemax/deltat+1;
q0=zeros(dimMKC-ru1-ru3-rtt,1);
y0=zeros(dimMKC-ru1-ru3-rtt,1);
if TESTdetype==2
    destart=30;
    deimpulsetime=2;
    deend=destart+deimpulsetime;
    F=zeros(length(q0),Nsize);
    F(p_u1+1-ru1:p_u1+p_u3-(ru1+ru3),destart/deltat+1:deend/deltat+1)=8*10^6;
else
    ststart=10;
    stend=timemax;
    F=zeros(length(q0),Nsize);
    F(p_u1+1-ru1:p_u1+p_u3-(ru1+ru3),ststart/deltat+1:stend/deltat+1)=8*10^6;
end
f0=F(:,1);
x0=M\(f0-C*y0-K*q0);
a0=1/(Npalpha.*(deltat).^2);
a1=Npdelta./(Npalpha.*deltat);
a2=1./(Npalpha.*deltat);
a3=1./(2.*Npalpha)-1;
a4=Npdelta/Npalpha-1;
a5=0.5.*deltat.*(Npdelta./Npalpha-2);
a6=deltat.*(1-Npdelta);
a7=Npdelta.*deltat;
Kef=K+a0.*M+a1.*C;
x_i=zeros(length(q0),Nsize);
y_i=zeros(length(q0),Nsize);
q_i=zeros(length(q0),Nsize);
x_i(:,1)=x0; %Acceleration at a given ith instant
y_i(:,1)=y0; %Velocity at a given ith instant
q_i(:,1)=q0; %Displacement at a given ith instant
for i=2:Nsize
    Fef=F(:,i)+M*(a0.*q_i(:,i-1)+a2.*y_i(:,i-1)+a3.*x_i(:,i-1))+C*(a1.*q_i(:,i-1)+a4.*y_i(:,i-1)+a5.*x_i(:,i-1));
    q_i(:,i)=Kef\Fef;
    x_i(:,i)=a0.*(q_i(:,i)-q_i(:,i-1))-a2.*y_i(:,i-1)-a3.*x_i(:,i-1);
    y_i(:,i)=y_i(:,i-1)+a6.*x_i(:,i-1)+a7.*x_i(:,i);
end
```

```
        ffu1=zeros(p_u1,1);
        j=1;
        for i=1:length(f)
            if i<p_u1-1 || i>length(f)-2
                ffu1(j,1)=f{i,1}(1);
                j=j+1;
            end
        end
        if ru1r==1
            ffu1(end-1,:)=[];
        end
        u1=transpose(ffu1)*q_i(1:p_u1-ru1,:);
        ffu3=zeros(p_u3,1);
        j=1;
        for i=1:length(f)
            if i<p_u3-1 || i>length(f)-2
                ffu3(j,1)=f{i,1}(1);
                j=j+1;
            end
        end
        if ru3r==1
            ffu3(end-1,:)=[];
        end
        u3=transpose(ffu3)*q_i(p_u1-(ru1+ru31)+1:p_u1+p_u3-(ru1+
            ru3),:);
        fftt=zeros(p_tt,1);
        j=1;
        for i=1:length(f)
            if i<p_tt-1 || i>length(f)-2
                fftt(j,1)=f{i,1}(1);
                j=j+1;
            end
        end
        if rttr==1
            fftt(end-1,:)=[];
        end
        tt=transpose(fftt)*q_i(p_u1+p_u3+1-(ru1+ru3+rttl):end,:)
            ;
        figure(1)
        plot(0:deltat:timemax,u1)
        xlabel('t / s')
        ylabel('u_1^{pile top}(t) / m')
        title(Nmtitle)
        figure(2)
        plot(0:deltat:timemax,u3)
        xlabel('t / s')
        ylabel('u_3^{pile top}(t) / m')
        title(Nmtitle)
```

```
        figure(3)
        plot(0:deltat:timemax,tt)
        xlabel('t / s')
        ylabel('\theta^{pile top}(t) / rad')
        title(Nmtitle)
end
```